Proteomic dissection of Alzheimer's disease pathology

Hondius, David Carolus

2022

document version
Publisher's PDF, also known as Version of record

PROTEOMIC DISSECTION OF ALZHEIMER'S DISEASE PATHOLOGY

David C. Hondius

Provided by thesis specialist Ridderprint, ridderprint.nl
Printing: Ridderprint
Layout and design: Anna Bleeker, persoonlijkproefschrift.nl

Printing of this thesis was financially supported by Alzheimer Nederland (Amersfoort) and the Center for Neurogenomics and Cognitive Research (CNCR) (Amsterdam)

VRIJE UNIVERSITEIT

PROTEOMIC DISSECTION OF ALZHEIMER'S DISEASE PATHOLOGY

ACADEMISCH PROEFSCHRIFT

ter verkrijging van de graad Doctor aan
de Vrije Universiteit Amsterdam,
op gezag van de rector magnificus
prof.dr. C.M. van Praag,
in het openbaar te verdedigen
ten overstaan van de promotiecommissie
van de Faculteit der Bètawetenschappen
op dinsdag 15 februari 2022 om 11.45 uur
in een bijeenkomst van de universiteit,
De Boelelaan 1105

door

David Carolus Hondius

geboren te Edam-Volendam

promotoren:	prof.dr. A.B. Smit prof.dr. J.M. Rozemuller
copromotor:	dr. J.J.M. Hoozemans
promotiecommissie:	dr. F.H. Bouwman prof.dr. P. Lucassen prof.dr. D.R. Thal prof.dr. W.E. van Nostrand dr. W. Scheper prof.dr. H.D. Mansvelder

Voor Kim, Ilse, Jasper en Tygo

Voor mijn ouders

CONTENTS

CHAPTER 1

General Introduction

INTRODUCTION

Alzheimer's disease

Alzheimer's disease (AD) is the most common form of dementia in the elderly and is becoming increasingly more prevalent due to the increase in live expectancy and the ageing population. An estimated number of 50 million people suffer from dementia worldwide and this is estimated to nearly triple by the year 2050. In approximately 2/3rd of these patients AD is the primary cause of dementia [37]. In early phases of AD the initial symptoms are memory complaints, difficulties in learning, word finding problems and disorientation. As AD develops, patients experience progressive loss of memory and deterioration of all cognitive functions, eventually resulting in complete dependence on others for daily living. On average, death occurs 9 years after diagnosis. Currently only limited symptomatic treatment is possible and attempts to stop or slow the underlying pathogenesis have been unsuccessful.

AD risk and genetics

The majority of AD cases are sporadic and have no specific genetic predisposition. The most important risk factor for sporadic AD is ageing. In addition, modifiable risk factors include elevated blood pressure, high body mass index (BMI), elevated total cholesterol levels, diabetes mellitus, smoking, depression, physical inactivity, cognitive inactivity, poor diet, and low educational level. Improvement of these factors may delay the age of onset of AD [12].

Much research has been done to identify genes that affect the risk of developing AD. The most well-known genetic risk factor for AD is APOE which comes in 3 alleles, ε2, ε3 and ε4. APOE ε4 carriers have a two- to three-fold increased risk of developing AD while two copies of ε4 can increase the risk by 12 times [39]. APOE ε4 carriers on average experience an earlier onset of the disease. APOE is involved in lipid metabolism as well as processing and transport of Aβ. Other genes that affect the risk for development, found in genome wide association studies, include CLU, SORL1, ABCA7, BIN1, PICALM, CR1, CD33, MS4A, TREM2, CD2AP and EPHA1. These genes control processes that include inflammation, endocytosis and cholesterol metabolism [29, 46].

In addition, there are genetic factors that predispose to the development of the familial form of AD, often at a relatively young age. Genetic causes for AD lay in the amyloid precursor protein (APP) gene, and genes coding for proteins involved in amyloid beta (Aβ) generation from the APP protein, presenilin (PSEN)1 and PSEN2. Individuals carrying certain mutations in these genes or those carrying a duplication of the APP gene are predisposed to develop pre-senile dementia of the AD type[7]. Interestingly, also a protective mutation in the APP gene has been described [28].

Pathology of AD

Post mortem macroscopic examination of the AD brain at the end stage of the disease, reveals severe brain atrophy in specific regions. These regions include the hippocampus, the neocortex,

the amygdala and the entorhinal cortex. Widening of the sulci, narrowing of the gyri and enlargement of the ventricles is often seen and is a direct result of massive neuronal loss [4].

Microscopically, several pathological hallmarks are observed which are inseparably connected with AD. The most well-known hallmarks of AD are senile plaques, composed of the aggregated Aβ peptide, and neurofibrillary tangles which are intracellular accumulations of hyperphosphorylated tau. The presence of these fibrillar structures were already observed and described in 1907 by Alois Alzheimer in a patient that died with pre-senile dementia [3, 61]. In addition, neuritic plaques were first described in that same year by Oscar Fisher in cases with senile dementia [15]. Less research has been invested in amyloid angiopathy, defined by the accumulation of Aβ aggregates at the brain vasculature, which is a common feature in AD, and granulovacuolar degeneration (GVD), which are neuronal lesions that are also present in all AD cases.

Plaque pathology

Amyloid plaques are extracellular aggregates of Aβ peptides which are a proteolytic cleavage product of amyloid precursor protein (APP) [18]. Aβ is cleaved from APP by β-secretase 1 (BACE1) and the γ-secretase multi-subunit protease complex (consisting of presenilins, NCSTN, APH1A and PEN2) [62]. Aβ is an aggregation prone peptide and has neurotoxic properties [10, 34, 52, 76]. Different forms of Aβ exist ranging from 36 to 43 amino acids, with Aβ40 and Aβ42 being the predominant forms. First, smaller oligomers of few Aβ molecules and subsequently Aβ fibrils are formed. Several studies have shown that the smaller oligomeric Aβ represents the most toxic species, inducing synaptic dysfunction, microglial and astrocytic activation and associated neuroinflammation, and tau pathology [71]. Extracellular aggregation might be a protective mechanism to scaffold these toxic Aβ species. Alternatively, the formation of amyloid fibrils could be required for the formation of tangles. This is supported by the occurrence of tangles in patients with other types of amyloid deposits, for example due to prion mutations or to chromosome 13 mutations, leading to various forms of dementia [55] (Fig. 1A-B).

Normally the production of Aβ is balanced with Aβ clearance. However, when production is high or removal is impaired this balance is lost and aggregation can occur. For familial AD, it is generally thought that an increased production of Aβ is the general cause. For sporadic AD however, insufficient clearance of Aβ may account for its accumulation (Fig. 1B). Removal of Aβ from the brain occurs by means of degradation via specific proteases [14, 49], through phagocytosis and degradation mainly by microglia [48] but also by astrocytes [45], via clearance through the blood brain barrier (BBB), by drainage along perivascular pathways [6, 74] and by drainage from the interstitial fluid to the CSF via the glymphatic pathway [50, 63].

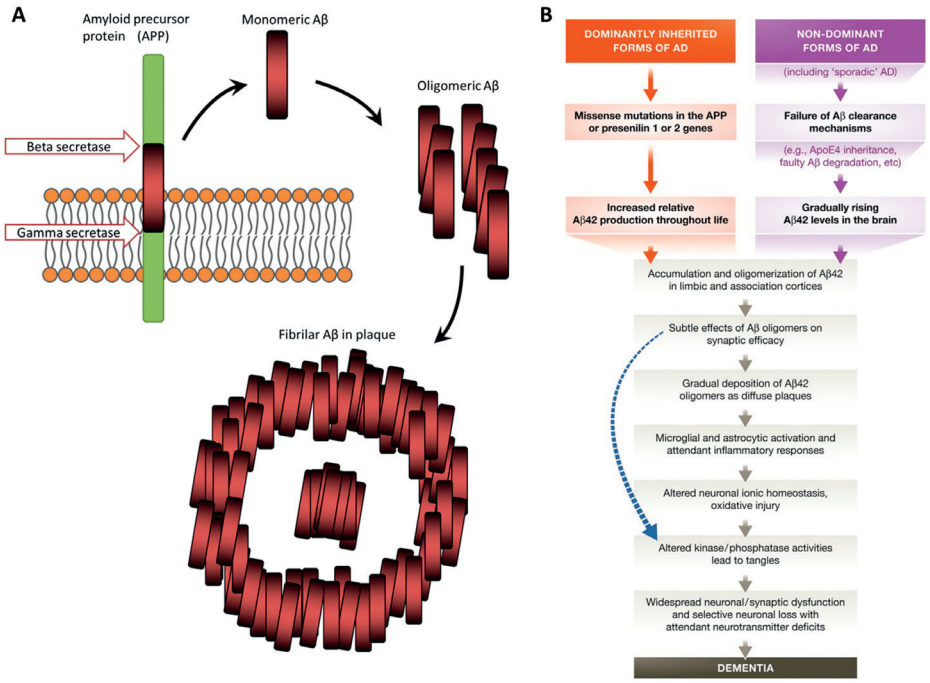

FIGURE 1 | A: Aβ is the proteolytic cleavage product of APP facilitated by β-secretase and the γ-secretase complex. In this amyloidogenic pathway Aβ is secreted to the interstitial fluid, a process that is increased with neuronal activity. After secretion, Aβ forms oligomers and fibrils that can contribute to AD pathogenesis at various disease stages. B: (Taken from [57]) The sequence of events that lead to AD as proposed by the amyloid cascade hypothesis. The curved blue arrow indicates that Aβ oligomers may directly damage synapses and neurites and induce tau hyperphosporylation [35, 57].

There are several proteins associated with Aβ deposits, including APO-E [43], APO-J [16], various factors of the complement system [67, 68] and serum amyloid P component, which can influence aggregation properties and toxicity, as well as modulating uptake of Aβ and eliciting a neuroinflammatory response [77].

Different types of plaques, with varying morphology and molecular composition, can be found in a typical AD brain, e.g. diffuse plaques (Fig. 3A), cored/classic plaques (Fig. 3B), coarse grained plaques (Fig. 3C) and neuritic plaques (Fig. 3F). This last type, being characterised by the presence of swollen neurites, also contains tau aggregates. In addition, less common plaque types exist, like for example cotton wool plaques which are mostly associated with certain mutations [58] (Fig. 3E). Although the presence of Aβ plaques is a requirement for the diagnosis of AD, Aβ pathology alone is not sufficient for symptomatic AD as many elderly display a significant amount of plaques but live without any symptoms of dementia [44].

Neurofibrillary tangles

Neurofibrillary tangles are intraneuronal aggregates of hyperphosphorylated tau protein (Fig 3I) [20, 21]. Normally, tau protein is involved in stabilisation of the microtubules and its association with microtubuli is regulated by phosphorylation of the protein as an essential part of microtubule dynamics. In AD, the tau protein gets abnormally hyperphosphorylated, which changes it from a normal functional protein into a neurotoxic protein that has aggregation properties and also possesses a prion-like templating activity [23, 42, 72]. Aggregated tau is observed in the neuronal cell body as tangles and in the neuronal extensions as neuropil threads.

Tangles become apparent in a progressive manner with early involvement of the hippocampus and gradual spreading to almost all other cortical regions, subcortical nuclei and brainstem as the disease progresses [7, 8]. The consistent way of spreading of tau pathology throughout the brain in typical AD allows objective pathological staging of the tangle pathology in AD using the Braak staging [8, 9] (Fig. 2). The Braak stage for tangle pathology ranges from stage 0 to stage VI with increasing NFT pathology. The severity and location of NFT pathology correlates well with the clinical manifestation of AD.

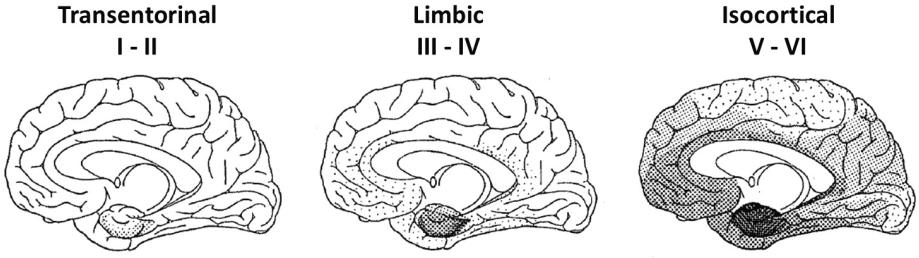

FIGURE 2 | Spreading of neurofibrillary tangles and neuropil threads during the course of AD defining the Braak stages I to VI. Darker grey shading indicates higher amounts of neurofibrillary changes. From Braak and Braak, 1991 [8].

Cerebral amyloid angiopathy

The Aβ peptide is not only found to aggregate into plaques in the parenchyma, but is also found to regularly aggregate at the brain vasculature. Vascular Aβ deposits are referred to as cerebral amyloid angiopathy (CAA). CAA is a common feature of AD as it is present in varying amounts in over 80% of all AD cases. There are two types of CAA with Aβ deposition. When CAA is present in larger vessels and also in brain capillaries it is called CAA type-1 [64] (Fig 3D). When CAA is present only in larger blood vessels, including leptomeningeal vessels, cortical arteries and arterioles, it is referred to as CAA type-2 [5, 64, 65]. Many cases with CAA type-1 exhibit dyshoric changes were Aβ pathology is associated with surrounding neuropil, and is often accompanied by microglial activation and tau pathology [53, 64]. Aβ deposition at the vessel wall is associated with impaired vascular response to changes in local metabolic demand [11] and increased risk of cerebral infarction, cerebral haemorrhage and micro-bleeds [69, 73]. Presence of the APOE ε4 allele is linked to the presence and severity of especially CAA type-1.

CAA type-1 correlates with clinical symptoms, it contributes to the clinical manifestation of AD and in severe forms it can be the primary cause of dementia [13, 19, 54]. Often, these patients are homozygous for APOE ε4 [64]. In AD there is an inverse correlation between the presence of Aβ plaque pathology in a certain region and CAA type-1 in the same region. Furthermore, CAA can also be genetically linked, as certain mutations in the genes that predispose for AD can also specifically give rise to a severe CAA type-1 or type-2 phenotype. Especially mutations in the APP gene, e.g. the Dutch E693Q (HCHWAD or Katwijk disease) lead to type-2 CAA and the Iowa D694N mutation, gives rise to very severe CAA type-1 in an autosomal dominant manner.

Granulovacuolar degeneration

As early as 1911 Teofil Simchowicz described changes in hippocampal pyramidal neurons which are now referred to as granulovacuolar degeneration (GVD) [22, 59]. GVD is characterized by neurons containing rimmed vacuoles with a dense pit, which become apparent predominantly in hippocampal pyramidal neurons (Fig 3G, H) [32, 47]. Co-occurrence of these double membrane-bound bodies with neurofibrillary tangles was noted [17, 32]. In AD, GVD arises first in the hippocampal regions CA2, CA1 and the subiculum and a gradual increase in the percentage of neurons with GVD takes place over the Braak stages [26], correlating with the increase of tau pathology within these regions. Also spreading of GVD to other brain regions, such as the temporal lobe and in a later stage the hypothalamus and the amygdala occurs with disease progression and are staged according to Thal et al. [66]. Moreover, the presence of GVD is associated with pre-tangle neurons, as GVD frequently shows co-occurrence in the same neuron with diffuse phospho-tau (pTau) staining, early (p)Tau epitopes and also with some aggregated tau [24, 26, 32]. GVD granules show immunoreactivity for markers related to the unfolded protein response (pPERK, pIRE1 and peIF2α) [25, 26], endocytosis pathway (CHMP2B) [75] and late stage autophagy markers (cathepsin-D, LAMP1) [17] suggesting a role in the autophagy-lysosomal pathway and activation of the unfolded protein response, two important mechanisms to manage an overload of misfolded proteins. In addition, markers that indicate necrosome activation (pRIPK1, pRIPK3 and pMLKL) are also found associated with GVD [33]. Commonly used marker proteins also include casein kinase 1 (CK1) α, δ and ε. These kinases are involved in various cellular processes and are capable of tau phosphorylation [31, 60].

Aβ depositions, tau pathology and GVD can all be observed to a certain extent in the brains of healthy elderly. As such, some degree of AD related pathology can be considered a pre-clinical stage of AD, but also as a part of normal ageing. The preclinical phase of AD is generally considered to span around 15 -20 years on average as was demonstrated in longitudinal studies that monitor cognitive function, CSF and neuroimaging biomarkers over time [35].

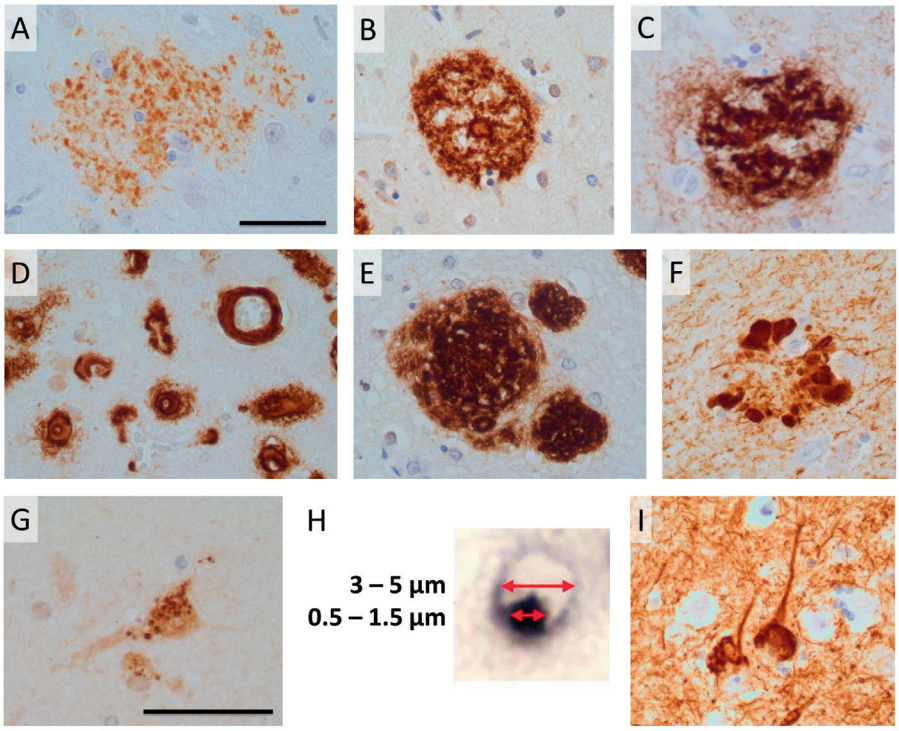

FIGURE 3 | Several types of AD related pathological features are shown. Diffuse non fibrillar plaque (A), cored or classical plaque (B), coarse grained plaque (C), affected capillaries in type-1 CAA (D) cotton wool plaque (E), all stained using an anti-Aβ antibody. Neuritic plaque is shown using an anti-p-tau antibody (F), granulovacuolar degeneration is shown using an anti-CK1δ antibody (G) and at high magnification (H) (from [32]). Tangles and neuropil threads are visualized using an anti-p-tau antibody (I). Scale bar in A represents 50µm and applies to A - F, scale bar in G represents 50µm and applies to G and I.

Diagnosis and treatment of AD

Diagnosis of AD is currently made according the "recommendations from the National Institute on Aging-Alzheimer's Association workgroups on diagnostic guidelines for Alzheimer's disease" and is based on clinical symptoms, neuropsychological testing, cerebrospinal fluid (CSF) biomarkers, magnetic resonance imaging (MRI), positron emission tomography (PET) scanning for amyloid [2, 38]. CSF biomarkers that are currently used for diagnosis of MCI and dementia due to AD are Aβ42, total tau and phospho-tau.

At this moment a clinical diagnosis does not reach 100% accuracy and sensitivity and different techniques can result in contradicting results [51]. In addition, AD has a long pre-symptomatic phase that can last for approximately 15 - 20 years [70]. During the pre-symptomatic phase there is a build-up of amyloid deposits, glial activation and in a later phase development of tau pathology and impairment of neuronal function (Fig. 4). In the subsequent symptomatic

phase of AD cognitive decline is staged using the Clinical Dementia Rating (CDR) that provides a 5-point scale based on six domains of cognitive and functional performance [40].

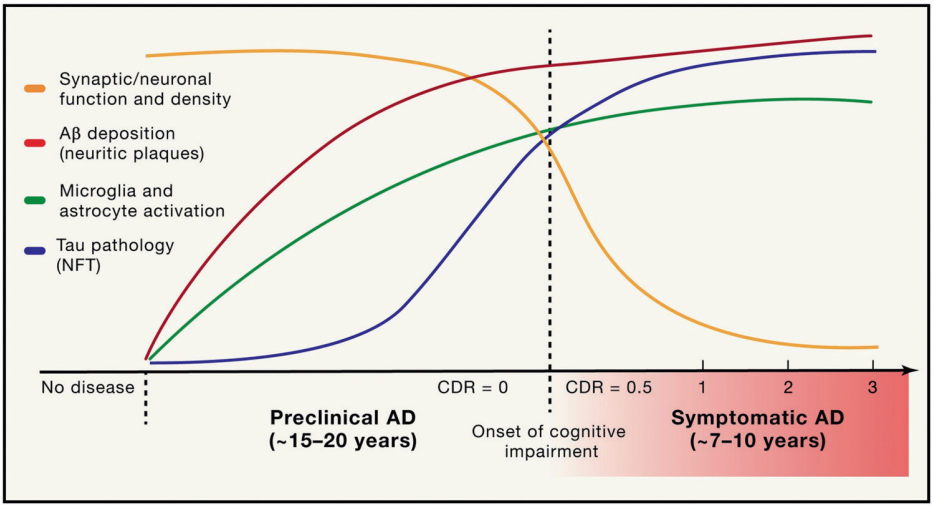

FIGURE 4 | Adapted from Long JM, Holtzman DM, Cell. 2019 [35]. AD is marked by a long pre-symptomatic phase during which Aβ deposition accompanied by glial activation already occurs. This is followed by an increase in tau pathology which in turn is associated with synaptic dysfunction and neuronal loss. The clinical symptoms after the onset of AD are staged using the Clinical Dementia Rating scale. A score of 0 indicates normal cognition and scores of 0.5, 1, 2, and 3 indicate questionable, mild, moderate, and severe dementia, respectively.

Currently, only symptomatic treatments exist for AD. The most commonly prescribed drugs for AD are cholinesterase inhibitors that aim to restore normal levels of the neurotransmitter acetylcholine. This treatment has a modest effect on symptoms of only a proportion of the AD patients and does not slow the underlying pathogenesis [35]. Many new therapeutics that have been tested, mainly focussing on reducing or preventing Aβ deposition, showed no benefits or appeared to have severe side effects [41, 56]. There are several reasons that could underlie this negative outcome. First, AD pathology starts decades before any symptoms arise and it is thought that by the time a diagnosis is made the damage in the brain is already very extensive and beyond repair. Secondly, AD is a heterogeneous disease, which is illustrated by the fact that patients can be symptomatically diverse, patients can be relatively young or very old, and the fact that AD can have a relatively fast or very slow progression. Also, AD pathology is heterogeneous, for example patients with AD can exhibit anything between no CAA and almost pure CAA and display a typical or an atypical distribution of tau pathology [30, 54]. Pathological and clinical diverse subtypes of AD will likely require different therapeutic approaches. Hence, it is very important to gain insight in early disease mechanisms and those associated with different pathological and clinical subtypes of AD.

Mass spectrometry-based proteomics

The proteome comprises all proteins that are present in a given sample. This can be, for example, a subcellular organelle, a cell, a tissue or an organism. Each individual cell contains thousands of different proteins that are needed to keep a cell alive and properly perform its function. Both the expression of genes and their translation into proteins is regulated and a cell can adjust the levels and repertoire of proteins to adapt to the specific requirements at that moment. As proteins essentially facilitate all functions performed in a cell, insight in the levels of specific proteins in different conditions provides information on their potential function, but is also important for the identification of processes that are affected under specific conditions, for example during a disease [1].

Global proteomics make use of liquid chromatography–tandem mass spectrometry (LC-MS/MS). This method identifies proteins or peptides based on their mass to charge ratio. As such, mass spectrometry studies allow unbiased insight in the proteome. The rapid development, in recent years, of mass spectrometers has resulted in remarkable increase in accuracy, sensitivity and speed [36]. It has become possible to directly quantify thousands of different proteins, sometimes including specific isoforms and post-translational modifications, from samples with a relatively low amount (<1µg) of total protein content [27]. This rapid evolution in the field of mass spectrometry makes it possible to perform unbiased analyses on small specific anatomical substructures or even groups of individually isolated cells.

The proteome of Alzheimer's disease

The brain is a highly complex and heterogeneously build organ, composed of different regions and anatomical layers each harbouring different combinations of cell types. On top of this, the aetiology of AD is complicated in nature as there is a slow progression, a long pre-symptomatic phase and different regions and cell types are affected differently and respond in diverse manners.

Combining (immuno-) histochemistry with laser microdissection (LMD) allows visualization and isolation of small anatomical regions or specific groups of individual cells with high accuracy of which the protein composition can be analysed using LC-MS/MS. A crucial step is to use high quality human brain tissue that has been extensively neuropathologically characterized and has a short post-mortem delay. Applying an unbiased proteomics approach at high resolution using LMD assisted LC-MS/MS has the potential to identify many proteins that have not previously been associated with AD and as such provide new insights into its pathogenesis.

Changes in the proteome can be determined in specific regions of interest either at different stages of AD, in different subtypes of AD or in association with specific pathological features. It is important to gain insight into the molecular mechanisms that are associated with different aspects of the disease. This will lead to new ideas on the aetiology and pathogenesis of AD and could ultimately lead to clues for the development of new post-mortem and clinically relevant diagnostic tools and therapeutic approaches.

Aims and outline

For the development of potential treatments increased insight in the aetiology and pathogenic mechanisms of AD is required. In addition, biomarkers that allow an accurate diagnosis at an early disease stage with possibility to stratify AD patients into subgroups are highly needed.

The main objective of the work described in this thesis is to identify and quantify differences in protein levels associated with 1) different pathological stages of AD 2), the development of tau pathology in neurons and 3) different subtypes of AD associated Aβ deposits. This information can provide insight in the molecular mechanisms associated with various aspects of AD and provide clues for therapeutic possibilities. In addition, some proteins can potentially be used as a protein biomarker in for example improved neuropathological characterisation, or clinically for early diagnosis, patient stratification and monitoring therapeutic efficacy.

Chapter 2 describes the proteomics analysis of a highly disease relevant region, the hippocampal subregions CA1 and subiculum, from 40 cases covering all stages of AD. We identified proteins that show changes in their abundance in early and late stages of AD, and changes that were transient over the disease course. Several identified AD related proteins were not previously associated with AD. In addition, we found that the different protein expression profiles over the disease stages are associated with different cell types and processes.

In **Chapter 3** we focus on proteomics analysis of laser micro-dissected human hippocampal pyramidal neurons and compare healthy neurons, pre-tangle neurons marked by GVD, and tangle bearing neurons. This provides neuron-specific insight in the temporal course of protein expression during tangle formation and allows deeper understanding of early mechanisms associated with the development of tau pathology and disease progression.

In **Chapter 4** we addressed the heterogeneity of AD by analysing two linked pathological hallmarks; the deposition of Aβ in plaques and CAA. We describe the proteomics analysis of human brain tissue with either Aβ plaque pathology or vascular Aβ deposits in CAA, with the aim to find specific protein markers that can be used to distinguish Aβ plaque pathology from vascular Aβ deposits. Several specific markers were identified and confirmed using immunohistochemistry and immunoblotting. In addition, specificity was assessed with respect to other brain vascular defects including prion CAA, CADASIL, CARASAL, and hypertension related small vessel disease.

Chapter 5 provides comprehensive instructions for performing a successful proteomics analysis on human post-mortem tissue with the aid of (immuno-) histochemistry and laser micro-dissection. This approach enables a focussed analysis on specific subareas, cells and cellular inclusions, and generates data on protein expression at high spatial resolution.

Chapter 6. Summarizes the findings of chapter 2 to 5 and presents a general discussion of the previous chapters.

REFERENCES

1. Aebersold R, Mann M Mass-spectrometric exploration of proteome structure and function. doi: 10.1038/nature19949
2. Albert MS, DeKosky ST, Dickson D, Dubois B, Feldman HH, Fox NC, Gamst A, Holtzman DM, Jagust WJ, Petersen RC, Snyder PJ, Carrillo MC, Thies B, Phelps CH (2011) The diagnosis of mild cognitive impairment due to Alzheimer's disease: Recommendations from the National Institute on Aging-Alzheimer's Association workgroups on diagnostic guidelines for Alzheimer's disease. Alzheimer's Dement 7:270-279w. doi: 10.1016/j.jalz.2011.03.008
3. Alzheimer A (1907) [Über eine eigenartige Erkrankung der Hirnrinde] [Article in German]. Allg Zeitschrift fur Psychiatr und Psych Medizin 64:146–148.
4. Apostolova LG, Green AE, Babakchanian S, Hwang KS, Chou Y-Y, Toga AW, Thompson PM Hippocampal atrophy and ventricular enlargement in normal aging, mild cognitive impairment and Alzheimer's disease. doi: 10.1097/WAD.0b013e3182163b62
5. Attems J, Jellinger K, Thal DR, Van Nostrand W (2011) Review: Sporadic cerebral amyloid angiopathy. Neuropathol Appl Neurobiol 37:75–93. doi: 10.1111/j.1365-2990.2010.01137.x
6. Bakker ENTP, Bacskai BJ, Arbel-Ornath M, Aldea R, Bedussi B, Morris AWJ, Weller RO, Carare RO (2016) Lymphatic Clearance of the Brain: Perivascular, Paravascular and Significance for Neurodegenerative Diseases. Cell Mol Neurobiol 36:181–194. doi: 10.1007/s10571-015-0273-8
7. Bateman RJ, Aisen PS, De Strooper B, Fox NC, Lemere CA, Ringman JM, Salloway S, Sperling RA, Windisch M, Xiong C (2010) Autosomal-dominant Alzheimer's disease: a review and proposal for the prevention of Alzheimer's disease. Alzheimers Res Ther 3:1. doi: 10.1186/alzrt59
8. Braak H, Braak E (1991) Neuropathological stageing of Alzheimer-related changes. Acta Neuropathol 82:239–59.
9. Braak H, Braak E (1995) Staging of alzheimer's disease-related neurofibrillary changes. Neurobiol Aging 16:271–278. doi: 10.1016/0197-4580(95)00021-6
10. Deshpande A, Mina E, Glabe C, Busciglio J (2006) Different conformations of amyloid β induce neurotoxicity by distinct mechanisms in human cortical neurons. J Neurosci 26:6011–6018. doi: 10.1523/JNEUROSCI.1189-06.2006
11. Dumas A, Dierksen GA, Gurol ME, Halpin A, Martinez-Ramirez S, Schwab K, Rosand J, Viswanathan A, Salat DH, Polimeni JR, Greenberg SM (2012) Functional magnetic resonance imaging detection of vascular reactivity in cerebral amyloid angiopathy. Ann Neurol 72:76–81. doi: 10.1002/ana.23566
12. Eggink E, Moll van Charante EP, van Gool WA, Richard E (2019) A Population Perspective on Prevention of Dementia. J Clin Med 8:834. doi: 10.3390/jcm8060834
13. Eurelings LSM, Richard E, Carrano A, Eikelenboom P, van Gool WA, Rozemuller AJM (2010) Dyshoric capillary cerebral amyloid angiopathy mimicking Creutzfeldt–Jakob disease. J Neurol Sci 295:131–134. doi: 10.1016/j.jns.2010.04.020
14. Farris W, Mansourian S, Chang Y, Lindsley L, Eckman EA, Frosch MP, Eckman CB, Tanzi RE, Selkoe DJ, Guenette S (2003) Insulin-degrading enzyme regulates the levels of insulin, amyloid -protein, and the -amyloid precursor protein intracellular domain in vivo. Proc Natl Acad Sci 100:4162–4167. doi: 10.1073/pnas.0230450100
15. Fischer O. Miliaere Nekrosen mit drusigen Wucherungen der Neurofibrillen, eine regelmassige Veraenderung der Hirnrinde bei seniler Demenz. Monatsschr Psychiat Neurol. 1907 Jan 1;22:361-72.

16. Foster EM, Dangla-Valls A, Lovestone S, Ribe EM, Buckley NJ (2019) Clusterin in Alzheimer's disease: Mechanisms, genetics, and lessons from other pathologies. Front Neurosci 13:164. doi: 10.3389/fnins.2019.00164

17. Funk KE, Mrak RE, Kuret J (2011) Granulovacuolar degeneration (GVD) bodies of Alzheimer's disease (AD) resemble late-stage autophagic organelles. Neuropathol Appl Neurobiol 37:295–306. doi: 10.1111/j.1365-2990.2010.01135.x

18. Glenner GG, Wong CW (1984) Alzheimer's disease and Down's syndrome: Sharing of a unique cerebrovascular amyloid fibril protein. Biochem Biophys Res Commun 122:1131–1135. doi: 10.1016/0006-291X(84)91209-9

19. Greenberg SM, Bacskai BJ, Hernandez-Guillamon M, Pruzin J, Sperling R, van Veluw SJ (2020) Cerebral amyloid angiopathy and Alzheimer disease — one peptide, two pathways. Nat Rev Neurol 16:30–42. doi: 10.1038/s41582-019-0281-2

20. Grundke-Iqbal I, Iqbal K, Quinlan M, Tung YC, Zaidi MS, Wisniewski HM (1986) Microtubule-associated protein tau. A component of Alzheimer paired helical filaments. J Biol Chem 261:6084–6089.

21. Grundke-Iqbal I, Iqbal K, Tung YC, Quinlan M, Wisniewski HM, Binder LI (1986) Abnormal phosphorylation of the microtubule-associated protein tau (tau) in Alzheimer cytoskeletal pathology. Proc Natl Acad Sci U S A 83:4913–4917. doi: 10.1073/pnas.83.13.4913

22. Grzybowski A, Pięta A, Pugaczewska M (2017) Teofil Simchowicz (1879–1957). J Neurol 264:1831–1832. doi: 10.1007/s00415-017-8460-9

23. Guo T, Noble W, Hanger DP (2017) Roles of tau protein in health and disease. Acta Neuropathol 133:665–704. doi: 10.1007/s00401-017-1707-9

24. Hara M, Hirokawa K, Kamei S, Uchihara T (2013) Isoform transition from four-repeat to three-repeat tau underlies dendrosomatic and regional progression of neurofibrillary pathology. Acta Neuropathol 125:565–579. doi: 10.1007/s00401-013-1097-6

25. Hoozemans JJM, van Haastert ES, Eikelenboom P, de Vos RAI, Rozemuller JM, Scheper W (2007) Activation of the unfolded protein response in Parkinson's disease. Biochem Biophys Res Commun 354:707–711. doi: 10.1016/j.bbrc.2007.01.043

26. Hoozemans JJM, Van Haastert ES, Nijholt DAT, Rozemuller AJM, Eikelenboom P, Scheper W (2009) The unfolded protein response is activated in pretangle neurons in alzheimer's disease hippocampus. Am J Pathol 174:1241–1251. doi: 10.2353/ajpath.2009.080814

27. Hosp F, Mann M (2017) A Primer on Concepts and Applications of Proteomics in Neuroscience. Neuron 96:558–571. doi: 10.1016/j.neuron.2017.09.025

28. Jonsson T, Atwal JK, Steinberg S, Snaedal J, Jonsson P V., Bjornsson S, Stefansson H, Sulem P, Gudbjartsson D, Maloney J, Hoyte K, Gustafson A, Liu Y, Lu Y, Bhangale T, Graham RR, Huttenlocher J, Bjornsdottir G, Andreassen OA, Jonsson EG, Palotie A, Behrens TW, Magnusson OT, Kong A, Thorsteinsdottir U, Watts RJ, Stefansson K (2012) A mutation in APP protects against Alzheimer's disease and age-related cognitive decline. Nature 488:96. doi: 10.1038/nature11283

29. Karch CM, Goate AM (2015) Alzheimer's disease risk genes and mechanisms of disease pathogenesis. Biol Psychiatry 77:43–51. doi: 10.1016/j.biopsych.2014.05.006

30. Kawakatsu S, Kobayashi R, Hayashi H (2017) Typical and atypical appearance of early-onset Alzheimer's disease: A clinical, neuroimaging and neuropathological study. Neuropathology 37:150–173. doi: 10.1111/neup.12364

31. Knippschild U, Gocht A, Wolff S, Huber N, Löhler J, Stöter M (2005) The casein kinase 1 family: Participation in multiple cellular processes in eukaryotes. Cell Signal 17:675–689. doi: 10.1016/j.cellsig.2004.12.011

32. Köhler C (2016) Granulovacuolar degeneration: a neurodegenerative change that accompanies tau pathology. Acta Neuropathol 132:339–359. doi: 10.1007/s00401-016-1562-0

33. Koper MJ, Schoor E Van, Ospitalieri S, Vandenberghe R, Mathieu Vandenbulcke ·, Von Arnim CAF, Tousseyn T, Sriram Balusu ·, De Strooper B, Dietmar ·, Thal R (2020) Necrosome complex detected in granulovacuolar degeneration is associated with neuronal loss in Alzheimer's disease. Acta Neuropathol 139:463–484. doi: 10.1007/s00401-019-02103-y

34. Lambert MP, Barlow AK, Chromy BA, Edwards C, Freed R, Liosatos M, Morgan TE, Rozovsky I, Trommer B, Viola KL, Wals P, Zhang C, Finch CE, Krafft GA, Klein WL (1998) Diffusible, nonfibrillar ligands derived from Aβ1-42 are potent central nervous system neurotoxins. Proc Natl Acad Sci U S A 95:6448–6453. doi: 10.1073/pnas.95.11.6448

35. Long JM, Holtzman DM (2019) Alzheimer Disease: An Update on Pathobiology and Treatment Strategies. Cell 179:312–339. doi: 10.1016/j.cell.2019.09.001

36. Mann M (2019) The ever expanding scope of electrospray mass spectrometry—a 30 year journey. Nat Commun 10:1–3. doi: 10.1038/s41467-019-11747-z

37. Martin Prince A, Wimo A, Guerchet M, Gemma-Claire Ali M, Wu Y-T, Prina M, Yee Chan K, Xia Z (2015) World Alzheimer Report 2015 The Global Impact of Dementia An analysis of prevalence, incidence, cost & trends.

38. McKhann GM, Knopman DS, Chertkow H, Hyman BT, Jack CR, Kawas CH, Klunk WE, Koroshetz WJ, Manly JJ, Mayeux R, Mohs RC, Morris JC, Rossor MN, Scheltens P, Carrillo MC, Thies B, Weintraub S, Phelps CH (2011) The diagnosis of dementia due to Alzheimer's disease: Recommendations from the National Institute on Aging-Alzheimer's Association workgroups on diagnostic guidelines for Alzheimer's disease. Alzheimer's Dement 7:263–269. doi: 10.1016/j.jalz.2011.03.005

39. Michaelson DM (2014) APOE ε4: The most prevalent yet understudied risk factor for Alzheimer's disease. Alzheimer's Dement 10:861–868. doi: 10.1016/j.jalz.2014.06.015

40. Morris JC (1993) The clinical dementia rating (cdr): Current version and scoring rules. Neurology 43:2412–2414. doi: 10.1212/wnl.43.11.2412-a

41. Moussa-Pacha NM, Abdin SM, Omar HA, Alniss H, Al-Tel TH (2020) BACE1 inhibitors: Current status and future directions in treating Alzheimer's disease. Med Res Rev 40:339–384. doi: 10.1002/med.21622

42. Mudher A, Colin M, Dujardin S, Medina M, Dewachter I, Alavi Naini SM, Mandelkow EM, Mandelkow E, Buée L, Goedert M, Brion JP (2017) What is the evidence that tau pathology spreads through prion-like propagation? Acta Neuropathol Commun 5:99. doi: 10.1186/s40478-017-0488-7

43. Namba Y, Tomonaga M, Kawasaki H, Otomo E, Ikeda K (1991) Apolipoprotein E immunoreactivity in cerebral amyloid deposits and neurofibrillary tangles in Alzheimer's disease and kuru plaque amyloid in Creutzfeldt-Jakob disease. Brain Res 541:163–166. doi: 10.1016/0006-8993(91)91092-F

44. Nelson PT, Alafuzoff I, Bigio EH, Bouras C, Braak H, Cairns NJ, Castellani RJ, Crain BJ, Davies P, Tredici K Del, Duyckaerts C, Frosch MP, Haroutunian V, Hof PR, Hulette CM, Hyman BT, Iwatsubo T, Jellinger KA, Jicha GA, Kövari E, Kukull WA, Leverenz JB, Love S, Mackenzie IR, Mann DM, Masliah E, McKee AC, Montine TJ, Morris JC, Schneider JA, Sonnen JA, Thal DR, Trojanowski JQ, Troncoso JC, Wisniewski T, Woltjer RL, Beach TG (2012) Correlation of Alzheimer Disease Neuropathologic Changes With Cognitive Status: A Review of the Literature. J Neuropathol Exp Neurol 71:362–381. doi: 10.1097/NEN.0b013e31825018f7

45. Nielsen HM, Veerhuis R, Holmqvist B, Janciauskiene S (2009) Binding and uptake of Aβ1-42 by primary human astrocytes in vitro. Glia 57:978–988. doi: 10.1002/glia.20822

46. Nikolac Perkovic M, Pivac N (2019) Genetic Markers of Alzheimer's Disease. In: Adv. Exp. Med. Biol. Springer New York LLC, pp 27–52

47. Okamoto K, Hirai S, Iizuka T, Yanagisawa T, Watanabe M (1991) Reexamination of granulovacuolar degeneration. Acta Neuropathol 82:340–345. doi: 10.1007/BF00296544

48. Paresce DM, Ghosh RN, Maxfield FR (1996) Microglial cells internalize aggregates of the Alzheimer's disease amyloid β-protein via a scavenger receptor. Neuron 17:553–565. doi: 10.1016/S0896-6273(00)80187-7

49. Poepsel S, Sprengel A, Sacca B, Kaschani F, Kaiser M, Gatsogiannis C, Raunser S, Clausen T, Ehrmann M (2015) Determinants of amyloid fibril degradation by the PDZ protease HTRA1. Nat Chem Biol 11:862–869. doi: 10.1038/nchembio.1931

50. Rasmussen MK, Mestre H, Nedergaard M (2018) The glymphatic pathway in neurological disorders. Lancet Neurol 17:1016–1024. doi: 10.1016/S1474-4422(18)30318-1

51. Reimand J, Groot C, Teunissen CE, Windhorst AD, Boellaard R, Barkhof F, Nazarenko S, Van Der Flier WM, Van Berckel BNM, Scheltens P, Ossenkoppele R, Bouwman F Why Is Amyloid-β PET Requested After Performing Cerebrospinal Fluid Biomarkers? doi: 10.3233/JAD-190836

52. Resende R, Ferreiro E, Pereira C, Resende de Oliveira C (2008) Neurotoxic effect of oligomeric and fibrillar species of amyloid-beta peptide 1-42: Involvement of endoplasmic reticulum calcium release in oligomer-induced cell death. Neuroscience 155:725–737. doi: 10.1016/j.neuroscience.2008.06.036

53. Richard E, Carrano A, Hoozemans JJ, Van Horssen J, Van Haastert ES, Eurelings LS, De Vries HE, Thal DR, Eikelenboom P, Van Gool WA, Rozemuller AJM (2010) Characteristics of dyshoric capillary cerebral amyloid angiopathy. J Neuropathol Exp Neurol 69:1158–1167. doi: 10.1097/NEN.0b013e3181fab558

54. Richard E, Carrano A, Hoozemans JJ, Van Horssen J, Van Haastert ES, Eurelings LS, De Vries HE, Thal DR, Eikelenboom P, Van Gool WA, Rozemuller AJM (2010) Characteristics of dyshoric capillary cerebral amyloid angiopathy. J Neuropathol Exp Neurol 69:1158–1167. doi: 10.1097/NEN.0b013e3181fab558

55. Rostagno A, Tomidokoro Y, Lashley T, Ng D, Plant G, Holton J, Frangione B, Revesz T, Ghiso J (2005) Chromosome 13 dementias. Cell Mol Life Sci 62:1814–1825. doi: 10.1007/s00018-005-5092-5

56. Schilling S, Rahfeld JU, Lues I, Lemere CA (2018) Passive Aβ immunotherapy: Current achievements and future perspectives. Molecules. doi: 10.3390/molecules23051068

57. Selkoe DJ, Hardy J (2016) The amyloid hypothesis of Alzheimer's disease at 25 years. EMBO Mol Med 8:595–608. doi: 10.15252/emmm.201606210

58. Shepherd C, McCann H, Halliday GM (2009) Variations in the neuropathology of familial Alzheimer's disease. Acta Neuropathol 118:37–52. doi: 10.1007/s00401-009-0521-4

59. Simchowicz T (1911) Histologische Studien über die senile Demenz. Nissl F, Alzheimer A (eds) Histol und Histopathol Arb über die Grosshirnrinde mit Bes Berücksichtigung der Pathol Anat der Geistekrankheiten 267-444.

60. Singh TJ, Grundke-Iqbal I, Iqbal K (1995) Phosphorylation of τ Protein by Casein Kinase-1 Converts It to an Abnormal Alzheimer-Like State. J Neurochem 64:1420–1423. doi: 10.1046/j.1471-4159.1995.64031420.x

61. Stelzmann RA, Norman Schnitzlein H, Reed Murtagh F (1995) An english translation of alzheimer's 1907 paper, "Über eine eigenartige erkankung der hirnrinde." Clin Anat 8:429–431. doi: 10.1002/ca.980080612

62. De Strooper B (2003) Aph-1, Pen-2, and Nicastrin with Presenilin generate an active γ-Secretase complex. Neuron 38:9–12. doi: 10.1016/S0896-6273(03)00205-8

63. Tarasoff-Conway JM, Carare RO, Osorio RS, Glodzik L, Butler T, Fieremans E, Axel L, Rusinek H, Nicholson C, Zlokovic B V., Frangione B, Blennow K, Ménard J, Zetterberg H, Wisniewski T, De Leon MJ (2015) Clearance systems in the brain - Implications for Alzheimer disease. Nat Rev Neurol 11:457–470. doi: 10.1038/nrneurol.2015.119

64. Thal DR, Ghebremedhin E, Rüb U, Yamaguchi H, Del Tredici K, Braak H (2002) Two types of sporadic cerebral amyloid angiopathy. J Neuropathol Exp Neurol 61:282-293. doi: 10.1093/jnen/61.3.282

65. Thal DR, Griffin WST, de Vos RAI, Ghebremedhin E (2008) Cerebral amyloid angiopathy and its relationship to Alzheimer's disease. Acta Neuropathol 115:599–609. doi: 10.1007/s00401-008-0366-2

66. Thal DR, Del Tredici K, Ludolph AC, Hoozemans JJM, Rozemuller AJ, Braak H, Knippschild U (2011) Stages of granulovacuolar degeneration: Their relation to Alzheimer's disease and chronic stress response. Acta Neuropathol 122:577–589. doi: 10.1007/s00401-011-0871-6

67. Veerhuis R (2011) Histological and direct evidence for the role of complement in the neuroinflammation of AD. Curr Alzheimer Res 8:34–58. doi: 10.2174/156720511794604589

68. Veerhuis R, Nielsen HM, Tenner AJ (2011) Complement in the brain. Mol Immunol 48:1592–1603. doi: 10.1016/j.molimm.2011.04.003

69. van Veluw SJ, Kuijf HJ, Charidimou A, Viswanathan A, Biessels GJ, Rozemuller AJM, Frosch MP, Greenberg SM (2016) Reduced vascular amyloid burden at microhemorrhage sites in cerebral amyloid angiopathy. Acta Neuropathol 1–7. doi: 10.1007/s00401-016-1635-0

70. Vermunt L, Sikkes SAM, van den Hout A, Handels R, Bos I, van der Flier WM, Kern S, Ousset PJ, Maruff P, Skoog I, Verhey FRJ, Freund-Levi Y, Tsolaki M, Wallin ÅK, Olde Rikkert M, Soininen H, Spiru L, Zetterberg H, Blennow K, Scheltens P, Muniz-Terrera G, Visser PJ, Vellas B, Reynish E, Ousset PJ, Andrieu S, Burns A, Pasquier F, Frisoni G, Salmon E, Michel JP, Zekry DS, Boada M, Dartigues JF, Olde-Rikkert MGM, Rigaud AS, Winblad B, Malick A, Sinclair A, Frölich L, Scheltens P, Ribera C, Touchon J, Robert P, Salva A, Waldemar G, Bullock R, Tsolaki M, Rodriguez G, Spiru L, Jones RW, Stiens G, Stoppe G, Eriksdotter Jönhagen M, Cherubini A, Lage PM, Gomez-Isla T, Camus V, Agüera-Morales E, Lopez F, Savy S, Cantet C, Coley N (2019) Duration of preclinical, prodromal, and dementia stages of Alzheimer's disease in relation to age, sex, and APOE genotype. Alzheimer's Dement 15:888-898. doi: 10.1016/j.jalz.2019.04.001

71. Viola KL, Klein WL (2015) Amyloid β oligomers in Alzheimer's disease pathogenesis, treatment, and diagnosis. Acta Neuropathol 129:183–206. doi: 10.1007/s00401-015-1386-3

72. Vogels T, Leuzy A, Cicognola C, Ashton NJ, Smolek T, Novak M, Blennow K, Zetterberg H, Hromadka T, Zilka N, Schöll M (2019) Review Propagation of Tau Pathology: Integrating Insights From Postmortem and In Vivo Studies. doi: 10.1016/j.biopsych.2019.09.019

73. Weller RO, Nicoll J a R (2003) Cerebral amyloid angiopathy: pathogenesis and effects on the ageing and Alzheimer brain. Neurol Res 25:611–616. doi: 10.1179/016164103101202057

74. Weller RO, Subash M, Preston SD, Mazanti I, Carare RO (2008) Perivascular drainage of amyloid-β peptides from the brain and its failure in cerebral amyloid angiopathy and Alzheimer's disease. In: Brain Pathol. pp 253–266

75. Yamazaki Y, Takahashi T, Hiji M, Kurashige T, Izumi Y, Yamawaki T, Matsumoto M (2010) Immunopositivity for ESCRT-III subunit CHMP2B in granulovacuolar degeneration of neurons in the Alzheimer's disease hippocampus. Neurosci Lett 477:86–90. doi: 10.1016/j.neulet.2010.04.038

76. Yankner BA, Duffy LK, Kirschner DA (1990) Neurotrophic and neurotoxic effects of amyloid β protein: Reversal by tachykinin neuropeptides. Science (80-) 250:279–282. doi: 10.1126/science.2218531

77. Zhan SS, Veerhuis R, Kamphorst W, Eikelenboom P (1995) Distribution of beta amyloid associated proteins in plaques in Alzheimer's disease and in the non-demented elderly. Neurodegeneration 4:291–297. doi: 10.1016/1055-8330(95)90018-7

CHAPTER 2

Profiling the human hippocampal proteome at all pathological stages of Alzheimer's disease

David C. Hondius[1,2], Pim van Nierop[2], Ka Wan Li[2], Jeroen J.M. Hoozemans[1], Roel C. van der Schors[2], Elise S. van Haastert[1], Saskia M. van der Vies[1], Annemieke J.M. Rozemuller[1] and August B. Smit[2]

[1]Department of Pathology, VU University Medical Center, Neuroscience Campus Amsterdam, The Netherlands

[2]Department of Molecular and Cellular Neurobiology, Center for Neurogenomics and Cognitive Research, VU University Amsterdam, Neuroscience Campus Amsterdam, The Netherlands

Alzheimer's & Dementia 2016 Jun;12(6):654-68

ABSTRACT

Introduction: We performed a comprehensive quantitative proteomics study on human hippocampus tissue involving all Braak stages to assess changes in protein abundance over the various stages of Alzheimer's disease (AD).

Methods: Hippocampal subareas CA1 and subiculum of 40 cases were isolated using laser capture microdissection and analyzed using mass spectrometry. Immunoblotting and immunohistochemistry were used for validation.

Results: Over the Braak stages an altered expression was found for 372 proteins including changes in levels of extra cellular matrix components, and in calcium-dependent signaling proteins. Early changes were observed in levels of proteins related to cytoskeletal dynamics and in synaptic components including an increase in RIMS1 and GRIK4. Several synaptic proteins, such as BSN, LIN7A, DLG2,-3 and -4 exhibit an early-up, late-down expression pattern.

Discussion: This study provides new insight into AD dependent changes in protein levels in the hippocampus during AD pathology, identifying potential novel therapeutic targets and biomarkers.

INTRODUCTION

Alzheimer's disease (AD) is the most common cause of dementia in the elderly and is becoming more prevalent due to the ageing population. Substantial progress has been made in identifying disease-related molecular and cellular processes. Early disease-related processes, however, are not well understood despite their importance for targeting AD at an early stage. Also, there is a clinical need to identify novel biomarkers for early, pre-symptomatic diagnosis, or assessing therapeutics responsiveness [48]. A potentially important approach to identifying mechanisms underlying AD is to profile changes in protein expression during its development, in well-defined subsequent stages and using brain areas that belong to the early affected. One of the most vulnerable and early affected regions in AD is the hippocampus CA1 region and subiculum [34].

The main pathological hallmarks of AD are the extracellular deposition of β-amyloid (Aβ) peptides in plaques and the intracellular aggregation of hyperphosphorylated tau in neurofibrillary tangles (NFTs) [20, 22]. Clinico-pathological studies show a strong correlation between cognitive decline and the levels of tau pathology in AD [4, 42]. These pathological changes, and alterations in associated biomarkers, can be observed many years before any clinical symptoms are noticed [5, 29]. In the most common senile form of AD both neurofibrillary tangles and Aβ plaques spread during disease progression throughout the brain in a predictable manner, enabling an objective neuropathological diagnose and the classification into the different Braak stages [9, 10]. Here we grouped 40 cases according the Braak stages for tau pathology.

To gain insight in the molecular pathological mechanisms involved in AD, we used a liquid chromatography-tandem mass spectrometry (LC-MS/MS)-based proteomics approach, dedicated to reveal changes in protein expression during AD pathogenesis. Because of the defined anatomy of the hippocampus and its selective early affected CA1 and subiculum region, we excised these sub-regions with great precision using laser capture microdissection (LCM).

Several studies have applied mass spectrometry to search for changes in the proteome of the human hippocampus when comparing control with AD cases [2, 24, 33, 38, 41]. However, there are no studies that have examined the profile of hippocampal protein levels in progressive stages of AD. Our study is distinguished by (1) the high number of cases used (a total of 40), (2) the inclusion of all disease stages, and (3) the focus on specific, highly relevant, hippocampal sub-regions. By doing so, we gained insight into the magnitude and chronology of the changes in the proteome of the hippocampal regions CA1 and subiculum during AD progression, and revealed novel proteins and pathways, which might have great value as therapeutic target and/or biomarker.

MATERIAL AND METHODS

Case selection

Postmortem brain tissue was obtained from the Netherlands Brain Bank, Netherlands Institute for Neuroscience, Amsterdam. All material has been collected from donors whom written informed consent for brain autopsy and the use of the material and clinical information for research purposes has been obtained by the Netherlands Brain Bank. A total of 40 cases were selected based on clinical and neuropathological reports with 5 to 7 cases per Braak stage. All cases are listed in table S1 with in addition to the Braak stage the Thal phase for Aβ deposits [51]. An overview of the experimental workflow is shown in Fig. 1.

Brain tissue preparation and laser capture microdissection (LCM)

Sections (10 µm) of fresh frozen tissue were mounted on PEN-membrane slides (Leica, Herborn, DE), fixed in 100% ethanol for 1 min and stained using 1% (w/v) toluidine blue in H2O (Fluka analytical, Buchs, Switzerland) for 1 min. LCM was performed using a Leica AS LMD system (Leica, Herborn, DE). An equal volume of 1.2 x 10^9 μm^3 from the CA1 and subiculum regions was collected in Eppendorf tubes containing 30µl M-PER lysis buffer (Thermo scientific, Rockford IL, USA) supplemented with reducing SDS sample buffer (Thermo Scientific, Rockford IL, USA). Microdissected tissue was stored at -80°C until further use.

Protein separation by electrophoresis and in-gel digestion

Microdissected tissue lysates were incubated at 95°C for 5 min, followed by incubation with 50 mM iodoactamide for 30 min at RT in the dark. Proteins were size separated on a NuPAGE® 4-12% Bis-Tris acrylamide gel (Invitrogen, Carlsbad, CA, USA) using MOPS SDS running buffer (Invitrogen, Carlsbad, CA, USA) according the manufacturers protocol. Gels were fixed and stained with colloidal Coomassie blue G-250 overnight while shaking. After destaining in ultrapure H_2O each gel lane was sliced into 12 equal sized parts and each part was cut into blocks of approximately 1 mm^3 and collected in an Eppendorf tube. Destaining, trypsin digestion and peptide extraction was done as described previously [13].

Mass spectrometry analysis

The peptides were dissolved in 15 µL of 0.1% (v/v) acetic acid of which 10 µL was loaded onto a nano-liquid chromatography (nano-LC) system (Eksigent). The peptides were separated using a capillary reversed phase C18 column that had been equilibrated with 0.1% (v/v) acetic acid at a flow rate of 400 nL/min. The peptides were eluted by increasing the acetonitrile concentration linearly from 5 to 40% in 80 min and to 90% in 10 min, using the same flow rate. Eluted peptides were transferred into the LTQ Orbitrap Discovery (Thermo Scientific) by Electro Spray Ionisation (ESI). The mass spectrometer was operated in the range of m/z 350-2000 at a full width at half maximum resolution of 30,000 after accumulation to 500,000 in the LTQ with one microscan. The five most abundant precursor ions were selected for fragmentation by collision-induced dissociation (CID) with an isolation width of 2 Da.

Protein inference and relative protein quantification

MaxQuant software (version 1.3.0.5) was used for spectrum annotation, protein inference, and precursor area-based relative protein quantification [16]. Spectra were annotated against the Uniprot human reference proteome database (Build June 2012). Enzyme specificity was set to Trypsin/P, allowing at most two missed cleavages. Carbamido-methylation of cysteine was set as a fixed modification, and N-acetylation and methionine oxidation were set as variable modifications. Mass deviation tolerance was set to 20 ppm for monoisotopic precursor ions and 0.5 Da for MS/MS peaks. False-discovery rate (FDR) cut-offs for peptide and protein identifications were set to 1% for both. The minimum peptide length was seven amino acids. Identified proteins that had the same set, or a subset of peptides compared to another protein, were merged into one protein group. Peptides that were shared between different proteins were assigned to the protein the with most peptide evidence (so called 'Razor' peptides). Only protein groups with at least a single unique and a single Razor peptide were included. For relative protein quantification normalized LFQ intensities were used (MaxLFQ normalization based on at least a single shared peptide ratio between samples) [15].

Statistical analysis of differential protein expression

Significance of differential protein levels was established from the p-value for the F-test on a linear regression model in which Braak stages were treated as continuous variables with equal numerical distances. P-values were corrected for multiple testing according to Benjamini & Hochberg [6]. Significance of differential protein levels was assessed while adhering to a 10% FDR cut-off.

Hierarchical clustering of Braak stages

For clustering of Braak stages, distances were calculated for proteins with significantly altered abundance, of which mean Braak stage expression levels were calculated and centered to the overall mean expression level. For clustering of protein expression profiles across Braak stages, proteins were selected with at least a single LFQ intensity value in each experimental group (1904 proteins), and average quantification values were calculated and centered. Hierarchical clustering was performed using Euclidean distance, and Wards method [53] and plotted using the gplots library for the R language. Clusters of proteins with appropriate similarity between the protein expression profiles were arbitrarily defined by evaluating the dendrogram at increasing distances from the root.

Overrepresentation analysis

Manually curated annotations of genes expressed exclusively in astrocytes, microglia, neurons, or oligodendrocytes were used for overrepresentation analysis [21]. Significance of cell type overrepresentation was established using a one-sided Fisher's exact test. Significance of overrepresentation was determined at an alpha-level of 0.05. Pathway analysis was performed using QIAGEN's Ingenuity® Pathway Analysis (IPA®, QIAGEN Redwood City, www.qiagen.com/ingenuity, database version October 2014).

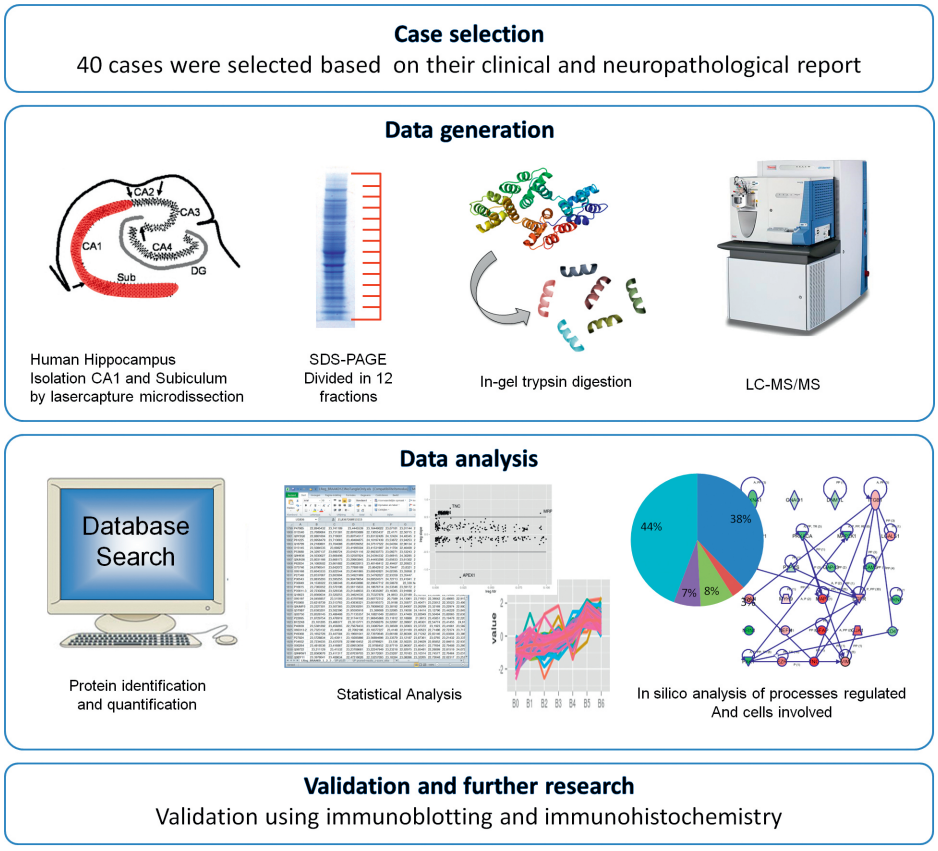

FIGURE 1 | Overview of experimental procedures performed in this study. 40 cases were selected for the analysis based on their clinical and neuropathological report. From these the CA1 and subiculum region, the area marked red in the displayed hippocampus, was isolated using laser micro-dissection. Proteins were separated using SDS-PAGE and subjected to in-gel trypsin digestion. Peptides were measured using LC-MS/MS. A database search for protein identification and protein quantification was performed using MaxQuant software. Linear regression and cluster analysis were used to identify significantly regulated proteins and proteins that show concomitant changes in their abundance. Pathway analysis was performed using Ingenuity to identify AD-enriched pathways. Abbreviations: LC-MS/MS, liquid chromatography-tandem mass spectrometry; AD, Alzheimer's disease.

Immunoblotting

Proteins were denatured at 95 °C for 5 min separated by SDS-PAGE using Criterion™ TGX stain-free™ precast gels (Bio-Rad, Hercules, CA, USA) and transferred (40 V overnight at 4°C) onto a 0.45 µm PVDF membrane. Blocking of the membrane was done using Odyssey blocking buffer (LI-COR). Primary antibodies and dilutions are shown in table S2. Secondary antibodies used were IRDye 800 CW Goat anti-Rabbit (LI-COR Biosciences, Lincoln, NE, USA) and IRDye 680

Goat anti-Mouse (LI-COR Biosciences, Lincoln, NE) both at a 1:15000 dilution. Quantification was performed using image-J software.

Immunohistochemical analysis

Fresh frozen human postmortem hippocampal tissue was cut (5µm sections), placed on a StarFrost Microscope Slide (Knittel glass) and air-dried overnight at room temperature (RT). Prior to staining procedure sections were fixed in 100% acetone for 10 min. Formalin fixed (4% for 24h) paraffin embedded tissue was cut (5µm sections), and placed on StarFrost Microscope Slides. After deparaffinising endogenous peroxidase activity was quenched by incubation with 0.3% (v/v) H_2O_2 in methanol for 30 min at RT. Antigen retrieval was performed by soaking the sections in 10 mM citrate buffer pH 6.0, heated and boiled for 10 min in a microwave oven.

The staining procedure was identical for both cryosections and paraffin sections and was performed as previously described [43]. All primary antibodies used are listed in table S2. Specificity of all antibodies used for immunohistochemistry (IHC) was confirmed by immunoblot analysis. Omission of the primary antibody was used as a negative control for all stainings. All samples were stained as part of the same batch. Quantification of the stainings, by determining the percentage of the surface that is stained, was performed with Image-J using the threshold colour plugin.

RESULTS

Identification of differentially expressed proteins

LC-MS/MS was performed on 40 laser-dissected tissue samples representing all Braak stages quantifying 3216 proteins in total and over 1500 per case (Fig. S1). The median coefficient of variation (CV) was determined for one case that was analyzed in triplicate and for each Braak stage as a group. The CV of measured protein abundance is constant across Braak stages at approximately 30% from which technical variation accounts for approximately 15% (Fig. S2). Changes in protein abundance were identified using a linear regression analysis at a significance cut off level of 10% FDR. This yielded a total of 372 proteins with significantly changed levels, comprising 166 proteins with increased levels and 206 proteins with decreased levels.

To identify early affected proteins, linear regression analysis was applied on the set of 372 changed proteins involving Braak stages 0-III. Proteins with a slope significantly deviating from zero ($p<0.05$) were regarded as early changed (Fig. S3). A total of 89 proteins met this criterion. The top 50 changed proteins including the significant p-values for early changed proteins are listed for proteins with increased levels (Table 1) and decreased levels (Table 2). The complete list of changed proteins is given in the supplemental data (Table S3). Peptide-level quantitative information is provided as supplemental data (Table S4).

TABLE 1 | Proteins with increased levels.

Name	Gene	FDR Braak 0-VI	P-val Braak 0-III	FC
Prolow-density lipoprotein receptor-related protein 1	LRP1	0.040	0.001	2.50
Plectin	PLEC	0.000	0.001	3.99
Microtubule-associated protein tau	MAPT	0.000	0.001	10.30
Regulating synaptic membrane exocytosis protein 1	RIMS1	0.049	0.002	6.88
Cathepsin D;Cathepsin D light chain;Cathepsin D heavy chain	CTSD	0.012	0.003	1.83
Proteasome inhibitor PI31 subunit	PSMF1	0.048	0.003	Inf
Glial fibrillary acidic protein	GFAP	0.000	0.004	12.09
Glutamate dehydrogenase 1, mitochondrial	GLUD1	0.000	0.006	2.62
Alpha-adducin	ADD1	0.011	0.008	1.68
Platelet-activating factor acetylhydrolase IB subunit gamma	PAFAH1B3	0.000	0.009	3.83
Four and a half LIM domains protein 1	FHL1	0.015	0.014	3.81
Glutathione S-transferase Mu 3	GSTM3	0.001	0.017	2.33
Pre-B-cell leukemia transcription factor-interacting protein 1	PBXIP1	0.038	0.017	9.06
Dystrobrevin alpha;Dystrobrevin beta	DTNA	0.022	0.020	5.53
Heat shock protein 105 kDa	HSPH1	0.069	0.021	1.30
Integrin alpha-V;Integrin alpha-V heavy chain;Integrin alpha-V light chain	ITGAV	0.050	0.021	1.69
LanC-like protein 1	LANCL1	0.004	0.023	2.07
Filamin-A	FLNA	0.000	0.023	13.64
Neuroblast differentiation-associated protein AHNAK	AHNAK	0.003	0.026	9.07
Cytosolic non-specific dipeptidase	CNDP2	0.003	0.028	5.64
Peptidyl-prolyl cis-trans isomerase A;Peptidyl-prolyl cis-trans isomerase	PPIA	0.058	0.029	4.03
Carbonyl reductase [NADPH] 1	CBR1	0.000	0.032	3.82
Protein-arginine deiminase type-2	PADI2	0.000	0.036	12.41
Phosphoserine aminotransferase	PSAT1	0.000	0.039	3.35
Secretogranin-2;Secretoneurin	SCG2	0.091	0.040	4.57
Alpha-aminoadipic semialdehyde dehydrogenase	ALDH7A1	0.048	0.040	4.43
Amine oxidase [flavin-containing] B	MAOB	0.001	0.042	2.27
Heat shock protein beta-1	HSPB1	0.000	0.044	4.87
Glutamate receptor, ionotropic kainate 4	GRIK4	0.001	0.046	9.23
ES1 protein homolog, mitochondrial	C21orf33	0.007	0.049	4.03
Brefeldin A-inhibited guanine nucleotide-exchange protein 3	KIAA1244	0.047	0.053	4.77
Ezrin	EZR	0.000		4.44
Gamma-adducin	ADD3	0.000		4.16
Annexin A5;Annexin	ANXA5	0.000		3.63

TABLE 1 | Continued

Name	Gene	FDR Braak 0-VI	P-val Braak 0-III	FC
Versican core protein	VCAN	0.000		3.42
Peroxiredoxin-1	PRDX1	0.000		2.35
Ferritin light chain;Ferritin	FTL	0.000		4.13
D-3-phosphoglycerate dehydrogenase	PHGDH	0.000		3.18
Glycogen phosphorylase, muscle form;Phosphorylase	PYGM	0.000		3.11
Septin-2	SEPT2	0.000		2.50
Heat shock 70 kDa protein 1A/1B	HSPA1B	0.000		1.82
1-phosphatidylinositol 4,5-bisphosphate phosphodiesterase delta-1	PLCD1	0.000		15.00
Hepatocyte cell adhesion molecule	HEPACAM	0.000		4.82
Band 4.1-like protein 2	EPB41L2	0.000		3.50
Vimentin	VIM	0.000		3.41
Guanine nucleotide-binding protein subunit alpha-13	GNA13	0.000		2.81
Aquaporin-4	AQP4	0.001		8.06
Delta-1-pyrroline-5-carboxylate dehydrogenase, mitochondrial	ALDH4A1	0.001		7.65
Transketolase	TKT	0.001		3.55
Excitatory amino acid transporter 1	SLC1A3	0.001		1.84

Abbreviations: FDR, false discovery rate; FC, fold change.
NOTE. Listed are the top 50 proteins with increased levels over the Braak stages as determined using a linear regression analysis with a false discovery cutoff of 10%. Proteins are ordered first on the P value for Braak 0–III (early regulated) from low to higher values. Next, they were ordered based on FDR for Braak 0–VI from low to high. The fold change represents the highest difference in protein abundance between any two Braak stages.

TABLE 2 | Proteins with decreased levels

Name	Gene	FDR Braak 0-VI	P-val Braak 0-III	FC
Amphiphysin	AMPH	0.035	0.000	1.65
Guanine nucleotide-binding protein G(z) subunit alpha	GNAZ	0.004	0.001	1.55
Protein LYRIC	MTDH	0.078	0.001	2.45
AP-2 complex subunit beta	AP2B1	0.006	0.001	1.51
Dual specificity mitogen-activated protein kinase kinase 4	MAP2K4	0.006	0.001	2.15
Cytohesin-3;Cytohesin-2;Cytohesin-1	CYTH2	0.013	0.002	2.57
V-type proton ATPase subunit C 1	ATP6V1C1	0.081	0.003	1.54

TABLE 2 | Continued

Name	Gene	FDR Braak 0-VI	P-val Braak 0-III	FC
Nck-associated protein 1	NCKAP1	0.001	0.003	1.81
Mitochondrial carrier homolog 1	MTCH1	0.085	0.004	1.95
Voltage-dependent calcium channel subunit alpha-2/delta-1	CACNA2D1	0.000	0.005	2.72
NADH dehydrogenase [ubiquinone] 1 beta subcomplex subunit 9	NDUFB9	0.013	0.007	1.69
AP-3 complex subunit delta-1	AP3D1	0.070	0.007	4.36
Cell adhesion molecule 1	CADM1	0.037	0.007	2.16
Dipeptidyl aminopeptidase-like protein 6	DPP6	0.000	0.009	2.04
Twinfilin-2	TWF2	0.015	0.009	3.03
AP-2 complex subunit alpha-1	AP2A1	0.005	0.009	1.43
Mitochondrial import inner membrane translocase subunit TIM44	TIMM44	0.058	0.009	1.70
Glycine--tRNA ligase	GARS	0.048	0.009	1.46
Serine/threonine-protein phosphatase 2A 65 kDa regulatory subunit A alpha isoform	PPP2R1A	0.005	0.010	1.77
Vacuolar protein sorting-associated protein 35	VPS35	0.062	0.010	1.33
cAMP-dependent protein kinase type II-beta regulatory subunit	PRKAR2B	0.000	0.010	3.06
Thy-1 membrane glycoprotein	THY1	0.018	0.011	2.18
SCY1-like protein 2	SCYL2	0.085	0.012	2.48
Cadherin-13	CDH13	0.003	0.013	2.08
Calcium/calmodulin-dependent protein kinase type II subunit alpha	CAMK2A	0.000	0.016	2.34
Voltage-gated potassium channel subunit beta-2	KCNAB2	0.070	0.016	inf
Exocyst complex component 3	EXOC3	0.053	0.018	2.80
Actin-related protein 2/3 complex subunit 3	ARPC3	0.001	0.019	2.07
Abl interactor 2	ABI2	0.048	0.021	3.53
Tubulin beta-3 chain	TUBB3	0.001	0.021	1.99
Endophilin-A1	SH3GL2	0.085	0.022	1.62
Glucose 1,6-bisphosphate synthase	PGM2L1	0.000	0.024	2.51
LETM1 and EF-hand domain-containing protein 1, mitochondrial	LETM1	0.006	0.024	1.66
Tubulin beta-4B chain	TUBB4B	0.000	0.024	1.60
Tubulin beta chain	TUBB	0.005	0.025	2.30
Ras GTPase-activating protein-binding protein 2	G3BP2	0.009	0.025	7.95
Protein NDRG4	NDRG4	0.010	0.026	2.12
Guanine nucleotide-binding protein G(o) subunit alpha	GNAO1	0.048	0.026	1.44
Protein kinase C and casein kinase substrate in neurons protein 1	PACSIN1	0.010	0.027	1.99

TABLE 2 | Continued

Name	Gene	FDR Braak 0-VI	P-val Braak 0-III	FC
Actin-related protein 3B	ACTR3B	0.042	0.028	3.14
Clathrin coat assembly protein AP180	SNAP91	0.009	0.030	1.78
Threonine--tRNA ligase, cytoplasmic	TARS	0.049	0.032	1.64
Alpha-actinin-1	ACTN1	0.000	0.032	1.82
26S proteasome non-ATPase regulatory subunit 12	PSMD12	0.007	0.033	2.52
Reticulon-1	RTN1	0.048	0.035	2.07
Glutamate receptor 2	GRIA2	0.001	0.038	2.99
Syntaxin-1B	STX1B	0.006	0.038	1.48
Tubulin alpha chain-like 3	TUBAL3	0.054	0.039	2.69
Ras-related protein Rab-1B;Putative Ras-related protein Rab-1C	RAB1B	0.079	0.039	1.30
Guanine nucleotide-binding protein G(i) subunit alpha-1	GNAI1	0.019	0.040	1.58

Abbreviations: FDR, false discovery rate; FC, fold change.
NOTE. Listed are the top 50 proteins with decreased levels over the Braak stages as determined using a linear regression analysis with a false discovery cutoff of 10%. Proteins were ordered first on the P value for Braak 0–III (early regulated) from low to higher values. Next, they were ordered based on the false discovery rate for Braak 0–VI from low to high. The fold change represents the highest difference in protein abundance between any two Braak stages.

Validity of the study

To assess the validity of our study we used several approaches. First, for proteins of which the expression is known to be highly elevated in AD, e.g. MAPT (tau), GFAP and CD44 we detected a large increase in expression level compared to Braak 0. With observed protein level increases of 10.3-fold for tau, 12.1-fold for GFAP, and 7.8-fold for CD44 (Fig. 2A) we confirm previous studies [1, 18, 32].

Second, to establish the relatedness of the Braak stages as determined by changes in protein abundance, we performed hierarchical clustering of experimental groups using quantitative protein expression data of the 372 proteins that were significantly changed. Protein expression patterns distinguish early Braak stages 0 to III and the late Braak stages IV to VI (Fig. 2B).

Third, we used immunohistochemistry (IHC) and immunoblotting to confirm protein expression data obtained by mass spectrometry. We selected GFAP, actin binding proteins FLNA, TLN, and VCL, the extracellular matrix (ECM) protein TNC, the adhesion molecule CD44, and calcium binding proteins ANXA2 and ANXA5). The selection of assessing these proteins for validation was based primarily on a large increase, as markers showing increased expression are the most promising to study as biomarker for a disease. In addition, these targets were selected on

either their established role in AD, novelty in AD pathology (e.g TLN and VCL), or their assumed extracellular localization (e.g. TNC, ANXA2 and ANXA5).

The immunoblots confirmed the increased levels of CD44, ANXA2 and -5, FLNA, VCL, TLN in tissue homogenates (Fig. 2C). In addition, using IHC we quantified immunoreactivity specifically in CA1 and subiculum. Hippocampal tissue of twenty-eight cases covering all Braak stages were stained for TNC, GFAP, CD44, FLNA, VCL, ANXA2 and -5 (Fig. S4) and four images were taken of the CA1 and subiculum regions from each case at 50x magnification. The immunoreactivity of these markers was quantified and confirmed increased levels of GFAP, TNC, CD44, ANXA2 and -5 (Fig. 2C). Taken together, this data validates of our mass spectrometry results using independent methods.

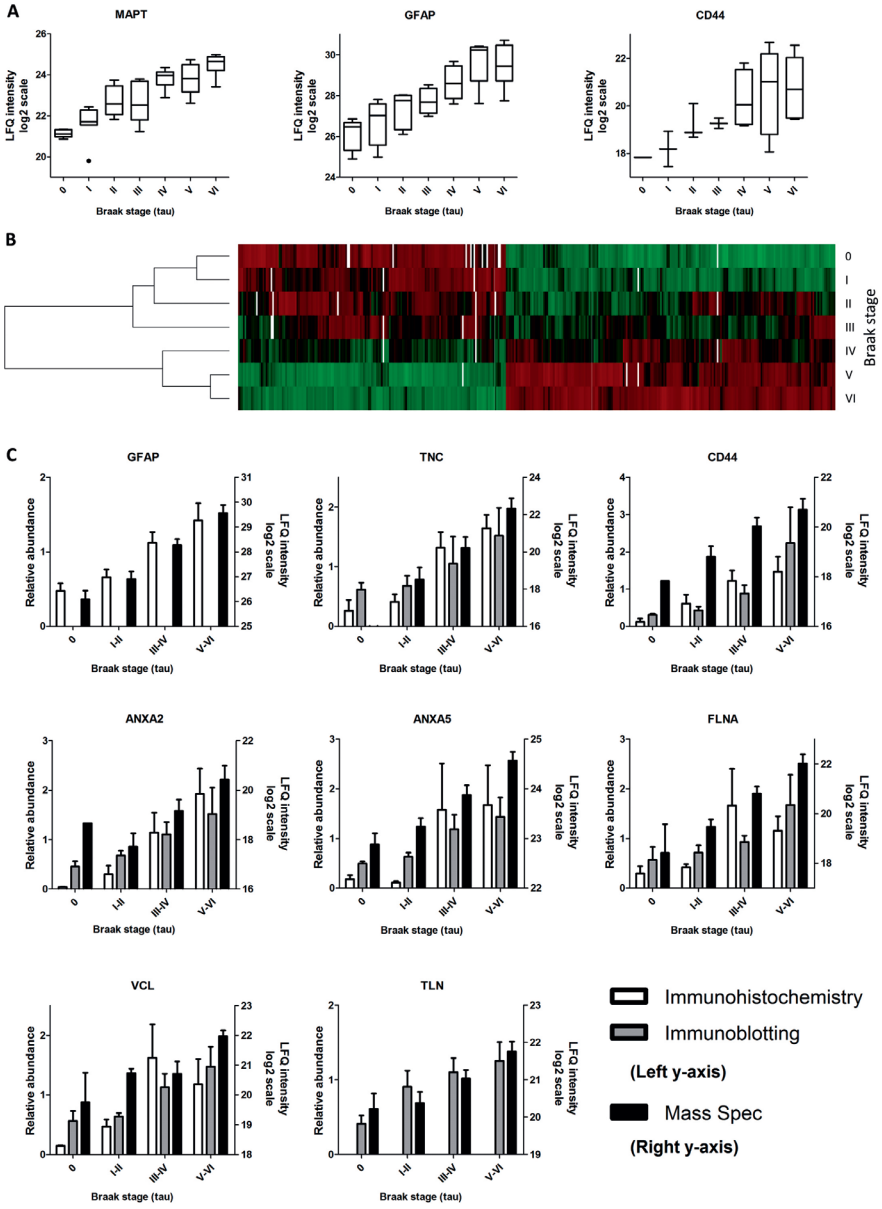

FIGURE 2 | Validation of mass spec data by different independent approaches. Label free quantification (LFQ) values in on a log2-scale of the proteins MAPT, GFAP and CD44, representing tangle pathology and glial activation and well-known to be increased in AD (A). Clustering analysis based on Euclidian distance to assess the relatedness of the different Braak stages to each other based on the protein expression profile of the proteins with significant changed levels. The mean LFQ intensity value of each protein per Braak stage was used and all values were centered around the mean for each protein. Values below the mean (red); above the mean (green); white indicates that a protein was not detected in that group. Based on the protein

profiles, the lower Braak stages (0-III) can be separated clearly from the higher Braak stages (IV-VI) (B). A selection of the proteins, as indicated above each graph, found regulated by mass spectrometry analysis, was quantified by immunohistochemistry (white bars) and immunoblotting (grey bars); values are associated with the left y-axis. As a reference the mass spectrometry quantitative values (LFQ intensity) are shown; values represented on the right y-axis. Significant ($p<0.05$) regulation was confirmed using immunohistochemistry for GFAP, TNC, CD44, ANXA2 and ANXA5. Significant ($p<0.05$) regulation was confirmed using immunoblotting for CD44, ANXA2, ANXA5, FLNA, VCL and TLN (C). Abbreviations: MAPT, microtubule-associated protein tau; GFAP, glial fibrillary acidic protein; AD, Alzheimer's disease; FLNA, filamin-A.

Identification of concomitant changes in protein levels and related pathways

We first used a discovery-driven approach to identify groups of proteins that display a similar expression profile and are potentially functionally related. Protein expression profiles that represent the abundance of individual proteins during the course of the disease were obtained using the mean expression values per Braak stage. Profiles were centered and clustered based on Euclidian distance resulting in twenty-one unsupervised defined clusters (Fig. S5). Four characteristic clusters (cluster M, S, Q and L) in which a distinction could be made into progressively decreased, an early-up, late-down profile and progressively increased, are depicted in Fig. 3A, -B, -C and -D, respectively.

The cellular composition of the CA1 and subiculum is diverse and includes neurons, astrocytes, microglia and oligodendrocytes. These cell types might be affected differentially and respond differently throughout the disease course. We hypothesized that some of the expression clusters represent responses of the various cell types. Hence, an overrepresentation analysis was performed using gene annotations from Goudriaan et al. [21] that defines genes with astrocyte-, oligodendrocyte-, neuron- or microglia-specific expression. By doing so we were able to assign protein clusters to specific cell types (Fig. 3). A progressive decreased pattern and an early up late-down pattern were associated to neurons. A progressive increased pattern was attributed predominantly to an astrocytic response.

To objectively explore the biological meaning of the expression changes, we performed an overrepresentation analysis with ingenuity pathway analysis (IPA) on the different expression clusters. The ten most significant overrepresented pathways of each cluster are displayed in Fig. 3. A complete overview of the overrepresentation analysis is available in the supplementary data (Table S5).

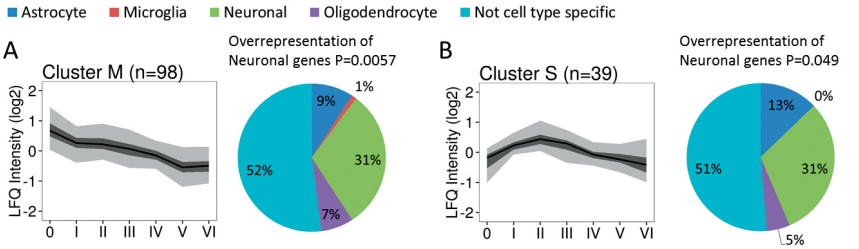

Cluster M
Synaptic Long Term Potentiation
CREB Signaling in Neurons
Calcium Signaling
Neuropathic Pain Signaling In Dorsal Horn Neurons
Role of NFAT in Cardiac Hypertrophy
GNRH Signaling
cAMP-mediated signaling
Melatonin Signaling
G-Protein Coupled Receptor Signaling
GM-CSF Signaling

Cluster S
Axonal Guidance Signaling
Oxidative Phosphorylation
Mitochondrial Dysfunction
Integrin Signaling
HIPPO signaling
PAK Signaling
Actin Cytoskeleton Signaling
Huntington's Disease Signaling
Pyrimidine Ribonucleotides Interconversion
Pyrimidine Ribonucleotides De Novo Biosynthesis

Cluster Q
NRF2-mediated Oxidative Stress Response
Glycolysis I
Serine Biosynthesis
Actin Cytoskeleton Signaling
Superpathway of Serine and Glycine Biosynthesis I
14-3-3-mediated Signaling
Regulation of Cellular Mechanics by Calpain Protease
Signaling by Rho Family GTPases
Aryl Hydrocarbon Receptor Signaling
Glutathione Redox Reactions I

Cluster L
LPS/IL-1 Mediated Inhibition of RXR Function
FAK Signaling
RhoGDI Signaling
Xenobiotic Metabolism Signaling
Regulation of Cellular Mechanics by Calpain Protease
Putrescine Degradation III
Aryl Hydrocarbon Receptor Signaling
Tryptophan Degradation X (Mammalian, via Tryptamine)
Caveolar-mediated Endocytosis Signaling
Molecular Mechanisms of Cancer

FIGURE 3 | Cluster analysis identifies concomitant changes in protein levels, related pathways and cell types. Cluster analysis of the different protein expression profiles based on Euclidian distance using the mean expression values centered to zero. Four typical clusters (clusters M, S, Q and L figure 3A, B, C, and D respectively) were selected based on the magnitude of expression changes and their pattern of expression (A, progressive decrease; B, early up, late down; C and D, progressive increase). Overrepresentation analysis of cell type specific gene expression using gene expression data for astrocytes, microglia, neurons and oligodendrocytes was performed and indicates the relative involvement of the different cell types in the different expression patterns observed. The proportions of different cell type specific genes on the basis of all 3216 quantified proteins are: astrocytes 13.1%, microglia 1.5%, neurons 16.5%, oligodendrocytes 9.8% and not cell type specific 59.0%. The ten most significant overrepresented pathways as determined using ingenuity pathway analysis (IPA) are displayed for each cluster. Abbreviations: IL, interleukin; cAMP, cyclic adenosine monophosphate; CREB, cAMP response element-binding protein; NFAT, nuclear factor of activated T-cells; GNRH, gonadotropinreleasing hormone; GM-CSF, granulocyte-macrophage colony-stimulating factor; NRF2, nuclear factor erythroid 2 -related factor 2; LPS, lipopolysaccharide.

Consistent changes in protein abundance across functionally related groups

AD is a multifactorial disease in which several processes have been reported involved in the progression of the disease. From our quantitative proteomics analysis several different proteins with an altered expression level are also functionally related. These include synaptic proteins, extracellular matrix-associated proteins, proteins involved in cytoskeletal reorganization, cell adhesion, microtubule-associated proteins, calcium binding proteins and proteins involved in response to cellular stress (Fig. 4). As from our findings many proteins turn out relevant to processes of synaptic function. Hence, a schematic overview was created to visualize proteins that affect synaptic function and/or their microenvironment (Fig. 5). This overview includes a proportion of our data that is associated with the synapse highlighting multiple synapse(-associated) processes which are affected during the course of AD.

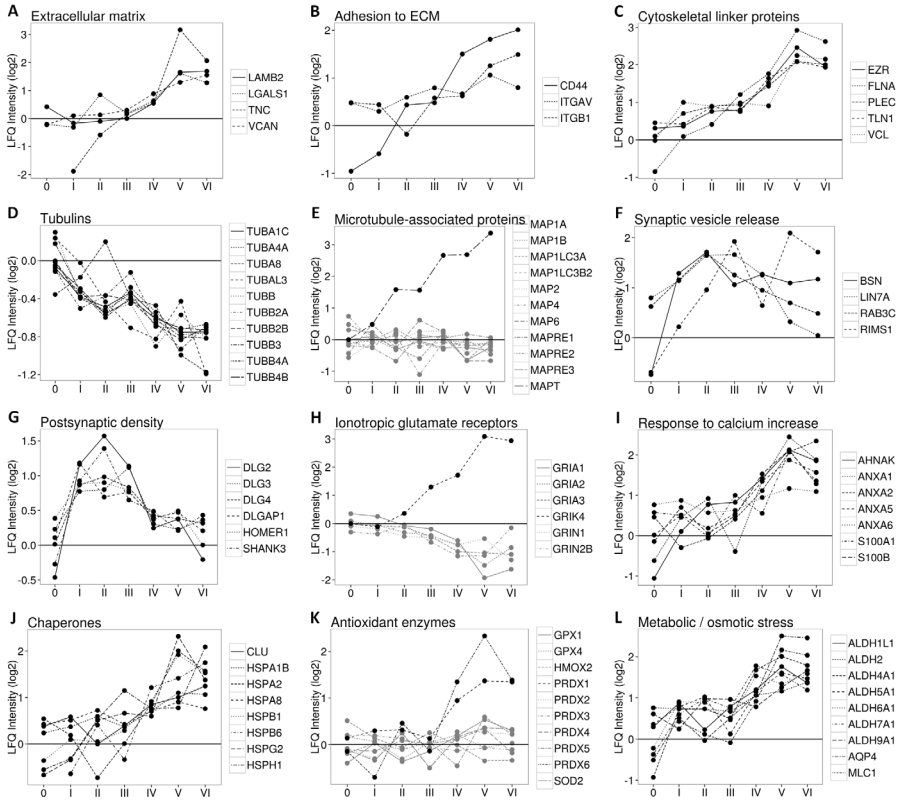

FIGURE 4 | Protein levels of selected proteins that belong to specific functional groups. Proteins of different functional groups are displayed in each panel. Over the Braak stages (0 to VI) we detected increased levels of extracellular matrix (ECM) proteins LAMB2, LGALS1, TNC and VCAN (A), increased levels of proteins that mediate the adhesion to the ECM (B), and higher abundance of cytoskeletal linker proteins (C). There is an overall decrease of tubulins (D), but no changes in the expression of microtubule-associated proteins except for large increase in MAPT and a slight reduction of MAPRE3 (E). There is an early-up, late-down expression pattern of proteins involved in synaptic vesicle release (F) and of the postsynaptic density (G). Ionotropic glutamate receptors are decreased over the Braak stages with the exception of GRIK4, which is highly increased (H). Proteins responding to increased intracellular calcium concentrations are increased (I). Several classes of stress-response proteins such as various chaperones are also increased (J). Only a few enzymes involved in anti-oxidant defense (PRDX1 and PRDX6) are increased, whereas others were not found changed (K). Levels of all detected members of the aldehyde dehydrogenase family, and AQP4 and MLC1, the latter of which are involved in counteracting metabolic and osmotic stress are found increased (L).

DISCUSSION

The CA1 and subiculum areas of the hippocampus represent a vulnerable and early affected region in AD pathology. This study provides a comprehensive overview of changes in protein

expression in these regions over the entire course of the disease, including the pre-symptomatic period of AD. We distinguish between early and late changes and cluster proteins together that have concomitant changes in abundance during the disease course. We find that proteins that show concomitant changes in abundance belong to specific functional groups and can be assigned to different cell types. The observation of transient changes in protein abundance underpins the importance of analyzing all disease stages, including the pre-symptomatic, instead of merely contrasting AD versus control cases.

Patient selection

To get insight in the mechanisms involved in the different stages of AD, it is essential to have a well characterized, age-matched patient cohort without comorbidities. However, due to the limited number of aged cases that meet the strict criteria for Braak stage 0, complete age-matching was not feasible. Nevertheless, we consider inclusion of these cases to be very important for this study as it represent a group without any AD pathology. Some Braak stage VI cases in our cohort are relatively young, as younger end-stage AD patients are more frequently brought to autopsy and are therefore over-represented. In one case, hereditary form of AD was suspected but not investigated. The CV (Fig S2) indicates similar variance in this group compared to the other groups indicating that the age variance has no or minor impact on the data.

Handling of inter-individual variability

We quantified the inter-individual variability by comparing the median CV obtained from technical replication (independent dissection/LC-MSMS of a single human subject in triplicate) with the median CV of Braak stage experimental group (Fig S2). We observed that the total variation was equal for all Braak stages amounting to approximately 30% variation within each group. Based on these data we estimated that approximately 15% of the variation within each Braak stage could be contributed by factors other than the LCM/LC-MSMS workflow. Changes in protein abundance were detected using a linear regression method on log-transformed protein expression values. We found that this method advances over statistical methods that compare variation between experimental groups (e.g. ANOVA) allowing the detection of more subtle differences.

Validation of the mass spectrometry results

We validated our results by different approaches. First, we reproduced results of established markers that showed increased expression in AD, such as MAPT, GFAP and CD44. Second, based on protein expression data of the hippocampus a clear separation between the early and late Braak stages is observed, indicative that our protein profiling corroborates pathological disease stage criteria. Third, we confirmed the expression of proteins using independent techniques of immunoblotting and immunohistochemistry, yielding high confidence in the data obtained by mass spectrometry. Significance was not reached using immunoblotting for TNC. This is most likely because the immunoblots were performed on whole hippocampal lysates instead of dissected material. This underscores the importance of targeting a proteomics analysis towards a specific region using LCM, as this improves resolution and as a consequence, results in

higher sensitivity to detect subtle changes in expression in the relevant brain area. In addition, IHC using 3,3'-Diaminobenzidine (DAB) is a semi quantitative analysis per definition, thereby variances may occur compared to the quantitative proteomics approach used in this study.

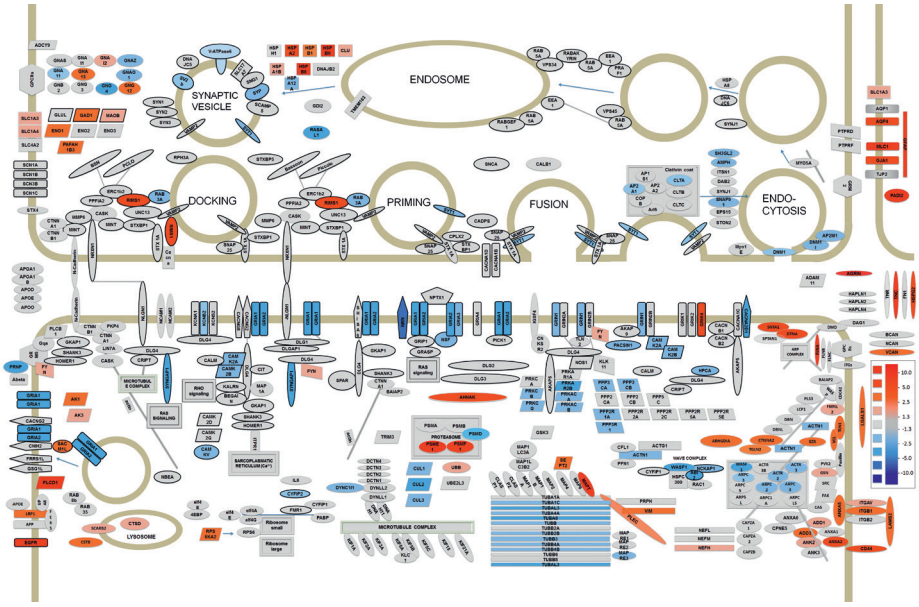

FIGURE 5 | Proteins with altered expression during the course of AD at the synapse. Altered protein levels during the course of AD with, depicted in red the proteins with increased levels and in blue the proteins with decreased levels relative to Braak 0. Brighter colors indicate a higher fold change in protein abundance (see scale at inset). In the pre-synapse increased levels are observed in components of the vesicle release machinery, solute carrier family proteins, heatshock proteins and several proteins involved in metabolic pathways. There is decrease of proteins involved in endocytosis. In the post-synapse glutamate receptors are decreased in levels, with the exception of GRIK4. Also decreased are the tubulins but there is strong increase of the microtubule stabilizing protein MAPT. We found increase of several adhesion molecules and proteins involved in cytoskeletal dynamics, such as PLEC, EZR, VCL, TLN1, CTNNA2 and TGLN2. Several astrocytic proteins (upper right corner) are upregulated, as are several ECM proteins altering the synaptic microenvironment. Proteins indicated with dark lining are only found in synapses, those without can also be found in other cellular compartments. Abbreviations: MAPT, microtubule-associated protein tau; GRIK4, glutamate receptor, ionotropic kainate 4; AD, Alzheimer's disease; ECM, extracellular matrix.

Pathways involved in Alzheimer's disease

By using a clustering analysis we were able to identify groups of proteins that show a similar expression pattern over the Braak stages. The hypothesis that these might represent different cellular responses exerted by different cell types is supported by the overrepresentation of astrocytic genes in cluster Q and L and neuronally expressed genes in cluster M and S (Fig. 3).

Pathway analysis using IPA provided some insight into the biology represented by the different clusters. In the neuronal clusters there is a loss in expression of genes involved in long term potentiation (PRKAR2B, CAMK2D, CAMK2A, GRM3, GRIA1, GRIA2, GRIA3, PPP3R1, MAP2K1, PPP3CA and PRKCG). The up-down cluster might reflect a compensatory mechanism and includes proteins involved in axonal guidance (ADAM22, TUBA8, NTRK3, WASL, PIK3R6, GSK3B, and GIT1), and oxidative phosphorylation (ATP5J, NDUFB11, NDUFA3 and MT-ND2) pathways. These might reflect a compensatory mechanism as there are no obvious cognitive symptoms during the "up" phase and these only occur during the "down" phase of this cluster. The astrocytic response is progressively up correlating well with the increasing astrogliosis during progression of AD. Astrogliosis is adding to a state of inflammation that might be harmful by itself. Processes involved in this cluster include proteins involved in NRF2-mediated oxidative stress response (AKR7A2, MGST1, FTL, PPIB, GSTP1 and CBR1), glycolysis (ENO1, TPI1 and PKM) and cytoskeletal rearrangements (FLNA, EZR, TLN1, VCL, GSN and GNG12).

Changes in protein abundance of functionally related protein groups

Notably, protein groups with related functions were identified. Protein abundance over the Braak stages was plotted for these groups to emphasize their concomitant change in abundance or to visualize notable exceptions within a group (Fig. 4), and proteins with a known or potential synaptic or synapse-related function were visualized (Fig. 5).

The extracellular matrix (ECM).

Several components of the ECM were found to have increased levels in AD, such as TNC, VCAN, LAMB2 and LGALS1 (Fig. 4A). The ECM is involved in the regulation of many processes including axonal growth during neural development, response to injury, inflammation and is also part of the synapse microenvironment (Fig. 5) involved in synaptic plasticity [7, 54]. In addition, we found a change in abundance for adhesion molecules that interact with the ECM, including CD44, ITGB1 and ITGAV (Fig. 4B) which are linked to inflammation in AD [19], and also to synaptic plasticity (Fig. 5) [11]. These transmembrane proteins signal via intracellular proteins linking the plasma membrane and the actin cytoskeleton.

Cytoskeletal associated proteins.

Many actin-associated proteins were found increased including early increase of PLEC, FLNA, TLN1, VCL and EZR (Fig. 4C), indicating increased signaling and cytoskeletal dynamics in early phases of AD. These early changes in proteins involved in cytoskeletal dynamics might reflect changes in (sub-)cellular morphology and structural plasticity of synaptic neuronal (Fig. 5) or glial processes, influencing synaptic plasticity and function or the extension of neuronal processes. In agreement with this we observed increased levels of GSN and DPYSL3 and a reduction of PAK1, TWF2, ABI2, NCKAP1 and CORO1A and -1C, all associated with the Arp2/3 -dependent actin cytoskeletal dynamics [12, 25].

Microtubules and associated proteins.
Microtubules are essential for transport of proteins, vesicles and organelles and can bind several signaling molecules. The levels of tubulins TUBA8, TUBB, TUBB3, TUBB2B, TUBB4B and TUBB4A were significantly decreased (Figs 4D and 5). Several microtubule-associated proteins which are essential for the formation and stabilization of the microtubules, are sequestered by hyperphosphorylated MAPT. This includes MAP1A, MAP1B, MAP2, and MAPT itself, and results in microtubule disruption [28]. We observed an early increase of MAPT and a decrease of MAPRE3, but no changes were observed in the expression of other microtubule associated proteins MAP1A, MAP1B or MAP2 (Fig. 4E and 5), which are involved in microtubule stability and are able to compensate for a loss of MAPT function [31].

Presynaptic signaling.
An up-down profile is observed for several proteins, which are present in the active zone of the pre-synapse and involved in vesicle priming and release, RAB3C, LIN7A, and BSN. In addition, RIMS1 is early increased (Fig. 4F), which might indicate an early disturbance in vesicle docking and release (Fig. 5) [14]. Typical vesicle integral proteins, such as VAMP1, VAMP2, YKT6, SLC17A7 and SV2A and show no change (Fig. 5), suggesting that vesicle numbers do not change early in AD. Synaptic plasticity critically depends on the process of endocytosis. We observed changed levels of several proteins involved in endocytosis, such as reduced levels of CLTA and AP2M1 and an early decrease of SNAP91, AP2A1, AP2B1 and DNM1, all suggesting early endocytic dysfunction (Fig. 5) [46].

Postsynaptic signaling.
The abundance of postsynaptic density proteins DLG2, -3 and -4, SHANK3, HOMER1 and DLGAP1 are clearly found changed in a concomitant early-up, late-down fashion, coinciding with what is observed presynaptically (Fig. 4G). We observed reduced levels of the glutamate AMPA-type receptor subunits GRIA1, GRIA2, and GRIA3, in accordance with the literature [3, 27], and reduction of the NMDA receptors GRIN1, GRIN2B. Interestingly, the kainate-type receptor GRIK4 is increased already early in AD (Fig. 4H), which might add to excitotoxicity [37], an effect possibly amplified by increased glutamate levels due to early increase of glutamate dehydrogenase 1 (GLUD1) [40].

Calcium activated proteins.
The Annexin family responds to increased intracellular calcium, and can subsequently interact with phospholipid membranes. Their functions involve membrane trafficking, endocytosis and exocytosis [36]. We observed an increase in the abundance of ANXA2 and ANXA5 (ANXA1 and ANXA6 follow this trend) (Fig. 4I), which might represent a protective response against membrane damage [17]. This is highlighted by the increase in expression of AHNAK (Fig. 4I), which together with S100A10 and ANXA2 forms a membrane repair complex [45]. Moreover, we found decreased levels of CAMK2A, CDH13 and PPP3R1. Increased intracellular calcium results in downstream signaling especially of CAMK2A, which is highly important for synaptic plasticity [55].

Response to cellular stress.
Heat shock proteins are induced upon cellular stress and are important in preventing potentially toxic protein misfolding and aggregation [23]. Significantly increased are HSPA1B, HSPH1, HSPB6, HSPB1, HSPB8, and HSPA2 of which the first two are designated as early increased (Fig. 4J). Changes in abundance of anti-oxidant repair enzymes were limited to increases of PRDX1 and PRDX6, whereas several other anti-oxidant enzymes showed no change in expression (Fig. 4K). We observed increased levels of ALDH2 ALDH4A1, ALDH6A1, ALDH7A1 (early increased), ALDH9A1, ALDH1L1 and other members of the aldehyde dehydrogenase family followed a similar trend (Fig. 4L). We observed increased MLC1 and AQP4 which play a role in maintaining the water balance [8, 44] and AQP4 has also been suggested to play a role in the clearance of Aβ [26].

Other early increased proteins include LRP1 which is linked to Aβ metabolism [30], CNDP2, the citrullinating enzyme PADI2, and the protease CTSD.

Potential biomarkers
Proteins that display early changes in abundance, but also their metabolic products, might serve to realize an early and specific diagnosis of AD, assess different aspects of the disease process or evaluate therapeutic efficacy. For several proteins in our study detection in CSF or serum has been demonstrated. For example TNC is detected in CSF and serum [49, 50], ANXA5 is found to be increased in serum of AD patients [47], CLU is detected in the CSF and associated with AD [35, 52] and SCG2 levels correlate with Aβ peptides in CSF [39]. Our study provides many novel opportunities in assessing proteins with early changes in abundance as potential biomarkers of AD.

CONCLUSION

In summary, using laser microdissection we isolated the CA1 and subiculum regions from the human hippocampus. By subsequent mass spectrometry analysis, we detected progressive changes in the expression of 372 proteins during the course of AD. By including all Braak stages, we were able to determine the chronological pattern in the regulation of several proteins and assigned expression patterns to different cell types. Several functional groups were found to display (early) changes in protein abundance, including proteins involved in the ECM, cytoskeletal dynamics, calcium signaling, synaptic vesicle release, synaptic plasticity and response to cellular stress. In further steps the functional role of many of the expression-changed proteins needs to be addressed in the context of AD. Alterations of protein levels can be indicative of adaptive mechanisms during the disease, which might turn out detrimental or potentially protective, yielding new entries into AD treatment and diagnosis at an early stage.

ACKNOWLEDGEMENTS

We thank the Netherlands Brain Bank (Amsterdam, the Netherlands) for supplying human brain tissue. This work was financially supported by the Neuroscience Campus Amsterdam, and parts of the work were made possible by a grant from Alzheimer Nederland (WE.03-2012-17).

REFERENCES

1. Akiyama H, Tooyama I, Kawamata T, Ikeda K, McGeer PL (1993) Morphological diversities of CD44 positive astrocytes in the cerebral cortex of normal subjects and patients with Alzheimer's disease. Brain Res 632:249–259. doi: 10.1016/0006-8993(93)91160-T
2. Andreev VP, Petyuk VA, Brewer HM, Karpievitch Y V., Xie F, Clarke J, Camp D, Smith RD, Lieberman AP, Albin RL, Nawaz Z, El Hokayem J, Myers AJ (2012) Label-free quantitative LC-MS proteomics of alzheimer's disease and normally aged human brains. J Proteome Res 11:3053–3067. doi: 10.1021/pr3001546
3. Armstrong DM, Ikonomovic MD (1996) AMPA-selective glutamate receptor subtype immunoreactivity in the hippocampal dentate gyrus of patients with Alzheimer disease: Evidence for hippocampal plasticity. In: Mol. Chem. Neuropathol. Humana Press Inc., pp 59–64
4. Arriagada P V., Growdon JH, Hedley-Whyte ET, Hyman BT (1992) Neurofibrillary tangles but not senile plaques parallel duration and severity of Alzheimer's disease. Neurology 42:631–639. doi: 10.1212/wnl.42.3.631
5. Bateman RJ, Xiong C, Benzinger TLS, Fagan AM, Goate A, Fox NC, Marcus DS, Cairns NJ, Xie X, Blazey TM, Holtzman DM, Santacruz A, Buckles V, Oliver A, Moulder K, Aisen PS, Ghetti B, Klunk WE, McDade E, Martins RN, Masters CL, Mayeux R, Ringman JM, Rossor MN, Schofield PR, Sperling RA, Salloway S, Morris JC (2012) Clinical and biomarker changes in dominantly inherited Alzheimer's disease. N Engl J Med 367:795–804. doi: 10.1056/NEJMoa1202753
6. Benjamini Y, Hochberg Y (1995) Controlling the False Discovery Rate: A Practical and Powerful Approach to Multiple Testing. J R Stat Soc Ser B 57:289–300. doi: 10.1111/j.2517-6161.1995.tb02031.x
7. Bonneh-Barkay D, Wiley CA (2009) Brain extracellular matrix in neurodegeneration. Brain Pathol 19:573–585. doi: 10.1111/j.1750-3639.2008.00195.x
8. Boor I, Nagtegaal M, Kamphorst W, van der Valk P, Pronk JC, van Horssen J, Dinopoulos A, Bove KE, Pascual-Castroviejo I, Muntoni F, Estévez R, Scheper GC, van der Knaap MS (2007) MLC1 is associated with the dystrophin-glycoprotein complex at astrocytic endfeet. Acta Neuropathol 114:403–410. doi: 10.1007/s00401-007-0247-0
9. Braak H, Braak E (1991) Neuropathological stageing of Alzheimer-related changes. Acta Neuropathol 82:239–59.
10. Braak H, Braak E (1995) Staging of alzheimer's disease-related neurofibrillary changes. Neurobiol Aging 16:271–278. doi: 10.1016/0197-4580(95)00021-6
11. Chan CS, Weeber EJ, Zong L, Fuchs E, Sweatt JD, Davis RL (2006) β1-integrins are required for hippocampal AMPA receptor-dependent synaptic transmission, synaptic plasticity, and working memory. J Neurosci 26:223–232. doi: 10.1523/JNEUROSCI.4110-05.2006
12. Chan KT, Creed SJ, Bear JE (2011) Unraveling the enigma: Progress towards understanding the coronin family of actin regulators. Trends Cell Biol 21:481–488. doi: 10.1016/j.tcb.2011.04.004
13. Chen N, Koopmans F, Gordon A, Paliukhovich I, Klaassen R V., Van Der Schors RC, Peles E, Verhage M, Smit AB, Li KW (2015) Interaction proteomics of canonical Caspr2 (CNTNAP2) reveals the presence of two Caspr2 isoforms with overlapping interactomes. Biochim Biophys Acta - Proteins Proteomics 1854:827–833. doi: 10.1016/j.bbapap.2015.02.008
14. Chua JJE, Kindler S, Boyken J, Jahn R (2010) The architecture of an excitatory synapse. J Cell Sci 123:819–823. doi: 10.1242/jcs.052696

15. Cox J, Hein MY, Luber CA, Paron I, Nagaraj N, Mann M (2014) Accurate proteome-wide label-free quantification by delayed normalization and maximal peptide ratio extraction, termed MaxLFQ. Mol Cell Proteomics 13:2513–2526. doi: 10.1074/mcp.M113.031591

16. Cox J, Mann M (2008) MaxQuant enables high peptide identification rates, individualized p.p.b.-range mass accuracies and proteome-wide protein quantification. Nat Biotechnol 26:1367–1372. doi: 10.1038/nbt.1511

17. Eberhard DA, Brown MD, VandenBerg SR (1994) Alterations of annexin expression in pathological neuronal and glial reactions: Immunohistochemical localization of annexins I, II (p36 and p11 subunits), IV, and VI in the human hippocampus. Am J Pathol 145:640–649.

18. Eikelenboom P, Van Gool WA (2004) Neuroinflammatory perspectives on the two faces of Al'zheimer's disease. J Neural Transm 111:281–294. doi: 10.1007/s00702-003-0055-1

19. Eikelenboom P, Zhan SS, Kamphorst W, van der Valk P, Rozemuller JM (1994) Cellular and substrate adhesion molecules (integrins) and their ligands in cerebral amyloid plaques in Alzheimer's disease. Virchows Arch 424:421–427. doi: 10.1007/BF00190565

20. Glenner GG, Wong CW (1984) Alzheimer's disease: Initial report of the purification and characterization of a novel cerebrovascular amyloid protein. Biochem Biophys Res Commun 120:885–890. doi: 10.1016/S0006-291X(84)80190-4

21. Goudriaan A, De Leeuw C, Ripke S, Hultman CM, Sklar P, Sullivan PF, Smit AB, Posthuma D, Verheijen MHG (2014) Specific glial functions contribute to Schizophrenia susceptibility. Schizophr Bull 40:925–935. doi: 10.1093/schbul/sbt109

22. Grundke-Iqbal I, Iqbal K, Quinlan M, Tung YC, Zaidi MS, Wisniewski HM (1986) Microtubule-associated protein tau. A component of Alzheimer paired helical filaments. J Biol Chem 261:6084–6089.

23. Hinault MP, Ben-Zvi A, Goloubinoff P (2006) Chaperones and proteases: Cellular fold-controlling factors of proteins in neurodegenerative diseases and aging. J Mol Neurosci 30:249–265. doi: 10.1385/JMN:30:3:249

24. Ho Kim J, Franck J, Kang T, Heinsen H, Ravid R, Ferrer I, Hee Cheon M, Lee JY, Shin Yoo J, Steinbusch HW, Salzet M, Fournier I, Mok Park Y (2015) Proteome-wide characterization of signalling interactions in the hippocampal CA4/DG subfield of patients with Alzheimer's disease. Sci Rep 5:1–15. doi: 10.1038/srep11138

25. Ibarra N, Pollitt A, Insall RH (2005) Regulation of actin assembly by SCAR/WAVE proteins. In: Biochem. Soc. Trans. Biochem Soc Trans, pp 1243–1246

26. Igarashi H, Suzuki Y, Kwee IL, Nakada T (2014) Water influx into cerebrospinal fluid is significantly reduced in senile plaque bearing transgenic mice, supporting beta-amyloid clearance hypothesis of Alzheimer's disease. Neurol Res 36:1094–1098. doi: 10.1179/1743132814Y.0000000434

27. Ikonomovic MD, Mizukami K, Davies P, Hamilton R, Sheffield R, Armstrong DM (1997) The loss of GluR2(3) immunoreactivity precedes neurofibrillary tangle formation in the entorhinal cortex and hippocampus of Alzheimer brains. J Neuropathol Exp Neurol 56:1018–1027. doi: 10.1097/00005072-199709000-00007

28. Iqbal K, Gong CX, Liu F (2013) Hyperphosphorylation-induced tau oligomers. Front Neurol. doi: 10.3389/fneur.2013.00112

29. Jack CR, Knopman DS, Jagust WJ, Petersen RC, Weiner MW, Aisen PS, Shaw LM, Vemuri P, Wiste HJ, Weigand SD, Lesnick TG, Pankratz VS, Donohue MC, Trojanowski JQ (2013) Tracking pathophysiological processes in Alzheimer's disease: An updated hypothetical model of dynamic biomarkers. Lancet Neurol 12:207–216. doi: 10.1016/S1474-4422(12)70291-0

30. Kanekiyo T, Bu G (2014) The low-density lipoprotein receptor-related protein 1 and amyloid-β clearance in Alzheimer's disease. Front Aging Neurosci 6:93. doi: 10.3389/fnagi.2014.00093

31. Ke YD, Suchowerska AK, Van Der Hoven J, De Silva DM, Wu CW, Van Eersel J, Ittner A, Ittner LM (2012) Lessons from Tau-deficient mice. Int J Alzheimers Dis. doi: 10.1155/2012/873270

32. Khatoon S, Grundke-Iqbal I, Iqbal K (1994) Levels of normal and abnormally phosphorylated tau in different cellular and regional compartments of Alzheimer disease and control brains. FEBS Lett 351:80–84. doi: 10.1016/0014-5793(94)00829-9

33. Korolainen MA, Nyman TA, Aittokallio T, Pirttilä T (2010) An update on clinical proteomics in Alzheimer's research. J Neurochem 112:1386-1414. doi: 10.1111/j.1471-4159.2009.06558.x

34. Lace G, Savva GM, Forster G, De Silva R, Brayne C, Matthews FE, Barclay JJ, Dakin L, Ince PG, Wharton SB (2009) Hippocampal tau pathology is related to neuroanatomical connections: An ageing population-based study. Brain 132:1324–1334. doi: 10.1093/brain/awp059

35. Lidström AM, Bogdanovic N, Hesse C, Volkman I, Davidsson P, Blennow K (1998) Clusterin (apolipoprotein J) protein levels are increased in hippocampus and in frontal cortex in Alzheimer's disease. Exp Neurol 154:511-521. doi: 10.1006/exnr.1998.6892

36. Lizarbe MA, Barrasa JI, Olmo N, Gavilanes F, Turnay J (2013) Annexin-phospholipid interactions. Functional implications. Int J Mol Sci 14:2652–2683. doi: 10.3390/ijms14022652

37. Lowry ER, Kruyer A, Norris EH, Cederroth CR, Strickland S (2013) The GluK4 kainate receptor subunit regulates memory, mood, and excitotoxic neurodegeneration. Neuroscience 235:215–225. doi: 10.1016/j.neuroscience.2013.01.029

38. Manavalan A, Mishra M, Feng L, Sze SK, Akatsu H, Heese K (2013) Brain site-specific proteome changes in aging-related dementia. Exp Mol Med 45:e39. doi: 10.1038/emm.2013.76

39. Mattsson N, Johansson P, Hansson O, Wallin A, Johansson JO, Andreasson U, Andersen O, Haghighi S, Olsson M, Stridsberg M, Svensson J, Blennow K, Zetterberg H (2010) Converging pathways of chromogranin and amyloid metabolism in the brain. J Alzheimer's Dis 20:1039–1048. doi: 10.3233/JAD-2010-091651

40. Michaelis EK, Wang X, Pal R, Bao X, Hascup KN, Wang Y, Wang WT, Hui D, Agbas A, Choi IY, Belousov A, Gerhardt GA (2011) Neuronal Glud1 (glutamate dehydrogenase 1) over-expressing mice: Increased glutamate formation and synaptic release, loss of synaptic activity, and adaptive changes in genomic expression. Neurochem Int 59:473–481. doi: 10.1016/j.neuint.2011.03.003

41. Musunuri S, Wetterhall M, Ingelsson M, Lannfelt L, Artemenko K, Bergquist J, Kultima K, Shevchenko G (2014) Quantification of the brain proteome in Alzheimer's disease using multiplexed mass spectrometry. J Proteome Res 13:2056–2068. doi: 10.1021/pr401202d

42. Nelson PT, Alafuzoff I, Bigio EH, Bouras C, Braak H, Cairns NJ, Castellani RJ, Crain BJ, Davies P, Tredici K Del, Duyckaerts C, Frosch MP, Haroutunian V, Hof PR, Hulette CM, Hyman BT, Iwatsubo T, Jellinger KA, Jicha GA, Kövari E, Kukull WA, Leverenz JB, Love S, MacKenzie IR, Mann DM, Masliah E, McKee AC, Montine TJ, Morris JC, Schneider JA, Sonnen JA, Thal DR, Trojanowski JQ, Troncoso JC, Wisniewski T, Woltjer RL, Beach TG (2012) Correlation of alzheimer disease neuropathologic changes with cognitive status: A review of the literature. J Neuropathol Exp Neurol 71:362–381. doi: 10.1097/NEN.0b013e31825018f7

43. Nijholt DAT, Van Haastert ES, Rozemuller AJM, Scheper W, Hoozemans JJM (2012) The unfolded protein response is associated with early tau pathology in the hippocampus of tauopathies. J Pathol 226:693–702. doi: 10.1002/path.3969

44. Pasantes-Morales H, Cruz-Rangel S (2010) Brain volume regulation: Osmolytes and aquaporin perspectives. Neuroscience 168:871–884. doi: 10.1016/j.neuroscience.2009.11.074

45. Rezvanpour A, Santamaria-Kisiel L, Shaw GS (2011) The S100A10-annexin A2 complex provides a novel asymmetric platform for membrane repair. J Biol Chem 286:40174–40183. doi: 10.1074/jbc.M111.244038

46. Schmid EM, McMahon HT (2007) Integrating molecular and network biology to decode endocytosis. Nature 448:883–888. doi: 10.1038/nature06031

47. Sohma H, Imai S ichi, Takei N, Honda H, Matsumoto K, Utsumi K, Matsuki K, Hashimoto E, Saito T, Kokai Y (2013) Evaluation of annexin A5 as a biomarker for Alzheimer's disease and dementia with lewy bodies. Front Aging Neurosci. doi: 10.3389/fnagi.2013.00015

48. Sperling RA, Karlawish J, Johnson KA (2013) Preclinical Alzheimer disease - The challenges ahead. Nat Rev Neurol 9:54–58. doi: 10.1038/nrneurol.2012.241

49. Suzuki H, Kanamaru K, Shiba M, Fujimoto M, Imanaka-Yoshida K, Yoshida T, Taki W (2011) Cerebrospinal fluid tenascin-C in cerebral vasospasm after aneurysmal subarachnoid hemorrhage. J Neurosurg Anesthesiol 23:310–317. doi: 10.1097/ANA.0b013e31822aa1f2

50. Suzuki H, Kanamaru K, Suzuki Y, Aimi Y, Matsubara N, Araki T, Takayasu M, Kinoshita N, Imanaka-Yoshida K, Yoshida T, Taki W (2010) Tenascin-C is induced in cerebral vasospasm after subarachnoid hemorrhage in rats and humans: A pilot study. Neurol Res 32:179–184. doi: 10.1179/174313208X355495

51. Thal DR, Rüb U, Schultz C, Sassin I, Ghebremedhin E, Del Tredici K, Braak E, Braak H (2000) Sequence of Aβ-protein deposition in the human medial temporal lobe. J Neuropathol Exp Neurol 59:733–748. doi: 10.1093/jnen/59.8.733

52. Thambisetty M, An Y, Kinsey A, Koka D, Saleem M, Guntert A, Kraut M, Ferrucci L, Davatzikos C, Lovestone S, Resnick SM (2012) Plasma clusterin concentration is associated with longitudinal brain atrophy in mild cognitive impairment. Neuroimage 59:212–217. doi: 10.1016/j.neuroimage.2011.07.056

53. Ward JH (1963) Hierarchical Grouping to Optimize an Objective Function. J Am Stat Assoc 58:236–244. doi: 10.1080/01621459.1963.10500845

54. Xie K, Liu Y, Hao W, Walter S, Penke B, Hartmann T, Schachner M, Fassbender K (2013) Tenascin-C deficiency ameliorates alzheimer's disease-related pathology in mice. Neurobiol Aging 34:2389–2398. doi: 10.1016/j.neurobiolaging.2013.04.013

55. Yamauchi T (2005) Neuronal Ca2+/calmodulin-dependent protein kinase II - Discovery, progress in a quarter of a century, and perspective: Implication for learning and memory. Biol Pharm Bull 28:1342–1354. doi: 10.1248/bpb.28.1342

SUPPLEMENTARY MATERIAL

TABLE S1

Braak tau	Thal Aβ	Sex	Age (y)	brain weight (g)	PMD hh:mm
0	0	M	56	1313	10:00
0	0	M	80	1331	7:15
0	0	M	56	1548	9:15
0	0	M	66	1560	7:46
0	0	F	62	ND	5:00
1	4	F	83	1274	5:30
1	0	M	79	1269	6:30
1	0	F	93	1203	4:25
1	2	M	77	1287	7:30
1	0	F	94	1048	4:05
1	1	F	86	1108	6:30
1	2	F	73	1444	7:45
2	3	F	85	958	4:20
2	2	F	99	1045	5:10
2	0	M	79	1225	4:30
2	1	M	88	1418	4:43
2	3	F	99	910	4:15
3	0	F	91	1080	5:20
3	1	F	86	1107	6:00
3	4	M	78	1102	4:40
3	2	F	83	1125	5:20
3	1	F	98	1221	6:05
4	4	F	93	970	2:30
4	4	M	93	1130	5:50
4	4	F	86	1193	4:50
4	4	F	86	930	5:55
4	4	F	92	1030	4:15
4	4	F	91	1118	6:05
4	4	F	96	1107	5:00
5	4	F	82	984	4:35
5	4	F	78	1035	4:50
5	4	F	89	1131	4:40
5	4	F	89	984	10:20
5	4	F	78	953	4:35
6	4	F	66	1026	5:20

TABLE S1 | Continued

Braak tau	Thal Aβ	Sex	Age (y)	brain weight (g)	PMD hh:mm
6	4	F	91	940	5:45
6	4	F	89	1095	4:30
6	4	M	73	872	6:15
6	4	M	68	1100	
6	4	F	62	1047	

Cases used for mass spectrometry analysis.
Aβ, amyloid-beta; AD, Alzheimer's disease; F, female; M, male; ND, not determined; PMD, postmortem delay

TABLE S2

Primary antibody	Species	Clonality	Dilution IHC	Dilution IB	Source
AT8	Mouse	Mono	1:800	-	Innogenetics (Gent, Belgium)
GFAP	Mouse	Mono	1:20	-	Monosan (Sanbio, Uden The Netherlands
Aβ	Mouse	Mono	1:50	-	Dako (Glostrup, Denmark)
CD44	Mouse	Mono	1:1600	1:10.000	R&D systems (Abingdon, UK)
Tenascin-C	Rabbit	Mono	1:50	1:1000	Abcam (cambridge, UK)
Filamin-A	Rabbit	Mono	1:200	1:5000	Abcam (cambridge, UK)
Talin	Mouse	Mono	-	1:500	Millipore
Annexin 2	Rabbit	Poly	1:400	1:1000	Abcam (cambridge, UK)
Annexin 5	Mouse	Mono	1:800	1:2000	Abcam (cambridge, UK)
Vinculin	Mouse	Mono	1:800	1:10.000	Sigma Aldrich

Antibodies and dilutions used in this study.
IHC, immunohistochemistry; IB, immunoblotting.

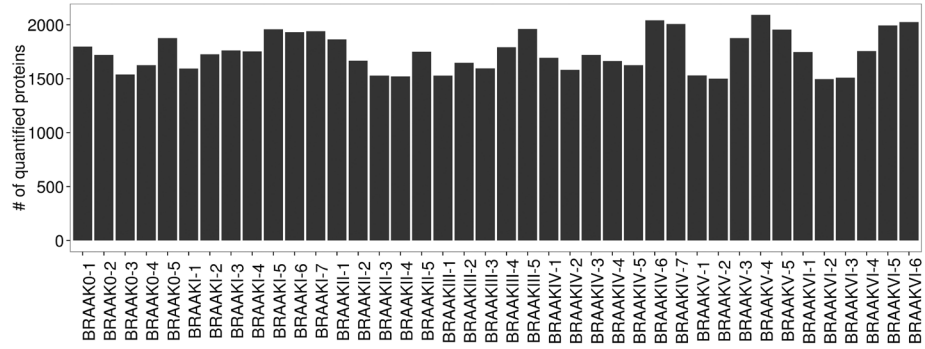

FIG. S1 | The number of quantifiable proteins per sample. At least 1500 proteins were quantified per sample. Represented here are the levels of proteins detected in each individual sample. In total, 3216 proteins were quantified.

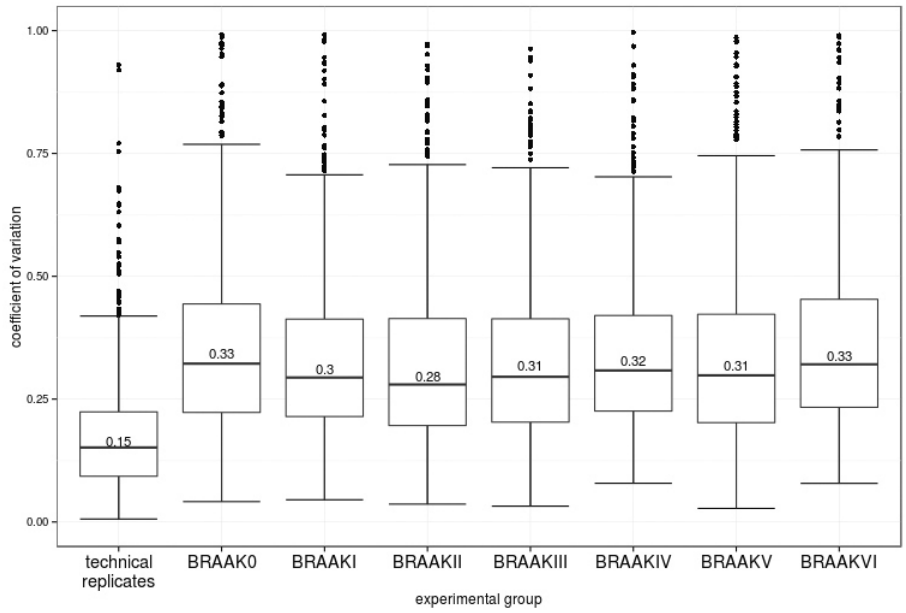

FIG. S2 | Coefficient of variation over the different Braak stages. Based on proteins that have quantitative values in all samples, the median coefficient of variation (CV) was determined. One case was dissected and analyzed in triplicate for which the CV is shown in the first column, referred to as "technical replicates." The CV of all seven groups representing the different Braak stages is shown in the remainder columns. The CV determined from technical replication is 15%. The CV of measured protein abundance is constant across Braak stages at approximately 30%.

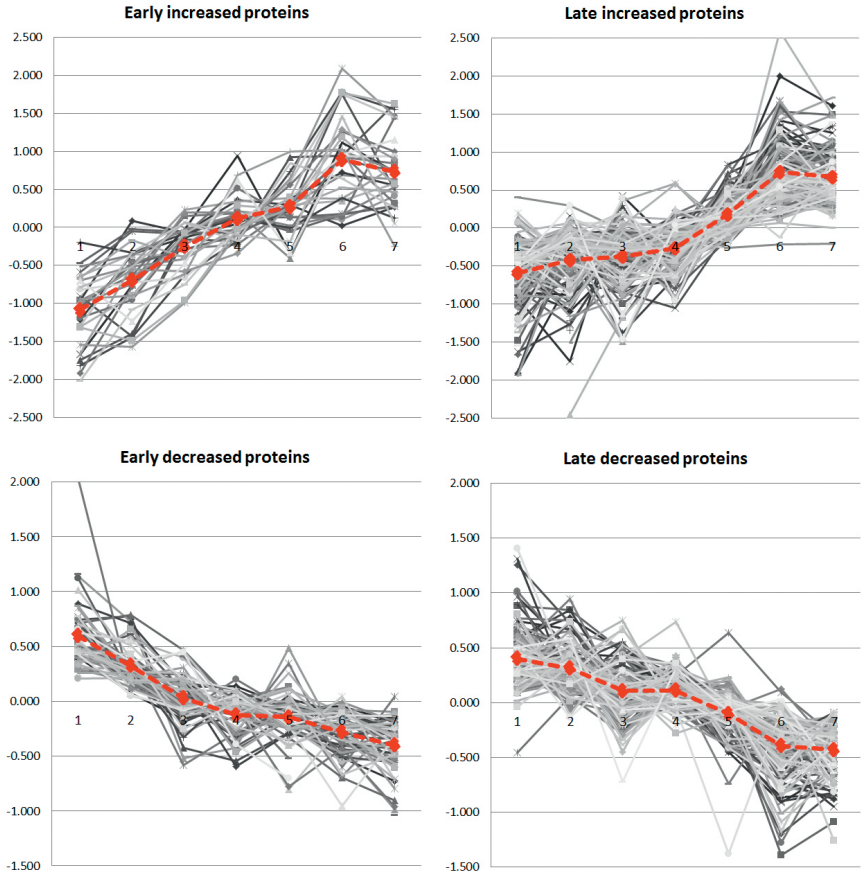

FIG. S3 | Early versus downregulated proteins. Proteins with a significant change in abundance (FDR <0.1) over the Braak stages (0-VI) were subjected to an additional linear regression analysis involving only the early Braak stages (0-III). Proteins with a significant change ($P < .05$) in this range were regarded as early changed. The gray lines are the mean values for individual proteins per Braak stage centered around zero. The striped red lines indicate the overall mean of all proteins in the graph per Braak stage. Abbreviation: FDR, false discovery rate.

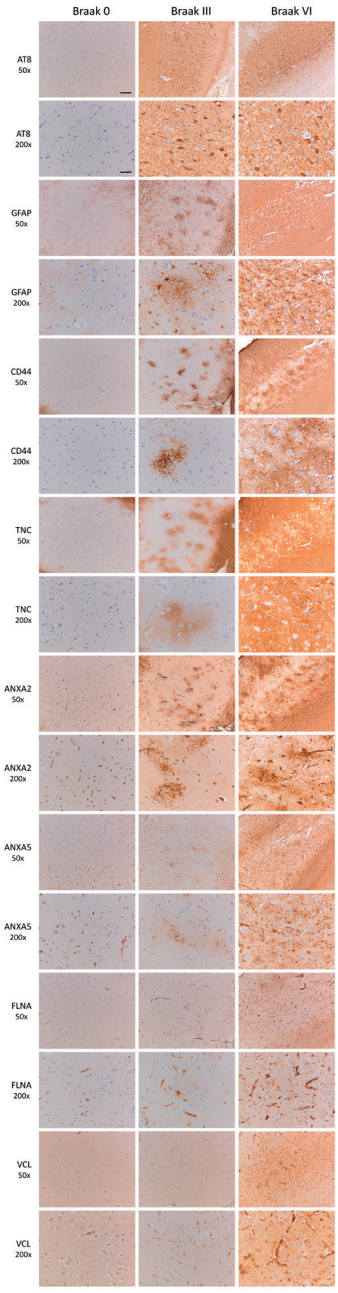

FIG. S4 | Immunohistochemical stainings were performed for GFAP, CD44, TNC, ANXA2, ANXA5, FLNA, and VCL. Images were taken at low (×50 original magnification) and high (×200 original magnification) magnification of a Braak stage 0, III, and VI case in the subiculum region. The scale bars, inserted in the AT8 staining of the Braak 0 case, are 200 µm in the ×50 magnification and 50 µm in the ×200 magnification. Abbreviations: GFAP, glial fibrillary acidic protein; FLNA, filamin-A.

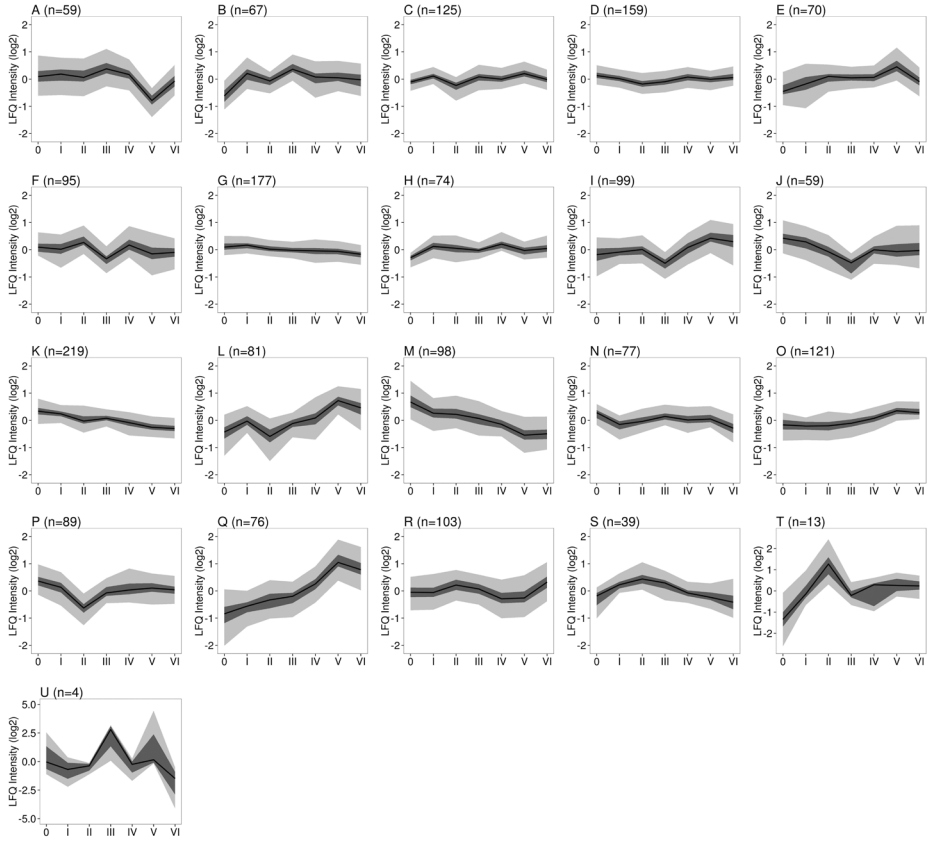

FIG. S5 | Proteins were clustered based on their expression profile. For each protein, the mean expression value per Braak stage was used and the expression profile based on the mean was centered around zero. Cluster analysis of the different protein expression profiles is based on Euclidian distance using the mean expression values centered to zero. Twenty-one clusters were generated each containing proteins displaying similar protein expression profiles. Abbreviation: LFQ, label-free quantification.

TABLE S3 | (increased proteins)

Gene (leading protein)	Pvalue BRAAK0-VI	FDR BRAAK0-VI	Slope BRAAK0-VI (LFQintensity Log2)	Max. fold change BRAAK0-VI	Pvalue BRAAK0-III	FDR BRAAK0-III	Slope BRAAK0-III (LFQintensity Log2)
LRP1	0.003	0.040	0.134	2.500	0.001	0.353	0.371
PLEC	0.000	0.000	0.315	3.990	0.001	0.353	0.265
MAPT	0.000	0.000	0.564	10.300	0.001	0.353	0.584
RIMS1	0.005	0.049	0.346	6.880	0.002	0.365	0.857
CTSD	0.001	0.011	0.111	1.830	0.003	0.381	0.208
PSMF1	0.004	0.048	0.195	Inf	0.003	0.381	0.419

TABLE S3 | Continued

Gene (leading protein)	Pvalue BRAAK0-VI	FDR BRAAK0-VI	Slope BRAAK0-VI (LFQintensity Log2)	Max. fold change BRAAK0-VI	Pvalue BRAAK0-III	FDR BRAAK0-III	Slope BRAAK0-III (LFQintensity Log2)
GFAP	0.000	0.000	0.625	12.090	0.004	0.381	0.559
GLUD1	0.000	0.000	0.251	2.620	0.006	0.416	0.219
ADD1	0.001	0.011	0.084	1.680	0.008	0.450	0.170
PAFAH1B3	0.000	0.000	0.267	3.830	0.009	0.450	0.381
FHL1	0.001	0.015	0.232	3.810	0.014	0.509	0.394
GSTM3	0.000	0.001	0.206	2.330	0.017	0.526	0.240
PBXIP1	0.003	0.038	0.418	9.060	0.017	0.532	0.539
DTNA	0.001	0.022	0.251	5.530	0.020	0.551	0.596
HSPH1	0.008	0.069	0.359	1.300	0.021	0.551	0.640
ITGAV	0.005	0.050	0.095	1.690	0.021	0.551	0.140
LANCL1	0.000	0.004	0.148	2.070	0.023	0.551	0.233
FLNA	0.000	0.000	0.601	13.640	0.023	0.551	0.627
AHNAK	0.000	0.003	0.456	9.070	0.026	0.551	0.603
CNDP2	0.000	0.003	0.340	5.640	0.028	0.551	0.545
PPIA	0.006	0.058	0.268	4.030	0.029	0.551	0.437
CBR1	0.000	0.000	0.295	3.820	0.032	0.551	0.284
PADI2	0.000	0.000	0.623	12.410	0.036	0.568	0.479
PSAT1	0.000	0.000	0.340	3.350	0.039	0.568	0.231
SCG2	0.012	0.091	0.322	4.570	0.040	0.568	0.580
ALDH7A1	0.004	0.048	0.244	4.430	0.040	0.568	0.446
MAOB	0.000	0.001	0.182	2.270	0.042	0.568	0.159
HSPB1	0.000	0.000	0.355	4.870	0.044	0.574	0.183
GRIK4	0.000	0.001	0.598	9.230	0.046	0.594	0.448
C21orf33	0.000	0.006	0.329	4.030	0.049	0.605	0.456
ARFGEF3	0.004	0.047	0.202	4.770	0.053	0.615	0.286
VCAN	0.000	0.000	0.300	3.420			
PRDX1	0.000	0.000	0.227	2.350			
EZR	0.000	0.000	0.350	4.440			
ANXA5	0.000	0.000	0.297	3.630			
ADD3	0.000	0.000	0.323	4.160			
PHGDH	0.000	0.000	0.276	3.180			
FTL	0.000	0.000	0.333	4.130			
PYGM	0.000	0.000	0.236	3.110			
SEPT2	0.000	0.000	0.208	2.500			

TABLE S3 | Continued

Gene (leading protein)	Pvalue BRAAK0-VI	FDR BRAAK0-VI	Slope BRAAK0-VI (LFQintensity Log2)	Max. fold change BRAAK0-VI	Pvalue BRAAK0-III	FDR BRAAK0-III	Slope BRAAK0-III (LFQintensity Log2)
HSPA1B	0.000	0.000	0.143	1.820			
HEPACAM	0.000	0.000	0.330	4.820			
EPB41L2	0.000	0.000	0.302	3.500			
PLCD1	0.000	0.000	0.591	15.000			
GNA13	0.000	0.000	0.189	2.810			
VIM	0.000	0.000	0.325	3.410			
AQP4	0.000	0.000	0.480	8.060			
ALDH4A1	0.000	0.001	0.390	7.650			
TKT	0.000	0.001	0.262	3.550			
SLC1A3	0.000	0.001	0.133	1.840			
CSTB	0.000	0.002	0.313	3.770			
GNG12	0.000	0.002	0.278	2.940			
CSRP1	0.000	0.002	0.415	5.890			
ALDH1L1	0.000	0.003	0.199	2.890			
GSN	0.000	0.003	0.215	2.430			
TLN1	0.000	0.003	0.307	3.160			
PRDX6	0.000	0.003	0.420	8.210			
HADHA	0.000	0.003	0.103	1.630			
METTL7A	0.000	0.004	0.259	3.220			
ACADVL	0.000	0.004	0.171	2.530			
GJA1	0.000	0.004	0.482	7.830			
PKM2	0.000	0.004	0.344	1.840			
GSTP1	0.000	0.004	0.203	3.540			
TAGLN2	0.000	0.004	0.270	4.710			
ENO1	0.000	0.005	0.347	4.430			
ARL3	0.000	0.005	0.205	2.340			
CLU	0.000	0.005	0.151	2.380			
FKBP3	0.000	0.005	0.130	1.810			
RPS6KA2	0.000	0.006	0.190	2.720			
HADHB	0.000	0.006	0.190	2.210			
AKR1A1	0.000	0.006	0.281	3.750			
MON2	0.000	0.006	0.156	2.040			
PPAP2B	0.000	0.007	0.296	4.500			
SLC1A4	0.000	0.008	0.190	2.470			

TABLE S3 | Continued

Gene (leading protein)	Pvalue BRAAK0-VI	FDR BRAAK0-VI	Slope BRAAK0-VI (LFQintensity Log2)	Max. fold change BRAAK0-VI	Pvalue BRAAK0-III	FDR BRAAK0-III	Slope BRAAK0-III (LFQintensity Log2)
EEF1A1	0.000	0.008	0.187	2.050			
NADKD1	0.000	0.009	0.328	Inf			
PEA15	0.000	0.009	0.175	2.630			
FYN	0.000	0.009	0.177	2.260			
TNC	0.001	0.010	0.869	Inf			
MLC1	0.001	0.010	0.472	Inf			
ACAA2	0.001	0.010	0.210	2.470			
LAMB2	0.001	0.011	0.320	3.610			
HSPA2	0.001	0.011	0.293	6.670			
CAPN2	0.001	0.012	0.197	2.330			
RAB6A	0.001	0.014	0.139	2.020			
CMBL	0.001	0.014	0.214	3.650			
KBTBD11	0.001	0.014	0.122	1.910			
ARHGDIA	0.001	0.014	0.303	4.870			
CD44	0.001	0.016	0.496	7.800			
ITGB1	0.001	0.016	0.190	3.190			
CTNNA2	0.001	0.017	0.170	2.860			
C4A	0.001	0.019	0.510	12.550			
MRPL19	0.001	0.019	0.538	Inf			
CA2	0.001	0.022	0.252	2.450			
ALDH6A1	0.002	0.022	0.239	3.510			
CLIC1	0.002	0.022	0.222	2.590			
FERMT2	0.002	0.025	0.203	2.770			
AK1	0.002	0.027	0.168	2.720			
HDHD3	0.002	0.027	0.372	Inf			
HINT2	0.002	0.027	0.185	2.270			
COTL1	0.002	0.027	0.197	2.860			
BLVRB	0.002	0.027	0.254	3.040			
HSPB6	0.002	0.028	0.483	Inf			
RBP1	0.002	0.029	0.359	Inf			
DPYSL3	0.002	0.029	0.259	3.990			
UBC	0.002	0.029	0.162	1.950			
NEFH	0.002	0.030	0.200	2.380			
AKR7A2	0.002	0.030	0.281	5.360			

TABLE S3 | Continued

Gene (leading protein)	Pvalue BRAAK0-VI	FDR BRAAK0-VI	Slope BRAAK0-VI (LFQintensity Log2)	Max. fold change BRAAK0-VI	Pvalue BRAAK0-III	FDR BRAAK0-III	Slope BRAAK0-III (LFQintensity Log2)
VCL	0.002	0.031	0.307	4.800			
GNAI2	0.002	0.032	0.132	2.170			
GPNMB	0.002	0.032	0.388	Inf			
PGAM1	0.003	0.033	0.139	2.010			
AK3	0.003	0.034	0.141	1.790			
PSME1	0.003	0.035	0.217	Inf			
STX8	0.003	0.036	0.182	Inf			
LGALS1	0.003	0.037	0.287	3.800			
GCLC	0.003	0.038	0.132	1.870			
TPI1	0.003	0.039	0.209	2.300			
FMNL2	0.003	0.039	0.163	2.470			
COMT	0.003	0.039	0.136	2.460			
MGST1	0.003	0.039	0.315	4.040			
HIBCH	0.003	0.040	0.160	2.240			
EGFR	0.004	0.042	0.260	Inf			
DDX6	0.004	0.044	0.309	5.360			
RAN	0.004	0.045	0.272	2.840			
ALDH2	0.004	0.045	0.110	1.640			
DDX3X	0.004	0.046	0.204	3.600			
SCRN1	0.004	0.046	0.121	1.690			
ANXA2	0.004	0.047	0.514	6.270			
TROVE2	0.004	0.048	0.189	3.510			
PDDC1	0.004	0.048	0.165	2.240			
RSU1	0.004	0.048	0.192	Inf			
GCSH	0.005	0.048	0.192	2.540			
HSPG2	0.005	0.050	0.347	7.940			
ERLIN2	0.005	0.051	0.180	2.650			
ALDH9A1	0.006	0.054	0.191	2.690			
ANK2	0.006	0.055	0.072	1.400			
SPTAN1	0.006	0.057	0.304	1.100			
SLC44A2	0.006	0.060	0.200	3.810			
TPPP3	0.006	0.060	0.201	Inf			
HGS	0.006	0.060	0.235	Inf			
ASAH1	0.007	0.063	0.087	1.500			

TABLE S3 | Continued

Gene (leading protein)	Pvalue BRAAK0-VI	FDR BRAAK0-VI	Slope BRAAK0-VI (LFQintensity Log2)	Max. fold change BRAAK0-VI	Pvalue BRAAK0-III	FDR BRAAK0-III	Slope BRAAK0-III (LFQintensity Log2)
PGD	0.007	0.067	0.265	4.300			
LDHB	0.008	0.070	0.096	1.690			
PPIB	0.008	0.072	0.265	3.290			
SNTA1	0.009	0.080	0.268	6.160			
RPL10A	0.009	0.081	0.187	3.200			
PGK1	0.010	0.081	0.163	2.390			
SNRPN	0.010	0.082	0.190	2.640			
HSD17B10	0.010	0.084	0.197	2.490			
HADH	0.010	0.085	0.195	2.790			
GSTM2	0.010	0.085	0.208	3.940			
IQGAP1	0.011	0.087	0.346	Inf			
SEPT7	0.011	0.088	0.093	1.710			
AKR1C3	0.011	0.088	0.207	2.500			
AGRN	0.011	0.090	0.149	2.290			
CAND2	0.012	0.091	0.494	Inf			
ANKFY1	0.012	0.092	0.163	2.130			
SACM1L	0.012	0.093	0.267	3.920			
GAD1	0.012	0.094	0.145	2.620			
HSPB8	0.012	0.095	0.334	Inf			
XRCC6	0.013	0.096	0.160	1.870			
G6PD	0.013	0.097	0.205	5.070			
ACAA1	0.013	0.097	0.157	Inf			
ARHGAP35	0.013	0.099	0.134	1.880			
SCARB2	0.013	0.100	0.127	1.970			

NOTE: Protein names and quantitative data on individual cases as present in original online version of supplementary table 3 can be found at http://dx.doi.org/10.1016/j.jalz.2015.11.002.

TABLE S3 | (decreased proteins)

Gene (leading protein)	Pvalue BRAAK0-VI	FDR BRAAK0-VI	Slope BRAAK0-VI (LFQintensity Log2)	Max. fold change BRAAK0-VI	Pvalue BRAAK0-III	FDR BRAAK0-III	Slope BRAAK0-III (LFQintensity Log2)
AMPH	0.003	0.035	-0.104	1.650	0.000	0.353	-0.254
GNAZ	0.000	0.004	-0.088	1.550	0.001	0.353	-0.179
MTDH	0.009	0.078	-0.156	2.450	0.001	0.353	-0.516
AP2B1	0.000	0.006	-0.068	1.510	0.001	0.353	-0.150
MAP2K4	0.000	0.006	-0.150	2.150	0.001	0.353	-0.247
CYTH3	0.001	0.013	-0.152	2.570	0.002	0.381	-0.313
ATP6V1C1	0.010	0.081	-0.081	1.540	0.003	0.381	-0.206
NCKAP1	0.000	0.001	-0.130	1.810	0.003	0.381	-0.212
MTCH1	0.011	0.085	-0.149	1.950	0.004	0.381	-0.306
CACNA2D1	0.000	0.000	-0.217	2.720	0.005	0.381	-0.189
NDUFB9	0.001	0.013	-0.126	1.690	0.007	0.445	-0.218
AP3D1	0.008	0.070	-0.265	4.360	0.007	0.445	-0.589
CADM1	0.003	0.037	-0.139	2.160	0.007	0.445	-0.284
DPP6	0.000	0.000	-0.159	2.040	0.009	0.450	-0.204
TWF2	0.001	0.015	-0.218	3.030	0.009	0.450	-0.463
AP2A1	0.000	0.005	-0.082	1.430	0.009	0.450	-0.115
TIMM44	0.006	0.058	-0.098	1.700	0.009	0.450	-0.239
GARS	0.004	0.048	-0.086	1.460	0.009	0.450	-0.168
PPP2R1A	0.000	0.005	-0.105	1.770	0.010	0.450	-0.181
VPS35	0.007	0.062	-0.057	1.330	0.010	0.452	-0.142
PRKAR2B	0.000	0.000	-0.301	3.060	0.010	0.452	-0.246
THY1	0.001	0.018	-0.160	2.180	0.011	0.452	-0.304
SCYL2	0.010	0.085	-0.171	2.480	0.012	0.470	-0.375
CDH13	0.000	0.003	-0.203	2.080	0.013	0.500	-0.211
CAMK2A	0.000	0.000	-0.202	2.340	0.016	0.526	-0.184
KCNAB2	0.008	0.070	-0.372	Inf	0.016	0.526	-0.389
EXOC3	0.005	0.053	-0.230	2.800	0.018	0.537	-0.475
ARPC3	0.000	0.001	-0.132	2.070	0.019	0.551	-0.168
ABI2	0.004	0.048	-0.206	3.530	0.021	0.551	-0.347
TUBB3	0.000	0.001	-0.137	1.990	0.021	0.551	-0.193
SH3GL2	0.010	0.085	-0.091	1.620	0.022	0.551	-0.193
PGM2L1	0.000	0.000	-0.171	2.510	0.024	0.551	-0.181
LETM1	0.000	0.006	-0.091	1.660	0.024	0.551	-0.152
TUBB4B	0.000	0.000	-0.103	1.600	0.024	0.551	-0.134

TABLE S3 | Continued

Gene (leading protein)	Pvalue BRAAK0-VI	FDR BRAAK0-VI	Slope BRAAK0-VI (LFQintensity Log2)	Max. fold change BRAAK0-VI	Pvalue BRAAK0-III	FDR BRAAK0-III	Slope BRAAK0-III (LFQintensity Log2)
TUBB	0.000	0.005	-0.142	2.300	0.025	0.551	-0.232
G3BP2	0.000	0.009	-0.438	7.950	0.025	0.551	-0.694
NDRG4	0.001	0.010	-0.178	2.120	0.026	0.551	-0.200
GNAO1	0.004	0.048	-0.069	1.440	0.026	0.551	-0.148
PACSIN1	0.000	0.010	-0.160	1.990	0.027	0.551	-0.230
ACTR3B	0.004	0.042	-0.217	3.140	0.028	0.551	-0.343
SNAP91	0.000	0.009	-0.100	1.780	0.030	0.551	-0.171
TARS	0.005	0.049	-0.117	1.640	0.032	0.551	-0.230
ACTN1	0.000	0.000	-0.149	1.820	0.032	0.551	-0.127
PSMD12	0.000	0.007	-0.165	2.520	0.033	0.551	-0.271
RTN1	0.004	0.048	-0.152	2.070	0.035	0.564	-0.287
GRIA2	0.000	0.001	-0.213	2.990	0.038	0.568	-0.181
STX1B	0.000	0.006	-0.084	1.480	0.038	0.568	-0.124
TUBAL3	0.006	0.054	-0.201	2.690	0.039	0.568	-0.326
RAB1B	0.009	0.079	-0.055	1.300	0.039	0.568	-0.104
GNAI1	0.001	0.019	-0.108	1.580	0.040	0.568	-0.146
BRK1	0.010	0.081	-0.142	2.060	0.041	0.568	-0.180
AP1G1	0.008	0.072	-0.073	1.550	0.042	0.568	-0.119
NSF	0.000	0.000	-0.108	1.550	0.043	0.568	-0.081
TAGLN3	0.006	0.054	-0.120	1.770	0.047	0.595	-0.201
COPS4	0.001	0.011	-0.138	1.920	0.050	0.612	-0.191
PRNP	0.005	0.048	-0.175	2.620	0.052	0.615	-0.275
ICAM5	0.000	0.001	-0.172	2.210	0.052	0.615	-0.150
RAB3D	0.010	0.085	-0.198	Inf	0.054	0.623	-0.282
ANKS1B	0.000	0.000	-0.298	2.900			
GRIA1	0.000	0.000	-0.373	4.840			
PRKCG	0.000	0.000	-0.182	2.060			
PPP3CA	0.000	0.000	-0.170	1.860			
SYT1	0.000	0.000	-0.099	1.450			
HPCA	0.000	0.000	-0.197	2.380			
RTN1	0.000	0.000	-0.160	1.880			
TUBB2B	0.000	0.000	-0.113	1.780			
BSG	0.000	0.000	-0.200	2.310			
PPP3R1	0.000	0.001	-0.200	2.150			

TABLE S3 | Continued

Gene (leading protein)	Pvalue BRAAK0-VI	FDR BRAAK0-VI	Slope BRAAK0-VI (LFQintensity Log2)	Max. fold change BRAAK0-VI	Pvalue BRAAK0-III	FDR BRAAK0-III	Slope BRAAK0-III (LFQintensity Log2)
PCDH1	0.000	0.001	-0.182	2.380			
NPTN	0.000	0.001	-0.203	2.350			
GNG4	0.000	0.002	-0.279	2.660			
RASAL1	0.000	0.003	-0.266	3.780			
AP3S1	0.000	0.003	-0.129	2.140			
TUBA4A	0.000	0.003	-0.098	1.590			
NAPB	0.000	0.003	-0.095	1.530			
CYFIP2	0.000	0.003	-0.086	1.380			
CORO1C	0.000	0.003	-0.255	2.970			
HK1	0.000	0.003	-0.075	1.530			
LSAMP	0.000	0.003	-0.115	1.600			
PPP3CB	0.000	0.003	-0.128	1.730			
RGS14	0.000	0.003	-0.272	3.140			
HSPA12A	0.000	0.003	-0.124	1.640			
TUBA1C	0.000	0.003	-0.099	1.600			
NDUFS2	0.000	0.003	-0.139	1.820			
ARPC2	0.000	0.004	-0.112	1.540			
PRKACB	0.000	0.004	-0.128	1.780			
GRIA3	0.000	0.004	-0.216	2.090			
CORO1A	0.000	0.004	-0.172	2.510			
NIPSNAP1	0.000	0.004	-0.155	1.950			
FAM49A	0.000	0.005	-0.144	1.760			
DLAT	0.000	0.005	-0.084	1.510			
ATP2B1	0.000	0.005	-0.114	1.780			
MAP2K1	0.000	0.005	-0.168	1.940			
TUBB4A	0.000	0.006	-0.096	1.630			
SYNGAP1	0.000	0.006	-0.224	2.950			
NCDN	0.000	0.006	-0.119	1.750			
ACTR2	0.000	0.006	-0.127	1.830			
PRKCB	0.000	0.006	-0.119	1.750			
VPS28	0.000	0.007	-0.220	2.590			
ARL15	0.000	0.008	-0.238	2.740			
PDHB	0.000	0.009	-0.090	1.710			
NDUFS8	0.000	0.009	-0.149	1.860			

TABLE S3 | Continued

Gene (leading protein)	Pvalue BRAAK0-VI	FDR BRAAK0-VI	Slope BRAAK0-VI (LFQintensity Log2)	Max. fold change BRAAK0-VI	Pvalue BRAAK0-III	FDR BRAAK0-III	Slope BRAAK0-III (LFQintensity Log2)
RPS7	0.000	0.009	-0.131	1.850			
DYNC1I1	0.000	0.010	-0.132	1.800			
CAMK2B	0.000	0.010	-0.146	1.780			
RAB2A	0.001	0.010	-0.086	1.530			
CUL1	0.001	0.010	-0.115	1.560			
RAB3A	0.001	0.010	-0.087	1.580			
PAK1	0.001	0.011	-0.201	2.370			
NDUFA12	0.001	0.011	-0.087	1.520			
ATP1B1	0.001	0.011	-0.091	1.520			
NDUFS1	0.001	0.012	-0.093	1.500			
DNM1	0.001	0.013	-0.060	1.340			
TXNDC5	0.001	0.013	-0.354	5.460			
AP2M1	0.001	0.014	-0.105	1.660			
CAMKV	0.001	0.014	-0.133	1.950			
PEX3	0.001	0.015	-0.315	4.620			
CUL2	0.001	0.017	-0.254	2.900			
ATP6V0C	0.001	0.017	-0.163	2.070			
ACTN2	0.001	0.019	-0.185	2.300			
FAM49B	0.001	0.019	-0.096	1.480			
PDE2A	0.001	0.020	-0.174	2.100			
NDUFA9	0.001	0.021	-0.114	1.670			
PTPRS	0.001	0.021	-0.086	1.470			
CUL3	0.001	0.022	-0.078	1.470			
SYP	0.001	0.022	-0.119	2.320			
ATP2B2	0.001	0.022	-0.137	2.000			
LANCL2	0.002	0.023	-0.282	4.910			
RARS	0.002	0.025	-0.263	3.240			
NEGR1	0.002	0.025	-0.144	1.840			
PRKACA	0.002	0.025	-0.156	2.130			
RAB27B	0.002	0.025	-0.196	2.740			
TIMM10	0.002	0.027	-0.258	Inf			
MAPRE3	0.002	0.029	-0.103	1.560			
GLS	0.002	0.030	-0.083	1.530			
PVRL1	0.002	0.031	-0.168	2.210			

TABLE S3 | Continued

Gene (leading protein)	Pvalue BRAAK0-VI	FDR BRAAK0-VI	Slope BRAAK0-VI (LFQintensity Log2)	Max. fold change BRAAK0-VI	Pvalue BRAAK0-III	FDR BRAAK0-III	Slope BRAAK0-III (LFQintensity Log2)
ACTR3	0.002	0.031	-0.106	1.740			
TMEM30A	0.002	0.031	-0.188	2.880			
TUSC2	0.002	0.031	-0.111	1.690			
CADM2	0.003	0.034	-0.207	2.410			
TNS1	0.003	0.035	-0.235	Inf			
GOT2	0.003	0.037	-0.094	1.620			
ATP2A2	0.003	0.039	-0.109	1.680			
CYLD	0.003	0.040	-0.132	Inf			
RAB4B	0.003	0.040	-0.175	2.400			
ATP6AP2	0.003	0.041	-0.144	1.980			
PTPN9	0.004	0.044	-0.143	1.700			
COX7A2L	0.004	0.046	-0.123	1.850			
OTUB1	0.004	0.047	-0.086	1.590			
SEPT5	0.004	0.047	-0.083	1.690			
OPA1	0.004	0.048	-0.128	1.800			
IMMT	0.005	0.048	-0.064	1.340			
BMP2KL	0.005	0.048	-0.107	1.600			
AGO61	0.005	0.048	-0.191	2.460			
GPD2	0.005	0.048	-0.071	1.470			
CAP2	0.005	0.050	-0.140	2.140			
TOM1L2	0.005	0.050	-0.205	2.370			
SLC8A2	0.005	0.050	-0.124	1.670			
CAMK1D	0.005	0.050	-0.100	1.720			
AGAP3	0.005	0.051	-0.136	1.900			
CCT3	0.005	0.052	-0.100	1.660			
ATP5C1	0.005	0.053	-0.081	1.420			
C17orf108	0.005	0.053	-0.254	3.540			
GDAP1	0.005	0.054	-0.077	1.540			
ATP6V0D1	0.006	0.055	-0.097	1.800			
CLTA	0.006	0.055	-0.153	2.020			
DNM1L	0.006	0.055	-0.090	1.560			
PDCD6IP	0.006	0.059	-0.137	2.260			
MBLAC2	0.006	0.060	-0.108	1.810			
BIN1	0.006	0.060	-0.129	1.910			

TABLE S3 | Continued

Gene (leading protein)	Pvalue BRAAK0-VI	FDR BRAAK0-VI	Slope BRAAK0-VI (LFQintensity Log2)	Max. fold change BRAAK0-VI	Pvalue BRAAK0-III	FDR BRAAK0-III	Slope BRAAK0-III (LFQintensity Log2)
NAP1L4	0.006	0.060	-0.097	1.600			
SV2B	0.007	0.062	-0.179	2.990			
NRN1	0.007	0.062	-0.332	6.890			
SAMM50	0.007	0.063	-0.082	1.560			
LRRC57	0.007	0.065	-0.100	1.610			
UQCRC1	0.007	0.066	-0.073	1.900			
CD200	0.007	0.068	-0.187	2.170			
IGSF21	0.007	0.068	-0.146	1.920			
GRIN1	0.008	0.070	-0.181	2.300			
MGLL	0.008	0.071	-0.129	2.070			
PTGES2	0.008	0.073	-0.096	1.500			
NDUFA13	0.009	0.074	-0.092	1.510			
C14orf166	0.009	0.074	-0.108	1.720			
SEP15	0.009	0.074	-0.122	2.020			
CHCHD3	0.009	0.075	-0.135	2.070			
MAL2	0.009	0.076	-0.150	2.100			
ATP5H	0.009	0.080	-0.062	1.640			
TUBA8	0.010	0.083	-0.169	3.260			
KCNAB2	0.010	0.085	-0.127	1.870			
ATP6AP1	0.010	0.085	-0.193	3.930			
MAB21L2	0.010	0.085	-0.107	Inf			
UQCRQ	0.010	0.085	-0.121	2.100			
WASF1	0.010	0.085	-0.167	2.690			
C6orf136	0.011	0.085	-0.185	2.170			
NCS1	0.011	0.085	-0.119	1.700			
FAM162A	0.011	0.085	-0.103	1.660			
ASH1L	0.011	0.086	-0.231	3.560			
AFG3L2	0.011	0.088	-0.108	1.640			
CADM3	0.011	0.090	-0.120	1.940			
YARS	0.012	0.091	-0.101	1.580			
RAB39B	0.012	0.091	-0.111	1.730			
RAC1	0.012	0.091	-0.070	1.450			
CD47	0.012	0.091	-0.124	2.230			
NDUFB6	0.013	0.097	-0.148	2.420			

TABLE S3 | Continued

Gene (leading protein)	Pvalue BRAAK0-VI	FDR BRAAK0-VI	Slope BRAAK0-VI (LFQintensity Log2)	Max. fold change BRAAK0-VI	Pvalue BRAAK0-III	FDR BRAAK0-III	Slope BRAAK0-III (LFQintensity Log2)
AGK	0.013	0.097	-0.139	1.730			
MTX2	0.013	0.099	-0.142	2.280			

NOTE: Protein names and quantitative data on individual cases as present in original online version of supplementary table 3 can be found at http://dx.doi.org/10.1016/j.jalz.2015.11.002.

TABLE S4 can be found at http://dx.doi.org/10.1016/j.jalz.2015.11.002.

TABLE S5 can be found at http://dx.doi.org/10.1016/j.jalz.2015.11.002.

CHAPTER 3

The proteome of granulovacuolar degeneration and neurofibrillary tangles in Alzheimer's disease

David C Hondius[1,2,§], Frank Koopmans[2,§], Conny Leistner[2], Débora Pita-Illobre[2], Regina M Peferoen-Baert[1], Fenna Marbus[1], Iryna Paliukhovich[2], Ka Wan Li[2], Annemieke JM Rozemuller[1], Jeroen JM Hoozemans[1*] and August B Smit[2*]

[1]Department of Pathology, Amsterdam Neuroscience, Amsterdam University Medical Centers, Location VUmc, Amsterdam, The Netherlands.

[2]Department of Molecular and Cellular Neurobiology, Center for Neurogenomics and Cognitive Research, Amsterdam Neuroscience, VU University Amsterdam, The Netherlands

[*]Contributed equally, [§]shared first authors

Acta Neuropathologica 2021 Mar 141(3):341-358.

ABSTRACT

Granulovacuolar degeneration (GVD) is a common feature in Alzheimer's disease (AD). The occurrence of GVD is closely associated with that of neurofibrillary tangles (NFTs) and GVD is even considered to be a pre-NFT stage in the disease process of AD. Currently, the composition of GVD bodies, the mechanisms associated with GVD and how GVD exactly relates to NFTs is not well understood.

By combining immunohistochemistry (IHC) and laser microdissection (LMD) we isolated neurons with GVD and those bearing tangles separately from human post-mortem AD hippocampus (n=12) using their typical markers casein kinase (CK)1δ and phosphorylated tau (AT8). Control neurons were isolated from cognitively healthy cases (n=12). 3000 neurons per sample were used for proteome analysis by label free LC-MS/MS.

In total 2596 proteins were quantified across samples and a significant change in abundance of 115 proteins in GVD and 197 in tangle bearing neurons was observed compared to control neurons. With IHC the presence of PPIA, TOMM34, HSP70, CHMP1A, TPPP and VXN was confirmed in GVD containing neurons. We found multiple proteins localizing specifically to the GVD bodies, with VXN and TOMM34 being the most prominent new protein markers for GVD bodies. In general, protein groups related protein folding, proteasomal function, the endolysosomal pathway, microtubule and cytoskeletal related function, RNA processing and glycolysis were found to be changed in GVD neurons. In addition to these protein groups, tangle bearing neurons show a decrease in ribosomal proteins, as well as in various proteins related to protein folding.

This study, for the first time, provides a comprehensive human based quantitative assessment of protein abundances in GVD and tangle bearing neurons. In line with previous functional data showing that tau pathology induces GVD, our data support the model that GVD is part of a pre-NFT stage representing a phase in which proteostasis and cellular homeostasis is disrupted. Elucidating the molecular mechanisms and cellular processes affected in GVD and its relation to the presence of tau pathology is highly relevant for the identification of new drug targets for therapy.

INTRODUCTION

Besides amyloid plaques and neurofibrillary tangles (NFTs), AD pathology is commonly featured by the presence of granulovacuolar degeneration (GVD) in neurons. GVD appears as rimmed vacuoles that are up to 5μm in diameter, harbouring a dense core, and are visible in a standard haematoxylin stain. These GVD bodies initially emerge predominantly in hippocampal pyramidal neurons in the hippocampal regions CA1, CA2 and subiculum. In later stages of AD, GVD presents in other brain regions, such as the temporal lobe, the hypothalamus and the amygdala [68]. Various studies [19, 23, 29, 46, 77] have pointed at an association between GVD and the onset of tau pathology. GVD is observed in non-demented cases that have a low Braak stage for tau pathology and is considered to be part of pre-clinical AD or normal aging. A gradual increase in the fraction of neurons with GVD is observed with the progression of AD and correlates with the increase of tau pathology in these regions [29, 47]. GVD is also present in Down's syndrome and primary tauopathies [45, 62, 65], as well as frontotemporal dementia cases with C9orf72 mutations and alpha synucleinopathies, such as Parkinson's disease (PD), Lewy body dementia (LBD) and multiple system atrophy (MSA) [18, 38, 58]. This indicates that GVD is not exclusively associated with the aggregation of tau, but occurs more broadly in neurodegenerative diseases affected by intracellular protein aggregates.

The cause or function of GVD in neurodegeneration is elusive. GVD bodies are known to contain proteins involved in the unfolded protein response (pPERK, pIRE1 and peIF2α) [19, 30], the endocytosis pathway (CHMP2B) [76] and late stage autophagy (LAMP1 and to some extent cathepsin-D) [10] representing mechanisms that are thought to manage an overload of misfolded proteins. Also necrosome activation markers were detected in GVD bodies as a possible cause of neuronal loss by delayed necroptosis [31]. In addition, various kinases are present in GVD including the protein kinases casein kinase 1 (CK1) α, δ and ε, and are commonly used markers to visualize GVD bodies [12]. These protein kinases are involved in numerous cellular processes and are capable of tau phosphorylation [28, 63]. The increased presence of the aforementioned proteins in GVD affected neurons points towards activation or malfunction of various cellular mechanisms related to stress responses, protein folding and protein degradation.

For various reasons it is hypothesized that GVD in AD brain is associated with an early stage in neurofibrillary tangle formation [29]. GVD frequently occurs in so-called pre-tangle neurons defined as neurons with diffuse hyperphosporylated tau (pTau) immunoreactivity [19]. GVD bodies are present in neurons with markers of early tangle formation including truncated tau, early pTau epitopes and high 4-repeat tau presence, but is not associated with late pTau markers like AT100 and AT270 and the presence of 3-repeat tau [15, 46]. Also, kinases that are known to phosphorylate tau are present in GVD containing neurons [6, 12, 34, 37, 44]. Although GVD is closely associated with markers for cellular stress and early stages of tau phosphorylation, it remains unclear whether GVD is a separate pathological process or part of a pre-stage of the neurofibrillary tangle. Currently, no comprehensive human based quantitative

assessment of protein abundances on GVD and tangle bearing neurons has been performed which could support this hypothesis. In addition, elucidating the molecular mechanisms and cellular processes affected in GVD and its relation to tangle pathology is highly relevant for the identification of new drug targets for future therapy.

To increase our insight in the role of GVD in the pathogenesis of AD, we have applied a combination of immunohistochemistry (IHC), cellular-resolution laser microdissection (LMD) and subsequently a mass spectrometry (LC-MS/MS) driven proteomics analysis. We isolated and analysed the proteome of separate populations of hippocampal pyramidal neurons, namely; 1) neurons with CK1δ positive GVD bodies, 2) neurons with pTau positive tangles, and 3) neurons negative for both CK1δ and pTau. This approach provides a highly sensitive, unbiased quantification of proteins at cellular resolution. Specifically, we were able to identify prominent cellular mechanisms involved in GVD, and show the coherence between GVD affected neurons and those with neurofibrillary tangles, supporting a model in which GVD is part of an early phase in tau pathology.

MATERIAL AND METHODS

Case selection

Post mortem brain tissue was obtained from the Netherlands Brain Bank (NBB), Netherlands Institute for Neuroscience (NIN), Amsterdam. All brain tissue was collected from donors with written informed consent for brain autopsy and the use of brain tissue and clinical information for research purposes. The brain donor program of the NBB was approved by the local medical ethics committee of the VU university medical center (Ref#2009/148). Brain tissue was selected based on clinical and neuropathological reports. Control cases used for proteomics had very little to no abnormalities including Aβ, tau, GVD, α-synuclein or p62 pathology in the hippocampus and were cognitively healthy. AD cases used for proteomics were typical AD cases with severe tau pathology in the hippocampus, but no other comorbidities in the hippocampal region. Per group 12 cases were used for LC/MS-MS analysis which are listed in Table 1. Samples were analysed in two separate batches which consisted of 6 cases per group, marked by batch "A" and batch "B" in table 1. Cases used for validation are listed in Table S1. AD pathology present as Aβ deposits, neurofibrillary tangles and neuritic plaques was staged [2, 3, 40] and also the ABC score is provided [2, 3, 40, 41, 67].

TABLE 1 | Cases used for mass spectrometry analysis

Batch	Case	Braak tau	Braak Aβ	ABC score	Gender	Age at death	PMD hh:mm	APOE genotype
1	Control 1	0	0	A0B0C0	M	56	9:15	ε3 ε4
1	Control 2	0	0	A0B0C0	M	74	8:05	ε3 ε3
1	Control 3	0	0	A0B0C0	M	49	6:15	ε2 ε3
1	Control 4	0	0	A0B0C0	M	76	6:45	ε3 ε3
1	Control 5	0	0	A0B0C0	F	62	5:00	ND
1	Control 6	0	0	A0B0C0	F	64	5:40	ε2 ε3
2	Control 7	1	A	A1B1C0	F	71	7:10	ε2 ε3
2	Control 8	1	0	A0B1C0	M	64	8:25	ε3 ε3
2	Control 9	0	0	A0B0C0	M	51	7:45	ε3 ε4
2	Control 10	1	0	A0B1C0	M	78	17:40	ε3 ε3
2	Control 11	1	0	A0B1C0	F	50	4:10	ND
2	Control 12	1	B	A1B1C0	M	80	3:18	ND
1	AD 1	6	B	A2B3C3	M	65	5:40	ε3 ε3
1	AD 2	5	C	A3B3C3	F	77	7:00	ε3 ε3
1	AD 3	5	C	A3B3C3	F	89	10:20	ε3 ε3
1	AD 4	5	C	A3B3C3	F	78	4:35	ε3 ε4
1	AD 5	6	C	A3B3C3	F	64	5:30	ε3 ε4
1	AD 6	5	C	A3B3C3	F	82	6:00	ε4 ε4
2	AD 7	5	C	A3B3C3	M	84	4:50	ε3 ε4
2	AD 8	5	C	A3B3C3	F	78	8:25	ND
2	AD 9	5	C	A3B3C3	F	81	6:10	ND
2	AD 10	5	C	A3B3C3	M	65	6:50	ε3 ε4
2	AD 11	6	C	A3B3C3	F	65	6:40	ε3 ε3
2	AD 12	6	C	A3B3C3	M	62	8:15	ND

AD: Alzheimer's disease, PMD: post-mortem delay, M: male, F: female, ND: not determined.

Fast immunohistochemistry for laser microdissection (LMD)

Sample preparation for mass spectrometry was performed as previously described [17]. Briefly, sections (10 µm) of fresh-frozen human hippocampus were mounted on PEN-membrane slides (Leica Wetzlar, Germany), air-dried and fixed in 100% ethanol for 1 minute. After air-drying the tissue was wetted with sterile phosphate-buffered saline (PBS) pH 7.4.

Tissue sections were immunostained for CK1δ (SantaCruz, sc-55553) at a 1:25 dilution in PBS pH 7.4 to detect GVD bodies, neurofibrillary tangles were detected using a pTau (AT8) antibody (Pierce Biotechnology, Rockford, IL, USA) at a 1:100 dilution in PBS pH 7.4. Both were incubated for 20 minutes and then briefly washed in sterile PBS pH 7.4 (3 x 30 sec). Next, HRP labelled rabbit anti-mouse (DAKO, Glostrup, Denmark) was applied at a 1:100 dilution in sterile PBS and

incubated for 15 minutes at RT and again briefly washed in sterile PBS pH 7.4 (3 x 30 sec). Freshly prepared 3,3' diaminobenzidine (DAB) solution (DAKO) was applied and left to incubate for 5 minutes to visualize antibody binding. Sections were thoroughly washed in ultra-pure H_2O and incubated with 1% (w/v) toluidine blue (Fluka Analytical, Buchs, Switzerland) in ultrapure H_2O for 1 minute as a counterstain. The toluidine blue counterstain allowed identification of control neurons in which no immunoreactivity was present. Sections were then washed in ultra-pure H_2O twice for 1 minute and twice in 100% ethanol for 1 minute and air dried.

Isolation of individual neurons using LMD

LMD was performed using a Leica LMD6500 system (Leica, Wetzlar, Germany). Control neurons were isolated from the CA1 and subiculum region in the hippocampus from healthy control cases that were negative for AT8 immunoreactivity and had no GVD marked by granular CK1δ staining. Neurons with GVD, marked by CK1δ staining, and tangle bearing neurons marked by AT8 positivity were isolated from the same region from AD cases (Fig. 1).

Per sample approximately 3.000 individual neurons were collected into caps of tubes (Sapphire PCR/Tubes, 0.5ml Greiner Bio-One, Solingen, Germany) containing 30 µl M-PER lysis buffer (Thermo Scientific) supplemented with reducing SDS sample buffer (Thermo Scientific). Micro-dissected tissue was stored at -80 °C until further use.

Protein in-gel digestion

Micro-dissected tissue lysates were incubated at 95 °C for 5 min to denature the proteins followed by incubation with 50 mM iodoacetamide for 30 minutes at room temperature (RT) in the dark. Samples were loaded onto a 10% acrylamide gel, of 1 mm thickness. Gels were composed of 10% acrylamide, 0.375M Tris–HCl (pH 8.8), ultra-pure H_2O, 0.1% (w/v) APS and 6 mL N,N,N',N'-tetramethylethylene-diamine (TEMED) per gel. Proteins were allowed to migrate into the gel by electrophoresis (150 V), until the sample progressed in the gel for a length of approximately 8–10 mm.

Gels were fixed overnight in a solution containing 50% (v/v) ethanol and 3% (v/v) phosphoric acid in H_2O at RT and stained with Colloidal Coomassie Blue (34% (v/v) methanol, 3% (v/v) phosphoric acid, 15% (w/v) ammonium Sulphate, and 0.1% (w/v) Coomassie brilliant blue G-250, for 1h while shaking. The gel was washed in ultra-pure water under gentle agitation for several hours to reduce background staining. Per sample the part of the gel containing the proteins was separated and cut into blocks of approximately 1 mm^3 and collected in an Eppendorf tube. Gel fragments were destained in ultrapure water with 50 mM NH_4HCO_3 and 50% (v/v) acetonitrile overnight. Gel fragments were dehydrated using acetonitrile for 20 min and dried for 30 min using a speedvac. The gel parts were rehydrated in 70 µl of ultra-pure water containing 50 mM NH_4HCO_3 and 10 ug/ ml trypsin (sequence grade; Promega) and incubated overnight at 37 °C to facilitate digestion of the proteins. Peptides were extracted twice with a solution containing 0.1% (v/v) trifluoroacetic acid and 50% (v/v) acetonitrile for 20 min. The samples were dried using a speedvac and stored at -20 °C until further analysis.

Mass spectrometry analysis

Peptides of the individual sample fractions were dissolved in 12 µL of 0.1% (v/v) acetic acid. In the first set, the sample was loaded onto an Ultimate 3000 LC system (Dionex, Thermo Scientific). Peptides were trapped on a 5mm Pepmap100 C18 column (Dionex) and fractionated on a 200 mm Alltima C18 column (100 µm id,3 µm particle size). In the second set, the sample was loaded onto a nanoLC 425 system (Sciex) and fractionated on a 120 mm C18 column (150 µm id column packed with 1.9 µm Reprosil-Pur 120 C18-AQ beads). Acetonitrile concentration in the mobile phase in 0.1% formic acid was increased from 5 to 18% in 88 min, to 25% at 98 min, 40% at 108 min, and to 90% at 110 min. The flow rate was 400nL/min. Peptides were electrosprayed into an SCIEX TripleTOF® 5600 mass spectrometer using an ion spray voltage of 2.5 kV, curtain gas at 35 p.s.i., nebulizer gas at 15 p.s.i., and an interface heater temperature of 150 °C. The MS survey scan range was m/z 350–1250 acquired for 250ms. The top 20 precursor ions were selected for 85 ms per MS/MS acquisition, with a threshold of 90 counts. Dynamic exclusion was 16 s. Rolling CID function was activated, with an energy spread of 15 eV. Analysis of one sample (tangle bearing neurons) failed due to technical problems and was removed from the analysis leaving an n=11 for the tangle bearing neurons.

Protein inference and relative protein quantification

Raw files were first converted from WIFF to mzML using ProteoWizard's qtofpeakpicker (version 3) with parameters " --resolution 20000 --area 1 --threshold 1 --smoothwidth 1.1" analogous to Schubert et al [61].

MetaMorpheus (version 0.0.311) was used to analyse the raw data [64]. The Uniprot human reference proteome database (SwissProt + TrEMBL, version 2020-04) was used to annotate spectra. Mass calibration was based on an initial search with 25ppm mass tolerance for both precursor and product ions, the dissociation type was set to CID and Carbaminomethyl(C) and Oxidation(M) were set as fixed and variable modifications respectively. For the main search, mass tolerances from the calibration task were used and acetylation of protein N-terminus was added as a variable modification. Label-free quantification by FlashLFQ was performed at 5ppm peakfinding tolerance with match-between-runs enabled. Normalization was disabled in MetaMorpheus. All other settings were left at default. The false discovery rate (FDR) cutoff for peptide and proteins identification using MetaMorpheus was set to 1%.

Statistical analysis of differential protein expression

MS-DAP 0.2.6.3 (https://github.com/ftwkoopmans/msdap) was used for downstream analysis of the MetaMorpheus output. In each statistical contrast of condition A versus B, only peptides observed in both sample group A and B in at least 2 samples were selected (per cohort). Normalization of peptide abundance values was then applied to this data subset and finally MSqRob was used for differential testing at the peptide level, accounting for the cohorts as a random variable in the regression model [13, 14]. P-values were adjusted for multiple testing with the Benjamini-Hochberg False Discovery Rate (FDR) procedure, the threshold for significance was set to 5% FDR. All statistical results are available in Table S3. The mass

spectrometry proteomics data have been deposited to the ProteomeXchange Consortium via the PRIDE [52] partner repository with the dataset identifier PXD023199.

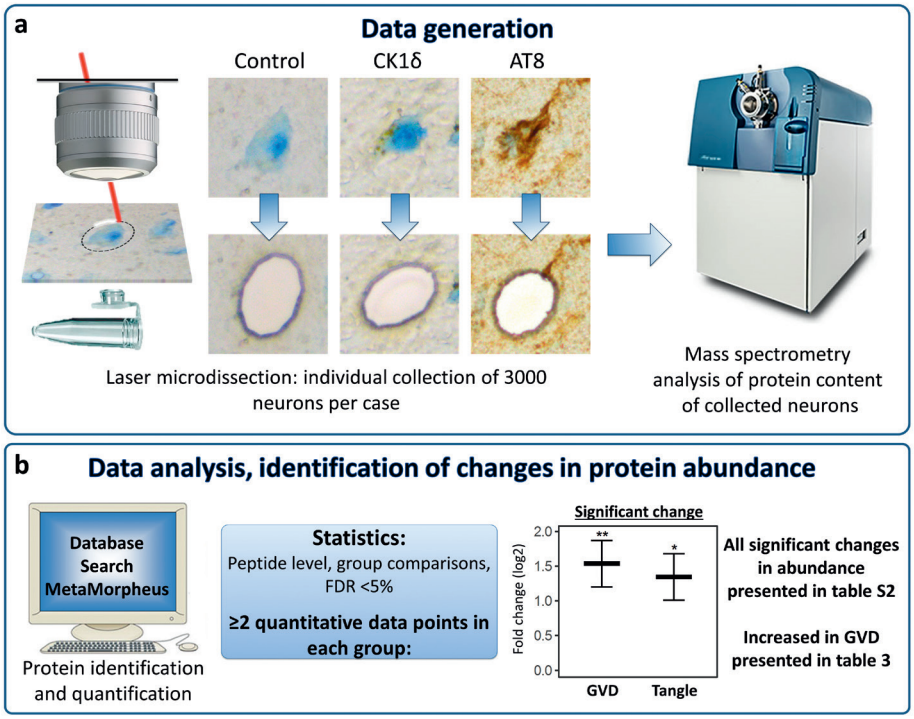

FIGURE 1 | Analysis workflow. Individual neurons were isolated from postmortem human hippocampal brain tissue by laser microdissection (LMD). Using immunohistochemistry three populations of neurons were visualized and isolated with high accuracy: 1. Control neurons, from cognitively healthy control cases that were negative for CK1δ and pTau (AT8) immunoreactivity, 2. granulovacuolar degeneration (GVD) bearing neurons, as recognised by the typical CK1δ positive granular staining pattern, and 3. pTau positive neurons, mostly tangle-bearing neurons, were isolated from AD cases. For each neuronal population 3000 individual neurons were isolated per case. The protein content of each sample was then analysed using mass spectrometry (a). Peptide level statistics were applied to identify proteins that are differentially expressed in neurons with GVD and neurons with pTau compared to control neurons (b). All resulting proteins are listed in table S2. The subset of proteins which are increased in GVD are listed in Table 3.

Immunohistochemical analysis

Paraffin embedded human hippocampus, of 71 cases representing all Braak stages for NFT pathology, was cut (5 µm) and the sections were placed on SuperFrost microscope slides (VWR) and air-dried overnight at 37 °C. Prior to staining the paraffin was removed by washing in xylene. Next, the sections were washed in decreasing concentrations of ethanol (100%, 96% and 70% (v/v)). Endogenous peroxidase activity was quenched by incubating in methanol with 0.3%

H_2O_2 for 30 minutes at RT. Next, antigen retrieval was performed by submerging the slides in citrate buffer (pH 6) and heating in an autoclave to 126 °C.

Primary antibodies (Table 2, Table S4) were diluted in normal antibody diluent (ImmunoLogic, Duiven, The Netherlands) and incubation was performed overnight at RT. After incubation the sections were thoroughly washed in PBS (pH 7.4), 3 times for 10 minutes followed by incubation with an HRP-labelled secondary antibody (Envision, DAKO) for 30 minutes. Again, the sections were thoroughly washed in PBS (pH 7.4) 3 times for 10 minutes and then incubated with DAB to visualize antibody binding. Counterstaining of the nuclei was performed by incubation in hematoxylin for 3 minutes followed by extensive washing in running tab water for 5 minutes. Next, the sections were dehydrated by incubation in increasing concentrations of ethanol consisting of 70% (v/v), 96% (v/v) and 100% (v/v) ethanol. The slides were then incubated in xylene and mounted using Quick-D mounting medium. A negative control was made by omission of the primary antibody. Primary antibodies used for data presented in the figures are present in Table 2 and all tested antibodies are listed in Table S4. Optimization of antibody dilution was achieved by titration of antibodies using both control and AD brain tissue.

TABLE 2 | Antibodies used in this study

Gene	Manufacturer	Order nr.	Clone	Species	Dilution IHC	Immunoblot	Fast IHC for MS
CK1δ	Santa Cruz	sc-55553	C-8	Mouse	1:800		1:25
Ck1ε	Santa Cruz	sc-25423	Polyclonal	Rabbit		1:1000	
pTau	ThermoFisher	MN1020	AT8	Mouse	1:800		1:100
VXN	OriGene	TA334828	Polyclonal	Rabbit	1:800	1:1000	
PPIA	Abcam	ab42408	Polyclonal	Rabbit	1:800		
TOMM34	Santa Cruz	sc-101284	S-05	Mouse	1:6400		
TOMM34	Protein tech	12196-1-AP	Polyclonal	Rabbit	1:6400		
HSP70	Santa Cruz	sc-24	W27	Mouse	1:200	1:1000	
CHMP1A	Santa Cruz	sc-271617	B-5	Mouse	1:12800		
TPPP	Santa Cruz	sc-515819	A-6	Mouse	1:3200		
CNDP2	Protein Tech	14925-1-AP	Polyclonal	Rabbit	1:6400		
PPIB	R&D systems	MAB5410	549205	Mouse		1:1000	

Assessment of the percentage of neurons with immunoreactivity for pTau and markers for GVD bodies.

The total number of neurons was determined in the CA1 and subiculum regions of the hippocampus. Unstained neurons were identified based on their morphology and the size of the nucleus. The number of neurons containing pTau (AT8) immunoreactivity or typical granular immunostaining of CK1δ, CK1ε, TOMM34 and VXN and a visible nucleus were determined. Differences between groups were identified using an ANOVA followed by Bonferroni's test for multiple comparisons. A p-value of <0.05 was considered significant.

Immunoblotting analysis

Protein extracts were prepared by lysis of hippocampal tissue in reducing SDS sample buffer. Proteins were denatured at 95 °C for 5 min separated by SDS-PAGE using Criterion™ TGX stain-free™ precast gels (Bio-Rad, Hercules, CA, USA) and transferred (100 V for 2 hours at 4 °C) onto a 0.45 µm PVDF membrane (Merck Millipore), which was pre-incubated in 100% methanol. Blocking of the membrane after transfer, was achieved using Odyssey blocking buffer (LI-COR). Subsequently the membrane was incubated with the primary antibody overnight. Primary antibodies and dilutions are listed in table 2.

After washing in Tris-buffered saline (pH 7.5) with 0.1% (v/v) Tween-20 (TBST) for 3 x 10 min, the membrane was incubated for 3h with the secondary antibody. Secondary antibodies used were IRDye 800 CW Goat anti-Rabbit (LI-COR Biosciences, Lincoln, NE, USA) and IRDye 680 Goat anti-Mouse (LI-COR Biosciences, Lincoln, NE) both at a 1:7000 dilution in Odyssey blocking buffer. Visualization was achieved using an Odyssey imaging system using excitation wavelengths of 700 nm and 800 nm. Total protein load was visualized using a chemidoc EZ (Bio-Rad) and the protein densitometric values were then used to normalize for their relative protein input. Quantification was performed using image-J software.

Gene ontology and pathway analysis

Gene ontology and pathway analysis was performed using g-profiler [56, 57]. The following databases were included: Gene ontology (GO), molecular function (MF), GO cellular component (CC), GO biological process (BP), KEGG pathways and Reactome pathways. G-profiler databases were updated July 2020. All detected proteins were used as a background dataset. Multiple testing corrected p-value was determined using Benjamini Hochberg FDR where an adjusted p-value of <0.05 was considered significant.

RESULTS

The proteomes of three populations of neurons from human post-mortem hippocampal tissue were assessed. These were (I) neurons with GVD marked by CK1δ positive granules (n=12) and (II) pTau (AT8) positive tangle bearing neurons, both from AD cases (n=12), and (III) neurons isolated from cognitively healthy control cases that contained no, or very little, AD related pathology (n=12) (Fig. 1). This analysis was performed in two separate batches containing an n=6 per group. Per case and for each sample 3000 neurons were analysed, resulting in an average quantification of 1981 (SD=137.5) proteins in control, 2034 (SD=120.9) proteins in CK1δ positive and 1935 (SD=146.6) proteins in pTau positive neurons in batch 1 and 2185 (SD=62.8) proteins in control, 2177 (SD=46.5) proteins in CK1δ positive and 2150 (SD=24.1) proteins in pTau positive neurons in batch 2. The integrated analysis accumulated in detecting a total of 2596 different proteins. There was no significant difference between the groups in the number of proteins identified within each batch (Fig. S1).

Proteins with altered abundance

To identify differentially expressed proteins in neurons with GVD or tangle bearing neurons compared to control a regular statistical approach was used for proteins with quantitative data in at least two cases per group (Fig 1b). We identified 92 proteins with significant higher expression level and 23 proteins with lower levels in the GVD bearing neurons and 82 proteins with significant higher expression level and 115 proteins with lower levels in the tangle bearing neurons, compared to control neurons (Fig. 2a). Proteins with increased expression in GVD compared to control are shown in Table 3. All proteins with an altered abundance in GVD and/or tangle bearing neurons are listed in Table S2, the complete dataset, with log2 fold changes and q-values in Table S3.

Within the differentially expressed groups of proteins, GVD and/or tangle bearing neurons versus controls, there are proteins unique to each group and proteins that are shared in GVD and tangle bearing neurons (Fig. 2a). There are relatively few proteins with decreased expression in the GVD positive neurons whereas in the tangle bearing neurons many proteins with decreased expression are observed.

The protein expression profile based on fold changes in GVD and tangle bearing neurons compared to control shows that most changes that occur in GVD and tangle bearing neurons are in the same direction, where the tangle bearing neurons generally show the largest change versus control. Only a small number of proteins is increased in GVD but not or less increased in tangle bearing neurons (Fig. 2b).

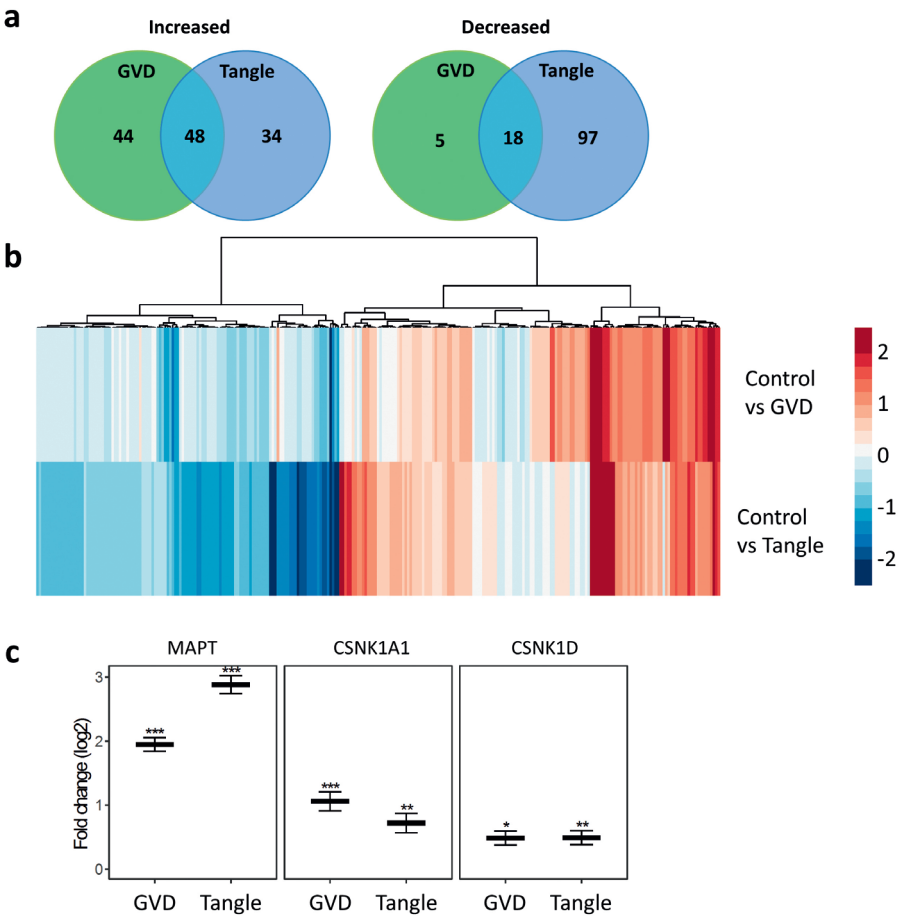

FIGURE 2 | Data overview. Shown are the number of proteins increased and decreased in each population and its overlap (a). The protein expression profile based on fold changes in GVD and tangle bearing neurons compared to control. Most differentially expressed proteins change in the same direction in GVD and tangle bearing neurons, in which tangle bearing neurons generally exhibit more severe changes. Few proteins are increased predominantly in GVD (b). Log2 fold changes of known markers of GVD, CSNK1A1 (CK1α) and CSNK1D (CK1δ) and tangles, MAPT (tau) are shown (c).

TABLE 3 | Proteins increased in GVD

Gene	Log2 FC C vs GVD	Log2 FC C vs Tangle	FDR C vs GVD	FDR C vs Tangle
MAPT	1.949	2.885	0.000	0.000
BRD2	1.785	0.404	0.004	ns
ARHGDIA	1.660	1.463	0.000	0.001
UBE2QL1	1.553	0.932	0.000	0.012
GFAP	1.538	1.575	0.000	0.001
PPIA	1.537	1.344	0.001	0.003
UBB*	1.434	2.051	0.000	0.000
CHMP1A	1.358	0.744	0.000	0.034
UNC13D	1.297	1.477	0.043	0.014
FKBP2	1.188	0.490	0.003	ns
PPIB	1.142	0.768	0.000	0.010
ENO1	1.128	1.070	0.012	0.026
PHPT1	1.065	0.000	0.005	ns
CSNK1A1	1.060	0.721	0.000	0.001
TOLLIP	1.006	0.933	0.023	0.028
PPIA	0.981	0.769	0.013	0.044
PEA15	0.980	0.838	0.000	0.000
PGAM1	0.957	0.914	0.000	0.001
TOMM34	0.944	0.793	0.000	0.000
CALR	0.928	0.416	0.002	ns
ENSG00000276612	0.862	0.797	0.003	0.045
HSPB1	0.807	1.064	0.000	0.000
CNRIP1	0.799	0.693	0.008	ns
PSD3	0.777	0.510	0.000	0.032
PITHD1	0.776	0.000	0.023	ns
ENO2	0.764	0.700	0.008	0.013
CLU	0.763	0.820	0.000	0.000
CBR1	0.755	0.637	0.000	0.009
HPCAL4	0.753	0.624	0.007	0.033
ENO1	0.752	0.829	0.015	0.005
MAP2	0.709	0.441	0.000	0.014
HPCA	0.709	0.432	0.019	ns
PAFAH1B3	0.709	0.365	0.001	ns
MLF2	0.704	0.409	0.000	0.040
DNAJB6	0.666	0.472	0.000	0.005
VIM	0.646	0.832	0.000	0.000
G3BP2	0.644	0.213	0.005	ns

TABLE 3 | Continued

Gene	Log2 FC C vs GVD	Log2 FC C vs Tangle	FDR C vs GVD	FDR C vs Tangle
SCRN1	0.644	0.530	0.005	0.034
CNDP2	0.642	0.642	0.003	0.016
SNX3	0.636	0.302	0.000	ns
EIF4H	0.608	0.439	0.000	0.007
GANAB	0.606	0.181	0.005	ns
HSD17B10	0.598	0.201	0.018	ns
AIMP1	0.577	0.000	0.020	ns
YWHAZ	0.569	0.498	0.002	0.006
CKB	0.568	0.391	0.044	ns
TKT	0.563	0.459	0.005	0.037
HSPA1B	0.554	0.445	0.003	0.020
EEF1B2	0.553	0.000	0.003	ns
TPI1	0.538	0.276	0.034	ns
PRDX5	0.533	0.468	0.008	0.033
GSN	0.523	0.437	0.005	0.064
VTI1B	0.519	0.161	0.044	ns
PALM	0.515	0.825	0.029	0.001
KARS1	0.514	0.183	0.001	ns
BLVRB	0.511	0.629	0.000	0.000
NEFL	0.502	0.398	0.000	0.015
CSNK1D	0.488	0.492	0.001	0.001
PAFAH1B1	0.478	0.325	0.044	ns
NEFM	0.478	0.362	0.000	0.059
SSB	0.478	0.000	0.001	ns
TPPP	0.473	0.462	0.022	0.008
PDIA3	0.456	0.000	0.004	ns
YWHAE	0.449	0.384	0.000	0.001
FSCN1	0.447	0.545	0.026	0.005
SYN1	0.441	0.458	0.043	0.062
PRKRA	0.438	0.000	0.004	ns
RTRAF	0.429	0.194	0.042	ns
AK1	0.405	0.368	0.003	0.020
NCL	0.398	0.000	0.013	ns
SNX12	0.392	0.259	0.026	ns
SDCBP	0.388	0.193	0.027	ns
EIF3CL	0.385	0.000	0.044	ns

TABLE 3 | Continued

Gene	Log2 FC C vs GVD	Log2 FC C vs Tangle	FDR C vs GVD	FDR C vs Tangle
CLINT1	0.379	0.000	0.017	ns
ANXA5	0.374	0.378	0.036	ns
INA	0.370	0.288	0.004	ns
CFL1	0.366	0.000	0.019	ns
PIN1	0.362	0.261	0.004	ns
MAP1B	0.352	0.072	0.002	ns
ATP6V1E1	0.341	0.400	0.008	0.022
VTA1	0.322	0.225	0.026	ns
CRYAB	0.321	0.576	0.048	0.043
HSPA8	0.295	0.331	0.046	0.006
ME1	0.290	0.071	0.001	ns
CAMK2D	0.289	0.070	0.026	ns
SND1	0.281	0.000	0.004	ns
LRRC47	0.275	0.000	0.005	ns
SUGT1	0.251	0.216	0.037	0.043
USO1	0.238	0.000	0.005	ns
PCBP1	0.222	0.000	0.020	ns
RAB6A	0.208	0.267	0.019	0.033
RTN4	0.207	0.129	0.044	ns

All proteins that have an increased abundance in GVD are shown. The full set of regulated proteins is presented in **Table S2.** * indicates this is the leading "razor protein", but based on the peptide data these proteins cannot be distinguished from some other highly similar proteins. These are presented in **Table S3**. FC; fold change, FDR; false discovery rate, ns; not significant, GVD; granulovacuolar degeneration.

Higher abundance and differential localization for selected proteins

Differentially expressed proteins included those known to be increased in AD, for example CSNK1A1 (CK1α), CSNK1D (CK1δ) and MAPT (Tau), which are associated with GVD and tau pathology respectively (Fig. 2d). The abundance of CK1δ and CK1α is increased in GVD bearing neurons and for CK1α to a lesser extent in tangle bearing neurons. MAPT on the other hand is increased in GVD and even more so in tangle bearing neurons.

Based on an increase in protein level in neurons with GVD and on antibody availability, 13 proteins were assessed by IHC (Fig. 3 and 4). Protein association with GVD and/or AD was confirmed by IHC with antibodies (Table 1) for PPIA, TOMM34, HSP70 (HSPA1B), CHMP1A and TPPP in at least n=3 per group. All tested antibodies are listed in Table S4. In addition, for proteins that have very low abundance in a particular group, proper statistical testing can be challenging as only few data points are available for statistics. In that case, differences in the number of peptides that are detected can be a useful indicator of a potential change in

expression. This differential detection in the number of individual peptides is then indicated as a z-score (Table S3). An example of a protein with a high z-score and data suggestive of a high increase in GVD is VXN (a.k.a. C8orf46), which was confirmed by additional IHC staining.

PPIA shows a strong increase in neuronal immunoreactivity that is localized to the GVD bodies (Fig. 4a, b). TOMM34 shows weak diffuse immunoreactivity across the neuronal cell body in control neurons. In AD, very strong immunoreactivity is present in cells with GVD bodies and the anti-TOMM34 antibody specifically stains GVD structures (Fig. 4c, d). Similar staining was observed using two different TOMM34 antibodies (Fig S2). HSP70 (HSPA1B) shows very little immunoreactivity in control cases and is increased in AD. Localization is mostly related to neurons, staining a proportion of the GVD bodies, and some glial cells (Fig. 4e, f). GVD is also visualized using 3 other HSP70 antibodies tested in this study (Fig S3). CHMP1A shows a granular staining pattern in control neurons. Surrounding the neurons also some immunoreactivity is found, that is possibly related to cellular protrusions. In AD, the level of immunoreactivity is largely increased in neurons, and mainly associated with cells containing GVD bodies and to a large extent localized in the GVD bodies (Fig. 4g, h). TPPP immunoreactivity is present in GVD bodies and in non-neuronal cells (Fig. 4i, j), presumably oligodendrocytes as the staining pattern matches a previous study by Kovacs et al. [32]. For VXN we observed a weak diffuse primarily neuronal staining in control tissue. An increase in immunoreactivity is seen in AD, that appears specifically localized in GVD bodies (Fig. 4m, n). In summary, IHC analysis of selected proteins that were found increased in laser-dissected GVD containing neurons, shows higher intensities in AD cases compared to control case and confirms the presence of these proteins in GVD.

When performing quantification of CK1ε, VXN, TOMM34 and PPIB using immunoblotting on whole hippocampal lysates of 7 control cases versus 6 AD cases, no significant change in abundance was found (Fig. S4), indicating that immunoblotting of whole hippocampal lysates does not provide sufficient resolution to match the laser-dissected cellular proteomics approach.

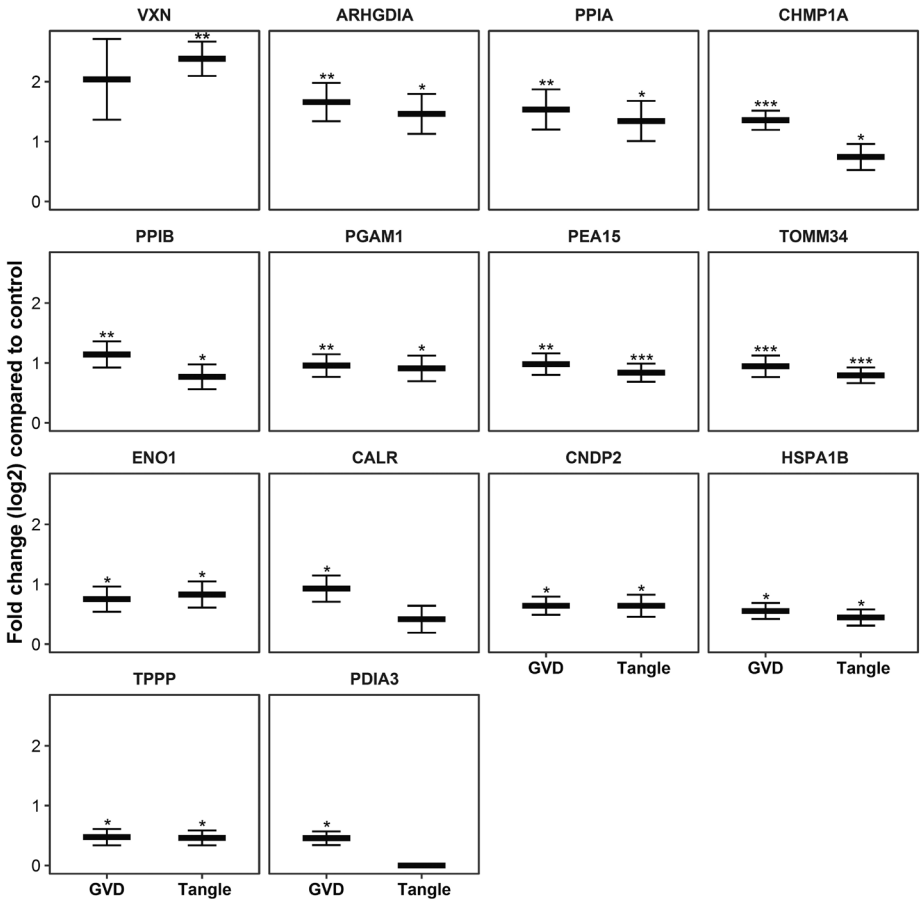

FIGURE 3 | Proteins selected for immunohistochemical analysis. Thirteen proteins that were found increased in neurons with GVD using the statistical approach, were selected for further analysis using immunohistochemistry (IHC). VXN was included for its high estimated fold change and a large increase in the number of individual peptides that was detected in GVD compared to control, indicated by a high z-score, suggestive of an increase in GVD. The log2 fold changes are indicated in GVD and tangles compared to control (a). * $q < 0.05$, **$q < 0.001$ and *** $q < 0.0001$.

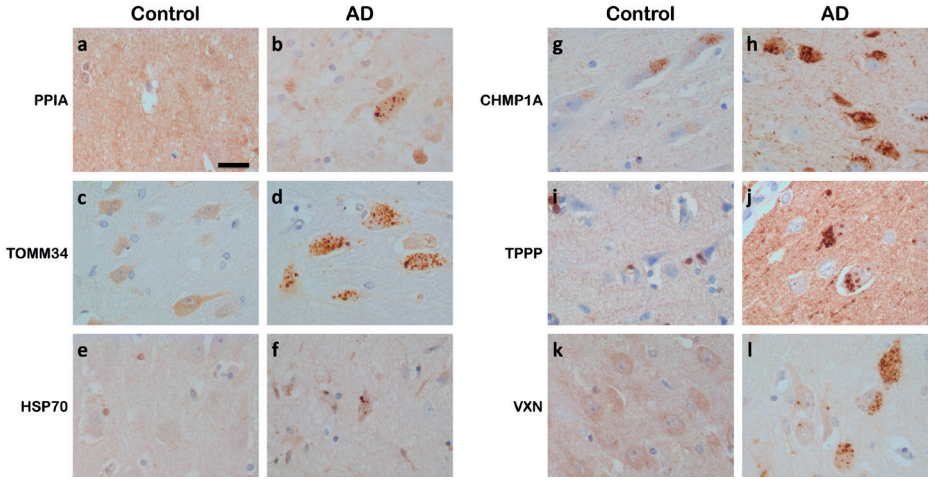

FIGURE 4 | Validation of differentially expressed proteins in GVD bearing neurons. Representative images are shown from immunohistochemical staining for proteins that are differentially expressed (PPIA, TOMM34, HSP70, CHMP1A, TPPP and VXN) in control cases (a, c, e, g, l, k and m, respectively) and AD cases (b, d, f, h, j, l and n, respectively). PPIA, TOMM34, HSP70, CHMP1A, TPPP, and VXN are localized in the GVD bodies in AD. All images are taken in the CA1 or subiculum subregion of the hippocampus. Scale bar in (a) indicates 25μm.

VXN and TOMM34 increase with pathology and parallels the presence of CK1δ, CK1ε and pTau in the hippocampus

Next, we selected the newly discovered markers VXN and TOMM34, which showed a high degree of association with GVD, to stain a large patient cohort (n=71), encompassing all Braak stages for NFT to quantify the percentage of positive neurons. The percentage of stained neurons was determined in the CA1 and subiculum subregion of the hippocampus (Fig. 5). Over the Braak stages there is a progressive increase in the fraction of neurons that are positive for TOMM34 and VXN. This increase proceeds to affect approximately 50% of all neurons in the hippocampus. The rate and extent of increase in percentage positive cells was similar to that of the known GVD associated proteins CK1δ and CK1ε and pTau (AT8) (Fig. 5).

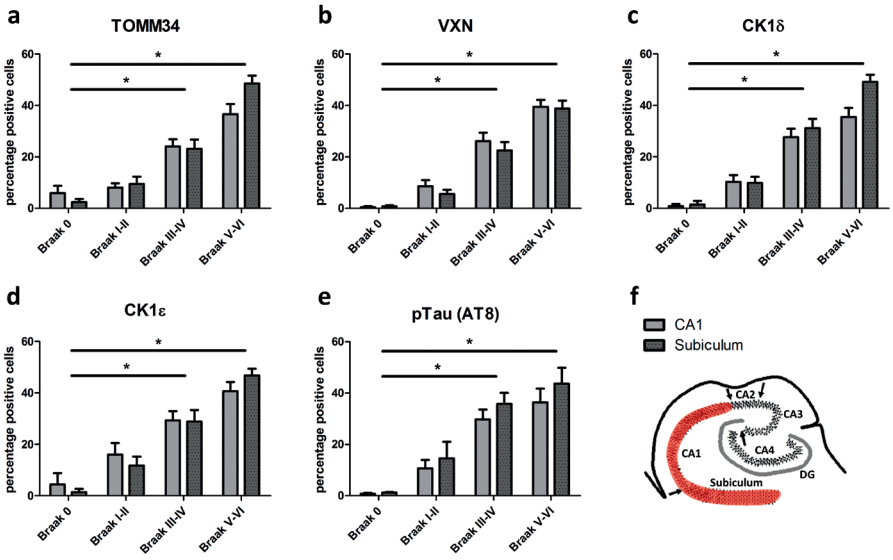

FIGURE 5 | Percentage of neurons containing pTau and markers for GVD bodies over the Braak stages. In the hippocampal subregions CA1 and Subiculum the percentage of neurons that displayed the typical GVD associated granular staining pattern was determined for new markers for GVD (TOMM34 and VXN) (a, b) and known markers of GVD (CK1δ, CK1ε) (c, d). In addition, the percentage of neurons that are positive for pTau (AT8) (e) was determined. A schematic representation of a human hippocampus with the quantified area marked in red is shown in (f). Significant differences ($p < 0.05$) compared to Braak stage 0 are indicated with an asterisk.

Processes associated with GVD and/or tangle bearing neurons

To obtain insight in disease mechanisms occurring in GVD and tangle bearing neurons an overrepresentation analysis in G-profiler was performed on significantly regulated proteins (Table S2). Separate subgroups defined as (I) increased in GVD, (II) decreased in GVD, (III) increased in tangle bearing neurons and (IV) decreased in tangle bearing neurons were analysed (Table S5).

(I) Considering all 92 proteins that are increased in GVD, this yielded 52 overrepresented terms with intermediate filament-based process being the most significant biological process (II) Proteins that are decreased in GVD containing neurons provided no enriched terms in our analysis. (III) Proteins increased in tangle bearing neurons yielded 159 GO and pathway terms, with neurogenesis being the most significantly affected biological process (IV) Proteins that were decreased in tangle bearing neurons primarily showed an overrepresentation in 251 terms with RNA catabolic process being the most significant biological process, but also included ribosomal proteins and cellular responses to stress.

Combining increased and decreased proteins in GVD or increased and decreased proteins in tangle bearing neurons did not result in any additional overrepresented GO terms or pathways for GVD but 49 additional significant terms for tangle bearing neurons were found (Table S5).

In addition to the overrepresentation analysis highlighting the proteins affected in GVD and tangles, an extensive, neurodegeneration relevant, overview and visualization of functionally related proteins and their changes in abundance related to GVD and tangles is presented (Fig. 6a – i). These include proteins involved in protein folding, proteasomal degradation, RNA processing, ribosome function, microtubule and cytoskeletal-related functions, endo-lysosomal function and glycolysis.

In AD, and neurons with GVD, accumulation of misfolded proteins occurs [19, 78]. An important response to misfolded proteins is via proteins that are involved in protein folding, as supported by GO/pathway analysis. Such proteins include PPIA, PPIB, CALR, HSPB1, CLU, DNAJB6, GANAB, HSPA1B, PDIA3, CRYAB, HSPA8 (GO:0006457), FKBP2 [36] and TOMM34 [9]. The mean fold change of each protein per group shows an increase in neurons with GVD (fig. 6a), whereas the increase in tangle bearing neurons is often less or not significant, appearing as an up-down profile when assuming consecutive stages from GVD to tangle bearing neurons. The ER resident proteins PDIA6, HSP90B1, HYOU1, PDIA4, MOGS and FKBP8, have functions involving protein folding and the unfolded protein response. These proteins are decreased only in tangle bearing neurons (Fig. 6b, Table S2). A well-known mechanism of removal of misfolded proteins is by proteasomal degradation. We observe a change in the abundance of proteins that are components of the proteasome complex including PSMC3, PSMD1, PSMD2, PSMD11, and PSMD12 and an increase of ubiquitin (UBB), the latter indicating accumulation of ubiquitinated proteins (Fig 6c, Table S2). Misfolded tau is also being degraded via the endolysosomal pathway and is found in early endosomes, multivesicular bodies, and lysosomes [72]. Several proteins related to this pathway (GO:0005764 lysosome, GO:0005768 endosome, GO:0005771 multivesicular body) are found regulated in neurons with GVD (Fig. 6d). These include CHMP1A, SNX3, VTI1B, PDIA3, SNX12, VTA1, RAB11A, UNC13D, TOLLIP, SDCBP and ATP6V1E1.

Regarding the neuronal cytoskeleton several proteins that are related to the microtubule, including MAPT, are found to have an altered abundance (Fig. 6e, Table S2). Also related to the actin cytoskeleton we find increased GSN, and FSCN1 and CFL1 as well as the neurofilament components VIM, NEFL, NEFM and INA in GVD and partially in tangles (Fig 6f). A decrease in expression was found for actin cytoskeleton regulators CORO1A, MYH9 and NCKAP1 in tangles and for ACTR3B in both GVD and tangles.

The abundance RNA processing proteins, specified by presence in “mRNA binding” (GO:0003729), “RNA splicing” (GO:0008380), “RNA processing” (GO:0006396), is changed in GVD and to even greater extent in tangles (Fig. 6g).

Ribosomal proteins as assigned to "structural constituent of ribosome" (GO:0003735) include RPS2, RPS3, RPL4, RPS4X, RPS7, RPS11, RPS14, RPS16, ENSG00000260836 (40S ribosomal protein S17), RPS23, RPS27L, RPL3, RPL7, RPL8, RPL15, RPL23, RPL28 and RPLP0 which are all decreased but only in the tangle bearing neurons (Fig. 6h). This indicates that in tangle bearing neurons protein synthesis might be impaired. We observe an increase in ENO1, PGAM1, ENO2 and TPI1 and a decrease of PGM2L1 in GVD and tangles (Fig. 6i) with the exception of TPI which does not reach significance in tangle bearing neurons. These proteins are facilitating sequential steps in glycolysis, the main energy source for the brain.

Interestingly, no proteins were found that are increased in GVD and decreased in tangle bearing neurons when compared to control, indicating no contradictory responses are found when comparing GVD to tangle bearing neurons.

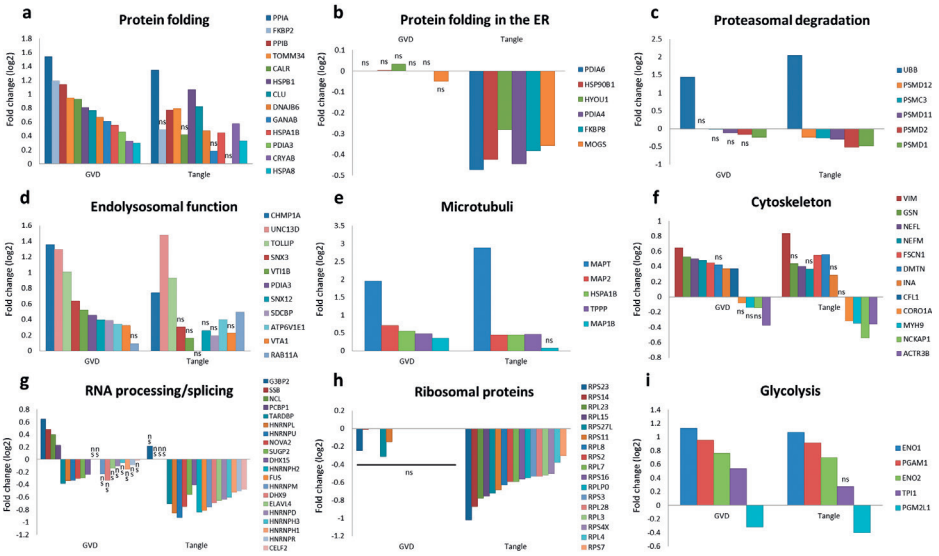

FIGURE 6 | Fold changes of selected proteins that belong to specific functional groups. Log2 fold changes compared to control are shown for proteins of different functional categories in panels a-i. Note that in panel a-i only proteins identified using the statistical approach are displayed. We detected increased levels of proteins related to protein folding in neurons with GVD compared to control while levels are generally lower in tangles compared to GVD (a). Several other proteins involved in protein folding, which in this case all function in the endoplasmic reticulum, remain unchanged in neurons with GVD but are reduced in tangles (b). Core components of the proteasome are found to be decreased in GVD and tangles while ubiquitin (UBB) builds up in GVD and to a greater extent in tangles (c). Several proteins related to the endolysosomal pathway are changed in expression, primarily in GVD and to a lesser extent in tangle bearing neurons (d). Several proteins related to the microtubule (e) and other neuronal cytoskeletal components (f) are elevated in GVD and tangles. Many proteins that are involved in RNA processing including several members of the Heterogeneous nuclear ribonucleoproteins (HNRNPs) are decreased in neurons with GVD and tangles, except for Nucleolin (NCL), Ras GTPase-activating protein-binding protein 2 (G3BP2), Lupus La protein (SSB) and heterogeneous nuclear ribonucleoprotein E1 (PCBP1) which are increased in GVD but unchanged in tangles (g). Several ribosomal proteins are decreased but only in tangles (h). Several enzymes facilitating sequential steps in glycolysis namely Alpha-enolase (ENO1), Phosphoglycerate mutase 1 (PGAM1), gamma-enolase (ENO2) and triosephosphate isomerase (TPI1) are increased in GVD and all, except for TPI1, also in tangles, while glucose 1,6-bisphosphate synthase (PGM2L1) was found decreased in GVD and tangle bearing neurons (i). (ns: not significant, nd: not detected)

DISCUSSION

Mass spectrometry-based proteomics analysis of laser dissected tissue or cells has become a useful technology to identify proteins specifically in pathological conditions [7, 16, 20]. In this study we applied a single-cell resolution proteomics approach that provides for the first time an overview of changes in the proteome of neurons containing GVD and in those containing neurofibrillary tangles. Using our approach, we have identified 115 differently expressed proteins that show changes in GVD bearing neurons and 197 proteins in tangle bearing neurons of which 66 proteins overlap between GVD and tangle bearing neurons. The identification of proteins differentially expressed in GVD containing neurons provides insight in the molecular mechanisms associated with GVD.

GVD is associated with activation of protein folding and degradation and dysregulation of RNA processing

As indicated by the GO/pathway overrepresentation analysis, several proteins associated with protein folding are increased, mostly in GVD containing neurons, and to a lesser extent in tangle bearing neurons (Fig.6a). TOMM34 is a cytosolic protein that is involved in protein folding and the transport of unfolded proteins into mitochondria [5, 9, 43]. HSP70 binds misfolded monomeric tau, oligomeric tau and to a lesser extent aggregated tau and is effective in preventing further aggregation [33, 51, 54]. Interestingly, TOMM34 interacts with HSP70 as a co-chaperone [70] and both were found in GVD bodies using IHC. The highest fold increase is seen in the cyclophilin family of peptidyl-prolyl isomerases PPIA, PPIB and FKBP2. Interestingly, inhibition or deficiency of PPIA results in increased aggregation and faster disease progression in models for prion disease [1, 50]. Other, mainly ER resident, protein folding associated proteins maintain normal expression in GVD but decrease in tangle bearing neurons (Fig. 6b).

A downregulation of components of the proteasome complex was observed, which was accompanied by an increase of UBB (Fig. 6c) indicating proteasomal dysfunction. Increased UBB has previously been suggested to be relevant in an early stage of tangle formation [4, 75]. In addition, several proteins related to early endosomes, multivesicular bodies, and lysosomes are found regulated in neurons with GVD. Of these proteins PDIA3, which is upregulated in GVD, has previously been implied as a possible therapeutic target by reducing Aβ pathology and subsequent tau pathology in an AD model [22, 69]. In addition gene variants of the GVD increased protein SNX3 are associated with AD [71]. Together, these results indicate increased protein folding mechanisms and impaired protein degradation in GVD affected neurons.

We also observe cytoskeletal alterations of microtubule, actin and intermediate filament related proteins in GVD and continuing in tangle bearing neurons (Fig. 6f). Next to MAPT, MAP2 and MAP1B are increased in GVD and could compensate microtubule instability [27]. In addition, MAP1B is important for synaptic plasticity and neurite outgrowth [24, 49]. Also TPPP is increased and localizes in the GVD bodies. TPPP is involved in modulation of microtubule dynamics and stability [32, 48] and can bind and inhibit the activity of tau kinase glycogen synthase kinase

3 [53]. Previously the regulator of actin dynamics and synaptic plasticity CFL1 was linked to synaptotoxicity in AD and CFL1 positive inclusions were shown associated with plaque and tangle pathology in AD [39, 59, 60]. In addition, the neurofilament components VIM, NEFL, NEFM and INA are increased in GVD and NEFL is also increased in tangle bearing neurons.

GO/pathway overrepresentation analysis showed a decrease in an exceptionally large number of proteins that are involved in the binding and processing of mRNA in GVD and to an even greater extent in tangle bearing neurons. Impaired functioning of RNA processing can induce cryptic splicing errors and the relation with tau pathology has been indicated recently [21]. In GVD bearing neurons several heterogeneous ribonucleoproteins are reduced including HNRNPL, HNRNPU, while PCBP1 (hnRNP E1) is increased (Fig. 6g). Moreover, in tangles the abundance of additional related proteins from this family, including HNRNPH2, HNRNPM, HNRNPD, HNRNPH3, HNRNPH1 and HNRNPR is reduced. This family of proteins is involved in the processing, splicing, stability and transport of RNA [11, 55]. The level of TARDBP (TDP43) was found elevated in GVD and immunodetection of phosphorylated TARDBP (pTDP-43) has been found associated previously with GVD [39]. G3BP2 is a scaffold protein functioning in the development of stress granules [35]. Several stress granule markers are also found frequently present in GVD [29]. Also increase of SSB, PCBP1 and the known GVD localized protein NCL [39] in GVD suggests disturbances in RNA metabolism and protein synthesis [25]. Our findings suggest that pathways associated with RNA processing are affected already in the GVD stage of tau pathology.

VXN was found highly increased in neurons with GVD and localized specifically to the GVD bodies. As such VXN is a robust and interesting new marker for GVD. VXN has functions in the nucleus where it is involved in neurogenesis. Aberrant methylation of VXN gene was found associated with development of ALS [42, 66].

In summary, we observed increased presence of proteins and activation of pathways that promote protein folding, synaptic plasticity, and neurogenesis could indicate that GVD is a homeostatic response to a disturbed homeostasis in the early stages of tau pathology.

Decreased ribosomal proteins and protein folding in the ER in tangle bearing neurons

In comparison with GVD neurons, tangle bearing neurons show further persistence or aggravation of changes in relation to protein folding, protein degradation, microtubule and other cytoskeletal proteins and RNA processing. In addition, several protein groups that were unaffected in GVD show changes in their abundance in tangle bearing neurons. Neurofibrillary tangle bearing neurons show a decrease in ER resident proteins which are involved in protein folding and the unfolded protein response (Fig. 6b). Also, a large collection of ribosomal proteins was selectively decreased in tangle neurons (Fig. 6h). Decreased synthesis of ribosomal components can be induced by misfolded, aggregated tau [8]. A decrease in ribosomal subunits may indicate a substantial reduction in the capacity for protein synthesis in tangle bearing neurons. Our data shows that the levels of these proteins are unchanged in GVD and proper ribosomal function might still be maintained in these neurons.

There is a great deal of overlap between GVD and tangles in regulated proteins and protein groups like RNA processing, the proteasome, endolysosomal function and glycolysis as shown in figure 6 and 7. In addition, MAPT is the main protein aggregate in the tangle and a 3.9-fold increase is already observed in GVD bearing neurons further increasing to approximately 7.4-fold in the tangle bearing neurons. Furthermore, the aggregation of tau in tangle bearing neurons coincides with the decrease of chaperone proteins, involved in protein folding and prevention of aggregation.

Recently, Wiersma et al. showed that tau seeds induce GVD-like pathology in primary neurons in vitro [74]. This study supports a functional link between tau pathology and GVD. Although we cannot draw conclusions on the link between tau seeding and GVD in the present study, it is interesting to see that both tau seed induced GVD and GVD in human post mortem brain show strong involvement of the endolysosomal pathway. In general, both studies support the strong connection between GVD and tau pathology. These results suggest that GVD and tangle formation are sequential events.

We propose a model were tau seeds initiate the accumulation of tau, resulting in a gradual increase in tau hyper-phosphorylation and misfolding in the neuron. During this process of cellular stress, GVD is initiated. While the increase of intracellular pTau levels might elicit GVD formation, it is still elusive whether GVD is a protective or degenerative response [73].

Some limitations may apply to this work. For laser dissection of neurons with GVD or tangles, we used the marker CK1δ and pTau respectively. A proportion of neurons showing GVD are also pTau positive and vice versa, as such there will be a percentage of double positive neurons present in both groups in the analysis. In addition, proteins were solubilized using SDS buffer under reducing conditions. Although this solubilizes most proteins in a sample it does not completely solubilize protein aggregates and consequently the representation of aggregated proteins in this analysis may be incomplete. The average age of the control cases used for proteome analysis was lower than the AD cases (9,5 years difference). It was recently reported that age difference affects the brain proteome only mildly [26], and the proteins involved in that study are not part of the processes that we attribute to GVD or tangles nor do these include any of the markers highlighted in our study. Age cannot be a contributing factor in changes selective for GVD or tangle bearing neurons as these samples are derived from the same group of AD cases. However, we cannot exclude that the average age difference has an effect on the comparison between control and AD cases.

Furthermore, mass spectrometric results may require confirmation using an independent technique to assess cellular changes in protein levels. We confirmed increased abundance of several proteins not previously associated with AD or GVD by immunohistochemistry, however, changes in the expression and the localization of many other proteins of interest still need to be investigated.

Previous immunohistochemistry studies have shown the presence of phosphorylated proteins in GVD bodies. The technique used in this study was suitable for the detection of proteins independent of their phosphorylation state, which provided an unbiased analysis independent of the specificity of antibodies directed to phospho-epitopes.

For quantification by immunoblotting, whole hippocampal lysates were used as the protein yield from laser-dissected neurons is too low for this technique. The abundance of CK1ε, VXN, TOMM34 and PPIB was analysed, but no significant change in abundance was detected. This indicates that immunoblotting of whole hippocampal lysates does not provide sufficient resolution to detect changes related to the subpopulation of neurons that display GVD. This explains why we identified many proteins that have not previously been associated with AD and argues for a cell-targeted proteomics discovery approach.

For the proteins with a clear localization to the GVD bodies, like TOMM34, PPIA, VXN, or known marker proteins such as CK1δ and CK1ε, we do not observe significant lower abundance in tangle bearing neurons. This might be due to several reasons. First, the mass spec analysis is on a partly double positive cell population as we cannot exclude the presence of GVD in part of the isolated pTau positive neurons. Second, proteins associated with GVD might still have elevated levels of these proteins in tangle bearing neurons compared to control, but these might be below the detection threshold of the IHC analysis.

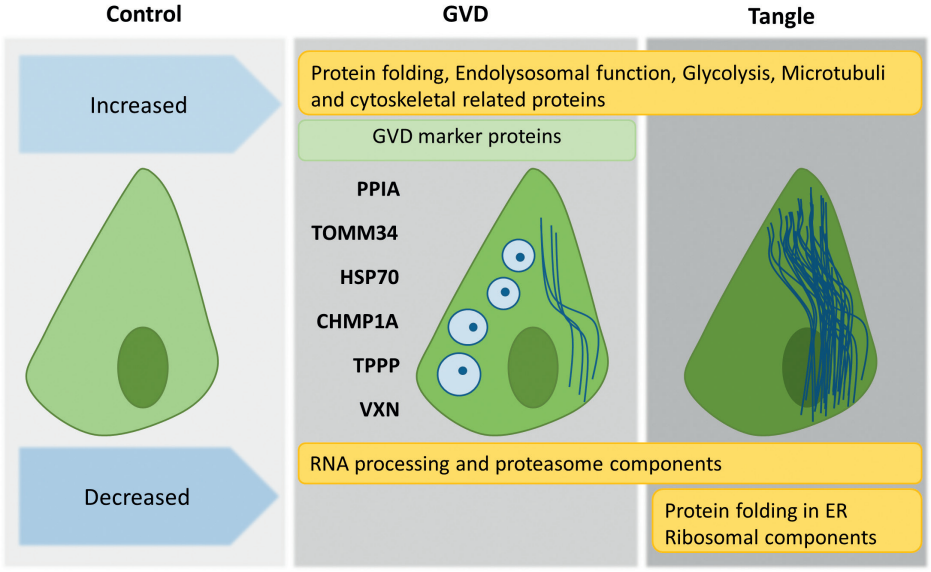

FIGURE 7 | Proteins and processes associated with GVD and tangles. Shown are the global proteome changes occurring in GVD containing neurons and tangle bearing neurons. In the top panel are the processes related to proteins that are increased and at the bottom row the processes related to decreased proteins. Several markers identified using LC-MS/MS and found to be associated with GVD using IHC in this study are placed at the left of the GVD bearing neuron.

CONCLUSION

Using a combination of IHC, LMD and LC-MS/MS we analysed the changes in the proteomes of neurons with GVD and neurons with tangles compared to control neurons, obtained from human post-mortem AD brain tissue. Our data show that GVD and neurofibrillary tangle bearing neurons are molecularly closely related and support that GVD represents a neuronal pre-tangle stage. Due to the high resolution of the analysis of specific neuronal populations this study identified many proteins that have not been associated previously with GVD or NFTs. Our results show that GVD bearing neurons have increased presence of proteins associated with protein folding, endolysosomal function and glycolysis, while there is a decrease of proteins involved in RNA processing and proteasome components. In addition, we find increased levels of proteins in GVD that promote protein folding, synaptic plasticity and neurogenesis suggesting that GVD is a response to a disturbed neuronal homeostasis in the early stages of tau pathology. We present new GVD associated proteins that provide insight in AD pathogenesis and novel leads for further research.

ACKNOWLEDGEMENTS

The authors thank the Netherlands Brain Bank (Amsterdam, the Netherlands) for supplying human brain tissue. This work was financially supported by Amsterdam Neuroscience and Alzheimer Nederland (grant NL-16054).

REFERENCES

1. Bouybayoune I, Comerio L, Pasetto L, Bertani I, Bonetto V, Chiesa R (2019) Cyclophillin A deficiency accelerates RML-induced prion disease. Neurobiol Dis 130:104498. doi: 10.1016/j.nbd.2019.104498
2. Braak H, Braak E (1991) Neuropathological stageing of Alzheimer-related changes. Acta Neuropathol 82:239–59.
3. Braak H, Braak E (1995) Staging of alzheimer's disease-related neurofibrillary changes. Neurobiol Aging 16:271–278. doi: 10.1016/0197-4580(95)00021-6
4. Chen JJ, Nathaniel DL, Raghavan P, Nelson M, Tian R, Tse E, Hong JY, See SK, Mok SA, Hein MY, Southworth DR, Grinberg LT, Gestwicki JE, Leonetti MD, Kampmann M (2019) Compromised function of the ESCRT pathway promotes endolysosomal escape of tau seeds and propagation of tau aggregation. J Biol Chem 294:18952–18966. doi: 10.1074/jbc.RA119.009432
5. Chewawiwat N, Yano M, Terada K, Hoogenraad NJ, Mori M (1999) Characterization of the novel mitochondrial protein import component, Tom34, in mammalian cells. J Biochem 125:721–7.
6. Derkinderen P, Scales TME, Hanger DP, Leung KY, Byers HL, Ward MA, Lenz C, Price C, Bird IN, Perera T, Kellie S, Williamson R, Noble W, Van Etten RA, Leroy K, Brion JP, Reynolds CH, Anderton BH (2005) Tyrosine 394 is phosphorylated in Alzheimer's paired helical filament tau and in fetal tau with c-Abl as the candidate tyrosine kinase. J Neurosci 25:6584–6593. doi: 10.1523/JNEUROSCI.1487-05.2005
7. Drummond E, Wisniewski T (2019) Using Proteomics to Understand Alzheimer's Disease Pathogenesis. In: Alzheimer's Dis. Codon Publications, pp 37–51
8. Evans HT, Benetatos J, van Roijen M, Bodea L, Götz J (2019) Decreased synthesis of ribosomal proteins in tauopathy revealed by non-canonical amino acid labelling. EMBO J. doi: 10.15252/embj.2018101174
9. Faou P, Hoogenraad NJ (2012) Tom34: A cytosolic cochaperone of the Hsp90/Hsp70 protein complex involved in mitochondrial protein import. Biochim Biophys Acta - Mol Cell Res 1823:348–357. doi: 10.1016/j.bbamcr.2011.12.001
10. Funk KE, Mrak RE, Kuret J (2011) Granulovacuolar degeneration (GVD) bodies of Alzheimer's disease (AD) resemble late-stage autophagic organelles. Neuropathol Appl Neurobiol 37:295–306. doi: 10.1111/j.1365-2990.2010.01135.x
11. Geuens T, Bouhy D, Timmerman V (2016) The hnRNP family: insights into their role in health and disease. Hum Genet 135:851–67. doi: 10.1007/s00439-016-1683-5
12. Ghoshal N, Smiley JF, DeMaggio AJ, Hoekstra MF, Cochran EJ, Binder LI, Kuret J (1999) A new molecular link between the fibrillar and granulovacuolar lesions of Alzheimer's disease. Am J Pathol 155:1163–1172. doi: 10.1016/S0002-9440(10)65219-4
13. Goeminne LJE, Gevaert K, Clement L (2016) Peptide-level Robust Ridge Regression Improves Estimation, Sensitivity, and Specificity in Data-dependent Quantitative Label-free Shotgun Proteomics. Mol Cell Proteomics 15:657–668. doi: 10.1074/mcp.M115.055897
14. Goeminne LJE, Gevaert K, Clement L (2018) Experimental design and data-analysis in label-free quantitative LC/MS proteomics: A tutorial with MSqRob. J Proteomics 171:23–36. doi: 10.1016/J.JPROT.2017.04.004

15. Hara M, Hirokawa K, Kamei S, Uchihara T (2013) Isoform transition from four-repeat to three-repeat tau underlies dendrosomatic and regional progression of neurofibrillary pathology. Acta Neuropathol 125:565–579. doi: 10.1007/s00401-013-1097-6

16. Hondius DC, Eigenhuis KN, Morrema THJ, van der Schors RC, van Nierop P, Bugiani M, Li KW, Hoozemans JJM, Smit AB, Rozemuller AJM (2018) Proteomics analysis identifies new markers associated with capillary cerebral amyloid angiopathy in Alzheimer's disease. Acta Neuropathol Commun 6:46. doi: 10.1186/s40478-018-0540-2

17. Hondius DC, Hoozemans JJM, Rozemuller AJM, Li KW, Smit AB (2018) A Laser Microdissection–Liquid Chromatography–Tandem Mass Spectrometry Workflow for Post-mortem Analysis of Brain Tissue. In: Methods Mol. Biol. pp 371–383

18. Hoozemans JJM, van Haastert ES, Eikelenboom P, de Vos RAI, Rozemuller JM, Scheper W (2007) Activation of the unfolded protein response in Parkinson's disease. Biochem Biophys Res Commun 354:707–711. doi: 10.1016/j.bbrc.2007.01.043

19. Hoozemans JJM, Van Haastert ES, Nijholt DAT, Rozemuller AJM, Eikelenboom P, Scheper W (2009) The unfolded protein response is activated in pretangle neurons in alzheimer's disease hippocampus. Am J Pathol 174:1241–1251. doi: 10.2353/ajpath.2009.080814

20. Hosp F, Mann M (2017) A Primer on Concepts and Applications of Proteomics in Neuroscience. Neuron 96:558–571. doi: 10.1016/j.neuron.2017.09.025

21. Hsieh YC, Guo C, Yalamanchili HK, Abreha M, Al-Ouran R, Li Y, Dammer EB, Lah JJ, Levey AI, Bennett DA, De Jager PL, Seyfried NT, Liu Z, Shulman JM (2019) Tau-Mediated Disruption of the Spliceosome Triggers Cryptic RNA Splicing and Neurodegeneration in Alzheimer's Disease. Cell Rep 29:301-316.e10. doi: 10.1016/j.celrep.2019.08.104

22. Hu W, Zhang L, Li MX, Shen J, Liu XD, Xiao ZG, Wu DL, Ho IHT, Wu JCY, Cheung CKY, Zhang YC, Lau AHY, Ashktorab H, Smoot DT, Fang EF, Chan MTV, Gin T, Gong W, Wu WKK, Cho CH (2019) Vitamin D3 activates the autolysosomal degradation function against Helicobacter pylori through the PDIA3 receptor in gastric epithelial cells. Autophagy 15:707–725. doi: 10.1080/15548627.2018.1557835

23. Ikegami K, Kimura T, Katsuragi S, Ono T, Yamamoto H, Miyamoto E, Miyakawa T (1996) Immunohistochemical examination of phosphorylated tau in granulovacuolar degeneration granules. Psychiatry Clin Neurosci 50:137–140. doi: 10.1111/j.1440-1819.1996.tb01678.x

24. Ishikawa Y, Okada M, Honda A, Ito Y, Tamada A, Endo N, Igarashi M (2019) Phosphorylation sites of microtubule-associated protein 1B (MAP 1B) are involved in axon growth and regeneration. Mol Brain. doi: 10.1186/s13041-019-0510-z

25. Jia W, Yao Z, Zhao J, Guan Q, Gao L (2017) New perspectives of physiological and pathological functions of nucleolin (NCL). Life Sci 186:1–10. doi: 10.1016/j.lfs.2017.07.025

26. Johnson ECB, Dammer EB, Duong DM, Ping L, Zhou M, Yin L, Higginbotham LA, Guajardo A, White B, Troncoso JC, Thambisetty M, Montine TJ, Lee EB, Trojanowski JQ, Beach TG, Reiman EM, Haroutunian V, Wang M, Schadt E, Zhang B, Dickson DW, Ertekin-Taner N, Golde TE, Petyuk VA, De Jager PL, Bennett DA, Wingo TS, Rangaraju S, Hajjar I, Shulman JM, Lah JJ, Levey AI, Seyfried NT (2020) Large-scale proteomic analysis of Alzheimer's disease brain and cerebrospinal fluid reveals early changes in energy metabolism associated with microglia and astrocyte activation. Nat Med. doi: 10.1038/s41591-020-0815-6

27. Ke YD, Suchowerska AK, Van Der Hoven J, De Silva DM, Wu CW, Van Eersel J, Ittner A, Ittner LM (2012) Lessons from Tau-deficient mice. Int J Alzheimers Dis. doi: 10.1155/2012/873270

28. Knippschild U, Gocht A, Wolff S, Huber N, Löhler J, Stöter M (2005) The casein kinase 1 family: Participation in multiple cellular processes in eukaryotes. Cell Signal 17:675-689. doi: 10.1016/j.cellsig.2004.12.011

29. Köhler C (2016) Granulovacuolar degeneration: a neurodegenerative change that accompanies tau pathology. Acta Neuropathol 132:339–359. doi: 10.1007/s00401-016-1562-0

30. Köhler C, Dinekov M, Götz J (2014) Granulovacuolar degeneration and unfolded protein response in mouse models of tauopathy and Aβ amyloidosis. Neurobiol Dis 71:169–179. doi: 10.1016/j.nbd.2014.07.006

31. Koper MJ, Schoor E Van, Ospitalieri S, Vandenberghe R, Mathieu Vandenbulcke ·, Von Arnim CAF, Tousseyn T, Sriram Balusu ·, De Strooper B, Dietmar ·, Thal R (2020) Necrosome complex detected in granulovacuolar degeneration is associated with neuronal loss in Alzheimer's disease. Acta Neuropathol 139:463–484. doi: 10.1007/s00401-019-02103-y

32. Kovács GG, László L, Kovács J, Jensen PH, Lindersson E, Botond G, Molnár T, Perczel A, Hudecz F, Mezo G, Erdei A, Tirián L, Lehotzky A, Gelpi E, Budka H, Ovádi J (2004) Natively unfolded tubulin polymerization promoting protein TPPP/p25 is a common marker of alpha-synucleinopathies. Neurobiol Dis 17:155-162. doi: 10.1016/j.nbd.2004.06.006

33. Kundel F, De S, Flagmeier P, Horrocks MH, Kjaergaard M, Shammas SL, Jackson SE, Dobson CM, Klenerman D (2018) Hsp70 Inhibits the Nucleation and Elongation of Tau and Sequesters Tau Aggregates with High Affinity. ACS Chem Biol 13:636–646. doi: 10.1021/acschembio.7b01039

34. Leroy K, Boutajangout A, Authelet M, Woodgett JR, Anderton BH, Brion JP (2002) The active form of glycogen synthase kinase-3β is associated with granulovacuolar degeneration in neurons in Alzheimers's disease. Acta Neuropathol 103:91–99. doi: 10.1007/s004010100435

35. Li T, Safitri M, Zhang K, Wang Y, Huang L, Zhu Y, Daniel R, Wu LJ, Qiu J, Wang G (2020) Downregulation of G3BP2 reduces atherosclerotic lesions in ApoE–/– mice. Atherosclerosis 310:64–74. doi: 10.1016/j.atherosclerosis.2020.08.003

36. Lu H, Yang Y, Allister EM, Wijesekara N, Wheeler MB (2008) The identification of potential factors associated with the development of type 2 diabetes: A quantitative proteomics approach. Mol Cell Proteomics 7:1434–1451. doi: 10.1074/mcp.M700478-MCP200

37. Lund H, Gustafsson E, Svensson A, Nilsson M, Berg M, Sunnemark D, von Euler G (2014) MARK4 and MARK3 associate with early tau phosphorylation in Alzheimer's disease granulovacuolar degeneration bodies. Acta Neuropathol Commun 2:22. doi: 10.1186/2051-5960-2-22

38. Makioka K, Yamazaki T, Takatama M, Ikeda M, Murayama S, Okamoto K, Ikeda Y (2016) Immunolocalization of Tom1 in relation to protein degradation systems in Alzheimer's disease. J Neurol Sci 365:101–107. doi: 10.1016/j.jns.2016.03.035

39. Minamide LS, Striegl AM, Boyle JA, Meberg PJ, Bamburg JR (2000) Neurodegenerative stimuli induce persistent ADF/cofilin-actin rods that disrupt distal neurite function. Nat Cell Biol 2:628–636. doi: 10.1038/35023579

40. Mirra SS, Heyman A, McKeel D, Sumi SM, Crain BJ, Brownlee LM, Vogel FS, Hughes JP, Belle G v., Berg L (1991) The Consortium to Establish a Registry for Alzheimer's Disease (CERAD): Part II. Standardization of the neuropathologic assessment of Alzheimer's disease. Neurology 41:479–479. doi: 10.1212/WNL.41.4.479

41. Montine TJ, Phelps CH, Beach TG, Bigio EH, Cairns NJ, Dickson DW, Duyckaerts C, Frosch MP, Masliah E, Mirra SS, Nelson PT, Schneider JA, Thal DR, Trojanowski JQ, Vinters H V, Hyman BT (2012) National institute on aging-Alzheimer's association guidelines for the neuropathologic assessment of Alzheimer's disease: A practical approach. Acta Neuropathol 123:1–11. doi: 10.1007/s00401-011-0910-3

42. Moore KB, Logan MA, Aldiri I, Roberts JM, Steele M, Vetter ML (2018) C8orf46 homolog encodes a novel protein Vexin that is required for neurogenesis in Xenopus laevis. Dev Biol 437:27–40. doi: 10.1016/j.ydbio.2018.03.003

43. Mukhopadhyay A, Avramova L V., Weiner H (2002) Tom34 unlike Tom20 does not interact with the leader sequences of mitochondrial precursor proteins. Arch Biochem Biophys 400:97–104. doi: 10.1006/abbi.2002.2777

44. Nakamori M, Takahashi T, Yamazaki Y, Kurashige T, Yamawaki T, Matsumoto M (2012) Cyclin-dependent kinase 5 immunoreactivity for granulovacuolar degeneration. Neuroreport 23:867–872. doi: 10.1097/WNR.0b013e328358720b

45. Nijholt DATA, van Haastert ES, Rozemuller AJMJ, Scheper W, Hoozemans JJJM (2012) The unfolded protein response is associated with early tau pathology in the hippocampus of tauopathies. 226:693–702. doi: 10.1002/path.3969

46. Nishikawa T, Takahashi T, Nakamori M, Hosomi N, Maruyama H, Miyazaki Y, Izumi Y, Matsumoto M (2016) The identification of raft-derived tau-associated vesicles that are incorporated into immature tangles and paired helical filaments. Neuropathol Appl Neurobiol 42:639–653. doi: 10.1111/nan.12288

47. Okamoto K, Hirai S, Iizuka T, Yanagisawa T, Watanabe M (1991) Reexamination of granulovacuolar degeneration. Acta Neuropathol 82:340–345. doi: 10.1007/BF00296544

48. Oláh J, Lehotzky A, Szunyogh S, Szénási T, Orosz F, Ovádi J (2020) Microtubule-Associated Proteins with Regulatory Functions by Day and Pathological Potency at Night. Cells 9:357. doi: 10.3390/cells9020357

49. Palenzuela R, Gutiérrez Y, Draffin JE, Lario A, Benoist M, Esteban JA (2017) MAP1B light chain modulates synaptic transmission via AMPA receptor intracellular trapping. J Neurosci 37:9945–9963. doi: 10.1523/JNEUROSCI.0505-17.2017

50. Pan I, Roitenberg N, Cohen E (2018) Vesicle-mediated secretion of misfolded prion protein molecules from cyclosporin A-treated cells. FASEB J 32:1479–1492. doi: 10.1096/fj.201700598RRR

51. Patterson KR, Ward SM, Combs B, Voss K, Kanaan NM, Morfini G, Brady ST, Gamblin TC, Binder LI (2011) Heat Shock Protein 70 Prevents both Tau Aggregation and the Inhibitory Effects of Preexisting Tau Aggregates on Fast Axonal Transport. Biochemistry 50:10300–10310. doi: 10.1021/bi2009147

52. Perez-Riverol Y, Csordas A, Bai J, Bernal-Llinares M, Hewapathirana S, Kundu DJ, Inuganti A, Griss J, Mayer G, Eisenacher M, Pérez E, Uszkoreit J, Pfeuffer J, Sachsenberg T, Yilmaz Ş, Tiwary S, Cox J, Audain E, Walzer M, Jarnuczak AF, Ternent T, Brazma A, Vizcaíno JA (2019) The PRIDE database and related tools and resources in 2019: Improving support for quantification data. Nucleic Acids Res 47:D442–D450. doi: 10.1093/nar/gky1106

53. Pérez Martín C, Vázquez J, Avila J, Moreno FJ (2002) P24, a glycogen synthase kinase 3 (GSK 3) inhibitor. Biochim Biophys Acta - Mol Basis Dis 1586:113–122. doi: 10.1016/S0925-4439(01)00092-8

54. Petrucelli L, Dickson D, Kehoe K, Taylor J, Snyder H, Grover A, De Lucia M, McGowan E, Lewis J, Prihar G, Kim J, Dillmann WH, Browne SE, Hall A, Voellmy R, Tsuboi Y, Dawson TM, Wolozin B, Hardy J, Hutton M (2004) CHIP and Hsp70 regulate tau ubiquitination, degradation and aggregation. Hum Mol Genet 13:703–714. doi: 10.1093/hmg/ddh083

55. Purice MD, Taylor JP (2018) Linking hnRNP function to ALS and FTD pathology. Front Neurosci. doi: 10.3389/fnins.2018.00326

56. Raudvere U, Kolberg L, Kuzmin I, Arak T, Adler P, Peterson H, Vilo J (2019) g:Profiler: a web server for functional enrichment analysis and conversions of gene lists (2019 update). Nucleic Acids Res. doi: 10.1093/nar/gkz369

57. Reimand J, Kull M, Peterson H, Hansen J, Vilo J (2007) G:Profiler-a web-based toolset for functional profiling of gene lists from large-scale experiments. Nucleic Acids Res 35:1–8. doi: 10.1093/nar/gkm226

58. Riku Y, Duyckaerts C, Boluda S, Plu I, Le Ber I, Millecamps S, Salachas F, Letournel F, Martin-Négrier ML, Chapon F, Godfraind C, Maurage CA, Deramecourt V, Meyronet D, Streichenberger N, Maues de Paula A, Rigau V, Vandenbos-Burel F, Milin S, Chiforeanu DC, Laquerrière A, Lannes B, Duchesne M, Yoshida M, Ando T, Katsuno M, Sobue G, Seilhean D (2019) Increased prevalence of granulovacuolar degeneration in C9orf72 mutation. Acta Neuropathol 138:783–793. doi: 10.1007/s00401-019-02028-6

59. Rush T, Martinez-Hernandez J, Dollmeyer M, Frandemiche ML, Borel E, Boisseau S, Jacquier-Sarlin M, Buisson A (2018) Synaptotoxicity in alzheimer's disease involved a dysregulation of actin cytoskeleton dynamics through cofilin 1 phosphorylation. J Neurosci 38:10349–10361. doi: 10.1523/JNEUROSCI.1409-18.2018

60. Rust MB (2015) ADF/cofilin: A crucial regulator of synapse physiology and behavior. Cell Mol Life Sci 72:3521–3529. doi: 10.1007/s00018-015-1941-z

61. Schubert OT, Gillet LC, Collins BC, Navarro P, Rosenberger G, Wolski WE, Lam H, Amodei D, Mallick P, Maclean B, Aebersold R (2015) Building high-quality assay libraries for targeted analysis of SWATH MS data. Nat Protoc 10:426–441. doi: 10.1038/nprot.2015.015

62. Schwab C, Demaggio AJ, Ghoshal N, Binder LI, Kuret J, McGeer PL (2000) Casein kinase 1 delta is associated with pathological accumulation of tau in several neurodegenerative diseases. Neurobiol Aging 21:503–510. doi: 10.1016/S0197-4580(00)00110-X

63. Singh TJ, Grundke-Iqbal I, Iqbal K (1995) Phosphorylation of τ Protein by Casein Kinase-1 Converts It to an Abnormal Alzheimer-Like State. J Neurochem 64:1420–1423. doi: 10.1046/j.1471-4159.1995.64031420.x

64. Solntsev SK, Shortreed MR, Frey BL, Smith LM (2018) Enhanced Global Post-translational Modification Discovery with MetaMorpheus. J Proteome Res 17:1844–1851. doi: 10.1021/acs.jproteome.7b00873

65. Stutzbach LD, Xie SX, Naj AC, Albin R, Gilman S, PSP Genetics Study Group VMY, Lee VMY, Trojanowski JQ, Devlin B, Schellenberg GD (2013) The unfolded protein response is activated in disease-affected brain regions in progressive supranuclear palsy and Alzheimer's disease. Acta Neuropathol Commun 1:31. doi: 10.1186/2051-5960-1-31

66. Tarr IS, McCann EP, Benyamin B, Peters TJ, Twine NA, Zhang KY, Zhao Q, Zhang Z-H, Rowe DB, Nicholson GA, Bauer D, Clark SJ, Blair IP, Williams KL (2019) Monozygotic twins and triplets discordant for amyotrophic lateral sclerosis display differential methylation and gene expression. Sci Rep 9:8254. doi: 10.1038/s41598-019-44765-4

67. Thal DR, Rüb U, Schultz C, Sassin I, Ghebremedhin E, Del Tredici K, Braak E, Braak H (2000) Sequence of Aβ-protein deposition in the human medial temporal lobe. J Neuropathol Exp Neurol 59:733–748. doi: 10.1093/jnen/59.8.733

68. Thal DR, Del Tredici K, Ludolph AC, Hoozemans JJM, Rozemuller AJ, Braak H, Knippschild U (2011) Stages of granulovacuolar degeneration: Their relation to Alzheimer's disease and chronic stress response. Acta Neuropathol 122:577–589. doi: 10.1007/s00401-011-0871-6

69. Tohda C, Urano T, Umezaki M, Nemere I, Kuboyama T (2012) Diosgenin is an exogenous activator of 1,25D 3-MARRS/Pdia3/ERp57 and improves Alzheimer's disease pathologies in 5XFAD mice. Sci Rep. doi: 10.1038/srep00535

70. Trcka F, Durech M, Man P, Hernychova L, Muller P, Vojtesek B (2014) The assembly and intermolecular properties of the Hsp70-Tomm34-Hsp90 molecular chaperone complex. J Biol Chem 289:9887–9901. doi: 10.1074/jbc.M113.526046

71. Vardarajan BN, Bruesegem SY, Harbour ME, St. George-Hyslop P, Seaman MNJ, Farrer LA (2012) Identification of Alzheimer disease-associated variants in genes that regulate retromer function. Neurobiol Aging 33:2231.e15-2231.e30. doi: 10.1016/j.neurobiolaging.2012.04.020

72. Vaz-Silva J, Gomes P, Jin Q, Zhu M, Zhuravleva V, Quintremil S, Meira T, Silva J, Dioli C, Soares-Cunha C, Daskalakis NP, Sousa N, Sotiropoulos I, Waites CL (2018) Endolysosomal degradation of Tau and its role in glucocorticoid-driven hippocampal malfunction. EMBO J. doi: 10.15252/embj.201899084

73. Wiersma VI, Hoozemans JJM, Scheper W (2020) Untangling the origin and function of granulovacuolar degeneration bodies in neurodegenerative proteinopathies. Acta Neuropathol Commun 8:153. doi: 10.1186/s40478-020-00996-5

74. Wiersma VI, van Ziel AM, Vazquez-Sanchez S, Nölle A, Berenjeno-Correa E, Bonaterra-Pastra A, Clavaguera F, Tolnay M, Musters RJP, van Weering JRT, Verhage M, Hoozemans JJM, Scheper W (2019) Granulovacuolar degeneration bodies are neuron-selective lysosomal structures induced by intracellular tau pathology. Acta Neuropathol 138:943–970. doi: 10.1007/s00401-019-02046-4

75. Williams RL, Urbé S (2007) The emerging shape of the ESCRT machinery. Nat Rev Mol Cell Biol 8:355-368. doi: 10.1038/nrm2162

76. Yamazaki Y, Takahashi T, Hiji M, Kurashige T, Izumi Y, Yamawaki T, Matsumoto M (2010) Immunopositivity for ESCRT-III subunit CHMP2B in granulovacuolar degeneration of neurons in the Alzheimer's disease hippocampus. Neurosci Lett 477:86–90. doi: 10.1016/j.neulet.2010.04.038

77. Yasojima K, Kuret J, DeMaggio AJ, McGeer E, McGeer PL (2000) Casein kinase 1 delta mRNA is upregulated in Alzheimer disease brain. Brain Res 865:116–20. doi: 10.1016/s0006-8993(00)02200-9

78. Yerbury JJ, Ooi L, Dillin A, Saunders DN, Hatters DM, Beart PM, Cashman NR, Wilson MR, Ecroyd H (2016) Walking the tightrope: Proteostasis and neurodegenerative disease. J Neurochem 137:489–505. doi: 10.1111/jnc.13575

SUPPLEMENTARY MATERIAL

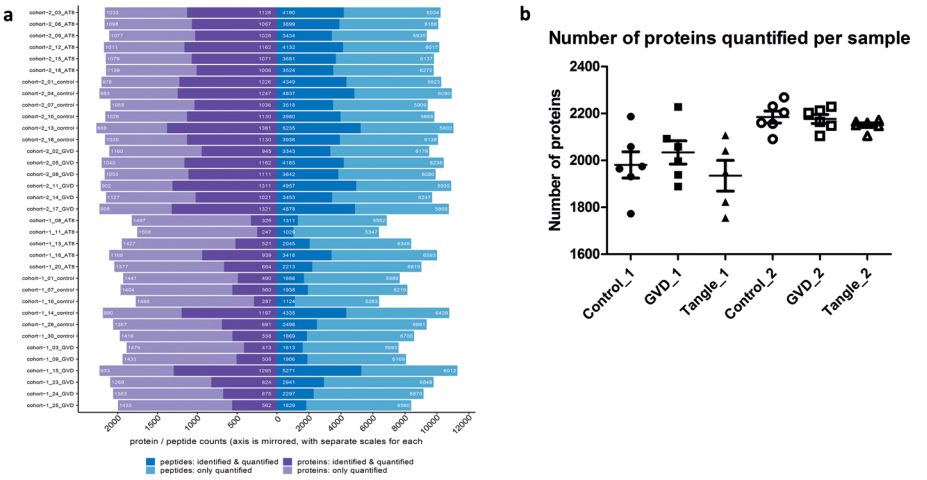

FIGURE S1 | Number of proteins quantified per case. The total number of proteins that was quantified using LC/MS-MS per case is shown per individual case. Both detection by MS/MS and quantification only via the match between runs option (MS1 only) are shown. Samples were analysed in two separate batches with each 6 samples per group. No significant differences exist between groups within each batch with respect to number of quantified proteins.

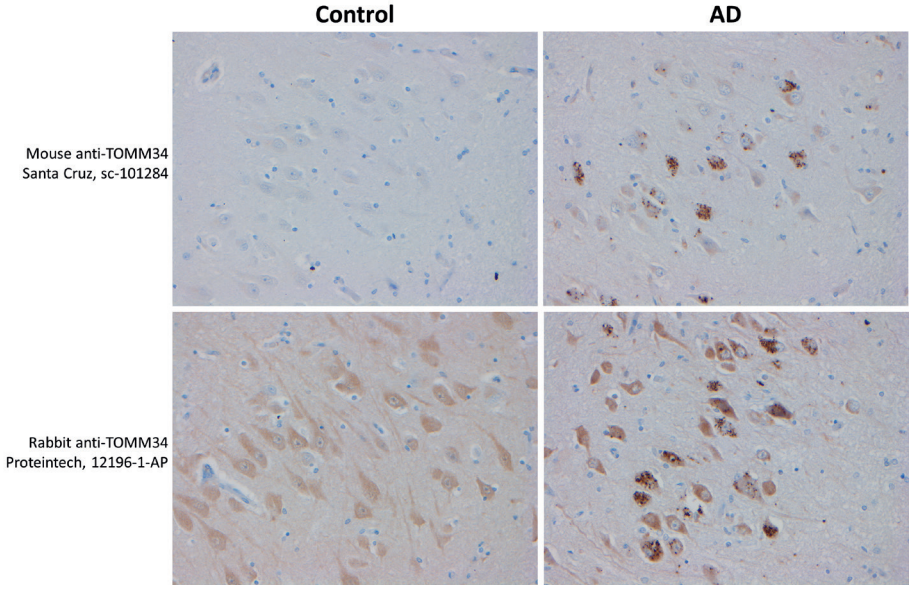

FIGURE S2 | IHC staining using two different anti-TOMM34 antibodies visualize GVD. Both anti-TOMM34 antibodies used in this study visualize GVD.

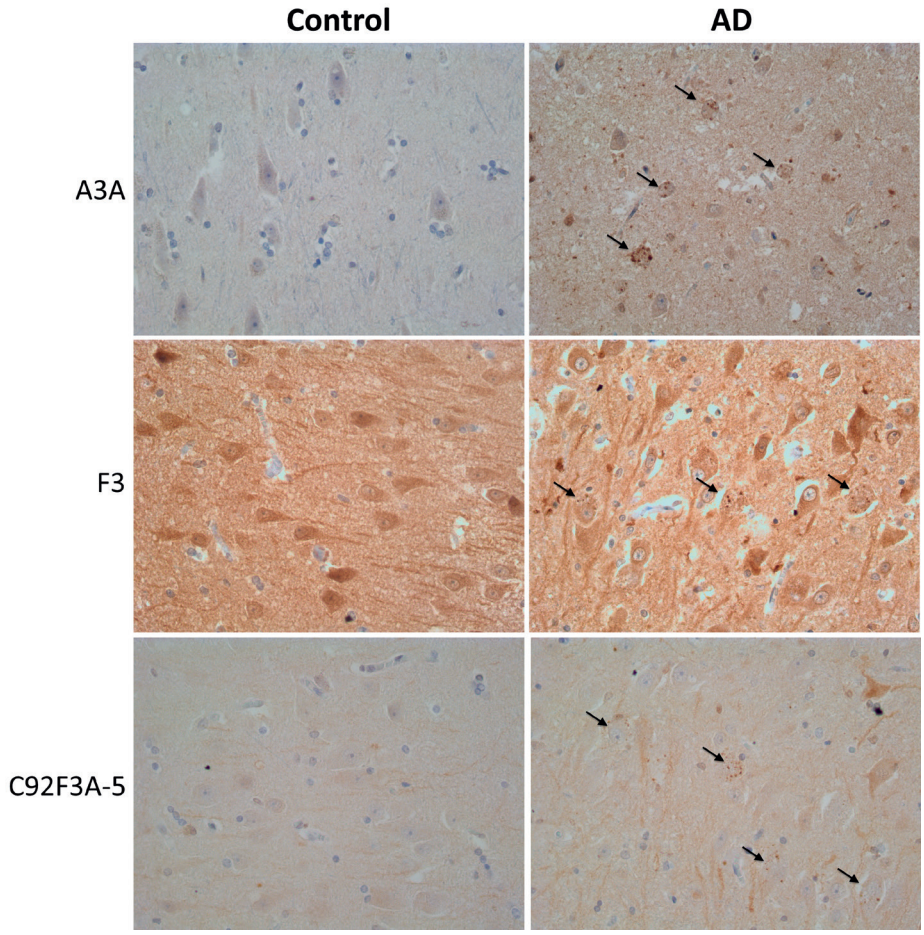

FIGURE S3 | IHC staining using three alternative anti-HSP70 antibodies visualize GVD. Three alternative anti-HSP70 antibodies that were tested in this studie also visualize GVD (arrows).

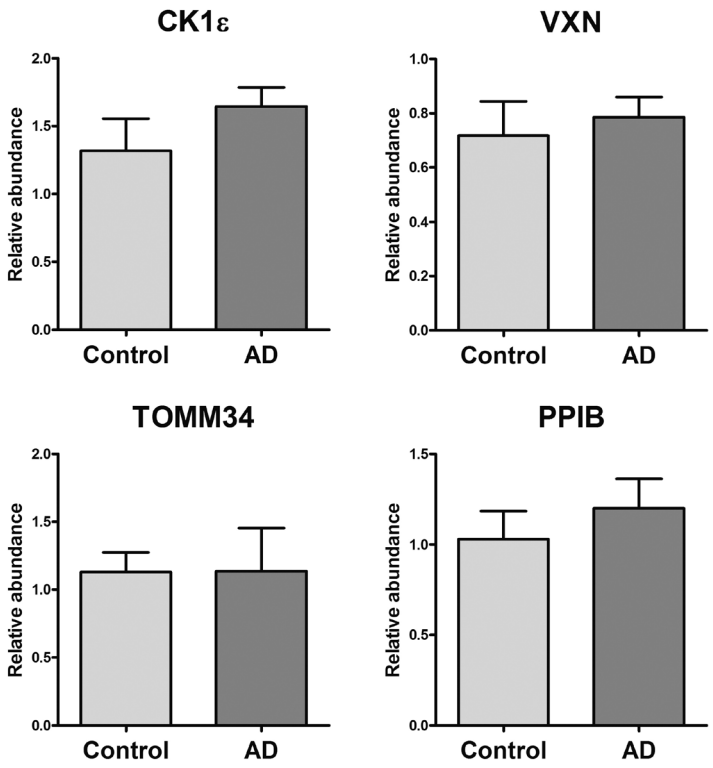

FIGURE S4 | Levels in whole hippocampus are not changed as determined using immunoblotting. Quantification of selected GVD associated proteins was performed on whole hippocampal lysates. Control (Braak 0 and I for tau pathology) was compared to AD cases (Braak stage V and VI). CK1ε, VXN, TOMM34, and PPIB were quantified and presented in a, b, c, and d, respectively. No differences in the abundance was found for any of these proteins when comparing control to AD.

TABLE S1 | Cases used for validation.

Case #	Braak Aβ [1]	Braak Tau [1,2]	ABC score [3]	Gender	Age at death (y)	Post-mortem delay (hh:mm)	APOE genotype	Diagnosis
1	0	0	A0B0C0	m	74	08:05	33	Non-demented control
2	0	0	A0B0C0	m	49	06:15	32	Non-demented control
3	0	0	A0B0C0	f	64	05:40	32	Non-demented control
4	0	0	A0B0C0	m	55	07:30	33	Non-demented control
5	0	0	A0B0C0	m	76	06:45	33	Non-demented control
6	0	0	A0B0C0	f	86	04:20	32	Non-demented control
7		0	A1B0C0	m	61	06:15	33	CAA HCHWAD
8	0	1	A0B1C0	m	93	05:05	33	Non-demented control

TABLE S1 | Continued

Case #	Braak Aβ [1]	Braak Tau [1,2]	ABC score [3]	Gender	Age at death (y)	Post-mortem delay (hh:mm)	APOE genotype	Diagnosis
9	A	1	A1B1C0	f	71	07:10	32	Non-demented control
10	0	1	A0B1C0	f	75	05:25	33	Non-demented control
11	B	1	A1B1C0	f	73	07:45	44	Non-demented control
12	B	1	A1B1C0	m	80	03:18	ND	Vascular dementia
13	A	1	A1B1C0	f	86	07:05	33	Non-demented control
14	0	1	A0B1C0	m	82	05:10	32	Non-demented control
15	B	1	A1B1C0	f	83	04:40	32	Non-demented control
16	A	1	A1B1C0	m	92	04:10	32	Dementia with Lewy bodies
17	A	1	A1B1C0	m	66	08:30	33	Motor neuron disease
18	B	1	A1B1C0	m	80	07:00	33	Non-demented control
19	B	1	A1B1C0	f	87	07:00	33	Non-demented control
20	0	2	A0B1C0	m	90	05:45	33	Non-demented control
21	B	2	A1B1C0	f	89	04:45	33	Non-demented control
22	C	2	A2B1C0	f	84	05:55	43	Non-demented control
23	A	2	A1B1C0	m	75	06:55	44	Vascular dementia
24	A	2	A1B1C0	f	95	05:15	33	Non-demented control
25	A	2	A1B1C0	f	70	06:15	33	Non-demented control
26	A	2	A1B1C0	m	79	06:30	32	Non-demented control
27	B	2	A2B1C0	f	83	06:03	44	Non-demented control
28	B	2	A1B1C0	f	84	06:45	33	Vascular dementia
29	C	2	A1B1C0	f	99	04:15	ND	Non-demented control
30	C	2	A3B1C0	m	80	04:25	43	Non-demented control
31	B	3	A1B2C0	f	96	04:00	32	AD/vascular dementia
32	B	3	A1B2C0	m	82	05:05	33	AD/MCI
33	A	3	A1B2C0	f	81	05:30	33	Non-demented control
34	A	3	A1B2C0	m	90	06:45	33	AD/tauopathy
35	A	3	A1B2C0	f	85	06:25	33	Non-demented control
36	B	3	A2B2C1	m	83	06:40	43	AD/vascular dementia
37	B	3	A1B2C0	f	95	05:40	33	Non-demented control
38	B	3	A1B2C0	f	86	06:25	33	Non-demented control
39	A	3	A1B2C0	f	87	02:35	43	Hippocampal sceloris
40	C	3	A2B2C1	f	94	06:15	43	AD with CAA
41	0	4	A0B2C0	m	88	05:40	43	Primary age related tauopathy

TABLE S1 | Continued

Case #	Braak Aβ [1]	Braak Tau [1,2]	ABC score [3]	Gender	Age at death (y)	Post-mortem delay (hh:mm)	APOE genotype	Diagnosis
42	B	4	A2B2C2	m	96	04:10	33	Non-demented control
43	B	4	A2B2C2	f	81	05:50	33	Non-demented control
44	A	4	A1B2C0	f	98	06:05	ND	AD
45	B	4	A2B2C1	m	89	04:56	33	AD
46	B	4	A2B2C1	f	96	07:20	33	AD
47	B	4	A2B2C2	f	80	08:55	43	Adrenoleukodystrophy
48	C	4	A2B2C1	f	100	05:15	43	AD
49	C	4	A2B2C2	m	77	05:00	33	AD
50	C	4	A2B2C1	f	87	06:40	33	AD/vascular dementia
51	C	4	A3B2C2	f	83	04:55	ND	AD
52	C	4	A2B2C1	m	79	04:05	44	AD
53	B	5	A2B3C1	f	94	06:30	32	AD/vascular dementia
54	C	5	A3B3C3	f	66	08:15	33	AD
55	C	5	A3B3C2	f	71	04:15	43	AD
56	C	5	A3B3C2	m	67	08:20	33	AD
57	C	5	A2B3C2	f	95	04:35	44	AD
58	B	5	A3B3C2	m	80	05:05	44	AD
59	C	5	A3B3C2	m	73	06:30	43	AD
60	C	5	A3B3C2	f	96	04:15	33	AD
61	C	5	A3B3C3	f	65	04:30	43	AD
62	C	5	A3B3C3	f	79	04:20	ND	AD
63	C	5	A3B3C3	f	85	04:05	43	AD
64	C	5	A3B3C3	f	75	05:00	ND	AD
65	C	6	A3B3C3	m	71	06:35	33	AD
66	C	6	A3B3C3	f	79	05:10	43	AD
67	C	6	A3B3C3	m	70	05:15	44	AD
68	C	6	A3B3C3	f	89	04:00	43	AD
69	C	6	A3B3C3	f	73	05:30	43	AD
70	C	6	A3B3C3	m	65	06:00	43	AD
71	C	6	A3B3C3	f	73	04:55	44	AD
72	C	6	A3B3C3	m	79	04:10	43	AD
73	C	6	A3B3C3	m	88	05:30	43	AD
74	C	6	A3B3C3	f	92	06:10	43	AD
75	C	6	A3B3C3	f	82	05:00	44	AD

TABLE S2 (adapted) | All proteins with a change in abundance.

Gene	FDR Control vs GVD	log2 FC Control vs GVD	FDR Control vs Tangle	log2 FC Control vs Tangle	Changed in GVD	Changed in Tangle
MAPT	0.000	1.949	0.000	2.885	1	1
UBB*	0.000	1.434	0.000	2.051	1	1
CLU	0.000	0.763	0.000	0.820	1	1
CSNK1A1	0.000	1.060	0.001	0.721	1	1
HSPB1	0.000	0.807	0.000	1.064	1	1
CHMP1A	0.000	1.358	0.034	0.744	1	1
DNAJB6	0.000	0.666	0.005	0.472	1	1
MAP2	0.000	0.709	0.014	0.441	1	1
NEFL	0.000	0.502	0.015	0.398	1	1
YWHAE	0.000	0.449	0.001	0.384	1	1
BLVRB	0.000	0.511	0.000	0.629	1	1
SNX3	0.000	0.636	0.148	0.302	1	0
PSD3	0.000	0.777	0.032	0.510	1	1
MLF2	0.000	0.704	0.040	0.409	1	1
TOMM34	0.000	0.944	0.000	0.793	1	1
PEA15	0.000	0.980	0.000	0.838	1	1
PGAM1	0.000	0.957	0.001	0.914	1	1
VIM	0.000	0.646	0.000	0.832	1	1
EIF4H	0.000	0.608	0.007	0.439	1	1
PPIB	0.000	1.142	0.010	0.768	1	1
ACTR3B	0.000	-0.371	0.018	-0.359	1	1
ARHGDIA	0.000	1.660	0.001	1.463	1	1
CBR1	0.000	0.755	0.009	0.637	1	1
NEFM	0.000	0.478	0.059	0.362	1	0
UBE2QL1	0.000	1.553	0.012	0.932	1	1
NOVA2	0.000	-0.302	0.000	-0.750	1	1
PSMD1	0.000	-0.241	0.000	-0.484	1	1
GFAP	0.000	1.538	0.001	1.575	1	1
EXOC4	0.000	-0.595	0.000	-0.734	1	1
SSB	0.001	0.478	1.000	0.000	1	0
PAFAH1B3	0.001	0.709	0.227	0.365	1	0
PPIA	0.001	1.537	0.003	1.344	1	1
ME1	0.001	0.290	0.967	0.071	1	0
KARS1	0.001	0.514	0.622	0.183	1	0
CSNK1D	0.001	0.488	0.001	0.492	1	1

TABLE S2 | Continued

Gene	FDR Control vs GVD	log2 FC Control vs GVD	FDR Control vs Tangle	log2 FC Control vs Tangle	Changed in GVD	Changed in Tangle
YWHAZ	0.002	0.569	0.006	0.498	1	1
MAP1B	0.002	0.352	0.886	0.072	1	0
CALR	0.002	0.928	0.373	0.416	1	0
EEF1B2	0.003	0.553	1.000	0.000	1	0
FKBP2	0.003	1.188	0.336	0.490	1	0
HSPA1B	0.003	0.554	0.020	0.445	1	1
CNDP2	0.003	0.642	0.016	0.642	1	1
ENSG00000276612	0.003	0.862	0.045	0.797	1	1
AK1	0.003	0.405	0.020	0.368	1	1
CAMK2B	0.004	-0.461	0.000	-0.652	1	1
TP53BP1	0.004	-0.518	0.005	-0.505	1	1
PIN1	0.004	0.362	0.097	0.261	1	0
SND1	0.004	0.281	1.000	0.000	1	0
PRKRA	0.004	0.438	1.000	0.000	1	0
PDIA3	0.004	0.456	1.000	0.000	1	0
INA	0.004	0.370	0.120	0.288	1	0
BRD2	0.004	1.785	0.847	0.404	1	0
TARDBP	0.004	-0.386	0.000	-0.707	1	1
USO1	0.005	0.238	1.000	0.000	1	0
GANAB	0.005	0.606	0.484	0.181	1	0
TKT	0.005	0.563	0.037	0.459	1	1
LRRC47	0.005	0.275	1.000	0.000	1	0
SUGP2	0.005	-0.297	0.000	-0.564	1	1
SYNE1	0.005	-0.415	0.011	-0.502	1	1
SCRN1	0.005	0.644	0.034	0.530	1	1
G3BP2	0.005	0.644	0.675	0.213	1	0
PHPT1	0.005	1.065	1.000	0.000	1	0
GSN	0.005	0.523	0.064	0.437	1	0
HPCAL4	0.007	0.753	0.033	0.624	1	1
ATP6V1E1	0.008	0.341	0.022	0.400	1	1
PRDX5	0.008	0.533	0.033	0.468	1	1
CNRIP1	0.008	0.799	0.057	0.693	1	0
ENO2	0.008	0.764	0.013	0.700	1	1
ENO1	0.012	1.128	0.026	1.070	1	1
PPIA	0.013	0.981	0.044	0.769	1	1

TABLE S2 | Continued

Gene	FDR Control vs GVD	log2 FC Control vs GVD	FDR Control vs Tangle	log2 FC Control vs Tangle	Changed in GVD	Changed in Tangle
NCL	0.013	0.398	1.000	0.000	1	0
SYNGAP1	0.015	-0.404	0.455	-0.248	1	0
ENO1	0.015	0.752	0.005	0.829	1	1
CLINT1	0.017	0.379	1.000	0.000	1	0
HSD17B10	0.018	0.598	0.854	0.201	1	0
DHX15	0.019	-0.236	0.002	-0.409	1	1
HPCA	0.019	0.709	0.163	0.432	1	0
CFL1	0.019	0.366	1.000	0.000	1	0
RAB6A	0.019	0.208	0.033	0.267	1	1
PCBP1	0.020	0.222	1.000	0.000	1	0
AIMP1	0.020	0.577	1.000	0.000	1	0
HNRNPUL2	0.020	-0.287	0.008	-0.416	1	1
RGS14	0.020	-0.507	0.279	-1.106	1	0
TPPP	0.022	0.473	0.008	0.462	1	1
TOLLIP	0.023	1.006	0.028	0.933	1	1
PITHD1	0.023	0.776	1.000	0.000	1	0
PGM2L1	0.023	-0.318	0.001	-0.401	1	1
FSCN1	0.026	0.447	0.005	0.545	1	1
CAMK2D	0.026	0.289	0.893	0.070	1	0
HNRNPL	0.026	-0.339	0.000	-0.857	1	1
SNX12	0.026	0.392	0.106	0.259	1	0
VTA1	0.026	0.322	0.155	0.225	1	0
SDCBP	0.027	0.388	0.549	0.193	1	0
PALM	0.029	0.515	0.001	0.825	1	1
TPI1	0.034	0.538	0.357	0.276	1	0
ANXA5	0.036	0.374	0.058	0.378	1	0
MYEF2	0.036	-0.285	0.001	-0.430	1	1
SUGT1	0.037	0.251	0.043	0.216	1	1
HNRNPU	0.039	-0.333	0.000	-0.928	1	1
RTRAF	0.042	0.429	0.472	0.194	1	0
ALDH5A1	0.042	-0.346	0.563	-0.169	1	0
UNC13D	0.043	1.297	0.014	1.477	1	1
SYN1	0.043	0.441	0.062	0.458	1	0
APMAP	0.043	-0.241	0.001	-0.376	1	1
CKB	0.044	0.568	0.262	0.391	1	0

TABLE S2 | Continued

Gene	FDR Control vs GVD	log2 FC Control vs GVD	FDR Control vs Tangle	log2 FC Control vs Tangle	Changed in GVD	Changed in Tangle
VTI1B	0.044	0.519	1.000	0.161	1	0
PAFAH1B1	0.044	0.478	0.239	0.325	1	0
EIF3CL	0.044	0.385	1.000	0.000	1	0
RTN4	0.044	0.207	0.340	0.129	1	0
CADPS	0.044	-0.165	0.005	-0.212	1	1
GRIA2	0.044	-0.284	0.000	-0.496	1	1
STXBP5L	0.044	-0.494	0.901	-0.139	1	0
PPP3CA	0.044	-0.289	0.896	-0.120	1	0
HSPA8	0.046	0.295	0.006	0.331	1	1
CRYAB	0.048	0.321	0.043	0.576	1	1
PIGR	0.055	0.482	0.038	0.539	0	1
DHX9	0.055	-0.333	0.000	-0.697	0	1
APP	0.067	0.464	0.029	0.641	0	1
CYFIP2	0.070	-0.304	0.000	-0.582	0	1
DOCK4	0.072	-0.710	0.018	-0.943	0	1
GNAQ	0.075	-0.389	0.049	-0.316	0	1
SLC25A12	0.081	-0.225	0.026	-0.255	0	1
DMTN	0.084	0.423	0.002	0.556	0	1
NPTXR	0.093	0.349	0.037	0.398	0	1
SHTN1	0.097	0.324	0.002	0.407	0	1
TRIM28	0.120	-0.302	0.000	-0.759	0	1
VXN	0.121	2.040	0.000	2.383	0	1
SQSTM1	0.127	0.531	0.000	1.334	0	1
C4A	0.162	0.497	0.005	0.792	0	1
PALM	0.163	0.341	0.005	0.620	0	1
FARSA	0.163	0.151	0.001	-0.309	0	1
PSMD11	0.171	-0.112	0.000	-0.294	0	1
HSPA4	0.183	-0.181	0.023	-0.214	0	1
SLC6A1	0.203	-0.498	0.025	-0.607	0	1
SSBP1	0.223	0.369	0.002	0.677	0	1
RPS27L	0.238	-0.310	0.001	-0.724	0	1
NOMO1	0.243	-0.151	0.000	-0.535	0	1
VCAN	0.250	0.334	0.003	0.642	0	1
GLS	0.302	0.254	0.018	0.363	0	1
RAB6B	0.306	0.259	0.049	0.299	0	1

TABLE S2 | Continued

Gene	FDR Control vs GVD	log2 FC Control vs GVD	FDR Control vs Tangle	log2 FC Control vs Tangle	Changed in GVD	Changed in Tangle
HNRNPM	0.316	-0.230	0.000	-0.761	0	1
MAPK1	0.323	0.250	0.049	0.294	0	1
SRP68	0.364	-0.221	0.028	-0.432	0	1
RUVBL2	0.365	-0.147	0.016	-0.265	0	1
CKAP4	0.434	-0.262	0.001	-0.405	0	1
EPB41L2	0.445	0.146	0.001	0.294	0	1
TPR	0.489	-0.147	0.020	-0.254	0	1
ARF1	0.496	0.261	0.033	0.454	0	1
PRKDC	0.505	-0.089	0.000	-0.326	0	1
CADM3	0.509	0.173	0.000	0.744	0	1
NCAM1	0.529	0.147	0.001	0.518	0	1
SH3GL2	0.531	0.189	0.040	0.302	0	1
ATP6V1B2	0.536	0.187	0.040	0.284	0	1
SPHKAP	0.536	-0.145	0.000	-0.566	0	1
HNRNPCL4*	0.536	-0.326	0.049	-0.885	0	1
IDH2	0.588	0.185	0.040	0.330	0	1
CSNK1E	0.605	0.377	0.033	0.558	0	1
PRKACB	0.649	-0.220	0.024	-0.562	0	1
ELAVL4	0.676	-0.144	0.000	-0.657	0	1
HNRNPH1	0.676	-0.159	0.002	-0.522	0	1
RPS11	0.707	-0.144	0.000	-0.682	0	1
LANCL2	0.710	-0.250	0.006	-0.503	0	1
NDRG1	0.742	-0.173	0.049	-0.337	0	1
MYH9	0.763	-0.137	0.000	-0.346	0	1
GSK3A	0.771	-0.124	0.002	-0.313	0	1
CAMK2A	0.775	-0.302	0.027	-0.763	0	1
NCKAP1	0.857	-0.145	0.000	-0.538	0	1
LMAN2	0.877	-0.131	0.005	-0.457	0	1
PSMD2	0.886	-0.156	0.003	-0.510	0	1
PRKAR1B	0.956	-0.093	0.040	-0.302	0	1
L1CAM	0.978	0.086	0.020	0.351	0	1
RAB11A	1.000	0.090	0.002	0.496	0	1
STX12	1.000	0.085	0.009	0.442	0	1
SHANK3	1.000	0.072	0.040	0.260	0	1
DNAJC5	1.000	0.063	0.014	0.737	0	1

TABLE S2 | Continued

Gene	FDR Control vs GVD	log2 FC Control vs GVD	FDR Control vs Tangle	log2 FC Control vs Tangle	Changed in GVD	Changed in Tangle
FXYD1	1.000	0.042	0.035	0.559	0	1
SEPTIN11	1.000	0.040	0.045	0.274	0	1
DARS1	1.000	0.032	0.049	-0.185	0	1
HYOU1	1.000	0.032	0.019	-0.282	0	1
HSP90B1	1.000	0.000	0.000	-0.424	0	1
FARSB	1.000	0.000	0.002	-0.464	0	1
RPL8	1.000	0.000	0.008	-0.628	0	1
RPL3	1.000	0.000	0.027	-0.518	0	1
RPL15	1.000	0.000	0.002	-0.753	0	1
RPL4	1.000	0.000	0.033	-0.377	0	1
FUS	1.000	0.000	0.020	-0.818	0	1
LARS1	1.000	0.000	0.000	-0.399	0	1
RPL23	1.000	0.000	0.000	-0.776	0	1
PURA	1.000	0.000	0.000	-0.581	0	1
PDIA6	1.000	0.000	0.000	-0.473	0	1
RPS2	1.000	0.000	0.000	-0.590	0	1
RPS3	1.000	0.000	0.000	-0.531	0	1
DDX3X	1.000	0.000	0.001	-0.393	0	1
PDIA4	1.000	0.000	0.002	-0.445	0	1
THY1	1.000	0.000	0.012	0.781	0	1
SYNJ1	1.000	0.000	0.014	-0.222	0	1
FKBP8	1.000	0.000	0.016	-0.382	0	1
IPO7	1.000	0.000	0.019	1.952	0	1
MATR3	1.000	0.000	0.022	-0.615	0	1
RPL9P8	1.000	0.000	0.027	-0.473	0	1
RPS7	1.000	0.000	0.032	-0.299	0	1
OPCML	1.000	0.000	0.034	0.608	0	1
HACD3	1.000	0.000	0.034	-0.275	0	1
NCLN	1.000	0.000	0.037	-0.335	0	1
SURF4	1.000	0.000	0.045	-0.472	0	1
BCL2L13	1.000	0.000	0.047	1.159	0	1
H3-3B	1.000	0.000	0.024	-0.547	0	1
RPN2	1.000	0.000	0.000	-0.349	0	1
RPS4X	1.000	0.000	0.000	-0.500	0	1
RPL7	1.000	0.000	0.003	-0.590	0	1

TABLE S2 | Continued

Gene	FDR Control vs GVD	log2 FC Control vs GVD	FDR Control vs Tangle	log2 FC Control vs Tangle	Changed in GVD	Changed in Tangle
RPLP0	1.000	0.000	0.000	-0.547	0	1
PSMD12	1.000	0.000	0.019	-0.239	0	1
GAP43	1.000	0.000	0.028	0.317	0	1
ATP2A2	1.000	0.000	0.000	-0.549	0	1
DDOST	1.000	0.000	0.001	-0.497	0	1
HNRNPH2	1.000	0.000	0.000	-0.843	0	1
RPL28	1.000	0.000	0.009	-0.529	0	1
ILF3	1.000	0.000	0.040	-0.401	0	1
CSDE1	1.000	0.000	0.033	-0.256	0	1
RPS16	1.000	0.000	0.000	-0.562	0	1
RALYL	1.000	0.000	0.049	-0.337	0	1
SLC25A12	1.000	0.000	0.049	-0.244	0	1
HDLBP	1.000	-0.009	0.005	-0.298	0	1
RPS14	1.000	-0.009	0.000	-0.868	0	1
NNT	1.000	-0.010	0.020	-0.287	0	1
PSMC3	1.000	-0.018	0.002	-0.264	0	1
CYRIB	1.000	-0.018	0.012	-4.460	0	1
CELF2	1.000	-0.019	0.047	-0.482	0	1
ACSL1	1.000	-0.033	0.046	-0.654	0	1
ATP5MG	1.000	-0.039	0.019	-0.401	0	1
RPN1	1.000	-0.041	0.002	-0.344	0	1
MOGS	1.000	-0.050	0.039	-0.357	0	1
TOMM70	1.000	-0.050	0.022	-0.194	0	1
HNRNPH3	1.000	-0.056	0.000	-0.606	0	1
ILF2	1.000	-0.061	0.032	-0.368	0	1
RNF170	1.000	-0.062	0.026	-0.372	0	1
ENSG00000260836*	1.000	-0.062	0.045	-0.540	0	1
AP2M1	1.000	-0.065	0.027	-0.234	0	1
CORO1A	1.000	-0.080	0.016	-0.317	0	1
HNRNPR	1.000	-0.084	0.002	-0.508	0	1
KPNB1	1.000	-0.088	0.001	-0.350	0	1
SORT1	1.000	-0.098	0.000	-0.427	0	1
HNRNPD	1.000	-0.102	0.000	-0.637	0	1
SLC2A3	1.000	-0.110	0.020	-0.406	0	1

TABLE S2 | Continued

Gene	FDR Control vs GVD	log2 FC Control vs GVD	FDR Control vs Tangle	log2 FC Control vs Tangle	Changed in GVD	Changed in Tangle
SEC61A1	1.000	-0.141	0.029	-0.578	0	1
RPS23	1.000	-0.241	0.020	-1.020	0	1

TABLE S3 | Quantitative data on all proteins detected, with log2 fold changes and q-values. Can be found at: https://link.springer.com/article/10.1007/s00401-020-02261-4#Sec23 as "Supplementary file 8 (XLSX 370 KB)".

TABLE S4 | All antibodies tested for IHC on FFPE tissue sections in this study.

Protein	Company	Order #	Species	Dilution IHC	IHC associated with GVD/AD	Remarks
VXN (C8orf46)	OriGene	TA334828	Rabbit	1:800	Yes	GVD
ARHGDIA	Santa Cruz	sc-271108	Mouse	1:3200	No	Probably microglia, some vessels
	Santa Cruz	sc-376473	Mouse	1:200	No	Neuronal staining, some microglia
PPIA	Abcam	ab42408	Rabbit	1:800	Yes	GVD
	Santa Cruz	sc-134310	Mouse	1:50	Weak	Hazy and some weak immunoreactivity to GVD
CHMP1A	Santa Cruz	sc-271617	Mouse	1:12800	Yes	GVD
PPIB	Santa Cruz	sc-390193	Mouse	1:400	No	Neuronal staining
	Santa Cruz	sc-130626	Mouse	1:50	No	Glia, some neuronal staining
PGAM1	Santa Cruz	sc-130334	Mouse		No	Neuronal cell body negative, diffuse staining
	Santa Cruz	sc-365677	Mouse		No	Neuronal cell body negative, diffuse staining
PEA15	Santa Cruz	sc-166678	Mouse	1:3200	No	Some neurons positive
TOMM34	Protein tech	12196-1-AP	Rabbit	1:6400	Yes	GVD
	Santa Cruz	sc-101284	Mouse	1:6400	Yes	GVD
ENO1	Santa Cruz	sc-101513	Mouse	1:50	No	Vascular staining, few neurons
	Santa Cruz	sc-271384	Mouse	1:3200	No	High background, vascular

TABLE S4 | Continued

Protein	Company	Order #	Species	Dilution IHC	IHC associated with GVD/AD	Remarks
CALR	Santa Cruz	sc-166837	Mouse	1:51200	No	Neuronal staining
	Santa Cruz	sc-373863	Mouse	1:3200	No	Neuronal staining
CNDP2	Protein tech	14925-1-AP	Rabbit	1:6400	Weak	Possibly some GVD, inconsistent
HSP70 (HSPA1B)	Santa Cruz	sc-24	Mouse	1:100/200	Yes	Part of the GVD positive, glia
	Santa Cruz	sc-32239	Mouse		Yes	Part of the GVD positive
	Santa Cruz	sc-373867	Mouse		Yes	Part of the GVD positive, neuronal cellbodies, surrounding tissue
	Santa Cruz	sc-66048	Mouse		Yes	Part of the GVD positive
	Santa Cruz	sc-66049	Mouse		No	No immunoreactivity at tested dillutions
TPPP	Santa Cruz	sc-515819	Mouse	1:3200	Yes	GVD
PDIA3	Santa Cruz	sc-23886	Mouse		No	No immunoreactivity at tested dillutions
	Protein tech	15967-1-AP	Rabbit	1:3200	No	Neuronal staining

TABLE S5 | Complete gene ontology/pathway analysis as performed using G:profiler. Can be found at: https://link.springer.com/article/10.1007/s00401-020-02261-4#Sec23 as "Supplementary file 10 (1949 KB)".

CHAPTER 4

Proteomics analysis identifies new markers associated with capillary cerebral amyloid angiopathy in Alzheimer's disease

David C Hondius[1,2], Kristel N Eigenhuis[2], Tjado HJ Morrema[1], Roel C van der Schors[2], Pim van Nierop[2], Marianna Bugiani[1], Ka Wan Li[2], Jeroen JM Hoozemans[1], August B Smit[2#] and Annemieke JM Rozemuller[1#]

[1]Department of Pathology, Amsterdam Neuroscience, VU University Medical Center, The Netherlands

[2]Department of Molecular and Cellular Neurobiology, Center for Neurogenomics and Cognitive Research, Amsterdam Neuroscience, VU University Amsterdam, The Netherlands.

[#] authors with equal contribution

Acta Neuropathologica Communications 2018 Jun 4;6(1):46.

ABSTRACT

Alzheimer's disease (AD) is characterized by amyloid beta (Aβ) deposits as plaques in the parenchyma and in the walls of cortical and leptomeningeal blood vessels of the brain called cerebral amyloid angiopathy (CAA). It is suggested that CAA type-1, which refers to amyloid deposition in both capillaries and larger vessels, adds to the symptomatic manifestation of AD and correlates with disease severity. Currently, CAA cannot be diagnosed pre-mortem and disease mechanisms involved in CAA are elusive. To obtain insight in the disease mechanism of CAA and to identify marker proteins specifically associated with CAA we performed a laser dissection microscopy assisted mass spectrometry analysis of post-mortem human brain tissue of (I) AD cases with only amyloid deposits in the brain parenchyma and no vascular related amyloid, (II) AD cases with severe CAA type-1 and no or low numbers of parenchymal amyloid deposits and (III) cognitively healthy controls without amyloid deposits. By contrasting the quantitative proteomics data between the three groups, 29 potential CAA-selective proteins were identified. A selection of these proteins was analysed by immunoblotting and immunohistochemistry to confirm regulation and to determine protein localization and their relation to brain pathology. In addition, specificity of these markers in relation to other small vessel diseases including prion CAA, CADASIL, CARASAL and hypertension related small vessel disease was assessed using immunohistochemistry.

Increased levels of clusterin (CLU), apolipoprotein E (APOE) and serum amyloid P-component (APCS) were observed in AD cases with CAA. In addition, we identified norrin (NDP) and collagen alpha-2(VI) (COL6A2) as highly selective markers that are clearly present in CAA yet virtually absent in relation to parenchymal amyloid plaque pathology. NDP showed the highest specificity to CAA when compared to other small vessel diseases. The specific changes in the proteome of CAA provide new insight in the pathogenesis and yields valuable selective biomarkers for the diagnosis of CAA.

INTRODUCTION

Alzheimer's disease (AD) pathology is characterized by the deposition of amyloid beta (Aβ) in the brain parenchyma as amyloid plaques and at the brain vasculature. The latter is referred to as cerebral amyloid angiopathy (CAA). Approximately 80 percent of AD cases have CAA pathology in varying degrees. When restricted to the larger blood vessels, including leptomeningeal vessels, cortical arteries and arterioles, this is referred to as CAA type-2. In approximately 50% of the AD cases also brain capillaries are affected, which is designated as CAA type-1 [3, 31]. Especially around the capillaries the Aβ deposits can extend into the parenchyma as perivascular Aβ also referred to as dyshoric changes [2]. In AD the observed plaque pathology and CAA type-1 capillary deposits have an inverse correlation [30].

Aβ deposition at the vessel wall in CAA correlates with an increase in the occurrence of cerebral infarction, cerebral haemorrhage and micro-bleeds. In addition, it causes a structural disruption of the vascular wall and might indirectly deteriorate the integrity of the microvascular network [41, 44]. Aβ peptide transport through the blood brain barrier (BBB) or via perivascular drainage is an important mechanism to clear the brain from Aβ. Disruption of Aβ clearance is thought to lead to increase in Aβ deposition in the walls of capillaries and blood vessels, which in turn further decreases drainage capacity resulting in further enhancement of Aβ deposition [5, 45].

CAA type-1 is clinically highly relevant, as it contributes to the symptomatic appearance of AD and, in severe form, CAA type-1 can present itself as the primary cause of rapidly progressive dementia [4, 16].

Currently, definitive diagnosis of AD and the occurrence of CAA can only be determined post-mortem. However, the presence or absence of CAA in AD patients might alter therapeutic options. In particular, a biomarker to detect CAA in patients might aid in stratification of patient groups, which is highly important when initiating, interpreting and improving outcome in clinical trials. Moreover, proteins selectively involved in CAA may function as therapeutic targets.

Proteomics analysis using mass spectrometry is a preferred method to obtain an unbiased insight into proteins involved in disease. For this, 20 cases were selected encompassing a group of AD patients with severe CAA type-1, a group with AD bearing severe plaque pathology but devoid of CAA, and a cognitively healthy control group without any pathology in the occipital lobe. Subsequently, we performed a proteomics analysis of small laser dissected occipital tissue sections containing either high plaque load, or severe CAA or no Aβ deposits. By contrasting the protein expression profiles of these subject groups we discovered proteins that are highly selective for CAA. These proteins also provide insight in specific pathogenic components of CAA, which might offer new targets for therapy.

MATERIAL AND METHODS

Case selection

Post mortem brain tissue was obtained from the Netherlands Brain Bank (NBB), Netherlands Institute for Neuroscience (NIN), Amsterdam. All brain tissue was collected from donors with written informed consent for brain autopsy and the use of the material and clinical information for research purposes has been obtained by the NBB. Brain tissue was selected based on clinical and neuropathological reports. Three groups were composed. Cognitively healthy control cases lacking any pathology, AD cases with severe plaque pathology but devoid of CAA and CAA type-1 cases with severe and (nearly) pure capillary CAA pathology (Thal stages 2 and 3 for CAA)[36]. All cases are listed in Table 1. Alzheimer's disease pathology present as Aβ deposits, neurofibrillary tangles and neuritic plaques is staged [9, 24, 37] and indicated conform the ABC criteria [26].

Fast immunohistochemistry for LCM

Sections (10 µm) of fresh frozen occipital tissue were mounted on PEN-membrane slides (Leica), air-dried and fixed in 100% ethanol for 1 minute. After air drying the tissue was wetted with sterile PBS. Anti-Aβ (clone IC16, detecting N-terminal part of Aβ [43]) was applied at a 1:100 dilution in sterile PBS (pH 7.5) and incubated for 20 minutes at RT. After washing 3 times for 30 seconds in sterile PBS, HRP labelled rabbit anti-mouse (DAKO) was applied at a 1:100 dilution in sterile PBS and incubated for 15 minutes at RT. Sections were briefly washed (3 x 30 s) and freshly prepared 3,3' diaminobenzidine (DAB) solution was applied and left to incubate for 5 minutes to visualize antibody binding. Sections were thoroughly washed in ultra-pure H2O and incubated with 1% (w/v) toluidine blue in ultrapure H2O for 1 minute as a counterstain. Sections were then washed in ultra-pure H2O twice for 1 minute and twice in 100% ethanol for 1 minute and air dried.

TABLE 1 | Patient data.

MS/ Validation	Case #	Diagnosis	M/F	Age (years)	Abeta	Tau	CERAD	PMD	APOE
MS	**1**	CAA type-1	F	75	A3	B3	C0‡	6:00	44
MS	**2**	CAA type-1	F	96	A3	B3	C0‡	4:20	43
MS	**3**	CAA type-1	M	68	A3*	B1	C0‡	6:05	44
MS	**4**	CAA type-1	F	78	A3	NA	C0‡	4:20	44
MS	**5**	CAA type-1	M	81	A3	B3	C2	6:30	44
MS	**6**	CAA type-1	F	95	A3	B3	C2	4:35	44
MS	**7**	CAA type-1	M	80	A3	B3	C0‡	5:05	44
MS	**8**	AD	F	82	A3	B3	C3	6:00	42
MS	**9**	AD	F	72	A3	B3	C3	6:30	44
MS	**10**	AD	F	81	A3	B3	C3	6:00	33
MS	**11**	AD	F	73	A3	B3	C3	5:55	44
MS	**12**	AD	M	84	A3	B3	C3	8:05	NA
MS	**13**	AD	F	87	A3	B3	C3	5:45	43
MS	**14**	AD	F	72	A3	B3	C3	5:55	23

TABLE 1 | Continued

MS/ Validation	Case #	Diagnosis	M/F	Age (years)	Abeta	Tau	CERAD	PMD	APOE
MS	**15**	Control	M	74	A0	B0	C0	8:05	33
MS	**16**	Control	F	80	A1	B1	C0	6:58	43
MS	**17**	Control	M	82	A0	B1	C0	5:10	23
MS	**18**	Control	M	78	A0	B1	C0	17:40	33
MS	**19**	Control	F	79	A0	B1	C0	18:13	33
MS	**20**	Control	F	81	A0	B1	C0	4:25	33
V	**21**	CAA type-1	F	94	A3	B3	C3	04:30	43
V	**22**	CAA type-1	M	74	A3	B3	C3	03:25	NA
V	**23**	CAA type-1	F	87	A3	B3	C3	08:00	44
V	**24**	CAA type-1	F	84	A3	B3	C2	04:45	NA
V	**25**	CAA type-1	M	88	A3	B3	C3	03:55	NA
V	**26**	CAA type-1	M	75	A3	B3	C0	03:15	NA
V	**27**	AD	M	64	A3	B3	C3	07:30	33
V	**28**	AD	F	81	A3	B3	C3	05:15	43
V	**29**	AD	F	90	A3	B3	C3	04:45	33
V	**30**	AD	M	65	A3	B3	C3	06:00	43
V	**31**	AD	F	73	A3	B3	C3	NA	NA
V	**32**	AD	F	90	A3	B3	C3	03:55	32
V	**33**	AD	M	88	A3	B3	C3	04:40	43
V	**34**	AD	M	74	A3	B3	C3	05:10	NA
V	**35**	Control	M	73	A0	B0	C0	24:45	33
V	**36**	Control	M	71	A0	B1	C0	07:40	33
V	**37**	Control	F	82	A0	B1	C0	07:00	33
V	**38**	Control	M	56	A0	B0	C0	09:15	43
V	**39**	Control	M	62	A0	B1	C0	07:20	33
V	**40**	Control	M	76	A0	B0	C0	06:45	33
V	**41**	Control	M	93	A0	B1	C0	05:05	33
V	**42**	Control	F	60	A0	B0	C0	08:10	32
V	**43**	Cotton wool	M	72	A3	B3	C0‡	05:15	43
V	**44**	Prp-CAA	F	57	A0	B0#	C0	24:00	NA
V	**45**	CADASIL	M	73	A0	B0	C0	31:45	NA
V	**46**	CARASAL	F	55	A1	B1	C0	04:00	NA
V	**47**	Hyper tension related SVD	F	92	A1	B2	C0	07:25	NA

Alzheimer's disease: AD, cerebral amyloid angiopathy: CAA, M: male, F: female, post mortem delay: PMD, not available / not applicable: NA, used for mass spectrometry analysis: MS, used for validation: V. (* Aβ only present as dysphoric CAA) (#Focal tau accumulation around blood vessels with prp-amyloid deposits) (‡ only dyshoric angiopathy in gallyas staining)

Brain tissue preparation and laser capture microdissection (LCM)
Laser capture microdissection (LCM) was performed as described previously [19]. LCM was performed using a Leica AS LMD system (Leica). Cortical layers II to VI which were randomly selected from control tissue and selected based on the presence of severe Aβ pathology in the case of AD and CAA were collected in Eppendorf tubes containing 30 µl M-PER lysis buffer (Thermo Scientific) supplemented with reducing SDS sample buffer (Thermo Scientific). Between 10 and 20 tissue sections with a thickness of 10 µm were captured using LCM, yielding an equal volume each of 1.0 x 10^9 µm3. Micro-dissected tissue was stored at -80 °C until further use.

Protein separation by electrophoresis and in-gel digestion
Micro-dissected tissue lysates were incubated at 95 °C for 5 min to denature the proteins, followed by incubation with 50 mM iodoacetamide for 30 min at RT in the dark to alkylate the cysteine residues. To reduce protein complexity, samples were size separated on a NuPAGE® 4-12% Bis-Tris acrylamide gel using MOPS SDS running buffer (Invitrogen) according to the manufacturers' protocol.

Gels were fixed in a solution containing 50% (v/v) ethanol and 3% (v/v) phosphoric acid in H_2O for 3h at RT and stained with Colloidal Coomassie Blue (34% (v/v) methanol, 3% (v/v) phosphoric acid, 15% (w/v) ammonium Sulphate, and 0.1% (w/v) Coomassie brilliant blue G-250 (Thermo Scientific), overnight while shaking. Destaining was performed in ultra-pure water under gentle agitation for several hours to reduce background staining (Fig. S1). Each gel lane was sliced into 12 equal sized parts to reduce sample complexity during later mass spectrometry analysis and each part was cut into blocks of approximately 1 mm^3 and collected in an Eppendorf tube. Gel fragments were destained in ultrapure water with 50 mM NH_4HCO_3 and 50% (v/v) acetonitrile overnight. Gel fragments were dehydrated using acetonitrile for 20 min and dried for 30 min using a SpeedVac. The gel parts were rehydrated in 70 µl of ultra-pure water containing 50 mM NH_4HCO_3 and 10 ug/ ml trypsin (sequence grade; Promega) and incubated overnight at 37 °C to facilitate digestion of the proteins. Peptides were extracted twice with a solution containing 0.1% (v/v) trifluoric acid and 50% (v/v) acetonitrile for 20 min. The samples were dried using a SpeedVac and stored at -20 °C until further analysis.

Mass spectrometry analysis
The peptides of the individual sample fractions were dissolved in 15 µL of 0.1% (v/v) acetic acid of which 10 µL was loaded onto a nano-liquid chromatography (nano-LC) system (Eksigent). The peptides were separated using a capillary reversed phase C18 column that had been equilibrated with 0.1% (v/v) acetic acid at a flow rate of 400 nL/min. The peptides were eluted by increasing the acetonitrile concentration linearly from 5 to 40% in 80 min and to 90% in 10 min, using the same flow rate. Eluted peptides were transferred into the LTQ/Orbitrap MS (Thermo Scientific) by Electro Spray Ionisation (ESI). The Orbitrap was operated in the range of m/z 350-2000 at a full width at half maximum resolution of 30,000 after accumulation to 500,000 in the LTQ with one microscan. The five most abundant precursor ions were selected for fragmentation by collision-induced dissociation (CID) with an isolation width of 2 Da.

Protein inference and relative protein quantification

MaxQuant software was used for spectrum annotation, protein inference, and relative protein quantification [14]. Spectra were annotated against the Uniprot human reference proteome database (version 2016_04). Enzyme specificity was set to Trypsin/P, allowing at most two missed cleavages. Carbamido-methylation of cysteine was set as a fixed modification, and N-acetylation and methionine oxidation were set as variable modifications. Mass deviation tolerance was set to 20 ppm for monoisotopic precursor ions and 0.5 Da for MS/MS peaks. False-discovery rate cut-offs for peptide and protein identifications were set to 1% for both. The minimum peptide length was seven amino acids. Identified proteins that had the same set of peptides or a subset of peptides compared to another protein, were merged into one protein group. Peptides that were shared between different proteins were assigned to the protein with most peptide evidence (so-called 'Razor' peptides). Only protein groups with at least a single unique and a single Razor peptide were included. For relative protein quantification MaxQuant LFQ intensities based on at least a single shared peptide ratio were used [13].

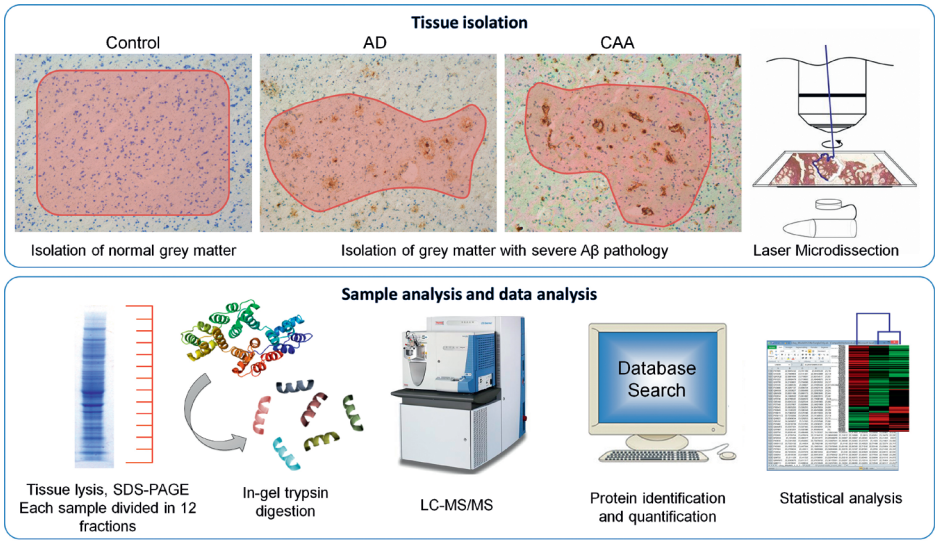

FIGURE 1 | Workflow used in this study. Amyloid Beta pathology was visualized in human postmortem occipital lobe tissue. Unaffected grey matter was isolated from healthy control cases. Grey matter with high burden of Aβ pathology was isolated from the AD and CAA cases thereby isolating tissue with high plaque load or high CAA type-1 burden, respectively.

Tissue was lysed and the proteins were separated using SDS-PAGE and subjected to in-gel trypsin digestion. Peptides were analysed using LC-MS-MS. A database search for protein identification and protein quantification was performed using MaxQuant software. ANOVA (Kruskall Wallis) and t-tests were performed to identify significantly regulated proteins.

Statistical analysis of differential protein expression

To identify proteins that differ in abundance between the different experimental groups an ANOVA (Kruskal–Wallis test) was performed using the Perseus software platform [40], adhering to a significance cut-off of p≤0.05. The p values were not corrected for multiple testing to include more proteins and provide a broad impression of the differences in the proteome.

Conditions that were set for inclusion of CAA selective proteins comprise of three approaches (A, B and C) that are visualized in figure 2. Approach A: T-tests (two-sided, assuming unequal variances, performed using Excel (Microsoft)) were performed contrasting the three experimental groups. When there was a significant difference ($p<0.05$) between both the control group versus CAA, and the AD group versus CAA, a protein was labelled as CAA specific. Approach B: If the number of quantitative values in the control group was zero or one while the AD and CAA groups both had two or more quantitative values, than a t-test was performed between the AD and the CAA group. When the AD group had zero or one quantitative values while the control and CAA groups both had two or more quantitative values a t-test was performed between the CAA and control group. Approach C: In the case of zero or single quantitative values in both the control and AD groups, proteins were included based exclusively on a minimum of four quantitative values in the CAA group. Also, we included proteins with zero or single quantitative values in the CAA group and four or more values in both the AD and control groups.

ANOVA (Kruskal–Wallis test) and posthoc Dunn's multiple comparison tests on immunoblot data and immunohistochemical data was performed using Graphpad Prism (GraphPad Software).

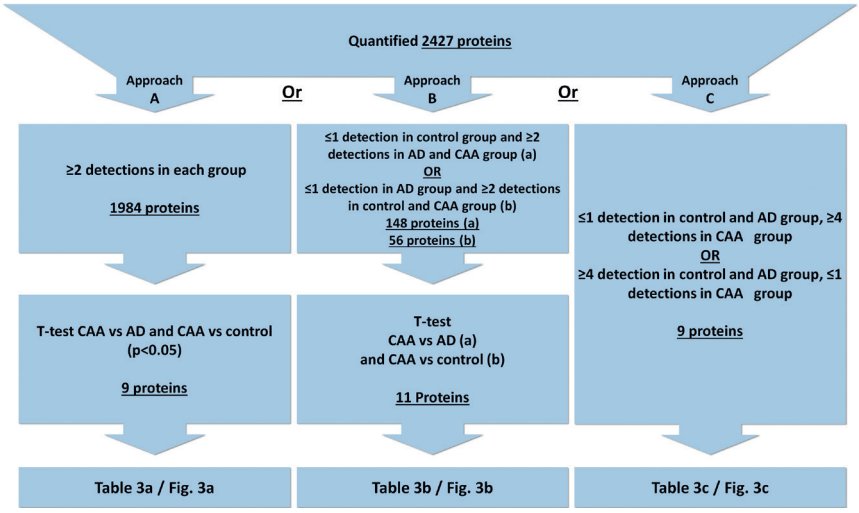

FIGURE 2 | Three strategies used to select proteins that are differentially expressed in CAA type-1 compared to control and AD brains. Criteria of each of the selection strategies are specified, numbers of resulted proteins indicated, and selected proteins are listed in tables and figures as indicated.

Immunoblot analysis

Protein extracts were prepared by lysis of whole occipital lobe tissue in reducing SDS sample buffer using a 1:20 tissue weight to lysis buffer ratio. Proteins were denatured at 95 °C for 5 min and separated by SDS-PAGE using precast Stain Free gradient gels (Bio-Rad) and transferred (40 V overnight at 4°C) onto a 0.45 µm PVDF membrane (Merck Millipore), which was pre-incubated in 100% methanol. The PVDF membrane was incubated in Odyssey blocking buffer for 1h and subsequently incubated with the primary antibody overnight. After washing in Tris-buffered saline (pH 7.5) with 0.1% (v/v) Tween-20 (TBST) for 3 x 10 min, the membrane was incubated for 3h with the secondary antibody. Visualization was achieved using an Odyssey imaging system using excitation wavelengths of 700 nm and 800 nm. Total protein load was visualized using a chemidoc EZ (Bio-Rad) after electro blotting (Fig. S2) and the protein densitometric values were then used to normalize for total protein input. Primary antibodies and dilutions are shown in Table 2. Secondary antibodies used were IRDye 800 CW Goat anti-Rabbit (LI-COR) and IRDye 680 conjugated Goat anti-Mouse (LI-COR) both were used at a 1:7.000 dilution. All antibodies were diluted in Odyssey blocking buffer (LI-COR). Quantification was performed using ImageJ software.

Immunohistochemical analysis

Fresh frozen or paraffin embedded human occipital tissue was cut (5 µm). For frozen tissue the sections were placed on a SuperFrost Microscope Slide (VWR, PA, USA) and air-dried overnight at room temperature (RT). Prior to staining, the sections were fixed in 100% acetone for 10 minutes. For paraffin sections the paraffin was removed by washing in xylene. Next, the sections were washed in decreasing concentrations of ethanol (100%, 96% and 70% (v/v)). Endogenous peroxidase activity was quenched by incubating in methanol with 0.3% H2O2 for 30 minutes at RT. Next, antigen retrieval was performed by submerging the slides in citrate buffer (pH 6) and heating in an autoclave.

Primary antibodies were diluted in antibody diluent (VWR) and incubation was performed overnight at 4 °C. All primary antibodies and corresponding dilutions used are listed in Table 2. After incubation the sections were thoroughly washed in PBS (pH 7.4) for 30 minutes followed by incubation of an HRP-labelled secondary antibody, Envision (DAKO) for 30 minutes. Again, the sections were thoroughly washed in PBS (pH 7.4) for 30 minutes and then incubated with DAB to visualize antibody binding. Counterstaining of the nuclei was performed by incubation in hematoxylin for 3 minutes followed by extensive washing in running tab water for 5 minutes. Next, the slides were dehydrated by incubation in increasing concentrations of ethanol consisting of 70% (v/v), 96% (v/v) and 100% (v/v) ethanol. The slides were then incubated in xylene and mounted using Quick-D mounting medium. A negative control was made by omission of the primary antibody. Quantification of the staining was done using ImageJ using the threshold colour plugin.

TABLE 2 | Antibodies used in this study.

Antibody	Source	Species	Ordernr.	Clone	Dilution (IHC)
Amyloid-beta	Kind gift of Prof. Dr. Korth, Heinrich Heine University, Düsseldorf, Germany	Mouse		IC16	1:200
APOE	Abcam	Mouse	ab1907	E6D7	1:3200
APOE	Santa Cruz Biotechnology	Mouse	sc-13521	A1.4	Used for immunoblot
NDP	Novus Biologicals	Rabbit	NBP1-84769	polyclonal	1:400
NDP	R&D systems	Mouse	MAB3014	#343711	1:800
HTRA1	R&D systems	Mouse	MAB2916	#275615	1:6400
APCS	Statens Serum Institut, SSI Antibodies	Mouse	#56585	HYB281-05	1:1600
COL6A2	Abnova	Mouse	H00001292-M01	2C5-F2	1:3200
COL6A2	Santa Cruz Biotechnology	Rabbit	SC-83607	polyclonal	1:1600

RESULTS

Selection of cases, controls and analysis of brain tissue

Three groups with a total of 20 cases were assembled based on careful neuro-pathological inspection: 1) cognitively healthy control cases (n=6) without any Aβ pathology or tau pathology, 2) AD cases with severe Aβ plaque pathology but no vascular deposits (no CAA) (n=7) and 3) AD cases with severe nearly pure CAA type-1 pathology and a negligible amount of plaque pathology (n=7). From here, these groups will be mentioned as "control", "AD" and "CAA", respectively. Inclusion of these cases was done based on histochemical analysis using Congo-red and additional IHC for Aβ on the occipital frozen tissue intended for LC-MS-MS analysis.

We focussed our analysis on the occipital lobe as this region is the most frequently and severely affected by CAA pathology. Tissue sections of human occipital lobe from all selected cases were mounted on PEN-foil slides and Aβ pathology was visualized using fast immunohistochemistry. Grey matter tissue was isolated using LCM. Tissue isolation from the AD cases and CAA cases was focused on occipital lobe grey matter areas with severe Aβ pathology, i.e. high plaque load or high CAA type-1 burden, respectively. This was done to selectively enrich the input material for the proteomics analysis for these types of Aβ pathology. For control cases occipital lobe grey matter areas from the same anatomical region were selected for isolation. LCM-collected tissue samples were lysed and proteins were separated using SDS-PAGE. Each PAGE sample lane was divided into 12 fractions and subjected to in-gel trypsin digestion (Fig. 1).

Protein quantification and global protein expression profiles

To identify and quantify proteins, liquid chromatography followed by mass spectrometry (LC-MS-MS) was performed on the 20 laser-dissected tissue samples. This allowed quantification of

2427 proteins in total and approximately 1500 proteins identified per individual case (Fig. S3), with a minimum of one tryptic peptide detected. All quantified proteins are listed in table S1.

To gain insight into the global similarities and differences between the three groups and the individual cases an ANOVA (Kruskall Wallis) was performed. This yielded 309 proteins that have a significant difference ($p<0.05$) in abundance between any of the experimental groups. Using these proteins in an unsupervised clustering analysis, three different expression signatures were obtained. The protein expression signatures of the AD and CAA groups appeared largely similar, whereas both were different from the control group (Fig. S4A). Unsupervised clustering analysis of the individual cases using the 309 ANOVA-identified proteins, separated the controls from the disease cases (Fig. S4B). The CAA and AD cases were not separated on the basis of the full set of differentially expressed proteins indicating that overall their protein expression profile is largely similar. One CAA case (case #5) clustered with the control cases indicating that the protein expression profile of this sample is more similar to the control cases than to other CAA or AD cases. Visualizing the expression profile of case #5 next to the average expression profiles of the three groups confirmed the resemblance of case #5 to the control group, but also showed several proteins that are similar in expression to the AD and or CAA groups (Fig. S5A).

Identification of proteins selectively altered in CAA type-1

To identify proteins that have a significantly different abundance in CAA type-1 compared to both the control and the AD group, and therefore represent unique features of CAA type-1, we performed student t-tests (two-sided, assuming unequal variances) for those proteins where at least two quantitative values per groups were available. When there was a significant difference ($p<0.05$) between both the control group versus CAA, and the AD group versus CAA, a protein was designated as CAA-specific (Fig. 3A and Table 3A). CLU, APOE, SUCLG2, PPP2R4, KTN1, ACTG1, TNR, COL6A3 and NFASC met these criteria. In addition, levels of CLU, APOE, SUCLG2, PPP2R4 and ACTG1 were also significantly different ($p<0.05$) when comparing the AD group with the control group.

After calculating the multiple testing corrected false discovery rate (FDR) only CLU was considered significant. This is likely due to the relatively low sample size of this exploratory study and the high inter-individual variance that is inevitably associated with the use of human tissue. Given the explorative nature of this study we relaxed criteria and adhered to the uncorrected p-values for protein inclusion.

Importantly, using label-free mass spectrometry to identify and quantify proteins, the absence of data for a number of proteins is observed. Despite great improvements in the speed and sensitivity of MS analysers missing data is almost unavoidable. When quantitative data are absent in one group while being present in the other group(s), this likely indicates differences in abundance, which might represent interesting candidate marker proteins. Therefore, absence of data in one or more patient groups required 2 additional approaches to also consider these proteins in this study. An overview of the 3 complementing strategies for protein inclusion is

shown in figure 2 and a complete description is present in the methods section. Note that any given protein is only considered using a single approach as these approaches are mutually exclusive.

Using approach B (Fig. 2), proteins with a significant difference were included, and APP, UBLCP1, SRI, NDP, PNP, C1orf123, DHX15, SYNPO, TPM1, CADPS2 and SERPINA3 (Fig. 3B and Table 3B) were identified as proteins selectively present in CAA type-1. Peptide data on APP indicates that quantification was based on two peptides in which the most abundantly detected peptide (LVFFAEDVGSNK) is part of Aβ.

Approach C (Fig. 2) resulted in the identification of HLA-DRA, HLA-DQA2, HTRA1, APCS, COL6A2, MOB2, POTEI, KIAA1468, TMF1 and SGIP1 (Fig. 3C and Table 3C) as CAA specific proteins.

Earlier, Case #5 was identified as having an expression profile resembling a control case. Case #5 was found positive for Alzheimer type 2 astrocytes, possibly related to high alcohol intake, and exhibited relatively low tau pathology. Otherwise, this case showed no pathological abnormalities when compared to the rest of the CAA type-1 group. However, the expression of several CAA selective markers that we identified was inspected for case #5. The levels of these markers correspond well with the other cases of the CAA group (Fig. S5B), indicating that these proteins are inseparably linked to the pathology of CAA type-1. In addition, although the number of cases is too small to do valid statistics, we observed no clear relation between gender and expression of the markers (Fig. S6).

To determine whether the above-described approaches were indeed appropriate in selecting CAA specific proteins, we performed additional immunoblotting and immunohistochemical (IHC) analysis.

TABLES 3A, 3B AND 3C | Proteins identified as selectively altered in CAA type-1.

Table 3A	**Significant CAA versus control and CAA versus Alzheimer's disease**									
Gene	**Protein**	**P-val C vs CAA**	**P-val AD vs CAA**	**FDR C vs CAA**	**FDR AD vs CAA**	**FC C vs CAA**	**FC AD vs CAA**	**# detections Control**	**# detections AD**	**# detections CAA**
CLU	Clusterin;Clusterin beta chain;Clusterin alpha chain	0.000	0.000	0.001	0.007	4.47	2.33	6	7	7
APOE	Apolipoprotein E	0.001	0.001	ns	ns	4.97	2.11	6	7	7
SUCLG2	Succinyl-CoA ligase [GDP-forming] subunit beta, mitochondrial	0.002	0.002	ns	ns	2.17	0.61	5	7	7
PPP2R4	Serine/threonine-protein phosphatase 2A activator	0.026	0.010	ns	ns	2.18	0.80	6	7	7
KTN1	Kinectin	0.015	0.021	ns	ns	0.34	0.40	2	2	3
ACTG1	Actin, cytoplasmic 2;Actin, cytoplasmic 2, N-terminally processed	0.000	0.035	ns	ns	0.80	0.90	6	7	7
TNR	Tenascin-R	0.007	0.017	ns	ns	0.82	0.82	6	7	7
COL6A3	Collagen alpha-3(VI) chain	0.016	0.024	ns	ns	7.79	4.95	3	5	7
NFASC	Neurofascin	0.028	0.040	ns	ns	0.86	0.87	6	7	7
Table 3B	**Significant CAA versus control or Alzheimer's disease and ≤1 detection in other group**									
Gene	**Protein**	**P-val C vs CAA**	**P-val AD vs CAA**	**FDR C vs CAA**	**FDR AD vs CAA**	**FC C vs CAA**	**FC AD vs CAA**	**# detections Control**	**# detections AD**	**# detections CAA**
APP	Amyloid beta A4 protein;N-APP;Soluble APP-alpha;Soluble APP-beta;	NA	0.000	NA	ns	NA	6.65	1	7	7
UBLCP1	Ubiquitin-like domain-containing CTD phosphatase 1	NA	0.007	NA	ns	NA	1.96	1	2	4
SRI	Sorcin	NA	0.011	NA	ns	NA	0.25	1	3	5
NDP	Norrin	NA	0.020	NA	ns	NA	5.16	0	4	7
PNP	Purine nucleoside phosphorylase	NA	0.030	NA	ns	NA	1.72	0	3	3

TABLES 3A, 3B AND 3C | Continued

Table 3B	**Significant CAA versus control or Alzheimer's disease and ≤1 detection in other group**									
C1orf123	UPF0587 protein C1orf123	NA	0.047	NA	ns	NA	0.71	0	6	6
DHX15	Putative pre-mRNA-splicing factor ATP-dependent RNA helicase DHX15	0.005	NA	ns	NA	0.44	NA	3	0	5
SYNPO	Synaptopodin	0.015	NA	ns	NA	0.44	NA	4	1	4
TPM1	Tropomyosin alpha-1 chain	0.021	NA	ns	NA	0.37	NA	3	1	3
CADPS2	Calcium-dependent secretion activator 2	0.042	NA	ns	NA	1.22	NA	2	1	3
SERPINA3	Alpha-1-antichymotrypsin;Alpha-1-antichymotrypsin His-Pro-less	0.042	NA	ns	NA	-0.86	NA	2	1	3

Table 3C	**≤1 in control and Alzheimer's disease and ≥4 in CAA OR ≤1 in CAA and ≥4 in Alzheimer's disease and control**									
Gene	**Protein**	**P-val C vs CAA**	**P-val AD vs CAA**	**FDR C vs CAA**	**FDR AD vs CAA**	**FC C vs CAA**	**FC AD vs CAA**	**# detections Control**	**# detections AD**	**# detections CAA**
HLA-DRA;HLA-DQA2	HLA class II histocompatibility antigen, DR alpha chain;HLA class II histocompatibility antigen, DQ alpha 2 chain	NA	NA	NA	NA	NA	NA	0	1	7
HTRA1	Serine protease HTRA1	NA	NA	NA	NA	NA	NA	0	1	7
APCS	Serum amyloid P-component;Serum amyloid P-component(1-203)	NA	NA	NA	NA	NA	NA	0	1	6
COL6A2	Collagen alpha-2(VI) chain	NA	NA	NA	NA	NA	NA	0	1	5
MOB2	MOB kinase activator 2	NA	NA	NA	NA	NA	NA	1	1	5
POTEI	POTE ankyrin domain family member I	NA	NA	NA	NA	NA	NA	1	0	4
KIAA1468	LisH domain and HEAT repeat-containing protein KIAA1468	NA	NA	NA	NA	NA	NA	1	0	4
TMF1	TATA element modulatory factor	NA	NA	NA	NA	NA	NA	0	1	4
SGIP1	SH3-containing GRB2-like protein 3-interacting protein 1	NA	NA	NA	NA	NA	NA	4	4	1

Alzheimer's disease, AD; cerebral amyloid angiopathy, CAA; false discovery rate, FDR; not applicable, NA; Not significant, NS; fold change, FC. Proteins were found using the three different selection methods as described in figure 2.

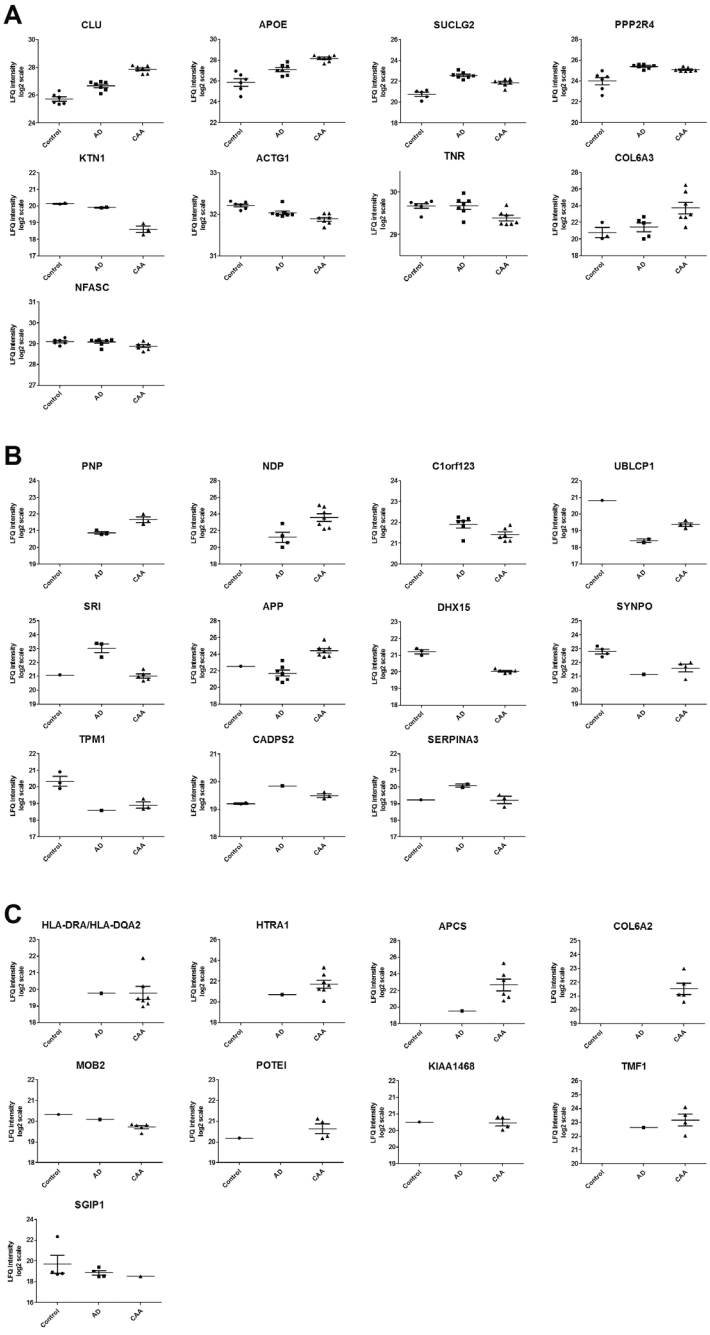

FIGURE 3 | Relative abundance of proteins with altered expression in CAA type-1 compared to Alzheimer's disease cases and controls as determined by MS. Three groups of selected proteins (panels A-C), with altered levels (MS-derived, log2 LFQ intensity values) in CAA type-1 compared to the control groups and the AD groups. Selection criteria are specified in Fig.2. Gene names are indicated.

Confirmation of MS data using immunoblotting and immunohistochemical analysis

Of the proteins described in table 3 we selected APOE (approach A), NDP (approach B), HTRA1, APSC and COL6A2 (approach C), based on the fold change or specific expression in the CAA type-1 group compared to the AD and control groups, to confirm our mass spectrometry results. Immunoblotting was performed on whole tissue lysates of the same cases as used for the mass spectrometry analysis. When comparing the CAA group with the control group we found significant differences in NDP expression (Fig. 4). For APOE, APCS and COL6A2, the data showed the same trend of increased abundance in the CAA group as the proteomics data, but the differences did not reach significance. A likely explanation for this is the higher variation of expression of these proteins in the tissue used for immunoblotting, which in contrast to the mass spectrometry exploratory analysis, was not selectively enriched for pathological burden using LCM, and instead included white matter, leptomeningeal vessels and grey matter with a lower pathological burden. To unequivocally demonstrate CAA related expression, we turned to IHC analysis of these same proteins, which, in contrast to immunoblotting, allows region specific analysis similar to the LCM-LC-MS-MS analysis. For this a separate cohort was used consisting of cognitively healthy control cases (n=8) without any Aβ or tau pathology, 2) AD cases with severe Aβ plaque pathology but no vascular deposits (no CAA)(n=8) and 3) AD cases with severe CAA type-1 pathology (n=6).

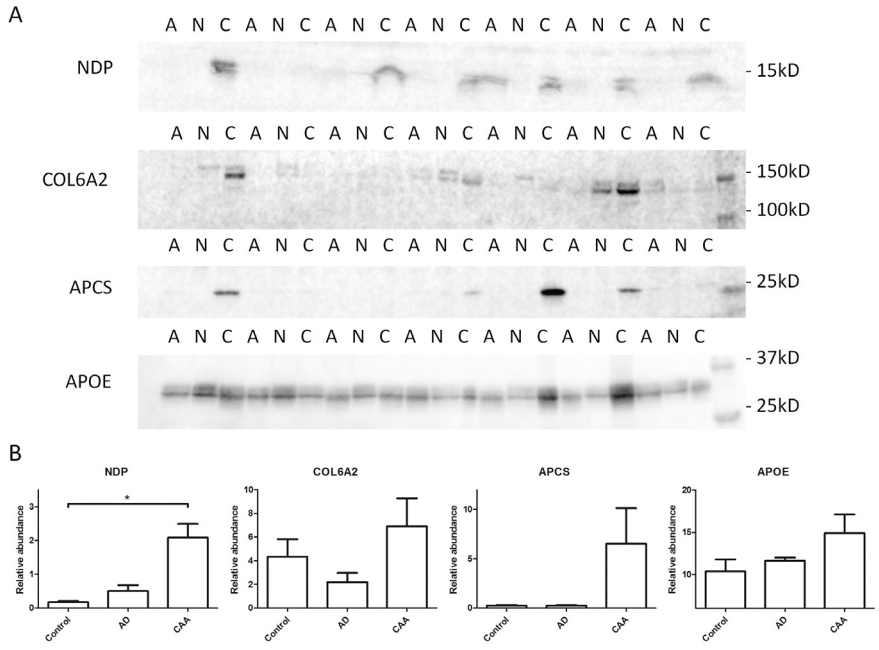

FIGURE 4 | Immunoblotting analysis of proteins with altered expression in CAA type-1. (A) Immunoblotting was performed for, NDP, COL6A2, APCS and APOE on occipital lobe tissue lysates of non-demented controls (N) AD cases (A) and CAA cases (C). Immunoreactivity was observed at the correct molecular weight for each protein. (B) A significant difference ($p < 0.05$) was found in the expression of NDP in the CAA group when compared to control but not when compared to the AD group. For COL6A2, APCS and APOE significance was not reached between any of the groups using this technique. Data are expressed as mean ± SEM.

First, Aβ pathology was visualized and its presence was confirmed in AD and CAA type-1 cases showing plaques and vascular Aβ pathology, respectively (Fig. 5B and Fig. 5C). Then, IHC analysis was performed to gain information on the localization of the selected proteins. IHC for NDP showed pronounced immunoreactivity in CAA type-1 cases that appeared associated to the vasculature. NDP immunostaining in CAA, appeared to be associated with both compact Aβ depositions as well as more diffuse staining in the parenchyma in cases that exhibit dyshoric Aβ deposits. Staining was more pronounced related to capillaries compared to larger vessels. The AD cases with plaques were nearly devoid of immunoreactivity, controls did not show any immunoreactivity for NDP (Fig. 5D, E and F). Different antibodies against NDP showed similar results (data not shown).

COL6A2 IHC showed some immunoreactivity in control and AD cases which was restricted to leptomeningeal vessels (Fig. S7) and a few large vessels in the brain tissue. In CAA type-1, immunoreactivity for COL6A2 was highly increased and includes brain capillaries and larger vessels. Immunoreactivity was mostly associated with the endothelium and / or the adventitia (Fig. 5G-I). Similar results were obtained using two different antibodies for COL6A2 (data not shown). HTRA1 IHC showed clear overlap with Aβ in both AD and CAA. Compact and diffuse staining was observed related to the vessels in the CAA cases and showed plaque pathology in the AD cases without CAA. Control cases were all negative for HTRA1 (Fig. 5J-L). IHC for APOE resulted in pronounced staining of the vasculature in CAA cases and appeared related to compact deposits as well as more diffuse dyshoric deposits. Also immunoreactivity of APOE was observed in the AD cases related to the Aβ plaques, although the staining was less intense than that related to the vascular amyloid in the CAA cases (Fig. 5P-R). APCS IHC illustrated the presence of this protein in relation with both diffuse and compact Aβ pathology in both the CAA and AD group. However, staining related to the plaque pathology was less intense than that related to the vascular Aβ pathology (Fig. 5M-O).

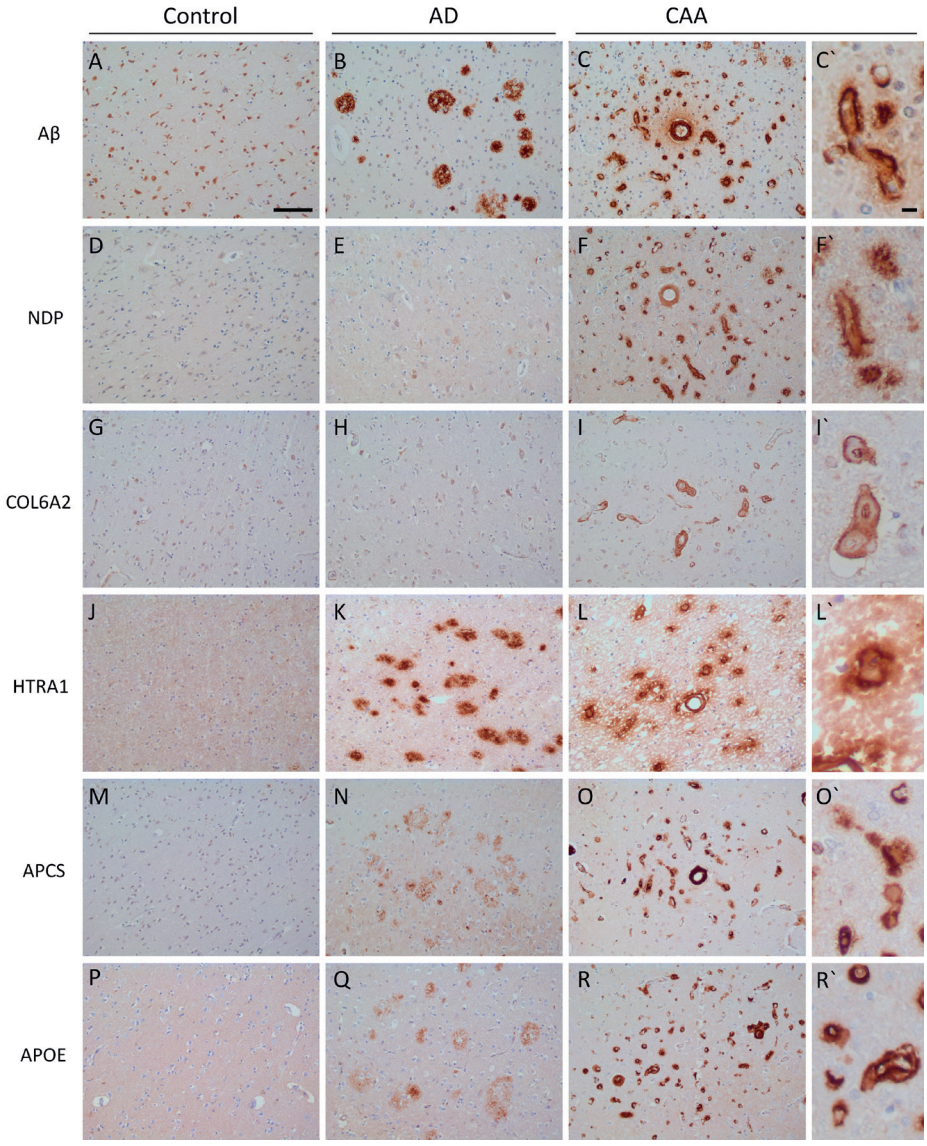

FIGURE 5 | Immunohistochemical analysis of selected proteins. Representative images were taken. Aβ pathology was visualized. (A) The control case does not have any Aβ pathology. (B) plaque pathology is confirmed in the AD case and (C) CAA type-1 pathology is confirmed in the CAA type-1 case. (D,E,F) Extensive NDP immunoreactivity is observed in the CAA type-1 cases whereas absent in both control and AD cases without CAA. (G,H,I) COL6A2 immunoreactivity is hardly observed in the control and AD cases, however, extensive immunoreactivity is observed in the CAA type cases and includes both capillaries and large vessels. (J,K,L) Immunoreactivity for HTRA1 is absent in control tissue, however, is observed both related to plaque pathology and CAA at comparable intensity. (M,N,O) Immunoreactivity for APCS is absent in control cases but is observed both related to plaque and CAA type-1 pathology. However, the intensity of

the staining observed in the AD cases is considerably less. (P,Q,R) Also, APOE immunoreactivity is observed related to both plaque and CAA type-1 pathology, yet its intensity in CAA type-1 is far greater. Scale bar, 100μm in images A to R. Scale bar in image (C`) 10μm and in all zoomed images, which are marked with a grave accent (`).

For quantification of the IHC, images were obtained at sites that, for the AD and CAA cases, had high Aβ pathological burden in nearby sections of the same tissue block. The percentage of positively stained pixels over a total of 5 images from each case was determined. Although this method is semi-quantitative, it allowed a region-specific analysis in line with the tissue obtained by laser capture dissection that was at the basis of the original mass spectrometry analysis. Using IHC quantification we observed strongly increased immunoreactivity in CAA type-1 cases for NDP and COL6A2, and moderate increases for APCS, HTRA1 and APOE, confirming the MS results (Fig. 6).

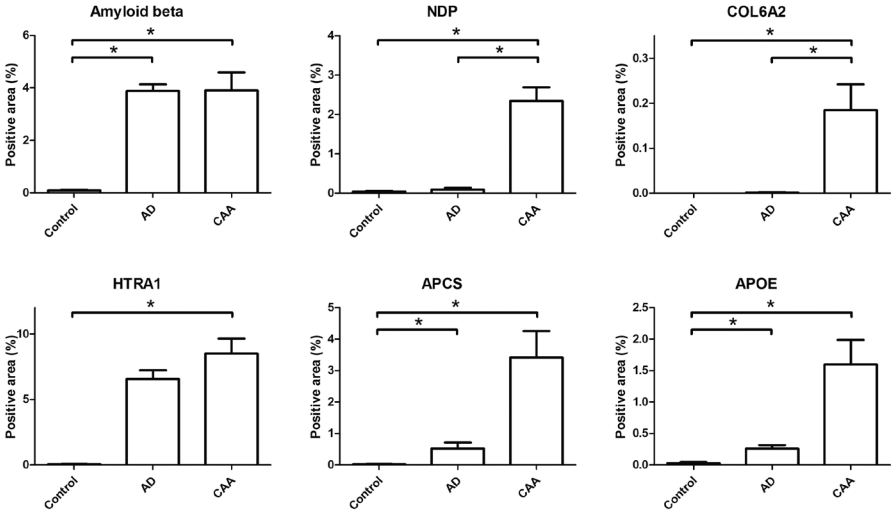

FIGURE 6 | Semi-quantitative analysis of immunohistochemical data of proteins with altered expression in CAA type-1. Immunohistochemical stainings were quantified by measuring the percentage of pixels that showed positive immunoreactivity. Significance was calculated using a one-way ANOVA (Kruskal-Wallis test) and posthoc Dunn's Multiple Comparison Test. A significant increase ($p<0.05$) in immunoreactivity in the CAA group compared to both control and AD groups was observed for NDP and COL6A2. For APOE, APCS and HTRA1 significant differences were only found when comparing CAA with control, but not with the AD group. Data are expressed as mean ± SEM.

Specificity in relation to other small vessel diseases

To assess the specificity of Aβ, NDP, COL6A2, APCS and APOE in relation to other small vessel diseases we performed additional IHC on cases that present various types of vascular defects, i.e., cotton wool plaque pathology, prion CAA, cerebral autosomal dominant arteriopathy with subcortical infarcts and leukoencephalopathy (CADASIL), hypertension related small vessel

disease and Cathepsin A-related arteriopathy with strokes and leukoencephalopathy (CARASAL). IHC was performed on sections that exhibited the relevant pathological characteristics of each disease, including an additional CAA type 1 case. Immunoreactivity for Aβ, NDP, COL6A2, APOE and APCS was confirmed in the CAA type 1 case (Fig. 7A-E). Immunoreactivity for these proteins was also assessed and confirmed in case exhibiting hereditary cerebral haemorrhage with amyloidosis Dutch type (HCHWA-D), which is a heredity form of CAA-type 1 (Fig. S8).

In tissue with cotton wool plaques, the pathology was confirmed using IHC for Aβ displaying pathology around capillaries and larger vessels with dyshoric changes extending deep into the parenchyma (Fig. 7F). Intense NDP immunoreactivity was observed related to capillaries and the dyshoric changes and to a lesser extend directly lining the larger vessels. COL6A2 showed intense immunoreactivity lining the capillaries and larger vessels (Fig. 7G). IHC for APOE and APCS presented a highly positive, staining that appeared similar to the Aβ staining.

The PrP-CAA tissue was confirmed negative for Aβ pathology (Fig. 7K) and showed positive for Prp (data not shown). NDP immunoreactivity was highly increased and localised to the affected vessels. NDP staining was more pronounced around affected capillaries than at affected larger vessels. COL6A2 immunoreactivity was clearly present around capillaries and larger affected vessels, of which the vascular pathology was clearly observed using haematoxylin. Although co-occurring in largely the same vessels COL6A2 did not generally co-localize with the deposits, but instead localized more internally as a component of the basal membrane. APOE and APCS were also highly present and co-localized with the Prp deposits.

In the white matter no immunoreactivity was seen for Aβ or any of the marker proteins (Fig. 7P-T) in the control case. The CADASIL case showed characteristic pathology in the white matter, thickened vessel walls, in the white matter as is common with this condition. No Aβ pathology was present (Fig. 7U) Mild immunoreactivity for NDP was present and of the assessed proteins COL62A staining was most pronounced. APOE and APCS also displayed mild immunoreactivity related to the affected vessels (Fig. 7V-Y).

In hypertension related small vessel disease the presence of COLA6A2 was most prominent, while immunoreactivity for NDP, APOE and APCS was low but present (Fig. 7Z-AD). Interestingly IHC analysis of the CARASAL cases showed only the prominent presence of COL6A2 in affected vessels while NDP, APOE and APCS were absent.

Taken our data together, from the tested panel of proteins, we recognize COL6A2 as a general small vessel disease marker. NDP, APOE and APCS are most prominent in CAA (type 1 and cotton wool) and Prp-CAA. Involvement of NDP APOE and APCS in other small vessel diseases is varying from non (CARASAL) to mild (CADASIL). Importantly, NDP is explicitly suitable to evidently separate CAA from Aβ plaque pathology (Table 4).

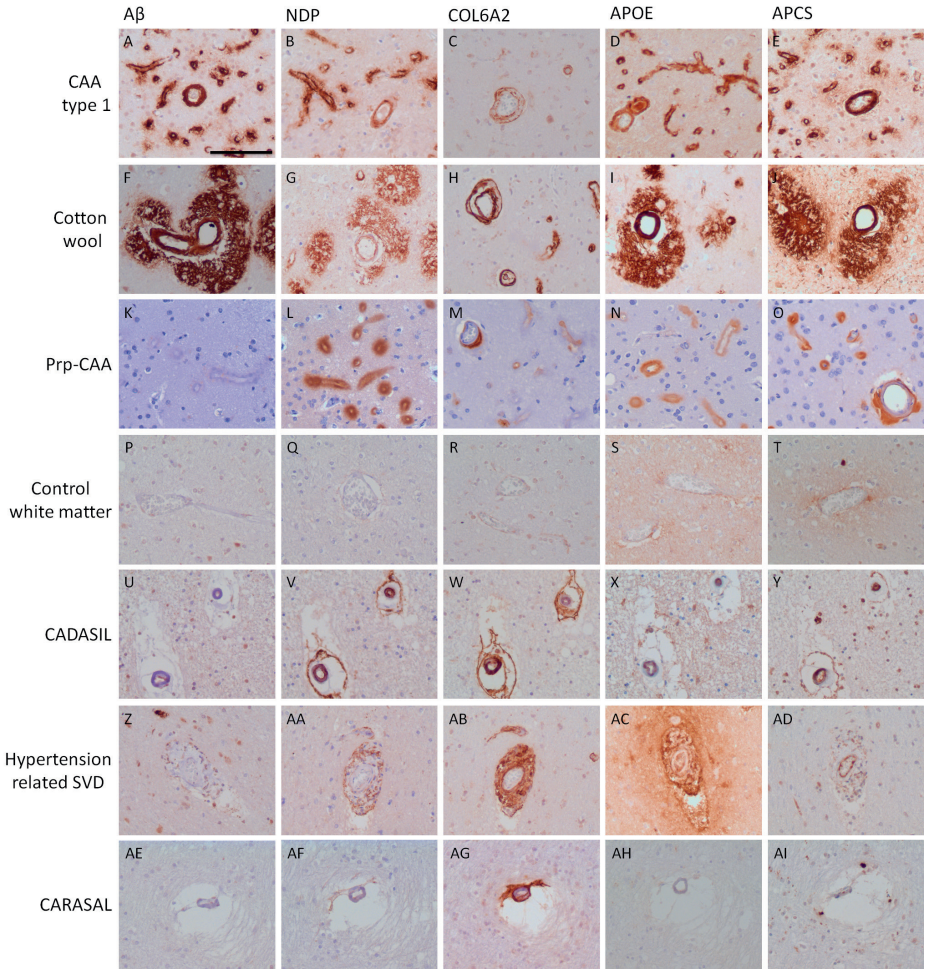

FIGURE 7 | Expression of CAA type-1 markers in other small vessel diseases. IHC for Aβ, NDP, COL6A2, APCS and APOE was performed. In a CAA type-1 case immunoreactivity for all marker proteins is confirmed (A-E). Also immunoreactivity is seen for all markers in the cotton wool case and Aβ pathology was confirmed (F). For NDP, APOE and APCS immunoreactivity is also seen localizing to severe dyshoric angiopathy (G, I and J). COL6A2 immunoreactivity is restricted to the vessel wall (H). In de Prp-CAA case Aβ pathology was absent (K). Extensive immunoreactivity was observed for NDP, COL6A2, APOE and APCS (L-O). No immunoreactivity was observed for Aβ, NDP, COL6A2, APOE and APCS in the white matter of control tissue (P-T). In the CADASIL case no Aβ pathology was present (U). Mild immunoreactivity for NDP (V) COL62A staining was most pronounced (W). APOE and APCS also displayed mild immunoreactivity related to the affected vessels (X, Y). In hypertension related small vessel disease no Aβ was detected (Z) immunoreactivity of COLA6A2 was moderate (AB) while immunoreactivity for NDP, APOE and APCS were low but present (AA, AC and AD). In the CARASAL case only prominent immunoreactivity of COL6A2 was seen in affected vessels (AG) while NDP, APOE and APCS were absent (AF, AH and AI). Scale bar in (A) indicates 100 µm.

TABLE 4 | Scoring of relative immunoreactivity of 5 CAA-1 positive markers in different small vessel diseases and AD plaque pathology.

	Aβ	NDP	COL6A2	APOE	APCS
CAA type 1	3	3	3	3	3
Cotton wool	3	3	3	3	3
Prp-CAA	0	3	3	3	3
Control white matter	0	0	0	0	0
CADASIL	0	2	2	1	1
Hypertension	0	1	2	1	1
CARASAL	0	0	2	0	0
AD plaques	3	0	0	2	2

0: no immunoreactivity, 1: mild immunoreactivity, 2: moderate immunoreactivity, 3: extensive immunoreactivity.

DISCUSSION

One of the most prevalent cerebro-vascular diseases in the elderly is sporadic CAA, characterized by vascular deposition of amyloid-beta protein. CAA can occur as an isolated disease or as part of the pathology in AD. Several studies have indicated CAA as an important cause of cognitive decline [1, 8, 16]. Currently, there is no treatment for CAA and its presence cannot be diagnosed pre-mortem. Therefore insight in the pathogenic mechanisms and the need for biomarkers are urgent. We performed an exploratory laser dissection-assisted LC-MS-MS analysis of AD brain tissue exhibiting severe CAA type-1 pathology, AD brain tissue without apparent involvement of CAA, and control brain tissue without AD related pathology. We show that the proteome of CAA type-1 is different from that of parenchymal plaque pathology in AD, which led to the identification of proteins selectively associated with CAA.

Next to identification of new CAA selective proteins, this study also confirmed the presence proteins already known to be involved in CAA pathology, e.g., CLU, APOE and APCS [22, 42]. Interestingly, CLU was detected in all samples included in the study and its abundance was sufficient to completely separate the CAA group from both the control group and the AD group. Moreover, CLU, APOE and APCS were markedly increased in AD compared to controls and APOE and APCS showed moderate immunoreactivity related to plaque pathology, in accordance with previous findings [42, 48]. Interestingly, increased levels of CLU have been reported in the plasma of CAA patients diagnosed according the modified Boston criteria [25].

Two recent proteomics studies focussed on CAA analysing leptomeningeal vessels [23] and leptomeningeal vessel combined with neocortical arterioles [20]. Some similarities were found with these studies, such as the increase in CLU and APOE. As expected also several differences exist as our analysis focussed on grey matter of CAA type 1 using micro dissected tissue that is enriched for areas with very high capillary associated Aβ pathology. These differences might indicate that other mechanisms are involved in the pathogenesis in CAA related to capillaries

compared to larger vessels, e.g., the findings of NDP and COL6A2. In contrast to these previous studies we compared CAA cases with both control and AD cases with plaque pathology and without CAA. There are many similarities in the response to CAA and AD and these proteins and processes can be cancelled out against each other, allowing CAA selective proteins to become apparent.

Importantly, we identified potential new key players in the development of CAA. NDP is found highly upregulated in CAA type 1, cotton wool Aβ pathology and Prp-CAA, and localizes around the affected vasculature. NDP immunoreactivity was only mildly increased in CADASIL and hypertension related small vessel disease. In addition, these diseases affect different anatomical regions, clearly identifiable with imaging studies, and present a distinct clinical picture, leaving NDP a promising biomarker for CAA.

NDP is a small, secreted protein with a molecular weight of approximately 15 kD. It has important function in the formation of the brain vasculature during development and in maintenance of a proper functioning BBB [15]. In the adult brain the NDP gene is primarily expressed by astrocytes [47]. NDP activates the canonical Wnt/β-catenin signalling pathway via the frizzled (Fzd)4/low-density lipoprotein receptor-related protein (Lrp)5/6 receptor complex [46]. In neural progenitor cells (NPCs) derived from FAD mutant PSEN1 subjects it was found that NDP mRNA is upregulated, but no increase in mRNA was found in AD human temporal lobe [35]. In the retina NDP was found to promote regrowth of capillaries and formation of intra-retinal vessels after oxygen-induced retinal damage [27]. Mice overexpressing NDP, had significantly less vascular loss following oxygen exposure. Mutations in the NDP gene result in Norrie disease, which is primarily an eye disease that leads to blindness. Interestingly, 30-50% of these patients display developmental delay, intellectual disability, behavioural abnormalities, or psychotic-like features [10, 33]. In addition, NDP has been shown to protect neurons against excitotoxicity induced by NMDA [32]. NDP seems to have protective properties for both endothelial cells and neurons, but whether NDP upregulation is beneficial in the context of CAA pathology is unknown.

Our proteomics data show COL6A2 expression in CAA cases, which is supported by a strong increase in COL6A2 immunoreactivity in the affected brain parenchyma. In addition to COL6A2 we also found COL6A3 highly increased in CAA type-1. COL6A2 immunoblotting did not show a significant difference between the experimental groups. This can be explained by the inclusion of leptomeningeal vessels, that express high levels of COL6A2 in all cases in varying amounts in the tissue lysates used for immunoblotting, as shown using IHC. COL6A2 was also found increased in the other small vessel diseases that were included for IHC analysis. This indicates that COL6A2 might be used as valuable indicator of vascular pathology in general, but not specific for CAA type pathology. COL6A2 is a non-fibril collagen and COL6 isoforms are present in various tissues including the vasculature [29]. COL6A2 encodes one of the three alpha chains of type VI collagen, which is found in most connective tissues. Type VI collagen anchors endothelial basement membranes by interacting with type IV collagen [21]. In the

brain, collagen VI was shown neuroprotective and its expression increased in animal models of AD [11].

HTRA1 is a trypsin-like serine protease which was detected in all CAA samples, with a single value in the AD group and zero quantitative values in the control group. Using immunohistochemistry we found a significant difference with the control groups but not with the AD group as HTRA1 marks normal plaque pathology as well. HTRA1 is relevant in neurodegeneration as this protease is involved in the degradation of APP and Aβ [17]. In addition, HTRA1 was found to degrade APOE4 more efficiently than APOE3 and the presence of APOE4 reduces digestion of MAPT by HTRA1 [12]. Moreover, mutations in HTRA1 are the cause of the hereditary small vessel disease CARASIL (cerebral autosomal recessive arteriopathy with subcortical infarcts and leukoencephalopathy) [18, 38].

As part of our LC-MS-MS exploratory study we identified other proteins that are potentially interesting for additional research in relation to CAA, but were not specifically followed up in this study. For instance, we observed significant high levels of HLA-DR/HLA-DQ in CAA type-1. This protein is associated with inflammation and high numbers of activated microglia [30]. PNP for which a single nucleotide polymorphism was found to be associated with faster progression of AD[39]. Its relation to CAA is yet unknown. SUCLG2 which is involved in clearance of Aβ1-42 [28] was found increased in CAA compared to control and even higher levels were observed in the AD cases. APP was identified with increased levels in CAA. Peptide data indicates that the most abundantly detected peptide is a part of Aβ, however this analysis cannot discriminate between Aβ or APP.

The proteins in this study, that show selective association with CAA type-1 pathology might serve as potential CAA type-1 biomarkers in patients. As larger vessels are also positive for the markers that were assessed using IHC, these markers might also be relevant in CAA type-2, although in the case of NDP the intensity of immunoreactivity is less in larger vessels compared to affected capillaries in CAA.

CAA selective markers might be used for pathological assessment of the severity of CAA. The association of Aβ with the vasculature, and in particular capillaries, is not always obvious in thin microscopic sections. Also, the use of these proteins as potential diagnostic markers should be explored. The need for a biomarker for CAA is urgent, in part for (early) diagnosis of CAA, but also for stratification of patients involved in clinical trials for AD. For instance, anti-amyloid immunotherapies in development may warrant separation of AD patients with or without CAA because of expected side effects associated with CAA, including vasogenic oedema and cerebral microhemorrhages [7, 34]. In addition, these markers would help to improve the assessment of the safety of anticoagulation therapy in patients with CAA as they increase the risk of intracerebral haemorrhage [6].

CONCLUSION

In conclusion, we present a set of marker proteins containing known and new markers representing valuable tools for both clinical and neuropathological diagnosis which can contribute to studies investigating the role of CAA in AD pathology. In addition to their use as biomarkers, the newly found proteins might be further investigated to increase our understanding of etiology and disease mechanism related to CAA, and ultimately may be used as therapeutic targets.

ACKNOWLEDGEMENTS

The authors thank the Netherlands Brain Bank (Amsterdam, the Netherlands) for supplying human brain tissue. The authors want to thank Will Hermsen, University Medical Center Utrecht, for performing the immunohistochemistry on the prion tissue. This work was financially supported by Amsterdam Neuroscience. David Hondius was supported by the CAVIA project (nr. 733050202), which has been made possible by ZonMW, part of the Dutch national 'Deltaplan for Dementia': zonmw.nl/dementiaresearch".

REFERENCES

1. Arvanitakis Z, Leurgans SE, Wang Z, Wilson RS, Bennett DA, Schneider JA (2011) Cerebral amyloid angiopathy pathology and cognitive domains in older persons. Ann Neurol 69:320–327. doi: 10.1002/ana.22112
2. Attems J (2005) Sporadic cerebral amyloid angiopathy: Pathology, clinical implications, and possible pathomechanisms. Acta Neuropathol 110:345–359. doi: 10.1007/s00401-005-1074-9
3. Attems J, Jellinger K, Thal DR, Van Nostrand W (2011) Review: Sporadic cerebral amyloid angiopathy. Neuropathol Appl Neurobiol 37:75–93. doi: 10.1111/j.1365-2990.2010.01137.x
4. Attems J, Jellinger KA (2004) Only cerebral capillary amyloid angiopathy correlates with Alzheimer pathology?a pilot study. Acta Neuropathol 107:83–90. doi: 10.1007/s00401-003-0796-9
5. Bakker ENTP, Bacskai BJ, Arbel-Ornath M, Aldea R, Bedussi B, Morris AWJ, Weller RO, Carare RO (2016) Lymphatic Clearance of the Brain: Perivascular, Paravascular and Significance for Neurodegenerative Diseases. Cell Mol Neurobiol 36:181–194. doi: 10.1007/s10571-015-0273-8
6. Banerjee G, Carare R, Cordonnier C, Greenberg SM, Schneider JA, Smith EE, Van Buchem M, Van Der Grond J, Verbeek MM, Werring DJ (2017) The increasing impact of cerebral amyloid angiopathy: Essential new insights for clinical practice. J Neurol Neurosurg Psychiatry 88:982–994. doi: 10.1136/jnnp-2016-314697
7. Boche D, Zotova E, Weller RO, Love S, Neal JW, Pickering RM, Wilkinson D, Holmes C, Nicoll JAR (2008) Consequence of Abeta immunization on the vasculature of human Alzheimer's disease brain. Brain 131:3299–310. doi: 10.1093/brain/awn261
8. Boyle PA, Yu L, Nag S, Leurgans S, Wilson RS, Bennett DA, Schneider JA (2015) Cerebral amyloid angiopathy and cognitive outcomes in community-based older persons. Neurology 85:1930–1936. doi: 10.1212/WNL.0000000000002175
9. Braak H, Braak E (1991) Neuropathological stageing of Alzheimer-related changes. Acta Neuropathol 82:239–59.
10. Braunger BM, Tamm @bullet E R, Braunger BM, Tamm ER, Tamm ER (2012) The Different Functions of Norrin. Adv Exp Med Biol. doi: 10.1007/978-1-4614-0631-0_86
11. Cheng JS, Dubal DB, Kim DH, Legleiter J, Cheng IH, Yu G-Q, Tesseur I, Wyss-Coray T, Bonaldo P, Mucke L (2009) Collagen VI protects neurons against Abeta toxicity. Nat Neurosci 12:119–21. doi: 10.1038/nn.2240
12. Chu Q, Diedrich JK, Vaughan JM, Donaldson CJ, Nunn MF, Lee K-F, Saghatelian A (2016) HtrA1 Proteolysis of ApoE In Vitro Is Allele Selective. J Am Chem Soc 138:9473–9478. doi: 10.1021/jacs.6b03463
13. Cox J, Hein MY, Luber CA, Paron I, Nagaraj N, Mann M (2014) Accurate Proteome-wide Label-free Quantification by Delayed Normalization and Maximal Peptide Ratio Extraction, Termed MaxLFQ. Mol Cell Proteomics 13:2513–2526. doi: 10.1074/mcp.M113.031591
14. Cox J, Mann M (2008) MaxQuant enables high peptide identification rates, individualized p.p.b.-range mass accuracies and proteome-wide protein quantification. Nat Biotechnol 26:1367–1372. doi: 10.1038/nbt.1511
15. Engelhardt B, Liebner S (2014) Novel insights into the development and maintenance of the blood–brain barrier. Cell Tissue Res 355:687–699. doi: 10.1007/s00441-014-1811-2
16. Eurelings LSM, Richard E, Carrano A, Eikelenboom P, van Gool WA, Rozemuller AJM (2010) Dyshoric capillary cerebral amyloid angiopathy mimicking Creutzfeldt–Jakob disease. J Neurol Sci 295:131–134. doi: 10.1016/j.jns.2010.04.020

17. Grau S, Baldi A, Bussani R, Tian X, Stefanescu R, Przybylski M, Richards P, Jones SA, Shridhar V, Clausen T, Ehrmann M (2005) Implications of the serine protease HtrA1 in amyloid precursor protein processing. Proc Natl Acad Sci 102:6021–6026. doi: 10.1073/pnas.0501823102

18. Hara K, Shiga A, Fukutake T, Nozaki H, Miyashita A, Yokoseki A, Kawata H, Koyama A, Arima K, Takahashi T, Ikeda M, Shiota H, Tamura M, Shimoe Y, Hirayama M, Arisato T, Yanagawa S, Tanaka A, Nakano I, Ikeda S, Yoshida Y, Yamamoto T, Ikeuchi T, Kuwano R, Nishizawa M, Tsuji S, Onodera O (2009) Association of HTRA1 Mutations and Familial Ischemic Cerebral Small-Vessel Disease. N Engl J Med 360:1729–1739. doi: 10.1056/NEJMoa0801560

19. Hondius DC, Van Nierop P, Li KW, Hoozemans JJM, Van Der Schors RC, Van Haastert ES, Van Der Vies SM, Rozemuller AJM, Smit AB (2016) Profiling the human hippocampal proteome at all pathologic stages of Alzheimer's disease. Alzheimer's Dement 12:654–668. doi: 10.1016/j.jalz.2015.11.002

20. Inoue Y, Ueda M, Tasaki M, Takeshima A, Nagatoshi A, Masuda T, Misumi Y, Kosaka T, Nomura T, Mizukami M, Matsumoto S, Yamashita T, Takahashi H, Kakita A, Ando Y (2017) Sushi repeat-containing protein 1: a novel disease-associated molecule in cerebral amyloid angiopathy. Acta Neuropathol 134:605–617. doi: 10.1007/s00401-017-1720-z

21. Kuo HJ, Maslen CL, Keene DR, Glanville RW (1997) Type VI collagen anchors endothelial basement membranes by interacting with type IV collagen. J Biol Chem 272:26522–9.

22. Manousopoulou A, Gatherer M, Smith C, Nicoll JAR, Woelk CH, Johnson M, Kalaria R, Attems J, Garbis SD, Carare RO (2016) Systems proteomic analysis reveals that clusterin and tissue inhibitor of metalloproteinases 3 increase in leptomeningeal arteries affected by cerebral amyloid angiopathy. Neuropathol Appl Neurobiol. doi: 10.1111/nan.12342

23. Manousopoulou A, Gatherer M, Smith C, Nicoll JAR, Woelk CH, Johnson M, Kalaria R, Attems J, Garbis SD, Carare RO (2017) Systems proteomic analysis reveals that clusterin and tissue inhibitor of metalloproteinases 3 increase in leptomeningeal arteries affected by cerebral amyloid angiopathy. Neuropathol Appl Neurobiol 43:492–504. doi: 10.1111/nan.12342

24. Mirra SS, Heyman A, McKeel D, Sumi SM, Crain BJ, Brownlee LM, Vogel FS, Hughes JP, Belle G v., Berg L (1991) The Consortium to Establish a Registry for Alzheimer's Disease (CERAD): Part II. Standardization of the neuropathologic assessment of Alzheimer's disease. Neurology 41:479–479. doi: 10.1212/WNL.41.4.479

25. Montañola A, de Retana SF, López-Rueda A, Merino-Zamorano C, Penalba A, Fernández-Álvarez P, Rodríguez-Luna D, Malagelada A, Pujadas F, Montaner J, Hernández-Guillamon M (2016) ApoA1, ApoJ and ApoE Plasma Levels and Genotype Frequencies in Cerebral Amyloid Angiopathy. NeuroMolecular Med 18:99-108. doi: 10.1007/s12017-015-8381-7

26. Montine TJ, Phelps CH, Beach TG, Bigio EH, Cairns NJ, Dickson DW, Duyckaerts C, Frosch MP, Masliah E, Mirra SS, Nelson PT, Schneider JA, Thal DR, Trojanowski JQ, Vinters H V, Hyman BT (2012) National institute on aging-Alzheimer's association guidelines for the neuropathologic assessment of Alzheimer's disease: A practical approach. Acta Neuropathol 123:1–11. doi: 10.1007/s00401-011-0910-3

27. Ohlmann A, Seitz R, Braunger B, Seitz D, Bösl MR, Tamm ER (2010) Norrin Promotes Vascular Regrowth after Oxygen-Induced Retinal Vessel Loss and Suppresses Retinopathy in Mice. J. Neurosci. 30:

28. Ramirez A, van der Flier WM, Herold C, Ramonet D, Heilmann S, Lewczuk P, Popp J, Lacour A, Drichel D, Louwersheimer E, Kummer MP, Cruchaga C, Hoffmann P, Teunissen C, Holstege H, Kornhuber J, Peters O, Naj AC, Chouraki V, Bellenguez C, Gerrish A, Heun R, Frolich L, Hull M, Buscemi L, Herms S, Kolsch H, Scheltens P, Breteler MM, Ruther E, Wiltfang J, Goate A, Jessen F, Maier W, Heneka MT, Becker T, Nothen MM (2014) SUCLG2 identified as both a determinator of CSF A 1-42 levels and an attenuator of cognitive decline in Alzheimer's disease. Hum Mol Genet 23:6644–6658. doi: 10.1093/hmg/ddu372

29. Ricard-Blum S (2011) The Collagen Family. Cold Spring Harb Perspect Biol 3:a004978–a004978. doi: 10.1101/cshperspect.a004978

30. Richard E, Carrano A, Hoozemans JJ, Van Horssen J, Van Haastert ES, Eurelings LS, De Vries HE, Thal DR, Eikelenboom P, Van Gool WA, Rozemuller AJM (2010) Characteristics of dyshoric capillary cerebral amyloid angiopathy. J Neuropathol Exp Neurol 69:1158–1167. doi: 10.1097/NEN.0b013e3181fab558

31. Rudolf Thal D, Sue GriYn WT, I de Vos RA, Ghebremedhin E (2008) Cerebral amyloid angiopathy and its relationship to Alzheimer's disease. Acta Neuropathol 115:599–609. doi: 10.1007/s00401-008-0366-2

32. Seitz R, Hackl S, Seibuchner T, Tamm ER, Ohlmann A (2010) Norrin Mediates Neuroprotective Effects on Retinal Ganglion Cells via Activation of the Wnt/ -Catenin Signaling Pathway and the Induction of Neuroprotective Growth Factors in Muller Cells. J Neurosci 30:5998–6010. doi: 10.1523/JNEUROSCI.0730-10.2010

33. Sims KB (1993) NDP-Related Retinopathies. University of Washington, Seattle

34. Sperling R, Salloway S, Brooks DJ, Tampieri D, Barakos J, Fox NC, Raskind M, Sabbagh M, Honig LS, Porsteinsson AP, Lieberburg I, Arrighi HM, Morris KA, Lu Y, Liu E, Gregg KM, Brashear HR, Kinney GG, Black R, Grundman M (2012) Amyloid-related imaging abnormalities in patients with Alzheimer's disease treated with bapineuzumab: a retrospective analysis. Lancet Neurol 11:241–9. doi: 10.1016/S1474-4422(12)70015-7

35. Sproul AA, Jacob S, Pre D, Kim SH, Nestor MW, Navarro-Sobrino M, Santa-Maria I, Zimmer M, Aubry S, Steele JW, Kahler DJ, Dranovsky A, Arancio O, Crary JF, Gandy S, Noggle SA (2014) Characterization and molecular profiling of PSEN1 familial alzheimer's disease iPSC-Derived neural progenitors. PLoS One. doi: 10.1371/journal.pone.0084547

36. Thal DR, Ghebremedhin E, Orantes M, Wiestler OD (2003) Vascular Pathology in Alzheimer Disease: Correlation of Cerebral Amyloid Angiopathy and Arteriosclerosis/Lipohyalinosis with Cognitive Decline. J Neuropathol Exp Neurol 62:1287–1301. doi: 10.1093/jnen/62.12.1287

37. Thal DR, Rüb U, Orantes M, Braak H (2002) Phases of Aβ-deposition in the human brain and its relevance for the development of AD. Neurology 58:1791–800. doi: 10.1212/WNL.58.12.1791

38. Tikka S, Baumann M, Siitonen M, Pasanen P, Pöyhönen M, Myllykangas L, Viitanen M, Fukutake T, Cognat E, Joutel A, Kalimo H (2014) CADASIL and CARASIL. Brain Pathol 24:525–544. doi: 10.1111/bpa.12181

39. Tumini E, Porcellini E, Chiappelli M, Conti CM, Beraudi A, Poli A, Caciagli F, Doyle R, Conti P, Licastro F (2007) The G51S purine nucleoside phosphorylase polymorphism is associated with cognitive decline in Alzheimer's disease patients. Hum Psychopharmacol Clin Exp 22:75–80. doi: 10.1002/hup.823

40. Tyanova S, Temu T, Sinitcyn P, Carlson A, Hein MY, Geiger T, Mann M, Cox J (2016) The Perseus computational platform for comprehensive analysis of (prote)omics data. Nat Methods 13:731–740. doi: 10.1038/nmeth.3901

41. van Veluw SJ, Kuijf HJ, Charidimou A, Viswanathan A, Biessels GJ, Rozemuller AJM, Frosch MP, Greenberg SM (2016) Reduced vascular amyloid burden at microhemorrhage sites in cerebral amyloid angiopathy. Acta Neuropathol 1–7. doi: 10.1007/s00401-016-1635-0

42. Verbeek MM, Otte-Höller I, Veerhuis R, Ruiter DJ, De Waal RMW (1998) Distribution of Aβ-associated proteins in cerebrovascular amyloid of Alzheimer's disease. Acta Neuropathol 96:628–636. doi: 10.1007/s004010050944

43. Verwey NA, Hoozemans JJM, Korth C, van Royen MR, Prikulis I, Wouters D, Twaalfhoven H a M, van Haastert ES, Schenk D, Scheltens P, Rozemuller AJM, Blankenstein MA, Veerhuis R (2013) Immunohistochemical characterization of novel monoclonal antibodies against the N-terminus of amyloid β-peptide. Amyloid 20:179–87. doi: 10.3109/13506129.2013.797389

44. Weller RO, Nicoll J a R (2003) Cerebral amyloid angiopathy: pathogenesis and effects on the ageing and Alzheimer brain. Neurol Res 25:611–616. doi: 10.1179/016164103101202057

45. Weller RO, Subash M, Preston SD, Mazanti I, Carare RO (2008) Perivascular drainage of amyloid-?? peptides from the brain and its failure in cerebral amyloid angiopathy and Alzheimer's disease. In: Brain Pathol. pp 253–266

46. Xu Q, Wang Y, Dabdoub A, Smallwood PM, Williams J, Woods C, Kelley MW, Jiang L, Tasman W, Zhang K, Nathans J (2004) Vascular development in the retina and inner ear: Control by Norrin and Frizzled-4, a high-affinity ligand-receptor pair. Cell 116:883–895. doi: 10.1016/S0092-8674(04)00216-8

47. Ye X, Smallwood P, Nathans J (2011) Expression of the Norrie disease gene (Ndp) in developing and adult mouse eye, ear, and brain. Gene Expr Patterns. doi: 10.1016/j.gep.2010.10.007

48. Zhan SS, Veerhuis R, Kamphorst W, Eikelenboom P (1995) Distribution of beta amyloid associated proteins in plaques in Alzheimer's disease and in the non-demented elderly. Neurodegeneration 4:291–7.

SUPPLEMENTARY MATERIAL

TABLE S1 | Complete dataset, containing log2 transformed quantitative values (LFQ values) of all quantified proteins per individual case. Table S1 can be found at : https://actaneurocomms.biomedcentral.com/articles/10.1186/s40478-018-0540-2

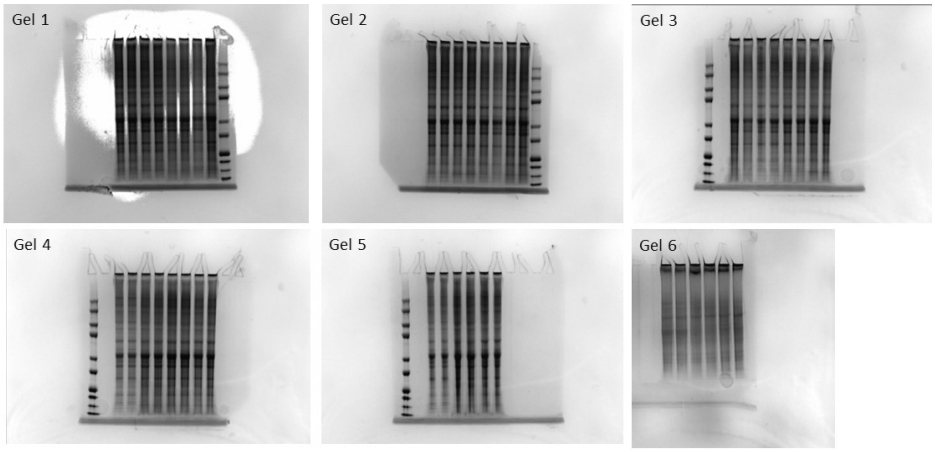

FIGURE S1 | Coomassie blue staining of the SDS PAGE gels containing the microdissected tissue lysates.

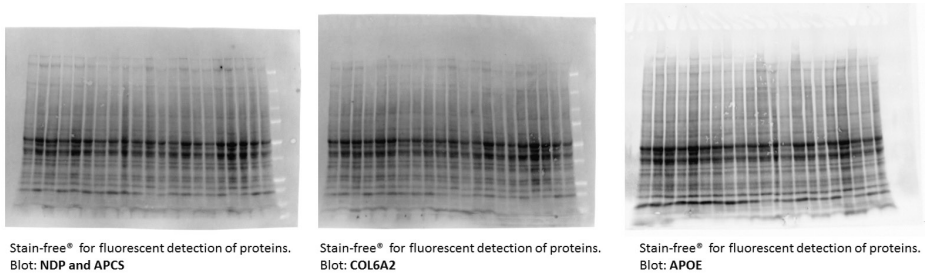

FIGURE S2 | Total protein fluorescent signal from blots used for immunoblot analysis. Total protein load was visualized using a chemidoc EZ (Bio-Rad) after electroblotting and used to obtain densitometric values which were then used to normalize for total protein input.

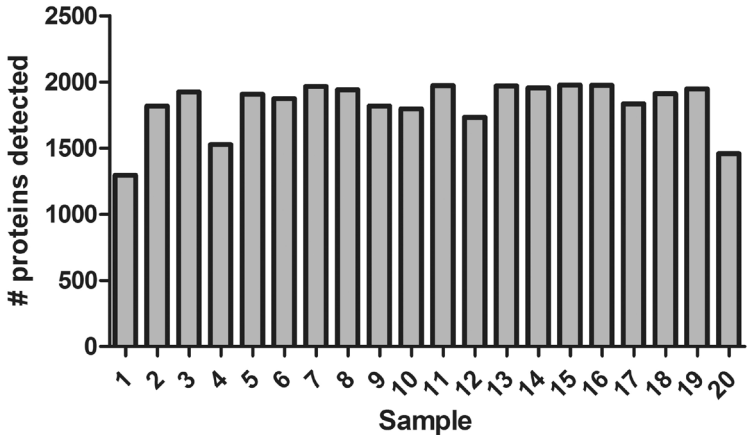

FIGURE S3 | Number of proteins detected per individual case. Proteins were quantified based on a minimum of one peptide and adhering to an FDR of < 0.01.

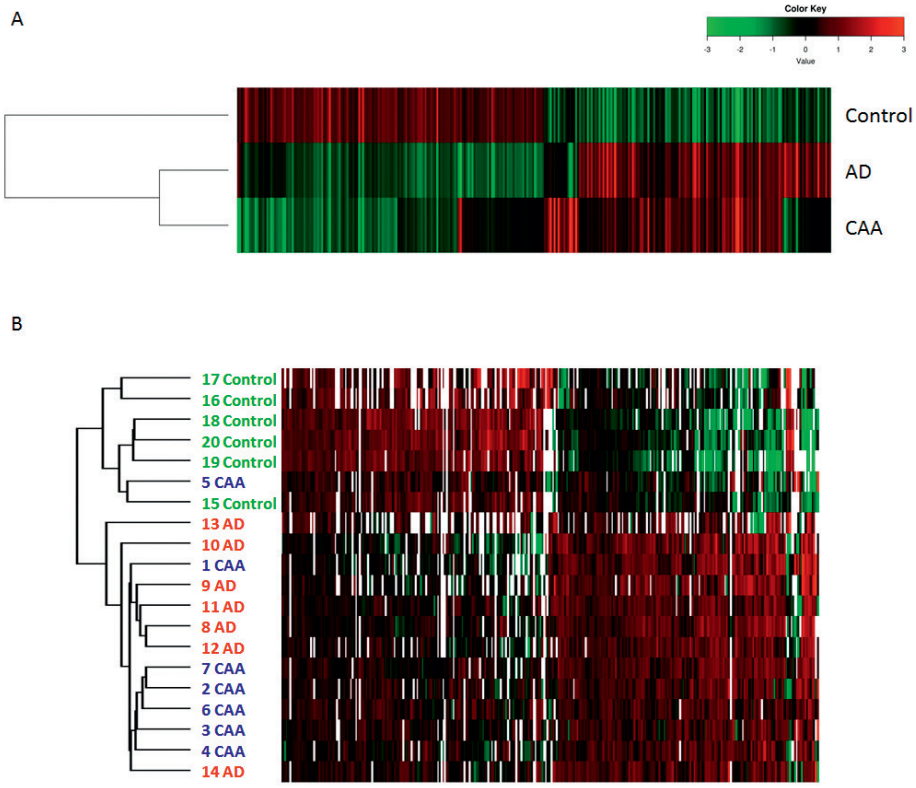

FIGURE S4 | Clustering analysis of experimental groups and individual cases. Clustering analysis and heat maps of the different experimental groups (A) and individual cases (B) based on proteins with a significant difference (ANOVA, $p < 0.05$) in expression between any of the groups.

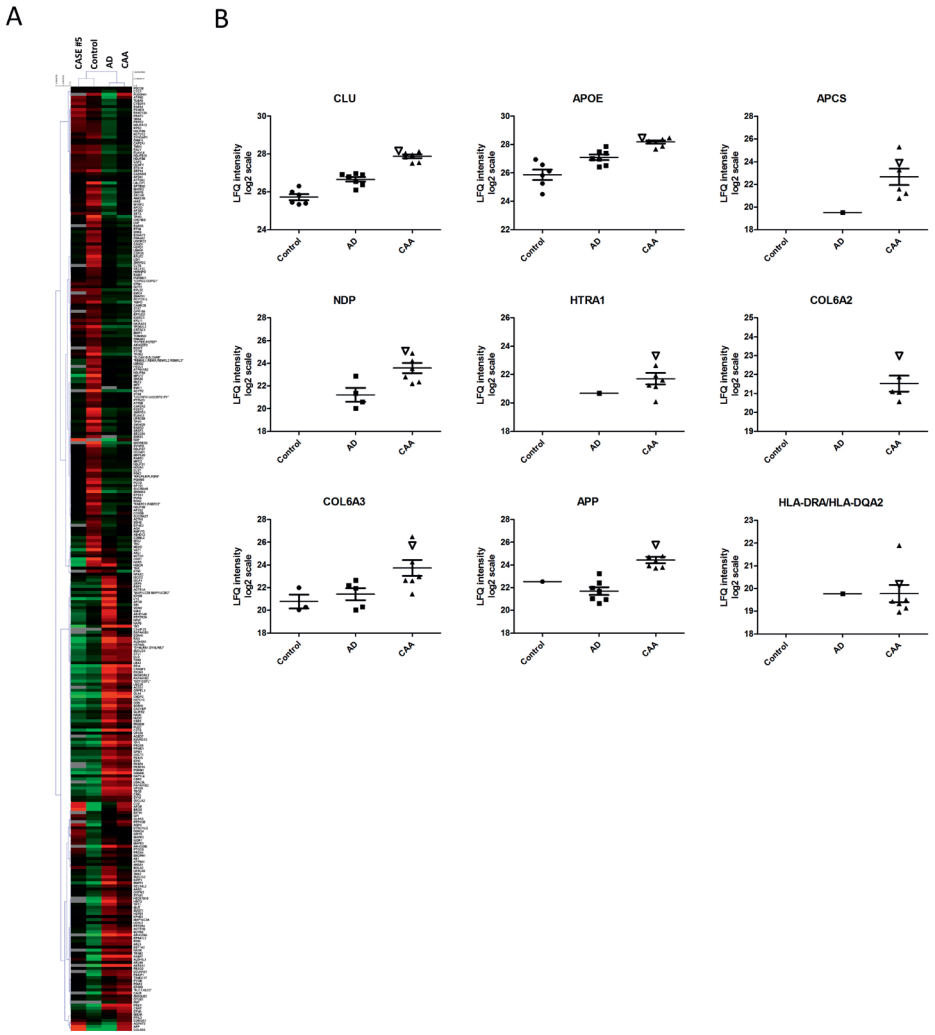

FIGURE S5 | Protein expression of CAA case #5 relative to the experimental groups and individual cases. (A) On the left the expression profile of case #5 compared to the average expression profile of the control group (2nd row), AD group (3rd row) and the CAA group (4th row). Green, expression below the overall mean; red, above the overall mean. The expression profile of case #5 is largely similar to that of the control groups but some proteins show a similar expression as in the AD and/or CAA groups. (B) Expression values (LFQ values) of several CAA specific proteins identified in this study with case #5 indicated as empty triangle pointing down. Case #5 does not differ from the CAA group in these markers.

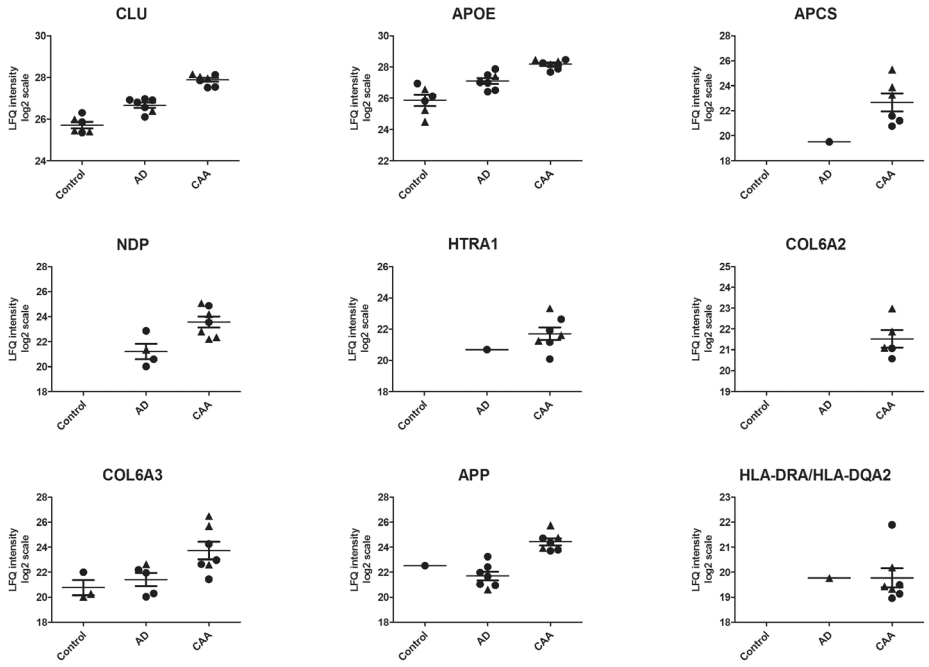

FIGURE S6 | Protein expression of males versus females. Quantitative data on several CAA selective data was plotted with males represented as triangles and females as dots. No clear relationship between gender and protein abundance was observed.

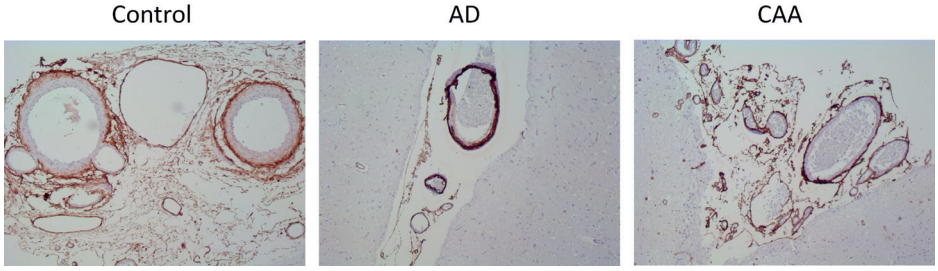

FIGURE S7 | Immunoreactivity for COL6A2 is equally present in leptomeningeal vessels in control, AD and CAA tissue.

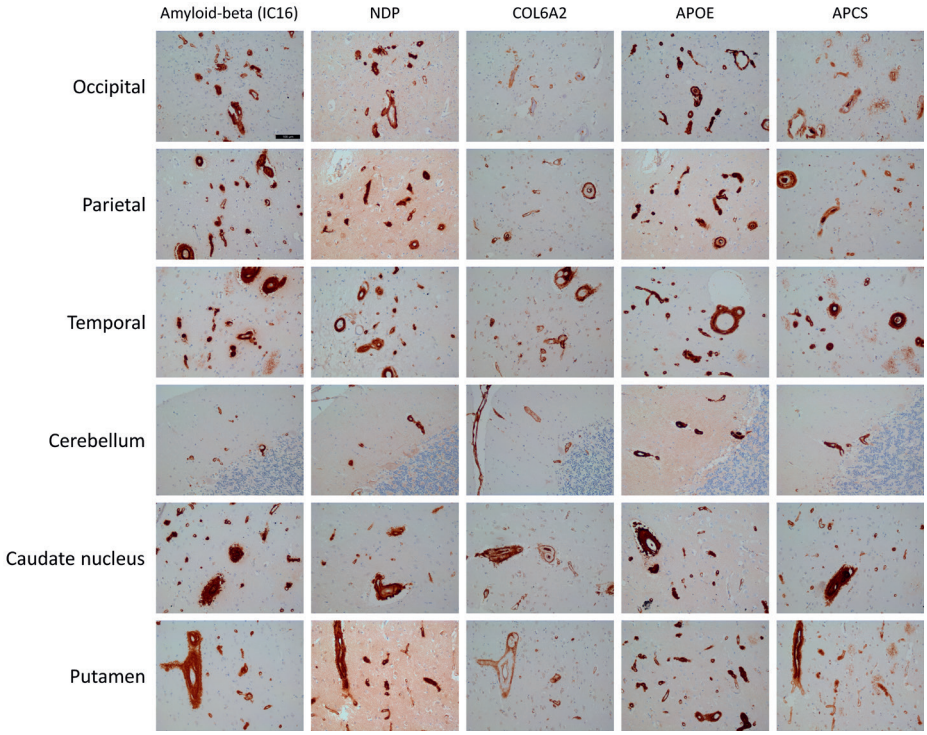

FIGURE S8 | Immunohistochemistry of Amyloid-beta, NDP, COL6A2, APOE and APCS on multiple brain regions of a HCHWA-D CAA type-1 case. Brain tissue of a case exhibiting a hereditary form of CAA type-1 was analyzed by immunohistochemistry of Amyloid-beta, NDP, COL6A2, APOE and APCS. Aβ pathology was confirmed and immunoreactivity associated with CAA type-1 pathology was found present for all markers. Scale bar in upper left picture represents 100 µm.

CHAPTER 5

A laser microdissection - liquid chromatography - tandem mass spectrometry workflow for post-mortem analysis of brain tissue

David C Hondius*[1,2], Jeroen JM Hoozemans[2], Annemieke JM Rozemuller[2], Ka Wan Li[1] and August B Smit[1]

[1]Department of Molecular and Cellular Neurobiology, Center for Neurogenomics and Cognitive Research, Amsterdam Neuroscience, VU University Amsterdam, The Netherlands.

[2]Department of Pathology, Amsterdam Neuroscience, VU University Medical Center, The Netherlands

Methods in Molecular Biology 2018;1723:371-383.

ABSTRACT

Improved speed and sensitivity of mass spectrometry allow the simultaneous quantification of high numbers of proteins from increasingly smaller quantities of tissue sample. Quantitative data of the proteome is highly valuable for providing unbiased information on, for example, protein expression changes related to disease or identifying related biomarkers. In brain diseases the affected area can be small and pathogenic events can be related to a specific cell type in an otherwise heterogeneous tissue type. An emerging approach dedicated to analyzing this type of samples is laser micro-dissection (LMD) combined with LC-MS/MS into a single workflow. In this chapter, we describe different options for isolating tissue suitable for LC-MS/MS analysis.

1. INTRODUCTION.

Improved speed and sensitivity of mass spectrometry allow the simultaneous quantification of high numbers of proteins from increasingly smaller quantities of tissue sample. Quantitative data of the proteome is highly valuable for providing unbiased information on, for example, protein expression changes related to disease or identifying related biomarkers.

In brain diseases the affected area can be small and pathogenic events can be related to a specific cell type in an otherwise heterogeneous tissue type. An emerging approach dedicated to analyzing this type of samples is laser micro-dissection (LMD) combined with LC-MS/MS into a single workflow. LMD enables isolation of small pieces of tissue, down to cells or even cellular inclusions, with high precision for mass spectrometric analysis [2].

In this chapter, we describe different options for isolating tissue suitable for LC-MS/MS analysis. Methods are divided into four variants. Protocol A describes tissue isolation from a specific brain area exemplified by the isolation of CA1 and subiculum from hippocampus, as published previously [1]. Protocol B describes tissue isolation of areas with high pathological burden, as visualized with a fast immunohistochemical (IHC) protocol. Protocol C describes isolation of inclusion bodies from separate cells using histochemical (HC) staining as published previously [3]. Protocol D describes isolation of separate cells that are positive for a specific marker using a fast IHC protocol.

The methods described here include tissue preparation, different visualization methods, know-how on the LMD procedure and further processing for MS analysis. Generally, we have made use of a Leica LMD 6500 system and in some cases of a Zeiss PALM microbeam system. We found that both systems deliver outstanding results. Depending on the tissue and the research question, the methods might require some adjustment. This chapter aims at providing the protocols to apply the LMD - LC-MS/MS workflow successfully.

2. MATERIALS

Prepare all solutions using ultrapure (sterile) water. Prepare and store all reagents at room temperature (unless indicated otherwise). It is important to work as clean as possible considering that the downstream MS analysis is very sensitive and will detect impurities that were introduced while preparing the tissue samples.

2.1. Preparation of tissue for LMD including (Immuno-)histochemical staining ((I)HC)

1. Snap frozen, post-mortem, human brain tissue with short (<12h) post-mortem delay (*see* **Note 1**).
2. Cryostat (Leica).
3. Polyethylene naphthalate (PEN)-foil membrane slides (Leica).
4. Ethanol 100%.
5. Ultrapure sterile H_2O.

6. Toluidine blue (Sigma-Aldrich) 1% (w/v) in sterile H_2O.
7. Hair dryer.
8. For additional protocol-specific requirements, *see* Subheading 2.1.2 (for protocols B and D) and Subheading 2.1.3 (for protocol C).

2.1.2. Preparation of tissue for LMD using an immunostaining (IHC) (Protocol B and D only)

1. Sterile PBS, (pH 7.4): NaCl 8.2g, Na_2HPO_4 $12H_2O$ 3.1g, NaH_2PO_4 $2H_2O$ 0.3g in 1000 mL.
2. Primary antibody (anti beta-amyloid (clone IC16, Kind gift of Prof. Carsten Korth) and anti phospho-tau (clone AT8, Thermo scientific) for protocol B and D, respectively).
3. HRP-labelled secondary antibody (protocol B and C only) Goat anti-mouse-HRP (DAKO).
4. 3,3'-diaminobenzidine (DAB) in chromogen solution (DAKO).

2.1.3. Preparation of tissue for LMD, applying a histochemical (HC) staining using eosin (Protocol C only)

1. Eosin staining solution: 50% (v/v) ethanol 0.2% (w/v) eosin and 0.04% (v/v) acetic acid.

2.2. Laser microdissection

1. Laser dissection microscope (here a Leica LMD6500 system was mostly used. Some experiments have also been performed using a Zeiss PALM MicroBeam system.)
2. 0.5 mL cap (Greiner Bio-one) or adhesive caps (Zeiss). Adhesive caps are obligatory when using a Zeiss PALM system but are useful in certain cases for the Leica system as well (*see* **Note 2**).
3. Pierce™ Lane Marker Reducing Sample Buffer 5x (Thermo scientific) (*see* **Note 2**).
4. M-PER lysis buffer (Thermo scientific).

2.3. SDS-PAGE

1. Centrifuge (Eppendorf, 5415D or comparable).
2. Pierce™ Lane Marker Reducing Sample Buffer 5x (Thermo scientific).
3. M-PER lysis buffer (Thermo scientific).
4. Water bath at 95°C.
5. Pre-stained protein ladder (Bio-Rad).
6. Gel fixation solution: 50% Ethanol (v/v), 3% Phosphoric Acid (from 85% stock) in H_2O.
7. Colloidal Coomassie blue: 34% (v/v) Methanol, 3% (v/v) Phosphoric Acid (from 85% stock) (Sigma Aldrich), 150g Ammonium Sulphate, 1g Coomassie brilliant blue G-250 (Thermo Scientific) in H_2O.

2.2.1. SDS PAGE for larger isolated areas (multiple fractions) (protocol A and B)

1. NuPAGE® 4-12% Bis-Tris acrylamide gel (Invitrogen).
2. MOPS running buffer (Invitrogen).

2.2.2. SDS page for single cell / inclusion body analysis (single fraction) (protocol C and D)

1. Acrylamide/Bis Solution, 19:1 (Bio-rad).
2. Tris 1.5 M, adjusted to pH 8.8 using HCl.
3. 10% w/v SDS.
4. Ultra pure (sterile) H_2O.
5. Ammonium persulfate: 10 % (w/v) solution in H_2O.
6. TEMED (Bio-rad).
7. Mini-PROTEAN® 3 Cell (Bio-rad).
8. Glass plates with 1mm spacers.
9. 10-well comb.
10. 10x Tris/Glycine/SDS (Bio-rad).

2.3. In gel digestion

1. Ammonium bicarbonate (100 mM): 0.78 g NH_3HCO_3 fill up to 100 mL with deionized water.
2. Acetonitrile (HPLC grade).
3. Capillary gel loading pipet tips (VWR)
4. Trypsin/Lys-C Mix, Mass spec Grade (20 µg per vial from Promega).

2.4. Mass spectrometry analysis

1. A capillary HPLC system with autosampler.
2. HPLC solvents A: 94.9% deionized water/5% acetonitrile/0.1% formic acid, and B: 95% acetonitrile/5% deionized water/0.1% formic acid.
3. An electrospray mass spectrometer. Mass spectrometers based on the use of either Orbitrap or quadrupole-time of flight mass analyser are preferred. We describe the use of the Sciex Triple TOF 5600 system as an example.

3. METHODS

Carry out all the procedures at room temperature unless otherwise specified.

3.1. Preparation of the slides for microdissection.

1. Prepare PEN-foil slides by placing them in UV light for 30 minutes according to the manufacturer's instructions.
2. Tissue sections are cut at the desired thickness in a cryostat at a temperature of -16°C to -18°C and applied on PEN-foil slides (*see* **Note 3**). For experiments A and B (larger areas of interest) typically the thickness used is between 10 - 50 µm depending on the tissue and the type of laser dissection microscope (*see* **Note 4**). For experiments C and D (separate cells/inclusion bodies) the thickness used is typically 10 µm or less (*see* **Note 5**).
3. Let the tissue sections air dry for at least 10 minutes.
4. Fix the sections in 100% ethanol for 1 minute (*see* **Note 6** and **7**).
5. Air dry for 10 minutes (or dry using a hair dryer, set to cool air, for 1 minute).

6. Proceed with Subheading 3.1.1 (protocol A), Subheading 3.1.2 (protocols B and D) or Subheading 3.1.3 (protocol D).

3.1.1. preparing section with toluidine blue staining (protocol A)

1. Briefly wet the sections with sterile ultra-pure H_2O by pipetting it on the sections.
2. Remove excess H_2O by tilting the slide.
3. Apply a few drops of toluidine (1% v/v in H_2O) onto the tissue in such a manner that all the tissue is covered. Incubate for 1 minute.
4. Wash the slides twice for 30 seconds in H_2O. (Use 2 containers with H_2O of 250 mL or more to do the washing).
5. Wash the slides in ethanol 100% three times 30 seconds.
6. Air dry for 10 minutes (or dry using a hair dryer, set to cool air, for 1 minute).
7. Store at room temperature (RT) till further use (within 1 week) (*see* **Note 8**).
    a. A typical image obtained using this protocol is shown in figure 1A.
8. Proceed to Subheading 3.2.

3.1.2. Fast IHC staining (protocol B and D)

1. Prepare all antibody dilutions in sterile PBS (*see* **Note 9**). Although depending on the section size, approximately 100 µl of diluted antibody is sufficient to completely cover the tissue section.
2. Prepare DAB solution according to the manufacturer's protocol.
3. Briefly wet the sections using sterile PBS (pH 7.4).
4. Remove excess fluid by tilting the slide.
5. Apply the primary antibody. Make sure the entire tissue section is covered. This can be done by distributing the liquid with the back of a pipet tip. Make sure not to touch the tissue or damage the membrane. Incubate for 20 minutes.
6. Wash 3 times 30 seconds in sterile PBS (pH 7.4) (Use 3 containers with H_2O of 250 mL or more to do the washing).
7. Apply the secondary HRP-labelled antibody. Use the highest dilution mentioned in the accompanying datasheet (DAKO) that is suitable for cytochemistry. Usually 1:100 is used but this depends on the antibody. Incubate for 20 minutes.
8. Wash 3 times 30 seconds in sterile PBS (pH 7.4).
9. Apply the DAB solution to the slides. Incubate 5 minutes in the dark.
10. Thoroughly wash repeatedly with ultrapure H_2O.
11. Incubate with 1% (w/v) toluidine blue in H_2O for 1 minute to implement a counterstain.
12. Wash the slides twice for 30 seconds in H_2O.
13. Wash the slides in ethanol 100% three times for 30 seconds.
14. Air dry for 10 minutes (or dry using a hair dryer, set to cool air, for 1 minute).
15. Store at RT till further use (within 1 week) (*see* **Note 8**).
    a. A typical image using this type of protocol is shown in figure 1B, D
16. Proceed to Subheading 3.2.

3.1.3. Histochemical staining for isolation of inclusion bodies (Protocol C)

1. Briefly wet the sections with sterile ultrapure H_2O by pipetting it on the sections.
2. Incubate in eosin solution for 30 seconds.
3. Wash the slides 30 seconds in H_2O.
4. Wash the slides in ethanol 100% 3 times 30 seconds.
5. Air dry for 10 minutes (or dry using a hair dryer, set to cool air, for 1 minute).
6. Store at room temperature (RT) till further use (within 1 week) (*see* **Note 8**).
    a. Figure 1C displays a typical staining obtained using this method.
7. Proceed to Subheading 3.2.

3.1. Laser dissection procedure

1. Place the PEN-foil slide holding the tissue section with the tissue facing down.
2. Depending on the availability and amount of material that has to be dissected, either load the cap with 30 µl of 1x reducing SDS loading buffer (diluted with M-PER lysis buffer), or place an adhesive cap in the cap holder below the specimen (*see* **Note 10**).
3. Proceed with Subheading 3.2.1 for protocols A and B or Subheading 3.2.2 for protocols C and D.

3.2.1. Laser dissection procedure (Protocol A and B)

1. To obtain approximately 40 µg grams of protein, a volume of $1x10^9$ μm^3 has to be isolated. This is best to be divided over two separate eppendorf tubes (60µl SDS loading buffer in total)
2. Select area(s) of interest and dissect the tissue using the LDM system as indicated by the manufacturer.
3. After tissue isolation freeze at -80 °C until further use.
4. Proceed with Subheading 3.3.1.

3.1.2. Laser dissection procedure (Protocol C and D)

1. Start with making a small hole in the PEN membrane at a location without tissue to let the air out (*see* **Note 11**).
2. Select shapes and dissect shapes as indicated by LCM manufacturer.
3. When the isolated material is in reducing SDS sample buffer, store in -80 °C until further use
4. When the isolated material is in an adhesive cap, then proceed with taking it up in reducing SDS sample buffer as follows:
    a. Add 25µl of reducing SDS sample buffer.
    b. Incubate for 10 minutes at RT.
    c. Pipet "up and down" repeatedly (5-10 times).
    d. Transfer to a new Eppendorf tube.
    e. Check the adhesive cap under a microscope to convince yourself that all material is removed from the adhesive cap.
    5. Store at -80 °C until further use.
    6. Proceed with Subheading 3.3.2

3.3. SDS-PAGE

3.3.1. SDS-PAGE for large areas of interest (Protocol A and B)

1. Let the sample defrost and warm up to RT.
2. Heat the samples to 95°C and incubate for 5 minutes
3. Let the samples cool down to RT
4. -optional- incubate with 50 mM iodoactamide for 30 min at RT in the dark
5. Separate protein based on their size on a NuPAGE® 4-12% Bis-Tris acrylamide gel (Invitrogen) using MOPS SDS running buffer (Invitrogen) according the manufacturers protocol.
6. After electrophoresis, remove the gel from the cassette.
7. Incubate the gel in gel fixing solution for at least 2 hours.
8. Wash the gel in ultra pure sterile water for 10 minutes
9. Incubate in Coomassie blue solution for 10 minutes
10. Wash the gel in ultra pure sterile H_2O for several hours, refreshing the H_2O repeatedly, until the gel is completely de-stained
11. The gel can now be cut into the required number of fractions, which depends on the type of mass spectrometer used. For the LTQ-Orbitrap mass spectrometer we used 12 fractions. For Triple TOF 5600 system we used 2-4 fractions. For a Fusion Lumos Orbitrap mass spectrometer it is possible to quantify 4000 proteins from a single fraction using a 2-3 hours HPLC gradient (*see* Subheading 3.3.2 for SDS-PAGE of proteins in a single fraction).
12. Proceed with in gel trypsin digestion protocol (Subheading 3.4)

3.3.2. SDS-PAGE for individually isolated cells or inclusion bodies (Protocol C and D)

1. Make a 10% gel, of 1mm thickness with 10 wells as follows (for 10 mL):
    a. Mix 3.3 mL of the 30% acrylamide, 1.5 mL 1.5M Tris (pH8.8) and 4.96 mL ultra pure H_2O.
    b. Add APS 0.1ml and TEMED 0.006ml, mix gently, and directly pipette this into the gel cast as polymerization starts directly. Place the 10 well comb and wait for the gel to polymerize (typically < 30 minutes).
2. Place the prepared gel in the Bio-rad electrophoresis system and fill up with TGS running buffer 1x.
3. Remove the comb.
4. Load the samples into the gel wells.
5. Let the proteins run into the gel by electrophoresis (150 V) until the sample is in the gel for a length of approximately 8 - 10 mm.
6. Remove the gel from the cask.
7. Incubate the gel in gel fixing solution for at least 2 hours.
8. Wash the gel in ultra pure sterile water for 10 minutes.
9. Incubate in Coomassie blue solution for 10 minutes or longer if desired (*see* **Note 12**).
10. Wash the gel in ultra pure sterile H_2O for several hours, refreshing the H_2O repeatedly, until the gel is completely de-stained.
11. Cut out the gel piece containing the sample and proceed with in gel digestion.
    a. The gel piece can be divided into two pieces (high and low molecular weight) if desired.
12. Proceed with in gel trypsin digestion protocol (Subheading 3.4).

3.4. In gel trypsin digestion

1. Cut the gel piece into small fragments of approximately 1 mm^3 using a razor blade. We often use two razor blades, one to maintain the gel piece in place and the other to cut the gel. Transfer the gel fragments into a 1.5 mL Eppendorf tube.
2. Add 1 mL of 50 mM ammonium bicarbonate/50% acetonitrile to the Eppendorf tube, invert the tube and put it on Table. This ensures a larger contact surface between the gel fragments and the destaining solution. Make sure that the gel fragments are at the bottom of the tube. Incubate for 2-3 hours.
3. Remove the solution and discard. Capillary gel loading pipet tips can be used for this.
4. Add 0.5 mL 100% acetonitrile. The gel fragments should turn white and shrink within a few minutes.
5. Remove acetonitrile and discard.
6. Add 0.5 mL 50 mM ammonium bicarbonate, incubate for 5 minutes, and then add 0.5 mL 100% acetonitrile.
7. Invert the Eppendorf tube, place on Table and incubate for 0ne hour or until the gel fragments are completely destained.
8. Remove solution and discard.
9. Add 0.5 mL 100% acetonitrile and incubate for 5 minutes.
10. Remove acetonitrile and discard.
11. Dry the gel fragments in Speedvac for 5 minutes.
12. Add 3 mL 50 mM ammonium bicarbonate to one vial of Promega Trypsin/Lys-C Mix, and vortex.
13. Add 0.1 mL Trypsin/Lys-C Mix to each Eppendorf tube containing the gel fragments, wait 5 minutes to determine if more trypsin/Lys-C Mix solution should be added to completely re-swell the gel fragments.
14. Add 0.1 mL 50 mM ammonium bicarbonate to the gel fragments, incubate overnight at 37°C.
15. Transfer the solution from the Eppendorf tube containing the gel fragments into a new Eppendorf tube.
16. Add 0.2 mL 50 mM ammonium bicarbonate/50% acetonitrile to the gel fragments, vortex for 20 minutes.
17. Transfer this solution to the Eppendorf tube from **step 15**.
18. Dry the pooled solution in a Speedvac. The samples can be stored in Eppendorf tube at -20°C for weeks before mass spectrometry analysis.

3.5. Mass spectometry analysis

1. HPLC and mass spectrometer from different vendors have their own specifications. The protocol described here is based on the use of an Ultimate 3000 LC system (Dionex) coupled to a Triple Tof 5600 mass spectrometer (Sciex). It services merely as a guideline.
2. Redissolve the dried tryptic peptides in 7 µL of HPLC solvent A. Vortex for 15 minutes.
3. Transfer the solution to a sample vial, cap the vial, and place it in the autosampler tray.
4. Load 6 µL to the 5mm Pepmap 100 C18 trap column (300µm internal diameter, 5µm particle size, Dionex).

5. Initiate the separation in the 100 µm (internal diameter) nano-LC column packed with C18 material (3 µm Altima C18 particle). The gradient is increased from 5 to 18% A in 88 min, to 25% at 98 min, 40% at 108 min, and to 90% at 110 min, at a flow rate of 400 nL/min.
6. Peptides are sprayed into the mass spectrometer, using an ion spray voltage of 2.5 kV, curtain gas at 35 p.s.i., nebulizer gas at 15 p.s.i., and an interface heater temperature of 150^{0}C. The MS survey scan range is *m/z* 350–1250 acquired for 250 ms. Select top 20 precursor ions for 85ms per MS/MS acquisition, with a threshold of 90 counts. Dynamic exclusion was 16 s. Rolling CID function was activated, with an energy spread of 15 eV.
7. Process raw data with MaxQuant. The match-between-run option can be activated to minimize the number of missing values across the samples.

4. NOTES

1. It is highly important that tissue is rapidly snap frozen in liquid nitrogen. When the freezing procedure is too slow, freezing artefacts will occur destroying the morphology and making the tissue crumble, when cutting the tissue, especially at larger thickness.

2. Adhesive caps can also be used on a Leica system. These can be of practical use, especially when isolating individual cells of a type that is low abundant and therefore requires multiple days of laser dissection. When using adhesive caps no buffer is required to collect the sample in.

3. Check if the foil is intact. When the foil is damaged then fluid will get between the foil and the glass, rendering the slide unusable for LMD. This is especially relevant when isolating larger areas of tissue (protocol A and B).

4. For analysis of larger areas of interest, usually thicker sections are better as that saves time in performing laser dissection and reduces the amount of (expensive) PEN-foil slides needed. Modern laser dissection microscopes, like the Leica LMD 6500, have sufficient laser power to cut through sections up to 50 µm. (Cutting sections on a cryostat does become increasingly difficult with increasing thickness. Lowering the temperature in the cryostat might help, but often one will have to settle with sections of a thickness below 50 µm.)

5. For the isolation of separate cells/inclusion bodies or other very small structures, sections are preferably thin, 10 µm or less. Thickness depends largely on the size of the objects that you wish to isolate, considering that when the section is thicker than the object of interest then tissue/material surrounding the object will be isolated as well, reducing the purity of your sample.

6. Typically we fix tissue in 100% ethanol, however, we experienced that some IHC stainings were incompatible with ethanol fixation, but were successful when fixing using 100% acetone. No negative effects were observed in the downstream LC-MS/MS analysis.

7. PEN-foil slides are easily damaged, and if so during the staining they can become unusable (also *see* **Note 3**). Therefore treat the slides with great care.

8. Proteins in the tissue are, when dry, very resistant to degradation. It is often preferred to store the slides at RT instead of freezing them. Freezing introduces the risk of deposition of moisture, and freeze thaw cycles are best avoided. However, fast (within a week) processing of the sections is recommendable. Meaning finishing the laser dissection and storing these in reducing SDS buffer at -80 °C.

9. Usually the antibody concentration used for a fast IHC staining is about tenfold higher as used in a normal overnight incubation for IHC. We recommend performing a test series prior to the actual experiment. Antibodies that produce a highly contrasted and specific staining will give the best chance of success, as the fast IHC protocol will produce a staining of lower quality than an overnight incubation. This combined with the absence of mounting medium will reduce the visual quality of a given specimen considerably. No blocking proteins are used as these are potentially picked up by the mass spectrometer, obscuring the results.

10. To decide for either the cap with SDS sample buffer or an adhesive cap is particularly valid when isolation separate cells/inclusion bodies (protocol C or D). For our experiments we found a number of 3000 cells/inclusion bodies to provide satisfactory results. Although even higher numbers will obviously result in more proteins that can be quantified as well as more reliable quantification. When a particular cell or structure of interest is very rare in the tissue, it can take several days to isolate sufficient cells for an successful MS analysis. Our experience is that it is then useful to capture the material in adhesive caps. It is then quite well fixed in place and you can store it at RT and easily continue then next day with dissection using the same cap.

11. Usually, dissection of small structures like separate cells, inclusion bodies or protein aggregates is done at high magnification, for example using the 20x or the 40x objective. The PEN-membrane glass slide usually has some air between the glass and the foil. When selecting a number of shapes to be dissected you will find that when the first hole is made in the foil, the air will come out and the foil will move to the glass. Consequentially, your tissue section will be out of focus for all remaining shapes, which will compromise the precision and effectivity of the dissection. This step is not necessary when metal frame slides are used.

12. Since only very little amount of protein is isolated the Coomassie staining will be very weak. Longer incubation time can increase the signal. However, complete lack of staining does not necessarily indicate absence of proteins. Successful quantification of a high number of proteins can still be realized using a very sensitive mass spectrometer.

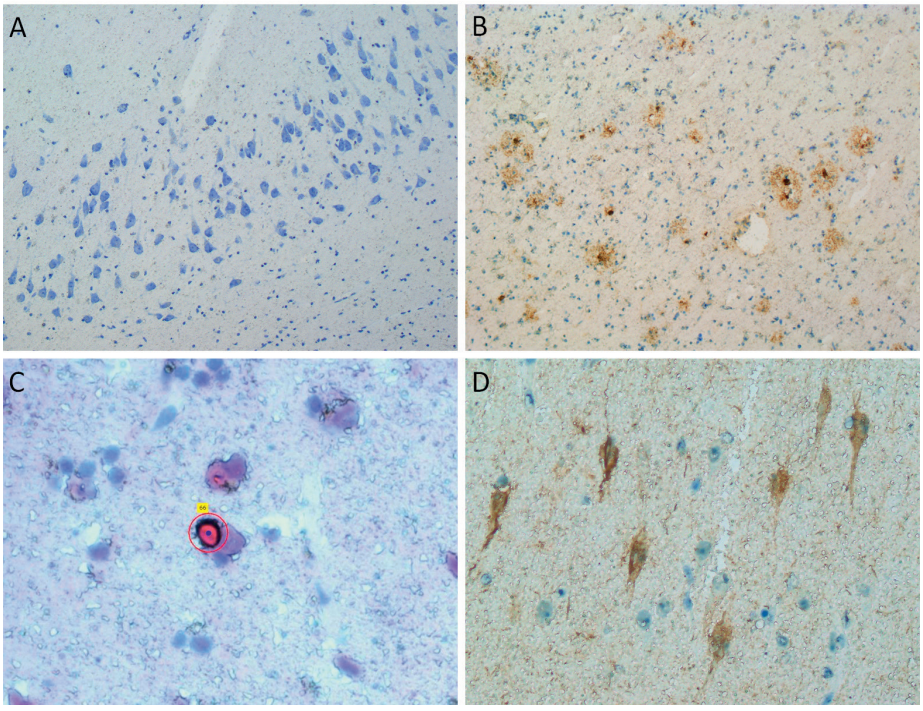

FIGURE 1 | Typical images obtained using the different (I)HC protocols. (A) Toluidine blue staining of human hippocampus. Shown is the CA1 region of the hippocampus. (B) Amyloid beta plaques identified using IHC. Immunodetection and visualization of beta-amyloid in plaques using DAB (brown). Toluidine blue was used as a counterstain (blue). (C) Inclusion body stained using eosin. (D) Cells displaying immunoreactivity for phospho-tau visualized using DAB (brown), toluidine blue was used as a counterstain (blue).

REFERENCES

1. Hondius DC, Van Nierop P, Li KW, Hoozemans JJM, Van Der Schors RC, Van Haastert ES, Van Der Vies SM, Rozemuller AJM, Smit AB (2016) Profiling the human hippocampal proteome at all pathologic stages of Alzheimer's disease. Alzheimer's Dement 12:654–668. doi: 10.1016/j.jalz.2015.11.002
2. Murray GI (2007) An overview of laser microdissection technologies. Acta Histochem 109:171–176. doi: 10.1016/j.acthis.2007.02.001
3. Wong TH, Chiu WZ, Breedveld GJ, Li KW, Verkerk AJMH, Hondius D, Hukema RK, Seelaar H, Frick P, Severijnen L-A, Lammers G-J, Lebbink JHG, Van Duinen SG, Kamphorst W, Rozemuller AJ, Bank NB, Bakker EB, Neumann M, Willemsen R, Bonifati V, Smit AB, Van Swieten J (2014) PRKAR1B mutation associated with a new neurodegenerative disorder with unique pathology. Brain. doi: 10.1093/brain/awu067

CHAPTER 6

Summary and General Discussion

SUMMARY

Alzheimer's disease (AD) is the main cause of dementia in the elderly and is becoming increasingly prevalent due to the increased life expectancy in the ageing population. AD pathology is characterized by the presence of amyloid beta (Aβ) aggregates, which occur in the brain parenchyma as plaques and in and around the brain vasculature as Cerebral Amyloid Angiopathy (CAA). Both plaques and CAA occur as a result of an imbalance in Aβ production and clearance. AD pathology is also hallmarked by the presence of intraneuronal aggregates of tau protein as neurofibrillary tangles (NFTs) and neuropil threads. Another important feature in AD is the increased presence of granulovacuolar degeneration (GVD) bodies. In general, there is a positive correlation between the increase and distribution of these features and the clinical symptoms. On the other hand, there is a long pre-symptomatic phase of AD, in which brain pathology builds up and neurodegeneration starts to occur. Hence, earlier diagnosis is probably essential for a better chance of success in treating AD. In addition, AD can be clinically and pathologically divers, for example, due to variations in the age of onset, clinical symptoms, rate of disease progression and variability in the presence, localization and extend of the individual pathological features. Disease heterogeneity, and possible differences in disease mechanisms, could also explain why past clinical trials have not yielded satisfying results, as different patients or patient groups might require different therapies.

Currently, no treatment options exist that delay, stop or reverse AD. The early changes in AD are still poorly described, and increased insight in the early disease mechanisms are highly needed. In particular, the early stage of AD may be open for treatment while progressed stages have already accumulated neuronal damage beyond the possibility of repair. Thus, increased insight in the molecular mechanisms associated with early phases of AD pathogenesis is likely of great importance for successfully developing new therapies. In addition, there is a clinical need to identify novel biomarkers for early, pre-symptomatic diagnosis, patient stratification and assessing therapy responsiveness. An important aspect of identifying potential molecular and/or cellular disease mechanisms underlying AD as well as specific markers associated with patient subgroups, is to identify changes in protein levels in brain tissue from AD patients. This aspect can be addressed by the unique combination of well-characterized human post-mortem brain tissue, selective isolation of the pathological tissue or cells, and an unbiased broad and in-depth assessment such as using proteomics. To identify molecular mechanisms that are involved in early phases of AD we analyzed the proteome of successive stages of AD as defined by the Braak stage for tau pathology (**Chapter 2**). The CA1 and subiculum regions from the hippocampus, which are early and severely affected subareas in AD brain, were isolated using laser microdissection (LMD). Proteome analysis of 40 cases derived from all Braak stages for tau pathology allowed differentiation between early and late changes in protein abundance during the development of AD pathology. In this pioneering study we showed that the abundance of 372 proteins was altered, which included several proteins that had not been linked to AD previously. Protein groups that displayed similar expression profiles over the disease course were identified and linked to specific cell-types and functional cellular processes.

Early changes included proteins related to the extracellular matrix, actin cytoskeleton, the synapse, endocytosis, protein folding and metabolic stress. In addition, an early-up, late-down expression pattern was observed for several proteins that are linked to synaptic vesicle release, the postsynaptic density and various other neuronal processes which together might represent a compensatory mechanism for early neuronal impairment.

Thanks to a combination in technical advances in mass spectrometry, laser microdissection and optimized IHC protocols, we successfully established a single cell type resolution proteomics workflow, which allowed us to obtain insight in the molecular mechanisms associated with GVD and early tau pathology in neurons (**Chapter 3**). GVD is considered to be associated with a pre-tangle stage in neuronal tau pathology, during which cellular homeostasis and proteostasis can possibly still be restored. Using IHC and LMD, unaffected neurons, neurons with GVD, and tangle-bearing neurons were isolated with high precision from human post-mortem hippocampus. In total 36 samples, each containing 3000 individually isolated neurons, were used for proteome analysis. A significant change in abundance compared to control neurons was found for 115 proteins in GVD- and 197 in tangle-bearing neurons. Affected processes in GVD-bearing neurons included protein folding, endolysosomal function and glycolysis, which are in agreement with findings in **Chapter 2.** Interestingly, profound alterations in RNA processing were apparent in GVD. In tangle-bearing neurons similar processes are affected, yet often more extensively, and in addition, ribosomal proteins and protein folding in the ER become dysregulated. Overall tangle-bearing neurons present a more severe phenotype compared to GVD-bearing neurons. Overlapping protein groups and a progressive increase in tau supports the hypothesis that GVD is associated with a pre-tangle stage. Together, **Chapter 2** and **Chapter 3** provided insight into the molecular mechanisms associated with early tau pathology, at both the regional (CA1 and subiculum) and the neuronal level. Importantly, confirmation of mass spectrometry results as well as association with GVD and other pathological lesions was provided by IHC and immunoblotting in independent study cohorts. Further assessment of the functional consequences of these early changes in protein expression in cellular – or animal models for AD may lead to new clues for future therapeutics.

CAA type-1 is characterized by the deposition of Aβ in the brain vasculature that includes brain capillaries next to larger vessels and is present in varying amounts in about 40% of all AD cases. CAA type-1 contributes to the clinical manifestation of AD and, in very severe forms, it can be the primary cause of dementia. Proteins that are specifically associated with CAA type-1 provide insight into associated disease mechanisms and could be used as diagnostic markers for the presence and extend of CAA type-1 pathology, which likely influences the treatment options for these AD patients. In addition, the presence of CAA can lead to haemorrhages. Therefore, it is advised not to use anticoagulants, as a treatment for thrombosis, in patients with CAA. Hence, in **Chapter 4** the proteome of the occipital lobe was analyzed in cases with severe CAA type-1, AD cases with severe plaque pathology but without vascular Aβ and cognitively heathy control subjects. IHC combined with LMD was used to visualize and isolate areas with high pathological burden from AD and CAA cases and grey matter without pathology from the control donors.

Although proteome changes in AD and CAA largely overlapped, 29 proteins were found selectively expressed/increased in CAA type-1. IHC analysis of selected proteins in brain tissue from AD, CAA type-1 and several other types of small vessel disease (SVD) cases, indicated that especially Norrin (NDP) is a highly specific marker for CAA, especially type-1 CAA, and is virtually absent in the presence of plaque pathology. In addition to a strong increase in CAA type-1, NDP was also associated with capillary pathology in a PrP-CAA case, indicating that increased NDP might be a consequence of capillary dysfunction rather than Aβ deposition. Considering that NDP is a secreted, low molecular weight protein that is localized to the (damaged) CAA-affected vessel wall, it represents a promising target for biomarker development, either in the form of a CSF or blood-based biomarker or as a target for a PET ligand. In addition, the role of NDP and other CAA specific proteins in CAA pathogenesis, e.g. with respect to Aβ transport, aggregation and toxicity, should be investigated.

Guidelines for performing a successful proteomics analysis on human post-mortem tissue with the aid of (immuno-) histochemistry and LMD are provided in **Chapter 5**. Different options for isolating tissue at the level of a microscopic area, individual cells and intracellular inclusion bodies suitable for subsequent LC-MS/MS analysis are described. The methods include tissue preparation, different visualization methods, know-how on the LMD procedure and further sample processing for LC-MS/MS analysis. The field of proteomics is rapidly evolving and new applications emerge allowing increased coverage, providing extensive insight into specific protein isoforms, analysis of posttranslational modifications and interaction proteomics in small samples, such as laser dissected cells.

Overall the results in this thesis improve insight in the molecular events that are involved at various stages in AD, both at a tissue level in different Braak stages for pathology, as well as at the cellular level during tangle formation. In addition, our data shows the heterogeneity in AD with respect to protein changes associated with Aβ plaque pathology compared to CAA. As such, the results presented in this thesis provide a stepping stone to new research directions, aimed to implement new biomarkers and further investigating early disease mechanisms in human brain tissue and available disease models.

GENERAL DISCUSSION

Alzheimer's disease (AD) is the main cause of dementia in the elderly and is currently incurable. To generate promising treatment options we need a better understanding of the aetiology and pathogenic mechanisms of AD and an accurate diagnosis at an early (pre-symptomatic) stage with potential to stratify AD patients into subgroups. Pathological features in human post-mortem brain tissue, which are associated with the progression of AD, have been extensively studied in the past and formed the foundation for our understanding of AD pathogenesis and its heterogeneity. To increase our insight in AD pathogenesis, there is an urgent need to map proteins and molecular pathways that are involved, as this will likely contribute to the development of diagnostics and future therapies.

Proteins that have an altered expression in disease are likely to be involved in disease related processes and are potential targets to modify disease progression. Assessment of RNA levels, referred to as transcriptomics, using high throughput techniques like microarrays and RNAseq, have been used extensively to identify changes in gene expression, and allowed a broad coverage of the gene expression profile. However, changes in RNA levels are often not reflected at the protein level [47]. With the emergence of high throughput and high sensitivity mass spectrometry based proteomics, direct quantification of thousands of proteins from relatively small amounts of total protein has become possible [29]. With the possibility to focus at high resolution on specific aspects of AD pathology using laser microdissection (LMD), it has become a powerful method that can increase our understanding of the molecular mechanisms underlying different aspects of AD pathogenesis. In this thesis, an optimized workflow is presented that combines (immuno-) histochemistry, LMD and LC-MS/MS, which enables the visualization, isolation and proteome analysis of small anatomical regions, pathologic structures and specific cell populations from human post mortem brain tissue.

To increase our understanding of the pathogenesis of AD and CAA we aimed to identify and quantify differences in protein levels in human post-mortem brain tissue to address the following:

- Proteins and potential pathways associated with the progression of AD, especially in early disease stages.
- Proteins and cellular processes involved in granulovacuolar degeneration and tangle pathology in neuronal cells, and the relation between these pathological features.
- Identification of proteins that are specifically associated with capillary Cerebral Amyloid Angiopathy (CAA type-1).

The long-term aim is to increase our insight in the molecular mechanisms associated with AD and CAA pathogenesis, and providing clues for therapeutic targets. Furthermore, the approach taken might deliver proteins that are suitable candidates for further assessment as protein biomarkers aimed to facilitate early diagnosis, patient stratification, monitoring therapeutic efficacy or improved neuropathological characterization.

Early changes in AD pathology

Chapter 2 and 3 describe pioneering studies that focus on the early changes in protein expression associated mainly with tangle pathology in AD. The analyses were performed at the regional tissue level, involving consecutive disease stages based on the Braak stages for tangle pathology [13, 14] in chapter 2 and on the cellular level considering the presence of GVD associated with a pre-tangle stage in chapter 3. In chapter 2 the whole CA1 and subiculum of the hippocampus regions were isolated using LMD. These regions are early and severely affected in AD pathogenesis and we analyzed 40 cases that cover all Braak stages, from 0 to VI, to identify changes in protein abundance at different stages of the disease.

In several proteomics studies human brain tissue of control subjects has been compared to AD tissue. Most studies were performed on whole tissue lysates. Although several recent studies compared control versus clinical AD [1, 26, 87], some studies included different disease stages like pre-symptomatic AD and MCI as well [24, 35, 36, 65]. It is important to note that these studies did not include control cases that were completely devoid of tau and amyloid pathology, which makes detection of early changes related to tau or amyloid beta difficult.

In chapter 2, an altered abundance of 372 proteins was found of which 89 proteins represent early changes that take place in Braak stage 0 to III. We observed an increase in proteins related to ECM alterations, neuroinflammation, protein folding and chaperoning, cytoskeleton, and cellular stress response. Changes in these processes are recurrently being identified in other studies as well, indicating good replication [1, 26, 35, 36, 65, 87]. Increased expression of proteins as reported in chapter 2 and commonly found in other studies include MAPT, CLU and APOE, but also markers that accompany glial activation, like GFAP and CD44. These markers correlate well with the classical pathological hallmarks of AD. In addition, in chapter 2 we observe an increase in the total number of proteins that show a change in abundance over the course of AD, which is also found in several other proteomics studies, pointing towards dysregulation of an increasing number of processes in later stages of the disease [24, 35, 36, 65]. Also more severely affected regions were found to display an increased number of dysregulated proteins [85]. Interestingly, this is also observed when comparing GVD to tangle bearing neurons, which supports that tangles are in a more progressed disease stage compared to GVD (Chapter 3).

Proteins related to synapse and neuronal function

In chapter 2 we show that synapse-related proteins and those related to neuronal functioning are primarily found decreased in AD, which is in accordance with the literature [43]. However, in addition we found that a subset of these proteins displays an early-up-/late-down type of expression profile (Chapter 2, Fig. 3b, Fig. 4f,g). Previous studies have not reported such an up/down profile, possibly because control cases that do not exhibit any pathology were not included in these studies [35, 36, 65].

The transiently increased synapse-related proteins, and other proteins that follow the same up/down type of expression profile, might represent an early compensatory mechanism to maintain

normal hippocampal functioning, in which the transition from Braak stage II to III appears to be a turning point, which roughly coincides with the appearance of clinical symptoms.

More specifically, this cluster is composed of proteins related to neuronal function, axonal guidance, mitochondrial oxidative phosphorylation, synaptic vesicle release and postsynaptic density function. High expression of such proteins was found associated with a stable cognitive trajectory at advanced age in a recent proteomics study [79]. This compensatory mechanism is likely unrelated to GVD bearing neurons as we did not observe changes in abundance of these proteins in GVD (Chapter 3). Hence, the transient increase of these neuronal proteins might be essential for maintaining neuronal and synaptic function whereas GVD-related processes are considered to counteract cellular stress caused by early tau pathology.

Early synaptic effects are also in agreement with the amyloid cascade hypothesis as increased levels of Aβ oligomers correlate with the extent of synaptic loss [44, 49, 64]. However, these effects might also relate to incipient tau pathology as we were not able to measure Aβ levels in CA1/subiculum samples, while an early increase in the total tau levels was clearly observed. In addition, Aβ pathology is not required for tangle pathology as is exemplified by Primary Age-related Tauopathy (PART) cases that exhibit AD like tangle pathology without elevated soluble Aβ levels or Aβ deposits [6, 34]. A distinction between Aβ- and tau-related changes might be made by direct proteomics comparison of PART and AD cases with equal amounts of tau pathology. Such a comparison could provide further insight in Aβ related pathological processes as well as increased insight in the relation between PART and AD. In addition, cortical brain regions are most likely more suitable to assess Aβ related changes as Aβ pathology is more prominent in these areas. As such the data from chapter 4 which was focused on the occipital lobe can be used to get more insight into differences between brain regions and protein expression changes related to general AD and Aβ-related changes.

GVD and neurofibrillary tangles

Prior to our study on GVD and tangle bearing neurons, the analysis of the protein content of laser dissected NFTs was performed in two small studies in which one and two samples were measured representing 3 and 4 pooled cases, respectively [51, 74]. These studies identified GAPDH and UCH-L1 to co-localize with pTau aggregates. In contrast to our study on tangle bearing neurons, no comparison was made with NFT negative neurons. As such, chapter 3 currently provides the largest proteomics study on NFTs, the only one on GVD containing neurons to date and is therefore the only study that provides a high level of insight into the changing neuronal proteome during tangle formation in AD. In addition, it provides for the first time quantitative protein data on the relation between GVD and NFTs and supports the model that the tangle bearing neurons are further progressed in the pathological process compared to GVD bearing neurons.

Applying mass spectrometry at cellular resolution in Chapter 3 identified changes in protein abundance specifically in neurons with GVD and tangle bearing neurons. Several new GVD-

associated proteins and processes were identified including changes related to protein folding, endolysosomal function, microtubules and cytoskeleton related proteins. This is in accordance with the identity of GVD bodies which are marked by several endolysosomal proteins and the onset of insipient tau pathology marked by disruption of the microtubule and counteracting protein misfolding [28, 39, 77].

In addition, reduced glycolysis is a known feature of AD and results in increased oxidative stress and reduced neuronal functioning [15]. We found that this process is affected in neurons with GVD and tangle bearing neurons as we observe an increase in the levels of proteins related to sequential steps in glycolysis. In addition, several proteins were found selectively increased or exclusively present in GVD containing neurons which may reflect a response to a disturbed homeostasis related to early tau pathology. Moreover, GVD bearing neurons also showed a striking difference in proteins related RNA processing. In addition to this, tangle bearing neurons also show dysregulation of ribosomal proteins and protein folding in the ER indicating disrupted protein synthesis and folding of newly synthesized proteins. Hence, there is a high degree of overlap in dysregulated processes between GVD and tangle bearing neurons in which tangle bearing neurons show a more extensive degree of dysregulation. This indicates a relation between GVD and tangle bearing neurons with the latter being in a more progressed phase of the disease. Also the stepwise increase in total tau levels supports the hypothesis that GVD is associated with a neuronal pre-tangle stage.

RNA processing

Although dysregulation of RNA metabolism has been linked to AD previously [2, 30, 36, 83] we found that it is an early neuronal event, that already occurs in GVD bearing pre-tangle neurons. Our results showed a decrease in RNA binding proteins, especially several proteins of the hnRNP family. Dysregulation of RNA processing can result in alternatively spliced protein isoforms [36], and mis-splicing events resulting in cryptic exon inclusion and synthesis of aberrant proteins [4]. As such, dysregulation of RNA processing can result in impaired neuronal functioning and decreased survival. In addition, it may affect the levels of different tau isoforms, disrupting the 3R and 4R tau isoform balance, impairing axonal transport and promoting tau pathology [4, 41].

Moreover, other studies found an increase in RNA binding proteins, especially snRNPs, in AD [24, 36, 45]. These RNA binding proteins have been found to bind and co-aggregate with tau and this interaction results in a disruption of pre-mRNA splicing in AD [9, 24, 30]. In addition, cryptic exon inclusion in AD has been suggested to occur in neurons that have either TDP-43 inclusions or where TDP-43 is depleted from the nucleus [69]. No changes in RNA metabolism were found with proteomics in a normal ageing cohort, which strengthens the connection between aberrant RNA processing and a pathogenic process [35].

Functional assessment of early AD regulated proteins

Proteins that showed a change in abundance in early disease stages or an up/down expression profile as shown in chapter 2 or those associated with early tau pathology identified in chapter

3 could be involved in onset and progression in early stages of AD pathogenesis. Hence, these might be used to modify disease progression. Therefore, the functional consequences of aberrant protein expression should be assessed in suitable models for AD. Several models for AD are available which capture various aspects of AD and are essential to increase our understanding of AD pathogenesis, test specific hypotheses and assess potential novel therapeutics [22]. Functional consequences and phenotypic alterations by changing the expression or activity of proteins associated with early AD can be assessed, for example in glia or neuronal cells [61, 62].

Specifically for the proteins found associated with GVD a useful neuronal cell model was recently developed by Wiersma et al. [78]. This model clearly shows a connection between the development of tau pathology and the presence of GVD bodies, as it shows GVD and its associated markers upon seeding induced intracellular tau pathology. The requirement of intracellular tau pathology for GVD formation in this model is in agreement with the presence of diffuse phosphorylated tau in GVD bearing neurons in post-mortem human brain tissue and with the increase in total tau levels detected in GVD bearing neurons (Chapter 3). Also the identification of CHMP1A as a GVD selective protein (Chapter 3) complies with the presence of late endocytic markers in the GVD bodies as observed in the model of Wiersma et al., as well as in post mortem tissue [78, 86]. The tau seed-induced GVD model would allow further study on the consequences of GVD formation, tau phosphorylation and tau aggregation upon knockdown, overexpression or functional modification of various newly identified GVD markers. Subsequently, animal models that display tau pathology and GVD might be used to further evaluate their therapeutic potential [40, 50]. Importantly, proper comparison between observations done in human post mortem tissue and those in various models are warranted to determine which effects are relevant for human disease and which features of the models diverge from the human condition.

In addition, to gain insight in the functional consequences of proteins that are early aberrantly expressed, or those associated with GVD and tangle formation, it is crucial to gain insight in the interaction partners of these proteins. This is possible using various techniques including co-immunoprecipitation, blue native gel electrophoresis or by proximity-based labelling followed by MS analysis [23, 38]. The role of these proteins in GVD and their association with other proteins or tau will shed light on their role in disease. Moreover, our findings could also be relevant in other neurodegenerative diseases including other tauopathies and proteinopathies.

Proteins with relevance for biomarker studies

Current biomarkers used for the clinical diagnosis of AD are based on the core components of its pathological hallmarks, Aβ and tau. This includes determining the levels of different Aβ isoforms and pTau and total tau in CSF or visualizing Aβ using a specific PET tracer [32]. Likewise, protein biomarkers can be measured in CSF or blood, or directly in the brain via the use of a PET tracer. Non-Aβ and non-tau protein biomarkers could be used to reflect processes related to various aspects of pathogenesis of AD, like prediction of the cognitive deterioration

rate, neuroinflammation and neuronal loss, which can aid to monitor these aspects of disease progression and/or therapy responsiveness [10, 56]. In addition, specific biomarkers or a combination thereof can be used for early diagnosis of AD and stratification of patients into clinically or pathologically defined subgroups. This might be of importance as different patient groups may respond differently when included in a clinical trial for a particular therapeutic intervention. As such, early diagnosis and stratification of patients into subgroups might pave the way to improve the success rate of clinical trials.

Several markers that we identified using a proteomics approach have been shown to be present in CSF or plasma and include CLU [37], TNC [25, 67], ANXA5 [68], Complement factor C4 [8, 17] and SCG2 [68]. Direct proteomics analysis of CSF or blood of patients is also possible for biomarker research as this is done in the field of clinical proteomics [57]. For example, detection and altered abundance of the early regulated proteins PPIA, YWHAZ, EZR and PBXIP1 was demonstrated this way [3, 63, 76]. Such studies would benefit from a post-mortem assessment of cases from which collected CSF or blood samples were analyzed. This would provide insight into the presence of early pathology in control cases, and provides the opportunity to distinguish associated biomarkers. In addition, co-morbidities in AD cases can be recognized, and it would allow for assessing correlations with the pathological features of AD [75].

However, detection of low-abundant proteins in CSF by LC-MS/MS is easily hindered by the presence of a small number of highly abundant proteins [58]. Low abundant CSF proteins that originate from the brain and might reflect a certain aspect of AD pathology, are thus more likely to be identified first in human brain tissue and can subsequently be quantified in blood or CSF using a targeted (immuno-) assay.

The pathology of CAA and NDP as a selective marker

CAA-specific proteins (Chapter 4) were identified by comparing the proteomes of human occipital lobe tissue from AD cases with severe CAA type-1, AD cases with severe plaque pathology without vascular Aβ, and control tissue without pathology. IHC was used to visualize Aβ pathology in grey matter areas and to select regions of interest for LMD and analysis by mass spectrometry. 29 proteins were identified that selectively associate with CAA type-1 of which 5 (APOE, APCS, HTRA1, NDP and COL6A2) were selected for additional IHC analysis. NDP was found to be the most promising marker protein for CAA type-1. NDP is mainly associated with capillary pathology as confirmed with IHC. This makes NDP a promising marker for CAA type-1 and possibly other brain capillary defects as it was not restricted to Aβ capillary pathology but was also found highly increased in a prion- (PrP-)CAA case that exhibited PrP accumulation around brain capillaries. Hence, increased NDP might be a consequence of capillary dysfunction rather than Aβ deposition. Recently, NDP immunoreactivity was also associated with an Aβ plaque type termed the “coarse grained plaque”, which is mainly associated with a form of early onset AD. This plaque type appears to have a vascular association and is linked to capillary damage [11]. Recently, the proteomic comparison of laser-dissected plaques of rapidly progressive (rp)AD and typical sporadic AD was described which was used to identify new

plaque-associated proteins but also differences in plaque composition between rpAD and typical AD [20]. This indicates differences in molecular mechanisms that underlie various types of Aβ pathology, which may have consequences for treatment [12, 20, 53].

Other proteomics studies focusing specifically on CAA in post-mortem human brains were described by Manousopoulou et al. [48] and Inoue et al. [31]. These studies were designed to identify proteins that co-accumulate with Aβ in CAA and were directed at isolated leptomeningeal arteries [48] and both leptomeningeal arteries and cerebral neocortical arterioles [31], while no comparison was made with AD cases with plaque pathology. We found several similarities with these proteomics studies, including the increase in abundance of proteins like CLU and APOE in CAA, both implicated in the development of the disease [66, 71, 82]. NDP was detected but was not found increased in CAA in these studies, supposedly because CAA affected capillaries were not included in these studies. Another study, aimed specifically at the sarkosyl-insoluble proteome in typical AD and thereby enriching for Aβ deposits and NFTs, indicated the correlation of APCS, NDP and HTRA1 with levels of Aβ pathology [24]. However, there is no mentioning of CAA in this study, but likely AD cases were included that exhibit capillary CAA, emphasizing the importance of validation, for example by IHC, and extensive neuropathological characterization of the cases analyzed by MS.

CAA biomarker proteins

NDP is well suited to be developed into a biomarker in various applications. NDP could serve as IHC biomarker in pathology and as a PET target or CSF/blood-based protein marker in the clinic. For neuropathological examination it would allow easy indication of any capillary-related Aβ pathology by the presence of NDP immunoreactivity. In addition, NDP has potential to be developed as a PET tracer for assessing the presence and amount of capillary CAA in AD patients. NDP is easily accessible in CAA as it is localized in the vessel wall and its accessibility is further improved by a reduced blood brain barrier function as a consequence of CAA [16, 46]. Currently, the Aβ binding PET tracer Pittsburgh compound B, cannot be used to distinguish between parenchymal Aβ and vascular Aβ depositions due to limited resolution of the scanning device. An NDP PET-tracer could provide this distinction.

For CSF or serum based analysis several proteins from this study, that are potentially useful biomarkers, were shown det ectable in CSF or serum, including CLU [10], APOE [57], APCS [73] and TNR [52]. As NDP is a small sized, secreted protein, which is primarily expressed in the brain, it could potentially reach the CSF or blood and show changes in abundance that reflect CAA severity or brain capillary dysfunction. This would allow stratification of AD patients based on the presence and extend of vascular pathology. In addition, CAA is counter indicative for the use of certain medication like anticoagulants, commonly known as blood thinners, as these increase the risk and severity of brain hemorrhages in CAA [5]. Although some increased NDP immunoreactivity was also found in other small vessel diseases, these can be easily distinguished from AD and CAA based on other clinical, CSF and/or genetic markers [33, 72].

Functional assessment of NDP and other CAA associated proteins

To get more insight in the potential role of NDP in pathogenesis of CAA type-1, it is important to clarify the phase in which NDP upregulation takes place and the mechanism by which it is induced in capillary CAA. Moreover, the effect of CAA on NDP signaling and the consequence of increased NDP on the pathogenesis of CAA needs to be investigated, e.g. by determining NDP interaction partners, assessing its effect on aggregation and toxicity of Aβ or its effect on blood brain barrier integrity or synaptic function. In addition, the relevance of NDP in existing animal models for CAA [18, 19] should be assessed, as well as the effect of modulation of NDP expression in these models.

Also, additional research on other identified CAA marker proteins is needed to better understand their relevance in CAA. Extensively studied proteins including APOE, CLU and APCS are known to affect the clearance, transport and aggregation of Aβ and are important for the development of CAA [7, 42, 54, 80–82]. But also less studied proteins could play an important role, e.g. TMF1 affects pericyte function and BBB integrity via PDGFRβ [55, 88] and the selective reduction of TNR might affect neuronal function and protection against stress [60, 70]. Increased HLA-DRA corresponds with increased microglial activation, as found previously in CAA type-1 especially when dyshoric changes are present [59].

Regional versus cellular resolution proteomics

As mentioned earlier, proteomics can be focused on cell populations, as shown in chapter 3, or subcellular disease-associated pathological features using LMD. Our first effort in this field is described in a paper from Wong et al. in 2014, in which the proteomics analysis of laser dissected intraneuronal inclusion bodies that were present in a neurodegenerative disease assisted to find the protein target among a multitude of genetic candidates [84]. As such, our proteomics data on the composition of the inclusion body revealed the causative gene of this illness. Similar approaches for the proteomics analysis of individual plaques and/or tangles have been described for both formalin fixed tissue [21], and fresh frozen brain tissue [27] (Chapter 5).

Several studies, including our own in Chapter 2, have assigned different expression profiles to different cell types. However, the best possible physical separation of cells and subcellular fractions will be essential to increase our understanding of AD related changes in protein expression. In addition, validation by IHC and immunofluorescence greatly contributes to a better understanding of spatial changes of protein expression and their relation with AD pathology.

In chapter 2 the complete area of CA1 and subiculum was analyzed whereas in chapter 3 individual pyramidal neurons from this same area were analyzed. There is some overlap in the proteins detected in both studies. However, several proteins that have an altered expression in neuronal cells with GVD or tangles do not show a change in expression when the whole CA1 and subiculum are assessed, and some were found to change in the opposite direction (Fig. 1). This emphasizes the importance of performing a proteomics analysis at various levels of resolution, in order to gain a more complete understanding of the proteins and associated

processes that play a role at different levels of AD pathogenesis. Sources of variation in the relative changes of proteins between regional and cellular resolution proteomics, may lie in the fact that in a brain area the cellular composition changes during AD by, for example, neuronal loss and gliosis. In addition, the same protein can be expressed by multiple cell types, but the change in abundance during AD can be different in each cell type.

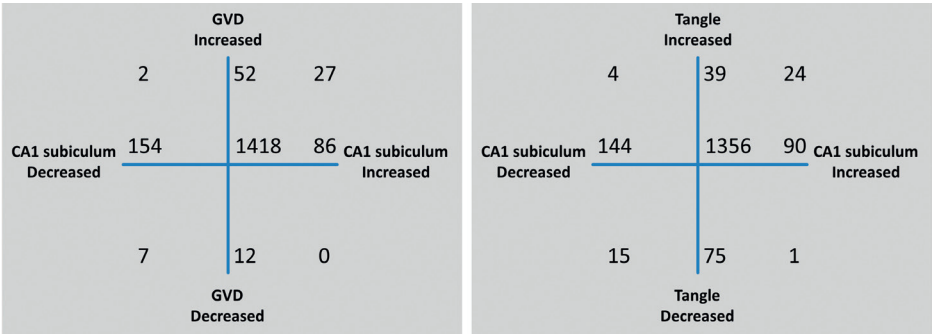

FIGURE 1 | Comparison of changes in expression found in the CA1 and subiculum region as a whole as determined in Chapter 2 and in neuronal cells with GVD and tangles as determined in Chapter 3. Only proteins detected in both studies are considered. The numbers indicate the number of proteins that overlap between the studies in Chapter 2 and Chapter 3. The position relative to the x-axis indicates any change in protein abundance in the CA1 and subiculum as determined in chapter 2, the position relative to the y-axis indicates any change in protein abundance in the CA1 and subiculum as determined in Chapter 3 in cells with GVD (a) and tangles (b). For both the x- and y-axes, the number at the crossing point indicates that no change has been observed.

Future perspectives of an (LMD assisted) LC-MS/MS workflow

Mass spectrometry-based proteomics is a field that is rapidly evolving. This will allow increasingly more in-depth analysis that will be valuable for research on AD and neurodegeneration. For example, increased understanding of disease-associated post translational modifications (PTMs) would provide insight in activity, localization, and interactions of proteins. In addition, abnormal PTMs might represent opportunities for diagnosis and treatment. Moreover, higher coverage of proteins in a brain sample will result in increased accuracy of protein quantification, and more importantly, it will provide data on an increased number of proteins and more detailed and reliable information on specific protein isoforms.

Increased sample number and inclusion of multiple brain regions including those severely affected and relatively unaffected may provide insight into the mechanisms underlying the relative vulnerability or resistance to different types of pathology. In addition to this, detailed comparison with other neurodegenerative diseases will give insight in potentially common pathogenic mechanisms, disease specific proteins and pathways, and increased understanding on predispositions and vulnerability in different affected regions. Moreover, systematic proteome characterization of disease models will increase our understanding of the similarities

and differences with human brain disease, as disease models may show specific pathological features induced in a non-physiological manner [22]. In contrast, disease models may indicate dysregulation of processes at early disease stage of which data in human postmortem brain is only scarce. Taken together, applied at the regional and cellular resolution, in-depth MS based studies will aid in gaining adequate understanding and proper comparison between regions, individuals and neurodegenerative diseases and selection or development of suitable disease models.

REFERENCES

1. Andreev VP, Petyuk VA, Brewer HM, Karpievitch Y V., Xie F, Clarke J, Camp D, Smith RD, Lieberman AP, Albin RL, Nawaz Z, El Hokayem J, Myers AJ (2012) Label-free quantitative LC-MS proteomics of alzheimer's disease and normally aged human brains. J Proteome Res 11:3053–3067. doi: 10.1021/pr3001546
2. Bader JM, Geyer PE, Müller JB, Strauss MT, Koch M, Leypoldt F, Koertvelyessy P, Bittner D, Schipke CG, Incesoy EI, Peters O, Deigendesch N, Simons M, Jensen MK, Zetterberg H, Mann M (2020) Proteome profiling in cerebrospinal fluid reveals novel biomarkers of Alzheimer's disease. Mol Syst Biol. doi: 10.15252/msb.20199356
3. Bampton A, Gittings LM, Fratta P, Lashley T, Gatt A (2020) The role of hnRNPs in frontotemporal dementia and amyotrophic lateral sclerosis. Acta Neuropathol. doi: 10.1007/s00401-020-02203-0
4. Banerjee G, Carare R, Cordonnier C, Greenberg SM, Schneider JA, Smith EE, Van Buchem M, Van Der Grond J, Verbeek MM, Werring DJ (2017) The increasing impact of cerebral amyloid angiopathy: Essential new insights for clinical practice. J Neurol Neurosurg Psychiatry 88:982–994. doi: 10.1136/jnnp-2016-314697
5. Bell WR, An Y, Kageyama Y, English C, Rudow GL, Pletnikova O, Thambisetty M, O'Brien R, Moghekar AR, Albert MS, Rabins P V., Resnick SM, Troncoso JC (2019) Neuropathologic, genetic, and longitudinal cognitive profiles in primary age-related tauopathy (PART) and Alzheimer's disease. 15:8–16. doi: 10.1016/j.jalz.2018.07.215
6. Belloy ME, Napolioni V, Greicius MD (2019) A Quarter Century of APOE and Alzheimer's Disease: Progress to Date and the Path Forward. Neuron 101:820–838. doi: 10.1016/j.neuron.2019.01.056
7. Bennett S, Grant M, Creese AJ, Mangialasche F, Cecchetti R, Cooper HJ, Mecocci P, Aldred S (2012) Plasma levels of complement 4a protein are increased in Alzheimer's disease. Alzheimer Dis Assoc Disord 26:329–334. doi: 10.1097/WAD.0b013e318239dcbd
8. Bishof I, Dammer EB, Duong DM, Kundinger SR, Gearing M, Lah JJ, Levey AI, Seyfried NT (2018) RNA-binding proteins with basic-acidic dipeptide (BAD) domains self-assemble and aggregate in Alzheimer's disease. J Biol Chem 293:11047–11066. doi: 10.1074/jbc.RA118.001747
9. Blennow K, Zetterberg H (2018) Biomarkers for Alzheimer's disease: current status and prospects for the future. J Intern Med 284:643–663. doi: 10.1111/joim.12816
10. Boon BDC, Bulk M, Jonker AJ, Morrema THJ, van den Berg E, Popovic M, Walter J, Kumar S, van der Lee SJ, Holstege H, Zhu X, Van Nostrand WE, Natté R, van der Weerd L, Bouwman FH, van de Berg WDJ, Rozemuller AJM, Hoozemans JJM (2020) The coarse-grained plaque: a divergent Aβ plaque-type in early-onset Alzheimer's disease. Acta Neuropathol 1:3. doi: 10.1007/s00401-020-02198-8

11. Boon BDC, Hoozemans JJM, Lopuhaä B, Eigenhuis KN, Scheltens P, Kamphorst W, Rozemuller AJM, Bouwman FH (2018) Neuroinflammation is increased in the parietal cortex of atypical Alzheimer's disease. J Neuroinflammation. doi: 10.1186/s12974-018-1180-y

12. Braak H, Braak E (1991) Neuropathological stageing of Alzheimer-related changes. Acta Neuropathol 82:239–259. doi: 10.1007/BF00308809

13. Braak H, Braak E (1995) Staging of alzheimer's disease-related neurofibrillary changes. Neurobiol Aging 16:271–278. doi: 10.1016/0197-4580(95)00021-6

14. Butterfield DA, Halliwell B (2019) Oxidative stress, dysfunctional glucose metabolism and Alzheimer disease. Nat Rev Neurosci 20:148–160. doi: 10.1038/s41583-019-0132-6

15. Carrano A, Hoozemans JJM, Van Der Vies SM, Van Horssen J, De Vries HE, Rozemuller AJM (2012) Neuroinflammation and blood-brain barrier changes in capillary amyloid angiopathy. Neurodegener Dis 10:329–331. doi: 10.1159/000334916

16. Daborg J, Andreasson U, Pekna M, Lautner R, Hanse E, Minthon L, Blennow K, Hansson O, Zetterberg H (2012) Cerebrospinal fluid levels of complement proteins C3, C4 and CR1 in Alzheimer's disease. J Neural Transm 119:789–797. doi: 10.1007/s00702-012-0797-8

17. Davis J, Xu F, Deane R, Romanov G, Previti M Lou, Zeigler K, Zlokovic B V., Van Nostrand WE (2004) Early-onset and Robust Cerebral Microvascular Accumulation of Amyloid β-Protein in Transgenic Mice Expressing Low Levels of a Vasculotropic Dutch/Iowa Mutant Form of Amyloid β-Protein Precursor. J Biol Chem 279:20296–20306. doi: 10.1074/jbc.M312946200

18. Davis J, Xu F, Hatfield J, Lee H, Hoos MD, Popescu D, Crooks E, Kim R, Smith SO, Robinson JK, Benveniste H, Van Nostrand WE (2018) A Novel Transgenic Rat Model of Robust Cerebral Microvascular Amyloid with Prominent Vasculopathy. Am J Pathol 188:2877–2889. doi: 10.1016/j.ajpath.2018.07.030

19. Drummond E, Nayak S, Faustin A, Pires G, Hickman RA, Askenazi M, Cohen M, Haldiman T, Kim C, Han X, Shao Y, Safar JG, Ueberheide B, Wisniewski T (2017) Proteomic differences in amyloid plaques in rapidly progressive and sporadic Alzheimer's disease. Acta Neuropathol 133:933–954. doi: 10.1007/s00401-017-1691-0

20. Drummond E, Nayak S, Pires G, Ueberheide B, Wisniewski T (2018) Isolation of amyloid plaques and neurofibrillary tangles from archived alzheimer's disease tissue using laser-capture microdissection for downstream proteomics. In: Methods Mol. Biol. Humana Press Inc., pp 319–334

21. Drummond E, Wisniewski T (2017) Alzheimer's disease: experimental models and reality. Acta Neuropathol 133:155–175. doi: 10.1007/s00401-016-1662-x

22. Gonzalez-Lozano MA, Koopmans F, Paliukhovich I, Smit AB, Li KW (2019) A Fast and Economical Sample Preparation Protocol for Interaction Proteomics Analysis. Proteomics. doi: 10.1002/pmic.201900027

23. Hales CM, Dammer EB, Deng Q, Duong DM, Gearing M, Troncoso JC, Thambisetty M, Lah JJ, Shulman JM, Levey AI, Seyfried NT (2016) Changes in the detergent-insoluble brain proteome linked to amyloid and tau in Alzheimer's Disease progression. Proteomics 16:3042–3053. doi: 10.1002/pmic.201600057

24. Hall JR, Johnson LA, Barber RC, Vo HT, Scott Winter A, O'Bryant SE (2012) Biomarkers of basic activities of daily living in Alzheimer's disease. J Alzheimer's Dis 31:429–437. doi: 10.3233/JAD-2012-111481

25. Ho Kim J, Franck J, Kang T, Heinsen H, Ravid R, Ferrer I, Hee Cheon M, Lee JY, Shin Yoo J, Steinbusch HW, Salzet M, Fournier I, Mok Park Y (2015) Proteome-wide characterization of signalling interactions in the hippocampal CA4/DG subfield of patients with Alzheimer's disease. Sci Rep 5:1–15. doi: 10.1038/srep11138

26. Hondius DC, Hoozemans JJM, Rozemuller AJM, Li KW, Smit AB (2018) A Laser Microdissection–Liquid Chromatography–Tandem Mass Spectrometry Workflow for Post-mortem Analysis of Brain Tissue. In: Methods Mol. Biol. pp 371–383

27. Hoozemans JJM, Van Haastert ES, Nijholt DAT, Rozemuller AJM, Eikelenboom P, Scheper W (2009) The unfolded protein response is activated in pretangle neurons in alzheimer's disease hippocampus. Am J Pathol 174:1241–1251. doi: 10.2353/ajpath.2009.080814

28. Hosp F, Mann M (2017) A Primer on Concepts and Applications of Proteomics in Neuroscience. Neuron 96:558–571. doi: 10.1016/j.neuron.2017.09.025

29. Hsieh YC, Guo C, Yalamanchili HK, Abreha M, Al-Ouran R, Li Y, Dammer EB, Lah JJ, Levey AI, Bennett DA, De Jager PL, Seyfried NT, Liu Z, Shulman JM (2019) Tau-Mediated Disruption of the Spliceosome Triggers Cryptic RNA Splicing and Neurodegeneration in Alzheimer's Disease. Cell Rep 29:301-316.e10. doi: 10.1016/j.celrep.2019.08.104

30. Inoue Y, Ueda M, Tasaki M, Takeshima A, Nagatoshi A, Masuda T, Misumi Y, Kosaka T, Nomura T, Mizukami M, Matsumoto S, Yamashita T, Takahashi H, Kakita A, Ando Y (2017) Sushi repeat-containing protein 1: a novel disease-associated molecule in cerebral amyloid angiopathy. Acta Neuropathol 134:605–617. doi: 10.1007/s00401-017-1720-z

31. Jack CR, Bennett DA, Blennow K, Carrillo MC, Dunn B, Haeberlein SB, Holtzman DM, Jagust W, Jessen F, Karlawish J, Liu E, Molinuevo JL, Montine T, Phelps C, Rankin KP, Rowe CC, Scheltens P, Siemers E, Snyder HM, Sperling R, Elliott C, Masliah E, Ryan L, Silverberg N (2018) NIA-AA Research Framework: Toward a biological definition of Alzheimer's disease. Alzheimer's Dement 14:535–562. doi: 10.1016/j.jalz.2018.02.018

32. Jansen C, Parchi P, Capellari S, Vermeij AJ, Corrado P, Baas F, Strammiello R, Van Gool WA, Van Swieten JC, Rozemuller AJM (2010) Prion protein amyloidosis with divergent phenotype associated with two novel nonsense mutations in PRNP. Acta Neuropathol 119:189–197. doi: 10.1007/s00401-009-0609-x

33. Jellinger KA, Alafuzoff I, Attems J, Beach TG, Cairns NJ, Crary JF, Dickson DW, Hof PR, Hyman BT, Jack CR, Jicha GA, Knopman DS, Kovacs GG, Mackenzie IR, Masliah E, Montine TJ, Nelson PT, Schmitt F, Schneider JA, Serrano-Pozo A, Thal DR, Toledo JB, Trojanowski JQ, Troncoso JC, Vonsattel JP, Wisniewski T (2015) PART, a distinct tauopathy, different from classical sporadic Alzheimer disease. Acta Neuropathol 129:757–762. doi: 10.1007/s00401-015-1407-2

34. Johnson ECB, Dammer EB, Duong DM, Ping L, Zhou M, Yin L, Higginbotham LA, Guajardo A, White B, Troncoso JC, Thambisetty M, Montine TJ, Lee EB, Trojanowski JQ, Beach TG, Reiman EM, Haroutunian V, Wang M, Schadt E, Zhang B, Dickson DW, Ertekin-Taner N, Golde TE, Petyuk VA, De Jager PL, Bennett DA, Wingo TS, Rangaraju S, Hajjar I, Shulman JM, Lah JJ, Levey AI, Seyfried NT (2020) Large-scale proteomic analysis of Alzheimer's disease brain and cerebrospinal fluid reveals early changes in energy metabolism associated with microglia and astrocyte activation. Nat Med. doi: 10.1038/s41591-020-0815-6

35. Johnson ECB, Dammer EB, Duong DM, Yin L, Thambisetty M, Troncoso JC, Lah JJ, Levey AI, Seyfried NT (2018) Deep proteomic network analysis of Alzheimer's disease brain reveals alterations in RNA binding proteins and RNA splicing associated with disease. Mol Neurodegener. doi: 10.1186/s13024-018-0282-4

36. Jongbloed W, Van Dijk KD, Mulder SD, Van De Berg WDJ, Blankenstein MA, Van Der Flier W, Veerhuis R (2015) Clusterin Levels in Plasma Predict Cognitive Decline and Progression to Alzheimer's Disease. J Alzheimer's Dis 46:1103–1110. doi: 10.3233/JAD-150036

37. Kim DI, Cutler JA, Na CH, Reckel S, Renuse S, Madugundu AK, Tahir R, Goldschmidt HL, Reddy KL, Huganir RL, Wu X, Zachara NE, Hantschel O, Pandey A (2018) BioSITe: A Method for Direct Detection and Quantitation of Site-Specific Biotinylation. J Proteome Res 17:759–769. doi: 10.1021/acs.jproteome.7b00775

38. Köhler C (2016) Granulovacuolar degeneration: a neurodegenerative change that accompanies tau pathology. Acta Neuropathol 132:339-359. doi: 10.1007/s00401-016-1562-0

39. Köhler C, Dinekov M, Götz J (2014) Granulovacuolar degeneration and unfolded protein response in mouse models of tauopathy and Aβ amyloidosis. Neurobiol Dis 71:169–179. doi: 10.1016/j.nbd.2014.07.006

40. Lacovich V, Espindola SL, Alloatti M, Devoto VP, Cromberg LE, Čarna ME, Forte G, Gallo JM, Bruno L, Stokin XB, Avale ME, Falzone TL (2017) Tau isoforms imbalance impairs the axonal transport of the amyloid precursor protein in human neurons. J Neurosci 37:58–69. doi: 10.1523/JNEUROSCI.2305-16.2016

41. Liu CC, Kanekiyo T, Xu H, Bu G (2013) Apolipoprotein e and Alzheimer disease: Risk, mechanisms and therapy. Nat Rev Neurol 9:106–118. doi: 10.1038/nrneurol.2012.263

42. Long JM, Holtzman DM (2019) Alzheimer Disease: An Update on Pathobiology and Treatment Strategies. Cell 179:312–339. doi: 10.1016/j.cell.2019.09.001

43. Lue LF, Kuo YM, Roher AE, Brachova L, Shen Y, Sue L, Beach T, Kurth JH, Rydel RE, Rogers J (1999) Soluble amyloid β peptide concentration as a predictor of synaptic change in Alzheimer's disease. Am J Pathol 155:853–862. doi: 10.1016/S0002-9440(10)65184-X

44. Lutz BM, Peng J (2018) Deep profiling of the aggregated proteome in Alzheimer's disease: From pathology to disease mechanisms. Proteomes 6:46. doi: 10.3390/proteomes6040046

45. Magaki S, Tang Z, Tung S, Williams CK, Lo D, Yong WH, Khanlou N, Vinters H V. (2018) The effects of cerebral amyloid angiopathy on integrity of the blood-brain barrier. Neurobiol Aging 70:70–77. doi: 10.1016/j.neurobiolaging.2018.06.004

46. Maier T, Güell M, Serrano L (2009) Correlation of mRNA and protein in complex biological samples. FEBS Lett 583:3966–3973. doi: 10.1016/j.febslet.2009.10.036

47. Manousopoulou A, Gatherer M, Smith C, Nicoll JAR, Woelk CH, Johnson M, Kalaria R, Attems J, Garbis SD, Carare RO (2017) Systems proteomic analysis reveals that clusterin and tissue inhibitor of metalloproteinases 3 increase in leptomeningeal arteries affected by cerebral amyloid angiopathy. Neuropathol Appl Neurobiol 43:492–504. doi: 10.1111/nan.12342

48. McLean CA, Cherny RA, Fraser FW, Fuller SJ, Smith MJ, Beyreuther K, Bush AI, Masters CL (1999) Soluble pool of Aβ amyloid as a determinant of severity of neurodegeneration in Alzheimer's disease. Ann Neurol 46:860–866. doi: 10.1002/1531-8249(199912)46:6<860::AID-ANA8>3.0.CO;2-M

49. Midani-Kurçak JS, Dinekov M, Puladi B, Arzberger T, Köhler C (2019) Effect of tau-pathology on charged multivesicular body protein 2b (CHMP2B). Brain Res 1706:224-236. doi: 10.1016/j.brainres.2018.11.008

50. Minjarez B, Rustarazo MLV, Sanchez Del Pino MM, González-Robles A, Sosa-Melgarejo JA, Luna-Muñoz J, Mena R, Luna-Arias JP (2013) Identification of polypeptides in neurofibrillary tangles and total homogenates of brains with Alzheimer's disease by tandem mass spectrometry. J Alzheimer's Dis 34:239-262. doi: 10.3233/JAD-121480

51. Minta K, Portelius E, Janelidze S, Hansson O, Zetterberg H, Blennow K, Andreasson U (2019) Cerebrospinal fluid concentrations of extracellular matrix proteins in Alzheimer's disease. J Alzheimer's Dis 69:1213–1220. doi: 10.3233/JAD-190187

52. Ossenkoppele R, Schonhaut DR, Schöll M, Lockhart SN, Ayakta N, Baker SL, O'Neil JP, Janabi M, Lazaris A, Cantwell A, Vogel J, Santos M, Miller ZA, Bettcher BM, Vossel KA, Kramer JH, Gorno-Tempini ML, Miller BL, Jagust WJ, Rabinovici GD (2016) Tau PET patterns mirror clinical and neuroanatomical variability in Alzheimer's disease. Brain 139:1551–1567. doi: 10.1093/brain/aww027

53. Ozawa D, Nomura R, Mangione PP, Hasegawa K, Okoshi T, Porcari R, Bellotti V, Naiki H (2016) Multifaceted anti-amyloidogenic and pro-amyloidogenic effects of C-reactive protein and serum amyloid P component in vitro. Sci Rep. doi: 10.1038/srep29077

54. Papadopoulos N, Lennartsson J, Heldin CH (2018) PDG FRβ translocates to the nucleus and regulates chromatin remodeling via TATA element-modifying factor 1. J Cell Biol 217:1701–1717. doi: 10.1083/jcb.201706118

55. Park SA, Han SM, Kim CE (2020) New fluid biomarkers tracking non-amyloid-β and non-tau pathology in Alzheimer's disease. Exp Mol Med 52:556–568. doi: 10.1038/s12276-020-0418-9

56. Pedrero-Prieto CM, García-Carpintero S, Frontiñán-Rubio J, Llanos-González E, Aguilera García C, Alcaín FJ, Lindberg I, Durán-Prado M, Peinado JR, Rabanal-Ruiz Y (2020) A comprehensive systematic review of CSF proteins and peptides that define Alzheimer's disease. Clin Proteomics 17:1–24. doi: 10.1186/s12014-020-09276-9

57. Portelius E, Brinkmalm G, Pannee J, Zetterberg H, Blennow K, Dahlén R, Brinkmalm A, Gobom J (2017) Proteomic studies of cerebrospinal fluid biomarkers of Alzheimer's disease: An update. Expert Rev Proteomics 14:1007–1020. doi: 10.1080/14789450.2017.1384697

58. Richard E, Carrano A, Hoozemans JJ, Van Horssen J, Van Haastert ES, Eurelings LS, De Vries HE, Thal DR, Eikelenboom P, Van Gool WA, Rozemuller AJM (2010) Characteristics of dyshoric capillary cerebral amyloid angiopathy. J Neuropathol Exp Neurol 69:1158–1167. doi: 10.1097/NEN.0b013e3181fab558

59. Roll L, Faissner A (2019) Tenascins in CNS lesions. Semin Cell Dev Biol 89:118–124. doi: 10.1016/j.semcdb.2018.09.012

60. Rosato M, Stringer S, Gebuis T, Paliukhovich I, Li KW, Posthuma D, Sullivan PF, Smit AB, van Kesteren RE (2019) Combined cellomics and proteomics analysis reveals shared neuronal morphology and molecular pathway phenotypes for multiple schizophrenia risk genes. Mol Psychiatry. doi: 10.1038/s41380-019-0436-y

61. Rosenberger AFN, Morrema THJ, Gerritsen WH, van Haastert ES, Snkhchyan H, Hilhorst R, Rozemuller AJM, Scheltens P, van der Vies SM, Hoozemans JJM (2016) Increased occurrence of protein kinase CK2 in astrocytes in Alzheimer's disease pathology. J Neuroinflammation. doi: 10.1186/s12974-015-0470-x

62. Sathe G, Na CH, Renuse S, Madugundu AK, Albert M, Moghekar A, Pandey A (2019) Quantitative Proteomic Profiling of Cerebrospinal Fluid to Identify Candidate Biomarkers for Alzheimer's Disease. Proteomics - Clin Appl 13:1800105. doi: 10.1002/prca.201800105

63. Selkoe DJ, Hardy J (2016) The amyloid hypothesis of Alzheimer's disease at 25 years. EMBO Mol Med 8:595–608. doi: 10.15252/emmm.201606210

64. Seyfried NT, Dammer EB, Swarup V, Nandakumar D, Duong DM, Yin L, Deng Q, Nguyen T, Hales CM, Wingo T, Glass J, Gearing M, Thambisetty M, Troncoso JC, Geschwind DH, Lah JJ, Levey AI (2017) A Multi-network Approach Identifies Protein-Specific Co-expression in Asymptomatic and Symptomatic Alzheimer's Disease. Cell Syst 4:60-72.e4. doi: 10.1016/j.cels.2016.11.006

65. Shinohara M, Murray ME, Frank RD, Shinohara M, DeTure M, Yamazaki Y, Tachibana M, Atagi Y, Davis MD, Liu CC, Zhao N, Painter MM, Petersen RC, Fryer JD, Crook JE, Dickson DW, Bu G, Kanekiyo T (2016) Impact of sex and APOE4 on cerebral amyloid angiopathy in Alzheimer's disease. Acta Neuropathol 132:225–234. doi: 10.1007/s00401-016-1580-y

66. Soares HD, Potter WZ, Pickering E, Kuhn M, Immermann FW, Shera DM, Ferm M, Dean RA, Simon AJ, Swenson F, Siuciak JA, Kaplow J, Thambisetty M, Zagouras P, Koroshetz WJ, Wan HI, Trojanowski JQ, Shaw LM (2012) Plasma biomarkers associated with the apolipoprotein E genotype and alzheimer disease. Arch Neurol 69:1310–1317. doi: 10.1001/archneurol.2012.1070

67. Sohma H, Imai S ichi, Takei N, Honda H, Matsumoto K, Utsumi K, Matsuki K, Hashimoto E, Saito T, Kokai Y (2013) Evaluation of annexin A5 as a biomarker for Alzheimer's disease and dementia with lewy bodies. Front Aging Neurosci. doi: 10.3389/fnagi.2013.00015

68. Sun M, Bell W, LaClair KD, Ling JP, Han H, Kageyama Y, Pletnikova O, Troncoso JC, Wong PC, Chen LL (2017) Cryptic exon incorporation occurs in Alzheimer's brain lacking TDP-43 inclusion but exhibiting nuclear clearance of TDP-43. Acta Neuropathol 133:923–931. doi: 10.1007/s00401-017-1701-2

69. Suttkus A, Rohn S, Weigel S, Glöckner P, Arendt T, Morawski M (2014) Aggrecan, link protein and tenascin-R are essential components of the perineuronal net to protect neurons against iron-induced oxidative stress. Cell Death Dis. doi: 10.1038/cddis.2014.25

70. Thal DR, Ghebremedhin E, Rüb U, Yamaguchi H, Del Tredici K, Braak H (2002) Two types of sporadic cerebral amyloid angiopathy. J Neuropathol Exp Neurol 61:282–93.

71. Tikka S, Baumann M, Siitonen M, Pasanen P, Pöyhönen M, Myllykangas L, Viitanen M, Fukutake T, Cognat E, Joutel A, Kalimo H (2014) CADASIL and CARASIL. Brain Pathol 24:525-544. doi: 10.1111/bpa.12181

72. Verwey NA, Schuitemaker A, Van Der Flier WM, Mulder SD, Mulder C, Hack CE, Scheltens P, Blankenstein MA, Veerhuis R (2008) Serum amyloid P component as a biomarker in mild cognitive impairment and Alzheimer's disease. Dement Geriatr Cogn Disord 26:522–527. doi: 10.1159/000178756

73. Wang Q, Woltjer RL, Cimino PJ, Pan C, Montine KS, Zhang J, Montine TJ (2005) Proteomic analysis of neurofibrillary tangles in Alzheimer disease identifies GAPDH as a detergent-insoluble paired helical filament tau binding protein. FASEB J 19:1–12. doi: 10.1096/fj.04-3210fje

74. Wesenhagen KEJ, Teunissen CE, Visser PJ, Tijms BM (2020) Cerebrospinal fluid proteomics and biological heterogeneity in Alzheimer's disease: A literature review. Crit Rev Clin Lab Sci 57:86–98. doi: 10.1080/10408363.2019.1670613

75. Whelan CD, Mattsson N, Nagle MW, Vijayaraghavan S, Hyde C, Janelidze S, Stomrud E, Lee J, Fitz L, Samad TA, Ramaswamy G, Margolin RA, Malarstig A, Hansson O (2019) Multiplex proteomics identifies novel CSF and plasma biomarkers of early Alzheimer's disease. Acta Neuropathol Commun 7:169. doi: 10.1186/s40478-019-0795-2

76. Wiersma VI, Hoozemans JJM, Scheper W (2020) Untangling the origin and function of granulovacuolar degeneration bodies in neurodegenerative proteinopathies. Acta Neuropathol Commun 8:153. doi: 10.1186/s40478-020-00996-5

77. Wiersma VI, van Ziel AM, Vazquez-Sanchez S, Nölle A, Berenjeno-Correa E, Bonaterra-Pastra A, Clavaguera F, Tolnay M, Musters RJP, van Weering JRT, Verhage M, Hoozemans JJM, Scheper W (2019) Granulovacuolar degeneration bodies are neuron-selective lysosomal structures induced by intracellular tau pathology. Acta Neuropathol 138:943–970. doi: 10.1007/s00401-019-02046-4

78. Wingo AP, Dammer EB, Breen MS, Logsdon BA, Duong DM, Troncosco JC, Thambisetty M, Beach TG, Serrano GE, Reiman EM, Caselli RJ, Lah JJ, Seyfried NT, Levey AI, Wingo TS (2019) Large-scale proteomic analysis of human brain identifies proteins associated with cognitive trajectory in advanced age. Nat Commun. doi: 10.1038/s41467-019-09613-z

79. Wisniewski T, Castaño EM, Golabek A, Vogel T, Frangione B (1994) Acceleration of Alzheimer's fibril formation by apolipoprotein E in vitro. Am J Pathol 145:1030-1035.

80. Wisniewski T, Drummond E (2019) Future horizons in Alzheimer's disease research. In: Prog. Mol. Biol. Transl. Sci. Elsevier B.V., pp 223–241

81. Wojtas AM, Kang SS, Olley BM, Gatherer M, Shinohara M, Lozano PA, Liu C-CC, Kurti A, Baker KE, Dickson DW, Yue M, Petrucelli L, Bu G, Carare RO, Fryer JD (2017) Loss of clusterin shifts amyloid deposition to the cerebrovasculature via disruption of perivascular drainage pathways. Proc Natl Acad Sci U S A 114:E6962–E6971. doi: 10.1073/pnas.1701137114

82. Wong TH, Chiu WZ, Breedveld GJ, Li KW, Verkerk AJMH, Hondius D, Hukema RK, Seelaar H, Frick P, Severijnen L-A, Lammers G-J, Lebbink JHG, Van Duinen SG, Kamphorst W, Rozemuller AJ, Bank NB, Bakker EB, Neumann M, Willemsen R, Bonifati V, Smit AB, Van Swieten J (2014) PRKAR1B mutation associated with a new neurodegenerative disorder with unique pathology. Brain. doi: 10.1093/brain/awu067

83. Xu J, Patassini S, Rustogi N, Riba-Garcia I, Hale BD, Phillips AM, Waldvogel H, Haines R, Bradbury P, Stevens A, Faull RLM, Dowsey AW, Cooper GJS, Unwin RD (2019) Regional protein expression in human Alzheimer's brain correlates with disease severity. Commun Biol 2:1–15. doi: 10.1038/s42003-018-0254-9

84. Yamazaki Y, Takahashi T, Hiji M, Kurashige T, Izumi Y, Yamawaki T, Matsumoto M (2010) Immunopositivity for ESCRT-III subunit CHMP2B in granulovacuolar degeneration of neurons in the Alzheimer's disease hippocampus. Neurosci Lett 477:86–90. doi: 10.1016/j.neulet.2010.04.038

85. Zhang Q, Ma C, Gearing M, Wang PG, Chin LS, Li L (2018) Integrated proteomics and network analysis identifies protein hubs and network alterations in Alzheimer's disease. Acta Neuropathol Commun 6:19. doi: 10.1186/s40478-018-0524-2

86. Zhang Y, Cedervall J, Hamidi A, Herre M, Viitaniemi K, D'Amico G, Miao Z, Valsala Madhavan Unnithan R, Vaccaro A, van Hooren L, Georganaki M, Thulin Å, Qiao Q, Andrae J, Siegbahn A, Heldin C-H, Alitalo K, Betsholtz C, Dimberg A, Olsson A-K (2020) Platelet-specific PDGFB ablation impairs tumor vessel integrity and promotes metastasis. Cancer Res canres.3533.2019. doi: 10.1158/0008-5472.CAN-19-3533

DANKWOORD

Het heeft even geduurd, maar nu is er dan toch echt een proefschrift uitgerold! Na al die jaren met veel leuk en interessant onderzoek, gezellige etentjes, borrels en congres bezoeken, ben ik een hoop mensen veel dank verschuldigd voor de leuke tijd en hun enorme bijdrage in het tot stand brengen van dit proefschrift.

Allereerst veel dank voor **Annemieke Rozemuller** en **Jeroen Hoozemans,** die mij al in 2008 verwelkomden bij de Neuropathologie. Ik heb ontzettend veel van jullie mogen leren en ben dankbaar voor de kans die ik gekregen heb om na vier jaar verder te gaan als promovendus. Ik heb het erg getroffen met jullie betrokkenheid, uitstekende begeleiding, vertrouwen en fijne samenwerking. Beste Annemieke, jou enthousiasme, optimisme en enorme kennis zijn altijd erg motiverend geweest. Beste Jeroen, wat fijn dat het altijd laagdrempelig was om bij jou aan te kloppen voor hulp en advies. Ik heb veel gehad aan je oplossingsgerichtheid, realistische kijk op dingen en je gevoel voor humor. **Guus Smit** bedankt voor de jarenlange enthousiaste begeleiding, support en scherpe maar opbouwende kritieken. Hierdoor zijn alle hoofdstukken in dit proefschrift veel beter geworden. Je enorme passie voor de wetenschap is altijd inspirerend geweest. Beste **Ka Wan Li**, dankzij jou als proteomics pionier en je enthousiasme voor het onderzoeken van neurodegeneratieve ziekten, zijn we heel wat proteomics pilot experimenten begonnen die uiteindelijk succesvolle projecten zijn geworden. Bedankt dat er altijd ruimte was om nieuwe dingen te proberen, ik heb veel van je geleerd.

Collega's van de Neuropathologie (waarvan sommige helaas ook alweer vertrokken zijn), het was gezellig en fijn werken, bedankt voor de vele mooie herinneringen. Ik heb erg genoten van de onderzoekservaringen, gezelligheid op het lab, borrels en congresbezoeken. Mijn dank gaat uit naar **Elise van Haastert** voor alle hulp met kleuringen en blotjes. **Andrea Rosenberger** thanks for the laughs, the funny stories and the good times, also during our visit to Vienna. Also lots of thanks to **Anna Carrano**, **Hripsime Snkhchyan** and **Kimberley Ummenthum** for making the most depressing office in the VUmc a cheerful place. **Anke Dijkstra, Andrea Ganz,** and **Anna Nölle** thank you for the nice conversations and the good atmosphere in the new office. **Jan Frits** bedankt voor de gezellige praatjes en de dagelijkse dosis gitaarmuziek en **Rob Veerhuis** voor de inspirerende ideeën voor met name het complement werk. **Regina Peferoen-Baert** bedankt voor alle mooie kleuringen, gezellige microscopie sessies en het stellen van goede vragen. **Marlies Jacobs** bedankt voor alle hulp, spoedbestellingen en gezelligheid en **Tjado Morrema** voor je gezelligheid op en om het lab en nimmer aflatende bereidheid om te helpen met kleuringen, coupes snijden en van alles en nog wat. **Baayla Boon** jou enthousiasme is altijd erg aanstekelijk! Bedankt voor de goede discussies, fijne samenwerking en gezelligheid. **Priya Gami-Patel** thank you very much for your interest and company at the neuro-PA and at conferences as a fellow PhD student and especially for joining me as my paranymph during my defence. Thanks to **Marianna Bugiani,** for making the CAA paper much better. **Vera Wiersma** bedankt voor de gezelligheid tijdens je stage, op congressen

en op de VU en natuurlijk het delen van de passie voor dalmatiërs. Collega's van de MS en white matter disease groepen; bedankt voor de gezelligheid en goede sfeer op het lab.

Collega's van het CNCR, en met name de neuroproteomics groep, bedankt! Ik heb altijd genoten van de enthousiaste sfeer, de gezelligheid en de proteomics dinners. Ik heb mij vanaf het begin af aan, erg welkom gevoeld. **Ning Chen**, thank you very much for helping me starting up the proteomics work. **Roel van der Schors**, bedankt voor jou enthousiasme, interesse en fijne samenwerking. Zonder jou waren we nooit zo succesvol begonnen. **Pim van Nierop** bedankt voor de magie op het gebied van dataverwerking en alle gezelligheid bij de vele analyses. Many thanks for the super-fast help with LMD-ing so many cells to **Débora Pita-Illobre**. **Iryna Paliukhovich** thanks for the nice conversations in the lab, your help, skills and getting the single cell measurements of unparalleled high quality. **Frank Koopmans**, heel erg bedankt voor je gezelligheid en gedrevenheid, mede dankzij jou is hoofdstuk 3 zo'n succes geworden.

Charlotte Teunissen, **Marta Del Campo Milan** and **Yanaika Hok-A-Hin** thanks for your help and interest in the NDP project. **Bea Kuiperij** en **Marcel Verbeek**, bedankt voor de fijne samenwerking in het CAVIA project. **John van Swieten** en **Tsz Hang Wong** bedankt voor de prettige samenwerking bij het PRKAR1B en VCP paper. Veel dank aan de Nederlandse Hersenbank en in het bijzonder **Michiel Kooreman**. Heel veel dank aan **Christiaan de Wijn**, ik ben blij dat je naast mij wilt staan bij de verdediging! Graag wil ik ook alle studenten bedanken; **Denise Kal, Sherida de Leeuw, Iris Lekkerkerker, Marina Sogorb González, Kristel Eigenhuis, Anne van Nifterick, Conny Leistner, Fenna Marbus, Melissa Peters, Florianne de Koning en Joris Geigenmüller** bedankt voor jullie harde werk en gezelligheid, ik denk er met veel plezier aan terug.

Tot slot, lieve familie en vrienden, heel erg bedankt voor jullie interesse in mijn werk, maar vooral ook de gezelligheid, steun, ontspanning, het fijn thuiskomen en het vieren van de weekenden en vakanties!

LIST OF PUBLICATIONS

Hondius DC, Koopmans F, Leistner C, Peferoen-Beart RM, Marbus F, Paliukhovich I, Li KW, Rozemuller AJM, Hoozemans JJM, Smit AB. The proteome of granulovacuolar degeneration and neurofibrillary tangles in Alzheimer's disease. *Under review, Acta Neuropathologica*

Hondius DC, Veerhuis R, van Nifterick AN, Kuiperij HB, Verbeek MM, Smit AB, Rozemuller AJM, Hoozemans JJM. Complement activation is associated with capillary cerebral amyloid angiopathy in Alzheimer's disease. *In preparation*

Kuiperij HB, **Hondius DC**, Kersten I, Versleijen AAM, Rozemuller AJM, Greenberg SM, Schreuder FHBM, Klijn CJM, Verbeek MM. Apolipoprotein D: a potential biomarker for cerebral amyloid angiopathy. Neuropathol Appl Neurobiol. 2019 Dec 23. doi: 10.1111/nan.12595. Epub ahead of print. PMID: 31872472.

Hondius DC, Hoozemans JJM, Rozemuller AJM, Smit AB. Laser microdissection for spatial proteomics of postmortem brain tissue. In Neuromethods (pp. 43-53). (Neuromethods; Vol. 146). Humana Press Inc. (2019). https://doi.org/10.1007/978-1-4939-9662-9_4

Hondius DC, Eigenhuis KN, Morrema THJ, van der Schors RC, van Nierop P, Bugiani M, Li KW, Hoozemans JJM, Smit AB, Rozemuller AJM. Proteomics analysis identifies new markers associated with capillary cerebral amyloid angiopathy in Alzheimer's disease. Acta Neuropathol Commun. 2018 Jun 4;6(1):46. doi: 10.1186/s40478-018-0540-2.

Wong TH, Pottier C, **Hondius DC**, Meeter LHH, van Rooij JGJ, Melhem S; Netherlands Brain bank, van Minkelen R, van Duijn CM, Rozemuller AJM, Seelaar H, Rademakers R, van Swieten JC. Three VCP Mutations in Patients with Frontotemporal Dementia. J Alzheimers Dis. 2018;65(4):1139-1146. doi: 10.3233/JAD-180301.

Hondius DC, Hoozemans JJM, Rozemuller AJM, Li KW, Smit AB. A Laser Microdissection-Liquid Chromatography-Tandem Mass Spectrometry Workflow for Post-mortem Analysis of Brain Tissue. Methods Mol Biol. 2018;1723:371-383. doi: 10.1007/978-1-4939-7558-7_21.

Hondius DC, van Nierop P, Li KW, Hoozemans JJ, van der Schors RC, van Haastert ES, van der Vies SM, Rozemuller AJ, Smit AB. (2016) Profiling the human hippocampal proteome at all pathologic stages of Alzheimer's disease. Alzheimers Dement. pii: S1552-5260(15)02987-8. doi: 10.1016/j.jalz.2015.11.002.

Wong TH, Chiu WZ, Breedveld GJ, Li KW, Verkerk AJ, **Hondius D**, Hukema RK, Seelaar H, Frick P, Severijnen LA, Lammers GJ, Lebbink JH, van Duinen SG, Kamphorst W, Rozemuller AJ; Netherlands Brain Bank, Bakker EB; International Parkinsonism Genetics Network, Neumann

M, Willemsen R, Bonifati V, Smit AB, van Swieten J. (2014) PRKAR1B mutation associated with a new neurodegenerative disorder with unique pathology. Brain 137:1361-1373.

Rozemuller AJ, Jansen C, Carrano A, van Haastert ES, **Hondius D**, van der Vies SM, Hoozemans JJ (2012) Neuroinflammation and common mechanism in Alzheimer's disease and prion amyloidosis: amyloid-associated proteins, neuroinflammation and neurofibrillary degeneration. Neurodegener Dis 10:301-304.

Kanters E, van RJ, Hensbergen PJ, **Hondius D**, Mul FP, Deelder AM, Sonnenberg A, van Buul JD, Hordijk PL (2008) Filamin B mediates ICAM-1-driven leukocyte transendothelial migration. J Biol Chem 283:31830-31839.

de Vries HE, Witte M, **Hondius D**, Rozemuller AJ, Drukarch B, Hoozemans J, van HJ (2008) Nrf2-induced antioxidant protection: a promising target to counteract ROS-mediated damage in neurodegenerative disease? Free Radic Biol Med 45:1375-1383.